Report
P-18-02
June 2018

SR-PSU (PSAR) Bedrock hydrogeology

TD18 – Temperate climate conditions

Johan Öhman
Magnus Odén

SVENSK KÄRNBRÄNSLEHANTERING AB

SWEDISH NUCLEAR FUEL
AND WASTE MANAGEMENT CO

Box 3091, SE-169 03 Solna
Phone +46 8 459 84 00
skb.se

SVENSK KÄRNBRÄNSLEHANTERING

ISSN 1651-4416
SKB P-18-02
ID 1668581

June 2018

SR-PSU (PSAR) Bedrock hydrogeology

TD18 – Temperate climate conditions

Johan Öhman, Geosigma AB

Magnus Odén, Svensk Kärnbränslehantering AB

Keywords: SFR, PSU, Hydrogeology, Bedrock, Modelling, Temperate, Forsmark, Safety assessment, Performance measures, Sensitivity analysis, Parameterisation.

Abstract

As a part of the license application for an extension of the existing repository for short-lived low and intermediate radioactive waste (SFR), the Swedish Nuclear Fuel and Waste Management Company (SKB) has undertaken a project to assess the radiological safety for the SFR repository after closure (SR-PSU). The SR-PSU project employs the groundwater flow model, developed in SDM-PSU, to perform hydrogeological modelling tasks that are defined in terms of so-called Task Descriptions (TDs). This report summarises the methodology, setup, and results of the groundwater flow modelling task TD18.

The objective of this study is to assess the repository performance in context of model uncertainty arising from: 1) bedrock heterogeneity, 2) parameterisation uncertainty, and 3) transient flow regime. The approach is to analyse a set of predefined performance measures in terms of a sensitivity analysis, which consists of 30 so-called bedrock cases (parameterisation variants) that are studied under nine selected stages of shoreline retreat. These bedrock cases have been selected based on a preceding inventory of model uncertainties to combine effects of uncertainty and variability in the bedrock parameterisation. Hence, the analysis is assumed to cover the range of flow through the disposal rooms.

The key outputs of this sensitivity analysis are: 1) demonstration of the dynamic hydrogeological setting of SFR, 2) quantification of the significance of model uncertainty for simulation results, and 3) delivery of performance measures to end users within SR-PSU.

The key performance measures from the groundwater flow modelling are:

- Disposal-room cross flow, Q (m^3/s).
- Particle exit location at the bedrock/regolith interface.
- Flow-related transport resistance along bedrock flow paths, Fr (y/m).
- Advective travel times along bedrock flow paths, $t_{w,r}$ (y).

The hydrogeological setting of SFR is strongly affected by the ongoing land uplift and as the seabed above SFR successively emerges above sea level, the flow regime will gradually conform to terrestrial conditions. Analysis of performance measures demonstrates that the flow regime remains in a transient state up to c. 3500 AD, after which it is stabilised by the influence of local topography, leading to a stationary appearance during later stages. The deeper location of the planned SFR extension (SFR 3) renders systematically longer path lengths, longer advective travel times, and higher flow-related transport resistance, as compared to SFR 1.

Out of the 30 studied bedrock cases, three are selected as representative for covering the range in observed cross flow through disposal rooms. The results of these three bedrock cases are presented in additional detail, and the flow solutions have been exported to near-field modelling teams.

Sammanfattning

Som en del av ansökan för utbyggnad av Slutförvaret för kortlivat radioaktivt avfall (SFR) har Svensk Kärnbränslehantering (SKB) genomfört ett projekt för att bedöma den radiologiska säkerheten för förvaret efter förslutning (SR-PSU). I SR-PSU tillämpas den grundvattenmodell som utvecklats i SDM-PSU för att genomföra olika hydrogeologiska modelleringsuppgifter, vilka finns definierade i särskilda uppgiftsbeskrivningar (*Eng:* Task Descriptions; TDs). Denna rapport sammanfattar ansats, genomförande och resultat för uppgiftsbeskrivningen.

Syftet är att bedöma de kombinerade effekterna av: 1) berggrundens heterogenitet, 2) parameterosäkerhet och 3) den transienta flödesregimen. Detta bedöms med hjälp av en känslighetsanalys, som består av 30 varianter av parameteruppsättning för berggrunden (*Eng:* bedrock cases), samtliga studeras för sex utvalda stadier av strandlinjeförskjutning.

Känslighetsanalysen medför tre huvudsakliga resultat: 1) förståelsen för den dynamiska hydrogeologiska omgivningen kring SFR demonstreras, 2) mått på bergets retentionsegenskaper (*Eng:* performance measures) levereras till användare inom SR-PSU och 3) nya modelleringsprinciper har tillförts DarcyToolsmiljön.

De huvudsakliga måtten på bergets retentionsegenskaper från simuleringarna är:

- Flöde genom förvarsutrymmen, Q (m^3/s).
- Partikelbanors passage vid övergången jord/berg.
- Flödesrelaterat transportmotstånd längs flödesbanor i berg, Fr (y/m).
- Advektiv gångtid längs flödesbanor i berg, $t_{w,r}$ (y).

Resultaten från partikelspårningen har levererats, för varje parameteruppsättning och stadie av strandlinjeförskjutning, till övriga modellörer inom SR-PSU.

I tidiga stadier av strandlinjeförskjutning, t.o.m. 3500 AD, påverkas bergets retentionsegenskaper påtagligt av den transienta flödesregimen, men därefter övergår flödesregimen gradvis mot stationära förhållanden som domineras av lokala topografiska gradienter, 5000 till 9000 AD. Den djupare belägenheten av den planerade utbyggnaden (SFR 3) ger upphov till systematsikt längre flödesbanor, längre advektiva gångtider och högre flödesrelaterat transportmotstånd, i jämförelse mot det existerande förvaret (SFR 1).

Av de 30 parameteruppsättningarna har tre valts ut som representativa för att täcka in intervallet av beräknade flöden genom förvarsutrymmen. Resultaten för de tre utvalda parameteruppsättningarna beskrivs extra utförligt och deras flödeslösningar har levererats till närfälts-modelleringen.

Contents

1 Introduction

1.1 Background of the SR-PSU project

The final repository for low and intermediate level short-lived radioactive waste (SFR) was constructed in its first stage and taken into operation in 1987. Today the SFR facility must be extended to manage the disposal volumes arising from: 1) the pending decommissioning of the closed reactors (Barsebäck, Studsvik, and Ågesta), 2) increased amounts of operational waste caused by the extended operating time of the remaining nuclear power plants, and 3) future decommission of the remaining nuclear power plants. The existing facility is denoted SFR 1, while its planned extension is denoted SFR 3. As a part of the license application for SFR 3, the Swedish Nuclear Fuel and Waste Management Company (SKB) initiated the SFR extension project (PSU). The radiological safety assessment for the entire SFR-repository after closure is referred to as SR-PSU.

All groundwater-flow modelling tasks within SR-PSU are defined in so-called Task Descriptions (TDs). A sensitivity analysis was carried out in support of the safety assessment for SR-PSU to address model sensitivity to parameterisation uncertainty and future shoreline retreat (i.e. TD11, Öhman et al. 2014). The model sensitivity was evaluated by means of hydrogeological flow simulations setup in the model code DarcyTools based on the site-descriptive hydrogeological model, SDM-PSU (SKB 2013) and quantified in terms of selected performance measures (flow through disposal rooms and bedrock retention along particle trajectories). Two different climate conditions were studied in SR-PSU (F-PSAR) (temperate and periglacial conditions; Odén et al. 2014). The original sensitivity analysis has been complemented by studies covering various aspects of relevance for SR-PSU (TD12; Öhman and Vidstrand 2014, TD14; Öhman and Odén 2017a, TD15; Öhman and Odén 2017b and TD16; Öhman and Odén 2017c). Since the performed modelling task in TD11 the plug geometry of SFR1 has been revised and a new repository layout of the planned SFR extension (version L.2.6; Odén and Öhman 2017) is available for SR-PSU (PSAR).

This report describes the model results of tasks defined in TD18 (Odén 2017), including input-data handling, numerical setup of model cases, simulation procedures, as well as, handling of output. This study assesses the impact of bedrock heterogeneity and parameterisation uncertainty on repository performance under post-closure conditions during temperate climate conditions, under various stages of shoreline retreat, by means of a sensitivity analysis.

1.2 Objectives

The main objective is to assess repository performance in the context of model uncertainties arising from heterogeneity and uncertainty in bedrock parameterisation. The approach is to quantify the impact of uncertainties in a sensitivity analysis of selected bedrock cases (Table 2-1). The performance measures are primarily affected by the bedrock properties in the proximity of SFR (i.e. local structures and local fracture network; e.g. Öhman et al. 2014), and therefore, the sensitivity analysis focusses on the parameterisation inside the SFR Regional domain (Figure 3-1) while keeping the properties outside fixed. However, based on the findings in earlier studies (e.g. Öhman and Odén 2017b), it has been decided to also address the bedrock properties outside the SFR Regional domain in a few model variants.

Two types of performance measures are used in the evaluation of simulation results (described in more detail in Section 1.3):

1. Flow through disposal rooms (both facilities SFR 1 and SFR 3).
2. Bedrock retention properties along flow paths through disposal rooms (quantified by means of particle tracking).

There are two reasons for this analysis. Firstly, the results demonstrate the understanding of the present day hydrogeological characteristics of the site, as well as, predict how these conditions will change during future stages of shoreline retreat. Secondly, results are delivered to the other modelling teams in SR-PSAR (near-field modelling and radionuclide transport modelling).

1.3 Considered performance measures

The key performance measures (output) from the groundwater flow modelling are:

- Disposal-room cross flow, Q (m^3/s).
- Particle exit location at the bedrock/regolith interface.
- Flow-related transport resistance along bedrock flow paths, Fr (y/m).
- Advective travel times along bedrock flow paths, $t_{w,r}$ (y).

A performance measure of supporting character is:

- Path length of bedrock flow paths, L_r (m).

As stated in Section 1.2, these performance measures are analysed to demonstrate the understanding of the hydrogeological characteristics of the site (Chapter 6), but also exported to downstream users within the SR-PSU project (e.g. radionuclide transport calculations, hydrogeochemistry, and biosphere analyses), for each bedrock case and time slice. The different performance measures are briefly described below.

The performance measures are evaluated from the steady-state flow solutions at different stages of shoreline retreat (time slices). The disposal-room cross flow, *Q*, refers to flow between tunnel and bedrock cells (Section 5.4.1), whereas the other performance measures refer to flow paths that cross the disposal rooms (Section 5.4.2). The performance measures F_r (y/m), $t_{w,r}$ (y), and L_r (m) are integrated bedrock properties along particle trajectories, as defined from a bedrock-entry point to a bedrock-exit point. The particle tracking is initiated by releasing particles spatially uniformly within disposal rooms. However, the analysis of bedrock properties starts at the bedrock entry (i.e. the tunnel-wall passage) and terminates at its exit (i.e. regolith interface passage). The underlying equations for determining these cumulative performance measures along flow paths are described in more detail in Section 5.4.2.

Disposal-room cross flow (Q)

Cross flow refers to the total flow, *Q* (m^3/s), over a predefined cross-sectional area in the computational grid. This area is defined as the outer walls of all grid cells representing each disposal room. Since this area is an enclosed surface, its net flow is zero, and therefore cross flow is defined by separate summation of inward- and outward-flow components (Section 5.4.1). Cross flow is an important output (performance measure) in the groundwater flow modelling as it affects the strength of the source term in radionuclide transport modelling.

Particle exit location

Exit locations are determined by means of forward particle tracking, and defined as the point where the particle passes the bedrock/regolith surface (expressed in RT90 coordinates).

Flow-related transport resistance (F_r)

The flow-related transport resistance in rock, F_r (y/m), is an entity, integrated along flow paths, that quantifies the flow-related (hydrodynamic) aspects of the possible retention of solutes transported in a fractured medium. It is an important output (performance measure) in groundwater flow modelling. In SR-PSU, information about the flow-related transport resistance governs the calculation of nuclide migration, hydrogeochemical calculations of salt diffusion into and out from the matrix, as well as oxygen ingress. In its most intuitive form, although not necessarily most generalised, the flow-related transport resistance is proportional to the ratio of flow-wetted fracture surface area (FWS) and flow rate (Joyce et al. 2010). An alternative definition is the ratio of FWS per unit volume of flowing water multiplied by the advective travel time.

Advective travel time ($t_{w,r}$)

The cumulative advective residence time for a particle along a trajectory in the rock, $t_{w,r}$ (y).

1.4 Settings

SFR is located in northern Uppland within the municipality of Östhammar, about 120 km north of Stockholm (Figure 1-1). The site is located about 2 km north of the site selected for the final repository for spent nuclear fuel (SDM-Site Forsmark).

The current ground surface in the Forsmark region forms a part of the sub-Cambrian peneplain in south-eastern Sweden. This peneplain represents a relatively flat topographic surface with a gentle dip towards the east that formed more than 540 million years ago. The Forsmark region is characterised by small-scale topography at low elevation (Figure 1-2). The whole area is located below the highest coastline associated with the last glaciation, and large parts of the area emerged from the Baltic Sea only during the last 2 000 years. The current landscape is strongly influenced by both the flat topography and the ongoing land uplift of about 6 mm/year. Sea bottoms are continuously transformed into new terrestrial areas or freshwater lakes, and lakes and wetlands are successively covered by peat. Most of the Forsmark-SFR site is currently covered by sea water (Figure 1-3), but the seabed will continue to rise and the seabed above SFR will be at the shoreline within about 1 000 years.

The existing repository facility, SFR 1, consists of four rock vaults and a vertically extending silo. The silo extends from c. –70 m to –140 m (elevation system RHB 70) and the four rock vaults of SFR 1 are located within the elevation range from c. –70 m to –90 m. The planned extension, SFR 3, consists of six rock vaults, which will extend from c. –120 m to –140 m (Figure 1-3 and Figure 3-2).

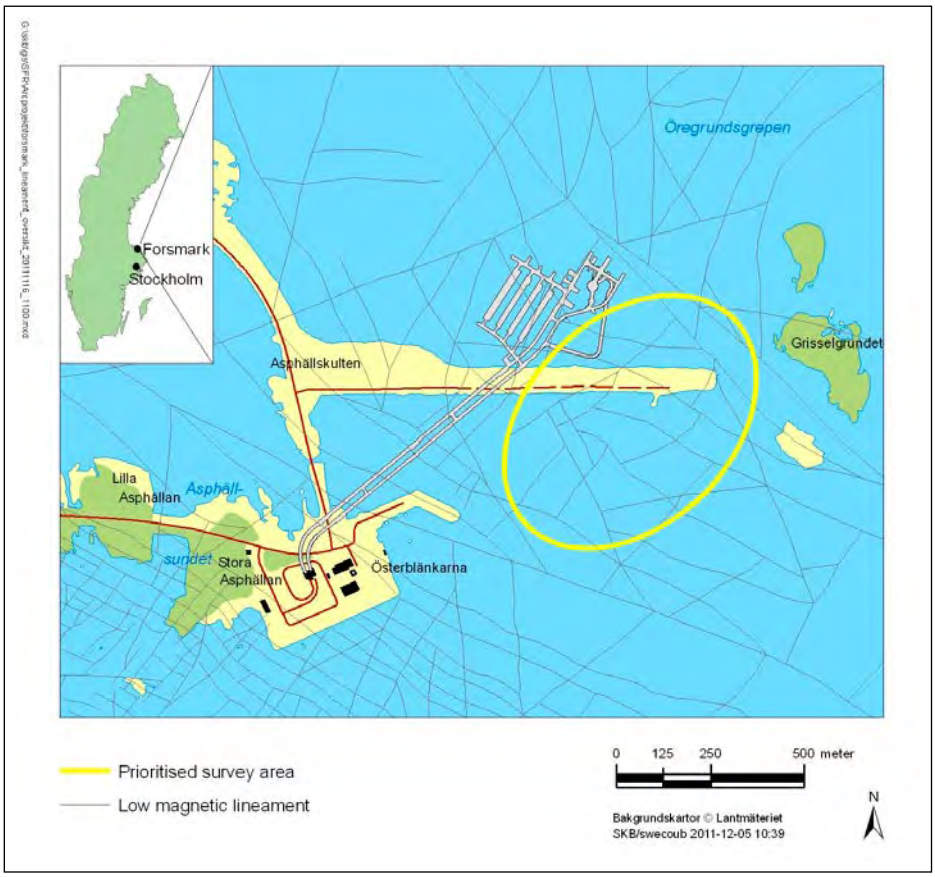

Figure 1-1. *Map of the Forsmark-SFR site showing the location of the existing SFR facility (SFR 1) and the prioritised survey area (yellow) for the SFR extension (SFR 3). In this report, the strip of land running above the existing SFR facility is referred to as the 'SFR Pier'.*

Figure 1-2. *Photograph showing the flat topography and the low-gradient shoreline with recently isolated bays due to land uplift, forming lakes with gradual vegetation ingrowth.*

Figure 1-3. *Figure showing the existing SFR facility (SFR 1) and the suggested area (yellow) for the SFR extension (SFR 3) in the foreground and the Forsmark nuclear power plant buildings in the background. The distance from SFR 1 to the shoreline is about 2 km. The man-made wave breaker running above SFR 1 is referred to as the 'SFR Pier', cf. Figure 1-1.*

1.5 Nomenclature

This report contains several terms and acronyms that are rarely used outside SKB work and makes several references to site-specific deformation zones. To facilitate the readability of the report these are listed in Table 1-1

Table 1-1. Acronyms and structures referred to in the report.

Acronym	Stands for	Explanation
DEM	Digital Elevation Model	Topographic model of the Forsmark area, covering both land and seafloor with a spatial resolution of 20 m in the horizontal plane.
DFN	Discrete Fracture Network	In DFN modelling, fractures, and fracture flow, are typically resolved as a network of planar geologic features.
ECPM	Equivalent Continuous Porous Medium	A hydrogeological modelling concept, where the hydraulic properties of a conductive fracture network are approximated by those of a porous medium. ECPM does not resolve explicit fracture flow, and hence is useful in large-scale simulations and on site-scale if fractures are resolved with fine enough discretization.
GEHYCO	GEnerate HYdraulic COnductivity	The module in DarcyTools used to translate a hydraulic DFN into an ECPM (Svensson et al. 2010).
HCD	Hydraulic Conductor Domain	Hydraulic representation of deterministically modelled deformation zones.
HRD	Hydraulic Rock mass Domain	Hydraulic representation of the bedrock outside deformation zones. Constant hydraulic conductivity cases are compared against ECPM parameterisation of stochastic DFN realisations.
HSD	Hydraulic Soil Domain	Hydraulic representation of the regolith (Quaternary deposits mainly).
L2.6	Layout for SFR 3	Currently studied layout geometry for the planned SFR extension (SFR 3).
PDZ	Possible Deformation Zone	A borehole section that has geologically been interpreted to have “deformation-zone like characteristics” (i.e. a possible deformation zone intercept). In the geological modelling, deterministic structures (ZFMxxx) are modelled in 3D by linking PDZs to surface lineaments. Remaining PDZs, which cannot be linked to lineaments, are referred to as “Unresolved PDZs”.
SDM	Site-Descriptive Model	A multi-disciplinary description of the site, including both qualitative and quantitative information, that is based on both direct observations and modelling studies.
SFR	SlutFörvaret för kortlivat Radioaktivt avfall	The existing final repository for short-lived radioactive waste. The existing repository is denoted SFR 1, while the planned extension is denoted SFR 3.
SKB	Svensk Kärnbränslehantering AB	The Swedish Nuclear Fuel and Waste Management Company.
ZFM	Deformation zone in the Forsmark area	Deterministically modelled deformation zone in the geological model. Modelled by linking borehole intercepts with “deformation-zone like characteristics” to surface lineaments (see acronym PDZ).

Table 1-2. Key deformation zones.

Key deformation zones (Figure 1-4) (Deterministic structures of the Geological model SFR v 1.0)		Alternatively known as: (Structures in early SFR models)
ZFMWNW0001	Core of the bounding Southern deformation zone belt (Curtis et al. 2011).	Singö deformation zone
ZFMNW0805A/B	Deformation zones that constitute a Northern boundary belt (Curtis et al. 2011).	Zone 8
ZFMNNW1034	Deformation zone of high transmissivity that cuts across the wedge defined by the intersection of the Northern and Southern boundary belts (Curtis et al. 2011).	Not included in previous SFR models.
ZFM871	Gently dipping deformation zone below the existing repository facility (SFR 1).	Zone H2
ZFMENE3115	A deformation zone that terminates ZFM871 to the southeast.	Not modelled in previous SFR models.
ZFMWNW0835	A deformation zone that intersects the SFR 3 rock vaults.	Not modelled in previous SFR models.
ZFMNE0870	Low-transmissive deformation zone parallel to the access tunnels.	Zone 9
ZFMNNE0869	High-transmissive deformation zone intersecting access tunnels.	Zone 3
ZFMNNW1209	A deformation zone that intersects the SFR 1 rock vaults.	Zone 6
ZFMWNW1035	A deformation zone that occurs at the northern rim of the Southern boundary belt (Curtis et al. 2011).	Zone 1

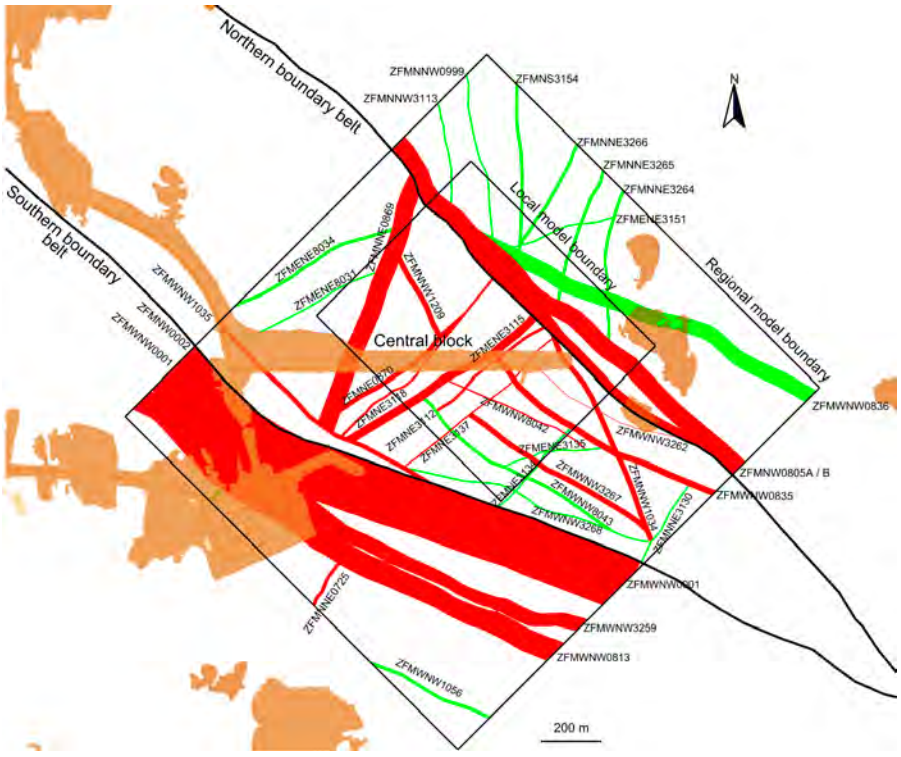

Figure 1-4. *Ground-surface intersection of deformation zone traces (Curtis et al. 2010). Coloured by confidence in existence: high = red, medium = green.*

2 Approach

As stated above, this study assesses the performance of SFR and its sensitivity to model uncertainty (Section 1.2). A sensitivity analysis is undertaken, in which groundwater flow is simulated for an ensemble of parameterisation variants (referred to as “bedrock cases”; Table 2-2) and the sensitivity to model uncertainties can be evaluated in terms of pre-defined performance measures (Section 1.3). This chapter outlines the approach taken.

The approach is divided into a description of the conceptual model components (Section 2.2) and the more detailed modelling sequence (or, numerical implementation; Section 2.3). The modelling sequence consists of the following key steps:

1. input geometry (Chapter 3),
2. model parameterisation (Chapter 4), and
3. simulation sequence (Chapter 5).

The flow-simulation code used, DarcyTools, has a central role in this modelling task, and therefore its inbuilt feasibilities/limitations/user control sets the framework for how the numerical approach can be designed. As the flow-simulation code has a significant influence on the numerical approach, this chapter starts with a brief presentation of DarcyTools (Section 2.1).

2.1 Modelling tool

The flow simulations in this study employ DarcyTools, which is a computer code that has been specifically developed for the analysis of a repository for spent nuclear fuel (Svensson et al. 2010).

DarcyTools is based on the Continuum Porous-Medium (CPM) approach (Svensson et al. 2010), in which the hydraulic properties of a flowing fracture network are approximated by those of a porous medium. DarcyTools allows transferring fracture-network characteristics, as observed in borehole data, onto its computational grid by means of geometrical upscaling over grid cells. These upscaled properties are referred to as Equivalent Continuous Porous Medium (ECPM) properties. As the ECPM approach is based on an underlying stochastic DFN model, the resulting ECPM properties are also stochastic. The uncertainty related to hydraulic heterogeneity can therefore be handled by addressing multiple DFN realisations.

The appeal of the ECPM approach is a significant reduction in computational demand and an upscaled bedrock parameterisation that bears the traits of an underlying fracture network, for example anisotropic correlation structures. Unfortunately, *geometrical* up-scaling does not always ensure *hydraulic* consistency between the complex heterogeneity of the underlying flowing fracture network and the approximated ECPM. It must therefore be emphasised that the term “equivalent” requires a fine resolution of the computational grid to be valid.

Another key feature in DarcyTools is its unstructured Cartesian grid system, which allows great flexibility in local grid refinement to represent detailed geometry of objects (e.g. tunnel layout). All grid geometry is handled via so-called DarcyTools objects (i.e. code-specific file format), which have been constructed from original CAD data geometry (see Chapter 3).

2.2 Conceptual model components

The groundwater flow model developed within SDM-PSU and SR-PSU consists of three conceptual hydrogeological units (see SKB 2013):

- HSD (Hydraulic Soil Domain), representing the regolith, i.e. any loose material covering the bedrock, e.g. Quaternary deposits, filling material, and peat,

- HCD (Hydraulic Conductor Domain), representing deformation zones, and
- HRD (Hydraulic Rock mass Domain), representing the less fractured bedrock in between the deformation zones.

The parameterisation of these three hydraulic-domain types is subject to uncertainty and heterogeneity, which is addressed by means of a sensitivity analysis (Section 1.2). This model task is delimited to assessing the sensitivity to uncertainty in bedrock parameterisation. Over the time span addressed in SR-PSU, the HSD is affected by landscape processes (marine sedimentation dynamics as well as terrestrial lake orogeny). These processes are modelled separately (Brydsten and Strömgren 2013) and the resulting regolith layers are implemented as time-variant input data for the flow simulations (Section 3.3). The HSD parameterisation is described in Section 4.5.

2.2.1 Bedrock parameterisation cases

The bedrock outside deformation zones, HRD, is described by means of a stochastic Discrete-Fracture Network (DFN) model, as well as, a stochastic conditional model for Unresolved PDZs (see details in SKB 2013). The heterogeneity in HRD is modelled by means of coupled stochastic realizations of the DFN and the Unresolved-PDZ models (examples presented in Section 4.3.1). Three homogeneous HRD parameterisation variants are also included as a reference for investigating the significance of the DFN model.

The HCD parameterisation involves two components of variability: 1) heterogeneity and 2) conceptual uncertainties (Section 4.3.2). The spatial heterogeneity is addressed by comparing homogeneous parameterisation versus heterogeneous realisations (Table 2-1). One of the conclusions from SKB (2013) was that the possible existence of a transmissivity depth trend could neither be supported by data, nor could it be rejected. The significance of this conceptual uncertainty in terms of repository performance has been evaluated by comparing HCD parameterisation variants that: 1) are based on an underlying depth-trend assumption, versus 2) variants that are not (Öhman et al. 2014). Earlier results have demonstrated that the depth-trend assumption is conservative (in terms of disposal-room crossflows), and therefore all bedrock cases in this study rely on the assumption of depth trend in HCD transmissivity.

Another conceptual uncertainty regards the confidence in local borehole conditioning of HCD parameterisation (i.e. the confidence of local data near disposal rooms, versus the large-scale interpretation of a zone). This uncertainty is addressed by comparing bore-hole conditioned HCD parameterisation, versus non-conditioned parameterisation (Table 2-1).

Finally, an uncertainty regarding the transverse hydraulic properties of the Singö deformation zone (i.e. the properties controlling flow across the zone) has been identified as potentially significant for flow during early stages of shoreline retreat.

2.2.2 Dynamic hydrogeological setting

The hydrogeological setting at SFR is a dynamic system, driven by the ongoing land uplift, which gradually alters the flow regime during the time span addressed in SR-PSU (e.g. Figure 2-1). The current setting for SFR will change from slow upward flow, driven by the regional-scale gradient, towards horizontal flow, driven by local topographical gradients. An important aspect is therefore to study the evolution of groundwater flow, from the surface (recharge areas) to the repository, and from the repository to the surface (discharge areas), and its impact on performance measures (Section 1.3). The altering flow regime is addressed by comparing results of steady-state flow solutions for selected shoreline positions (referred to as *time slices*). For the Global warming climate case (SKB 2014a) the identified shoreline positions correspond to the following time slices: 2000, 2100, 2250, 2500, 2750, 3000, 3500, 5000, and 9000 AD (Table 2-1).

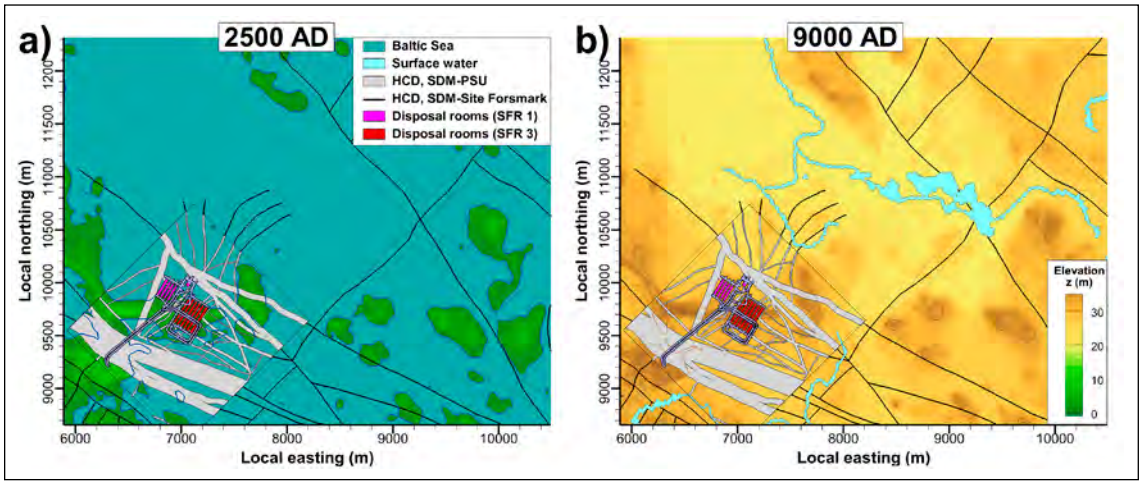

Figure 2-1. *Shoreline retreat between time slices 2500 AD and 9000 AD.*

2.2.3 Biosphere objects for SFR discharge

The output of this study is employed in another part of the PSU safety assessment (i.e. SR-PSU Biosphere), where radionuclide transport to the biosphere is calculated to predict the dose for humans. Earlier modelling tasks for SR-SPU have identified seven potential recipient areas for SFR discharge during future stages of shoreline retreat (Werner et al. 2013). These recipient areas are referred to as biosphere objects and are useful for classifying the output of particle-tracking (Figure 2-2).

Earlier simulations have demonstrated that the discharge areas, as modelled by particle-exit locations, exhibit modest variation with shoreline retreat and alternative bedrock parameterisation (Öhman et al. 2014). However, the general flow direction is north, and therefore the biosphere area 157_2 has been identified as the main recipient, with smaller fractions of discharge to 157_1 and 116. The main reasons for this are:

1. **Geology**: SFR discharge is more or less enclosed by three deformation zones: the steeply dipping ZFMNNE0869 and ZFMNW0805A/B and the gently dipping ZFM871 located just below the existing SFR facility. Their junction intersects ground-surface inside biosphere object 157_2 (Figure 2-3a).
2. **Location and topography**: The three biosphere objects, 157_1, 157_2 and 116, are located just north of SFR (i.e. downstream, in the general direction of flow). Biosphere object 157_2 is a local topographical depression, which forms a minor costal inlet at c. 3750 AD (Figure 2-3b).
3. **Sediment coverage**: the pier acts as a wave breaker, which allows accumulation of marine deposits south of the pier. North of the pier, the sea bottom is considerably more exposed to wave erosion, which is manifested by a redistribution of marine sediments towards deeper basins (marine sediment thickness contoured in Figure 2-3a). In particular, the costal inlet of object 157_2 is blocked to the north by thick deposits of low-conductive postglacial clay (Figure 2-3b). An overview of sediments in the SFR nearfield is provided in Figure 4-16.
4. **Model uncertainty outside the SFR Regional domain**: in addition to the hydrogeological conditions of object 157_2 stated above, previous studies (i.e. Öhman et al. 2014) may have underestimated the potential discharge to object 116. This study therefore includes variants of deformation-zone extension north and alternative HRD parameterisation in the area north of the SFR Regional domain (Sections 2.2.4 and 4.4).

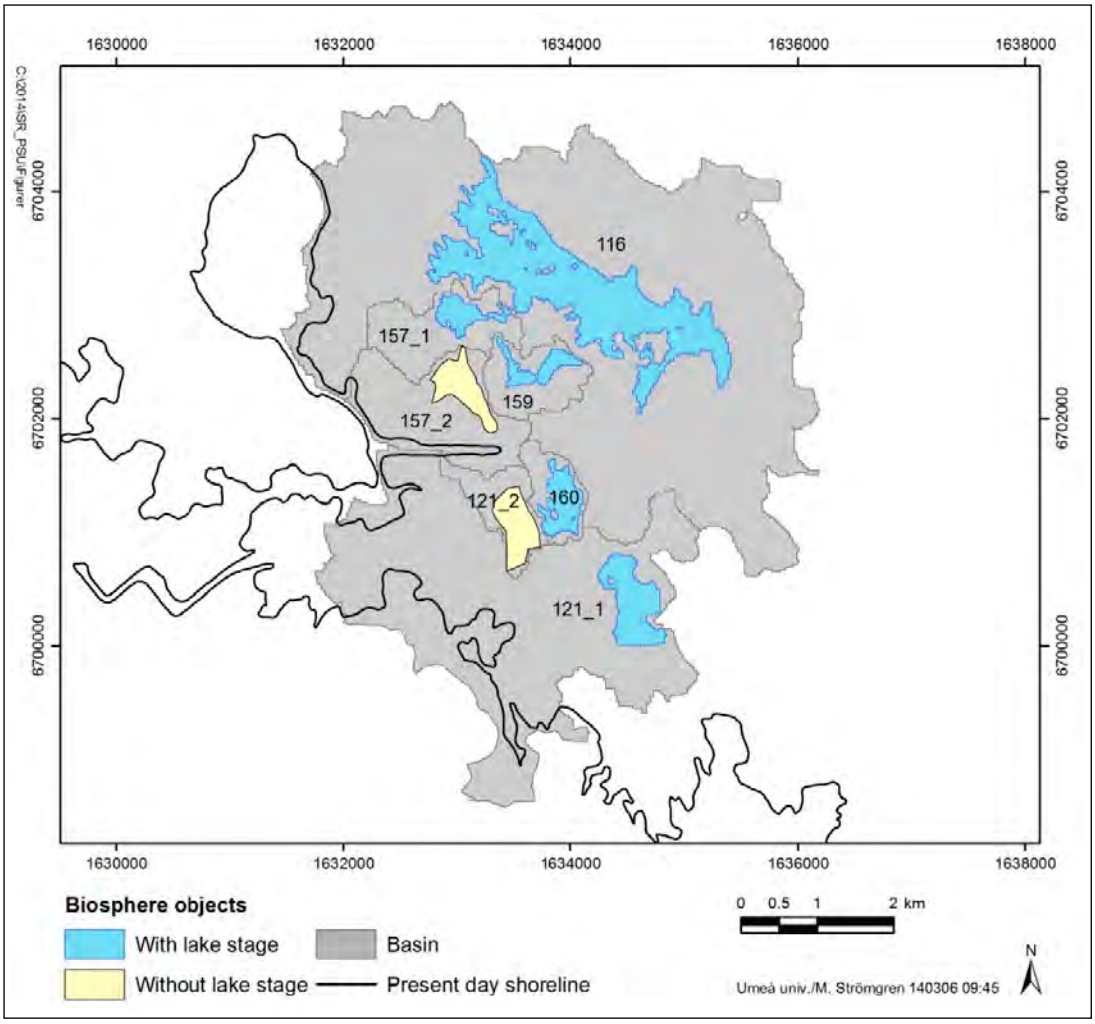

Figure 2-2. *Seven biosphere objects identified in Werner et al. (2013) as the key future recipients of SFR discharge (existing facility and its planned extension).*

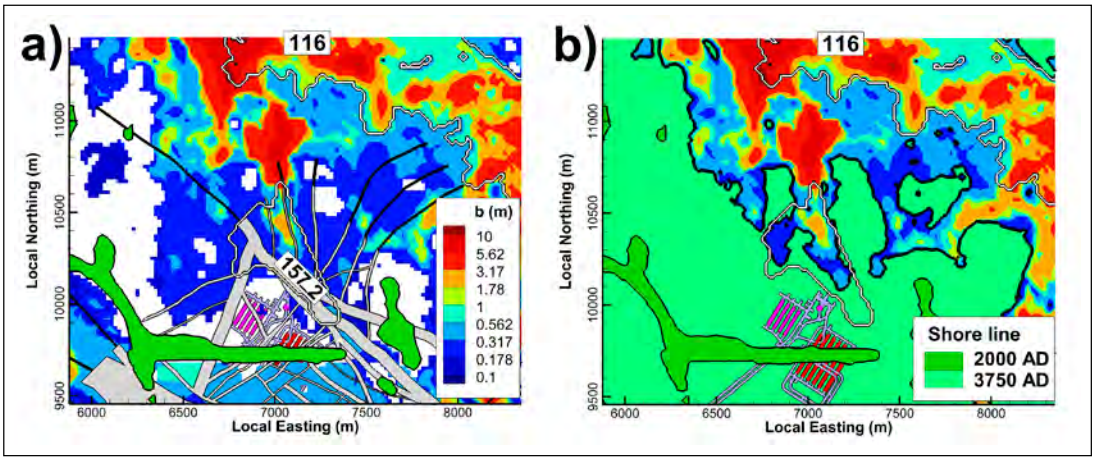

Figure 2-3. *Hydrogeological setting controlling SFR discharge (biosphere objects 157_2 and 116 outlined in white); a) ground-surface intercept of deformation-zone junction and b) topography forming a minor coastal inlet at c. 3750 AD. The occurrence of low-permeable marine deposits (contoured thickness, b) is concentrated to topographical basins.*

2.2.4 Model components in the sensitivity analysis

The different aspects in bedrock parameterisation (Section 2.2.1) combined with selected stages of future shoreline retreat (Section 2.2.2) comprise 270 model setups to solve in the sensitivity analysis. Each model setup, referred to as a "bedrock case", is a combination of a HCD parameterisation variant paired with a HRD variant/realisation. Moreover, the bedrock parameterisation is divided into domains: the "SFR host rock" (Table 2-1; i.e. inside the SFR Regional domain) and the "Remote bedrock" (Table 2-1; i.e. outside the SFR Regional domain). The number of combinations is reduced by selecting a few representative parameterisation variants of HCD and HRD (Table 2-1). The parameterisation variants have been selected as representative for covering the range of observed variability in disposal-room cross flow of the ensemble of analysed bedrock cases in Öhman et al. (2014). Out of the remaining possible bedrock-parameterisation combinations, 30 are selected for propagation to the sensitivity analysis (Table 2-2). These bedrock cases are considered to cover the range of flow through the disposal rooms (i.e. the range arising from bedrock parameterisation uncertainty). Moreover, nine representative time slices are selected for resolving the transition from submerged conditions into the fully matured terrestrial conditions.

The combined components of uncertainty/heterogeneity in the bedrock parameterisation are analysed in terms of a sensitivity analysis, where model performance is evaluated for a selection of 30 bedrock parameterisation cases under nine stages of shoreline retreat (Table 2-1).

Table 2-1. Model components varied in the sensitivity analysis.

Variable	Model component		Modelled cases
Host bedrock[1)]	HCD	Deterministic structures: • Deformation zones • SBA structures[2)]	• Base case (homogeneous) • Heterogeneity (R01, R07) • Borehole conditioning (y/n) • Singö cross-transmissivity (Si)
	HRD	Stochastic features: • DFN • Unresolved PDZ	Stochastic realisations: • R03, R18, R85
		Constant parameterisation: • KHRD	• KHRD = 6.5×10^{-9} m/s (± order one of magnitude)
Time slice	Shoreline retreat (sea-level displacement) Regolith layering Lake succession		Selected time slices (AD): 2000, 2100, 2250, 2500, 2750, 3000, 3500, 5000, and 9000
Remote bedrock[3)]	HCD	• Deformation zones[2)] • Sheet joints[2)] • Extension of North from SFR	Two extension variants (6 HCDs)
	HRD	Stochastic fractures: • DFN	Stochastic realisations: • R01, R02
		Constant parameterisation	• KHRD = 6.5×10^{-9} m/s

[1)] Bedrock *inside* the SFR Regional domain and consists of HCD and HRD parameterisation.

[2)] Parameterisation kept fixed in all bedrock cases.

[3)] Bedrock *outside* the SFR Regional domain and consists of HCD and HRD parameterisation.

The simulations are executed in two batches:

1. The three representative bedrock cases identified in TD11 (Öhman et al. 2014). These model setups were executed in advance to provide input for the near-field modelling (Abarca et al. 2014). These cases are directly comparable to the earlier sensitivity study for SR-PSU, as the gridding and file management is very similar to that used in TD11 (Öhman et al. 2014; see footnote 1 in Table 2-2).

2. The remaining 27 bedrock cases form selected combinations of the modelling aspects addressed in the sensitivity analysis. The gridding and file management (file-name conventions) were adjusted to manage addressing Singö-barrier effects and HCD extension north from SFR. Thus, both cases 1 and 30 employ identical bedrock parameterisation and represent the base case.

Table 2-2. Bedrock cases addressed in the sensitivity analysis.

		Inside SFR domain				Outside [1), 2)]	
		HCD					
No.	Bedrock case	Cond	Singö	Variability	HRD	HCD	HRD
1*	BASE_CASE1_DFN_R85_EXT1	Yes	–	Hom	R85	–	R01[1)]
2	BASE_CASE1_DFN_R85_EXT02	Yes	1	Hom	R85		R02[2)]
3	BASE_CASE1_DFN_R85_EXT11	Yes	1	Hom	R85	Ext.	R01
4	BASE_CASE1_DFN_R85_EXT12	Yes	1	Hom	R85	Ext.	R02
5	nc_Si1_HOM_HRD_C02_EXT01	No	1	Hom	C02		R01
6	nc_Si1_R01_HRD_C01_EXT01	No	1	R01	C01		R01
7	nc_Si1_R01_HRD_C02_EXT01	No	1	R01	C02		R01
8	nc_Si1_R01_HRD_C03_EXT01	No	1	R01	C03		R01
9	nc_Si1_R01_DFN_R03_EXT02	No	1	R01	R03		R02
10	nc_Si1_R01_DFN_R03_EXT01	No	1	R01	R03		R01
11*	nc_DEP_R07_DFN_R85_EXT1	No	–	R07	R85	–	R01
12	nc_Si1_R07_HRD_C02_EXT01	No	1	R07	C02		R01
13	CD_Si1_R07_DFN_R85_EXT01	Yes	1	R07	R85		R01
14	nc_Si1_R01_DFN_R85_EXT01	No	1	R01	R85		R01
15*	nc_NoD_R01_DFN_R18_EXT1	No	–	R01	R18	–	R01
16	nc_Si1_R07_DFN_R85_EXT02	No	1	R07	R85		R02
17	nc_Si1_R07_DFN_R18_EXT02	No	1	R07	R18		R02
18	nc_Si1_R07_DFN_R03_EXT02	No	1	R07	R03		R01
19	CD_Si2_HOM_DFN_R85_EXT01	Yes	2	Hom	R85		R01
20	CD_Si3_HOM_DFN_R85_EXT01	Yes	3	Hom	R85		R01
21	CD_Si4_HOM_DFN_R85_EXT01	Yes	4	Hom	R85		R01
22	nc_Si1_R07_DFN_R85_EXT11	No	1	R07	R85	Ext.	R01
23	nc_Si1_R07_DFN_R85_EXT12	No	1	R07	R85	Ext.	R02
24	nc_Si1_R01_DFN_R85_EXT11	No	1	R01	R85	Ext.	R01
25	nc_Si1_R01_DFN_R85_EXT12	No	1	R01	R85	Ext.	R02
26	BASE_CASE1_DFN_R85_EXT00	Yes	1	Hom	R85		K_{HRD}
27	BASE_CASE1_DFN_R85_EXT10	Yes	1	Hom	R85	Ext.	K_{HRD}
28	nc_Si1_HOM_HRD_C02_EXT00	No	1	Hom	C02		K_{HRD}
29	nc_Si1_HOM_HRD_C02_EXT10	No	1	Hom	C02	Ext.	K_{HRD}
30	BASE_CASE1_DFN_R85_EXT01	Yes	1	Hom	R85		R01[3)]

* Bedrock cases 1, 11, and 15 are referred to as the representative cases (i.e. base case and its bounding cases). The parameterisations are identical to those used in (Öhman et al. 2014). The output of these three cases will be delivered to the Comsol near-field simulations, and are therefore executed separately. Neither of these three cases involve variants of Singö, and hence their second sub string (char4:6) refers to the usage of depth trend (DEP = yes, NoD = No). Moreover, only one integer defines the remote-bedrock parameterisation: 1 for DFN realisation R01.

[1)] Two variants are compared for the extension of 6 deformation zones north from SFR Regional model domain.

[2)] Three parameterisation variants are compared for the HRD outside the SFR Regional domain:

- R01 refers to the static DFN used in Öhman et al. (2014), which comes from the SR-Site heterogeneity case. It is based on [SRS-FFM01-06_v4_alterFinal_nocpm_r1_sets1-65_all_96.asc], but expanded to cover the entire flow domain. Used file: [R_UPDATED_SERCO_DFN_WITH_HOLE].
- R02 refers to an anomalous realisation with unexpected impact on particle flow paths, identified in earlier SR-PSU modelling (Öhman and Odén 2017b). It is combined from two files [R_UPDATED_SERCO_DFN_HOLE_TEMPLATE] and [R_Connected_DFN_OUTSIDE_SFR_R02_knwn]. Explained in Section 2.5 of Öhman and Odén (2017b).
- KHRD refers to a constant parameterisation (not based on ECPM upscaling of fracture network).

[3)] Identical to case 1, except that the grid is meshed to allow introducing Singö-barrier variants.

2.3 Modelling sequence and traceability in data management

As explained above, the task is to analyse the differences between 30 bedrock cases, for nine stages of shoreline retreat (i.e. a total of 270 model setups). Even a single model setup, i.e. a given bedrock case/time-slice combination, is complex, involving multiple input files that must be processed in several steps (see flow chart in Figure A-1; Appendix A1). Therefore, at least three reasons are identified for applying automatized data-file management in the modelling sequence:

- minimisation of data-handling related errors: automatizing ensures that: 1) all model setups are handled consistently (i.e. all model setups are treated the same way), and 2) application of input files is consistent with the specified bedrock case/time-slice case (i.e. follows specifications in Table 2-1 and Table 2-2).
- traceability: automatizing provides traceable data management via the source codes, and also maintains a strict traceability between sequences by means of case-specific filenames for intermediate input and output (i.e. all I/O filenames are tagged by relevant specification to bedrock case and/or time-slice combination). Under no circumstances can output can be propagated unless all required input data are available.
- time efficiency: automatizing allows: 1) parallel processing in different working directories and 2) continuous processing over weeks, day and night.

Consequently, the data file management in execution is automatized as far as possible (all details provided in Appendix A). The modelling sequence is divided into four main routines, which are handled by separate file-managing that preserve full traceability between input and output (see flow chart in Figure A-1; Appendix A1). These four routines are:

a. **Data and grid preparation:** managed by a range of customized tools (Appendix A2).

b. **ECPM upscaling:** explained in Section 5.2 (details in Appendix A3).

c. **Final model setup and flow simulation** Section 5.3 (details in Appendix A3).

d. **Post processing** Section 5.4.1 and Section 5.4.2 (details in Appendix A4).

Quality Assurance (QA)

The automatized modelling chain used in this study employs several algorithms, file conversions, and management of input data that require verification on consistency (Quality Assessment; QA). However, most of the approach, including most of the input-data management, has been gradually developed during preceding modelling tasks for SR-PSU and therefore, most of the QA procedures have already been presented in earlier TDs (see references to earlier modelling tasks in Section 1.1).

Two main methods are used to verify the modelling sequence (input generation, execution, post-processing, and analysis of results):

1. **Visual 3D inspection** (manual analysis in TecPlot): all modelling steps generate graphical output in TecPlot format (all "*.plt" files tabulated in Appendix A). Several examples of such graphical confirmation are provided throughout this report (e.g. Figure 3-2, below). However, it is not meaningful to present all the 270 model setups of the sensitivity analysis in the report, nor to inspect them all in TecPlot. Instead the following principle is employed:
   a. The modelling sequence contains several functionalities that need verification (e.g. algorithms/data-managing steps, etc.).
   b. As these functionalities (e.g. retreating sea, or HSD parameterisation) are implemented into code, they are confirmed by means of a detailed visual inspection of a sample-group of model setups. These model setups may be arbitrarily selected, or specifically selected to demonstrate given phenomena.

   If the functionality can be confirmed to work properly in the samples studied, it is expected to work likewise in all setups in the automatized approach. As explained above, most of the QA has been established during preceding modelling tasks for SR-PSU (references in Section 1.1), and therefore the QA here focuses on the novelties in this report (e.g. Layout L2.6, six HCDs extending north from the SFR model domain, alternative Singö parameterisation, early time slices; Appendix D).

2. **Screening diagnostics** (automatized statistical calculations): the visual inspection (above) is time consuming, and therefore limited to focus on details (e.g. the sub-domain closest to SFR) and a few test cases (i.e. sample of the full model ensemble). To provide a more exhaustive error search, the simulation procedure is diagnosed in terms of a few monitored parameters (or statistics), which are indicative of modelling performance. The output is being stored in log files, which retrospectively can be screened and compared against earlier modelling tasks. Examples include ECPM parameterisation, mass balance in tunnel flow (Section 6.2.1) and convergence in flow solution (Appendix A5). It should be noted that this type of screening is limited to identifying unrealistic numerical errors (i.e. outliers and anomalies, which are clearly "out of bounds"); it does not capture errors which are incorrect, but within realistic bounds. On the other hand, both DarcyTools and the automatizing sequence are defensively coded, such that even small input mistakes will terminate simulation (i.e. reduce the risk of undetected errors "within reasonable bounds").

One way to circumvent the long execution times in QA (and in code development), is to first test the simulation sequence for a very small grid (e.g. 1 000 cells). The benefit of doing so is identifying and correcting errors beforehand, thus avoid having to re-run the real model setups.

The QA in this report focuses on conditions/aspects that are new or have been revised as compared to earlier SR-PSU modelling. These include:

- Layout L2.6 (Figure 3-2; Appendix B).
- HCD extension north from SFR (Section 4.4.1).
- Alternative Singö parameterisation (e.g. Figure 4-9).
- Early time slices (Appendix D).

3 Geometric data

3.1 Model domains

3.1.1 Flow domain

The flow domain defines the spatial extent covered in flow simulations. It extends vertically from +100 m to −1 100 m elevation. The configuration and size of this domain is set up in context of hydrological conditions with the goal to minimise the effects of boundary conditions in simulation (i.e. also accounting for future stages of shoreline retreat). The domain has undergone minor revisions during SR-PSU (Öhman et al. 2014).

The outer perimeter of the domain reflects the vertical sides of the three-dimensional computational grid in DarcyTools (red line in Figure 3-1). These vertical sides are associated to no-flow boundary conditions in flow simulations, and therefore the perimeter is defined based on topographical water divides of sub-catchments (current as well as future catchments). The north-eastern boundary follows a seafloor trench (the so-called Gräsörännan), as its symmetric converging flow can represent a no-flow boundary.

Sub-catchments that are currently below sea are included with respect to:

1. general expectations of the regional hydraulic gradient and shore line retreat,
2. modelled future topographical divides (Brydsten and Strömgren 2013),
3. the north-eastern seafloor trench (Gräsörännan).

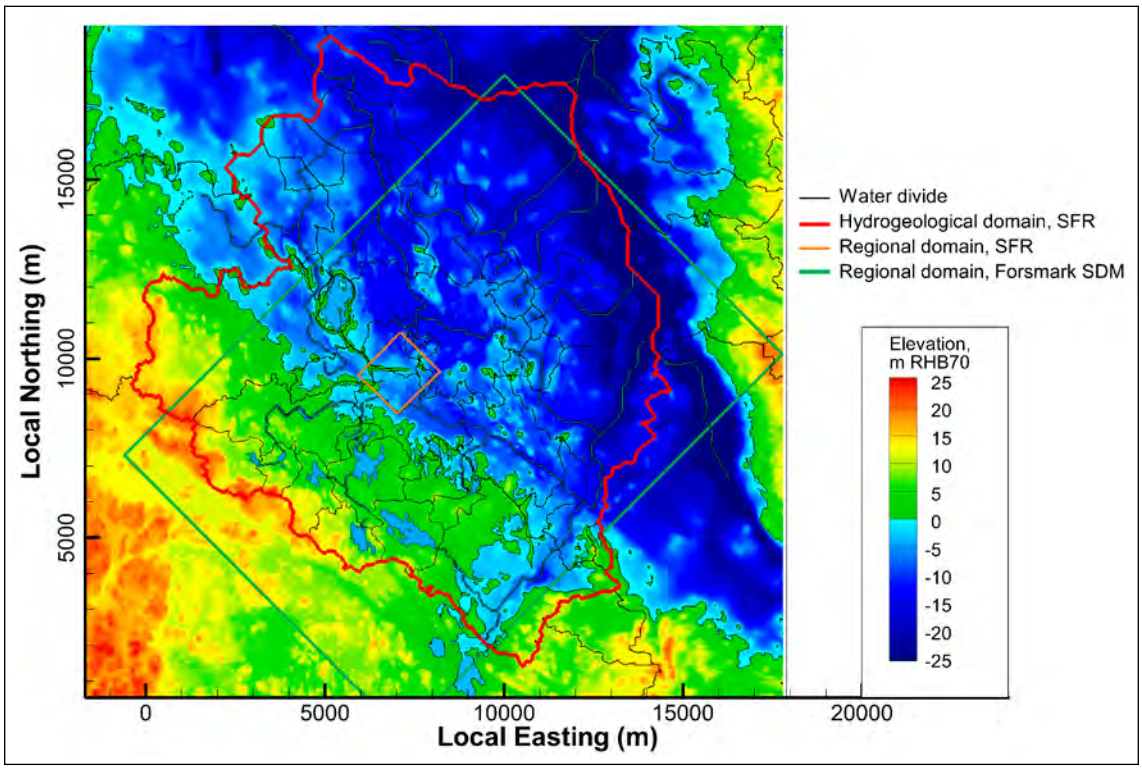

Figure 3-1. *The flow domain (red line) is the outer boundary in the model. The SFR Regional domain (orange line) is the boundary for bedrock parameterisation variants.*

3.1.2 SFR Regional domain

Two conceptual model scales for site-descriptive modelling were defined in the geoscientific execution programme for PSU: a local scale and a regional scale (SKB 2008). The local-scale model volume covers the near-field of SFR 1 and SFR 3, but has no practical role in this study. The regional-scale volume is referred to as the SFR Regional domain and defines a key boundary for the merging two types of bedrock parameterisation.

Neither of the two domains are supported by geological or hydrogeological inference. Instead, they are fictive modelling concepts with the purpose to draw a geometrical boundary between the applicability ranges of two Site-Descriptive Models:

1. The bedrock *inside* the SFR Regional domain is described in the SR-PSU/SDM-PSU project (SKB 2013).
2. The rock mass *outside* this domain is described in the SDM-Site/SR-Site Forsmark.

The repository performance is understood to be primarily controlled by the bedrock properties in the SFR nearfield. Therefore, the combined assessment of model uncertainty and hydraulic heterogeneity in this study primarily addresses the bedrock inside the SFR Regional domain (i.e. described by the SDM-PSU model), while keeping the bedrock properties outside this domain fixed. As the exception to this, a few cases of an alternative DFN realisation and lineament extension outside the SFR Regional domain are also included as bedrock parameterisation variants.

In summary, the SFR Regional domain is a practical concept for controlling and describing bedrock parameterisation variants which are combinations of two Site-Descriptive Models. The SFR Regional domain also controls grid generation and defines the boundaries for DFN generation. A discussion concerning the application of the DFN-model for model volumes is given in Appendix D of Öhman et al. (2014). The SFR Regional domain extends from +100 m to −1 100 m elevation and has horizontal extent of c. 1.5 km × 1.5 km (coordinates provided in Table 3-1).

Table 3-1. Coordinates defining SFR Regional domain.

Easting (m, RT90)	Northing (m, RT90)
1631920.0000	6701550.0000
1633111.7827	6702741.1671
1634207.5150	6701644.8685
1633015.7324	6700453.7014

3.2 Tunnel geometry

Tunnel geometry consists of laser-scanned tunnel walls of SFR1 as well as the latest layout of the planned SFR3 extension (layout L2.6; Odén and Öhman 2017; Figure 3-2). The design of SFR3 has matured in successive layout versions during the PSU project to accommodate construction-related requisites in context of hydrogeological conditions. As the result, earlier modelling tasks in SR-PSU has employed different prototype versions of the SFR3 design. The tunnel geometry of the present study has been revised in the following two main aspects, as compared to the preceding sensitivity analysis for SR-PSU (TD11; Öhman et al. 2014):

1. **updated layout for SFR3 (version L2.6)**: earlier designs of SFR3 were based on an initial plan to dispose intact reactor tanks in the rock cavern 1BRT (Swe: Bergsal för reaktortankar). The transportation of intact reactor tanks necessitated the construction of a third, separate ramp for access to ground surface (earlier referred to as 1RTT). Since then, a decision has been taken to dismount reactor tanks prior to disposal, which allows utilising the existing ramp (1BT) in the transportation of reactor tanks. A new transport tunnel, referred to as 2BT, is planned for the connection between 1BT and RTT (Figure 3-2).

2. **Updated closure plan:** the strategy for backfilling the repository at closure and the design of tunnel plugs has been established by Luterkort et al. (2014). The primary focus of the strategy is to describe the approach to resolving various practical aspects, such as the logistics of backfilling and tunnel plug construction. From the perspective of long-term safety, the backfill/tunnel-plug design described by Luterkort et al. (2014) is rather similar to that assumed in previous SR-PSU flow simulations (e.g. Öhman et al. 2014). However, one noteworthy difference is the installation of mechanical concrete plugs in bentonite-filled tunnels that connect to the Silo (blue and brown colours in Figure 3-2). The mechanical persistence of concrete, under the time span addressed in SR-PSU, is unclear and therefore a pessimistic hydraulic conductivity is assumed ($K = 10^{-6}$ m/s). Thus, the introduction of concrete plugs near the silo may reduce the retention properties of the particles tracked from the silo. On the other hand, it may be argued that this assumption is overly pessimistic.

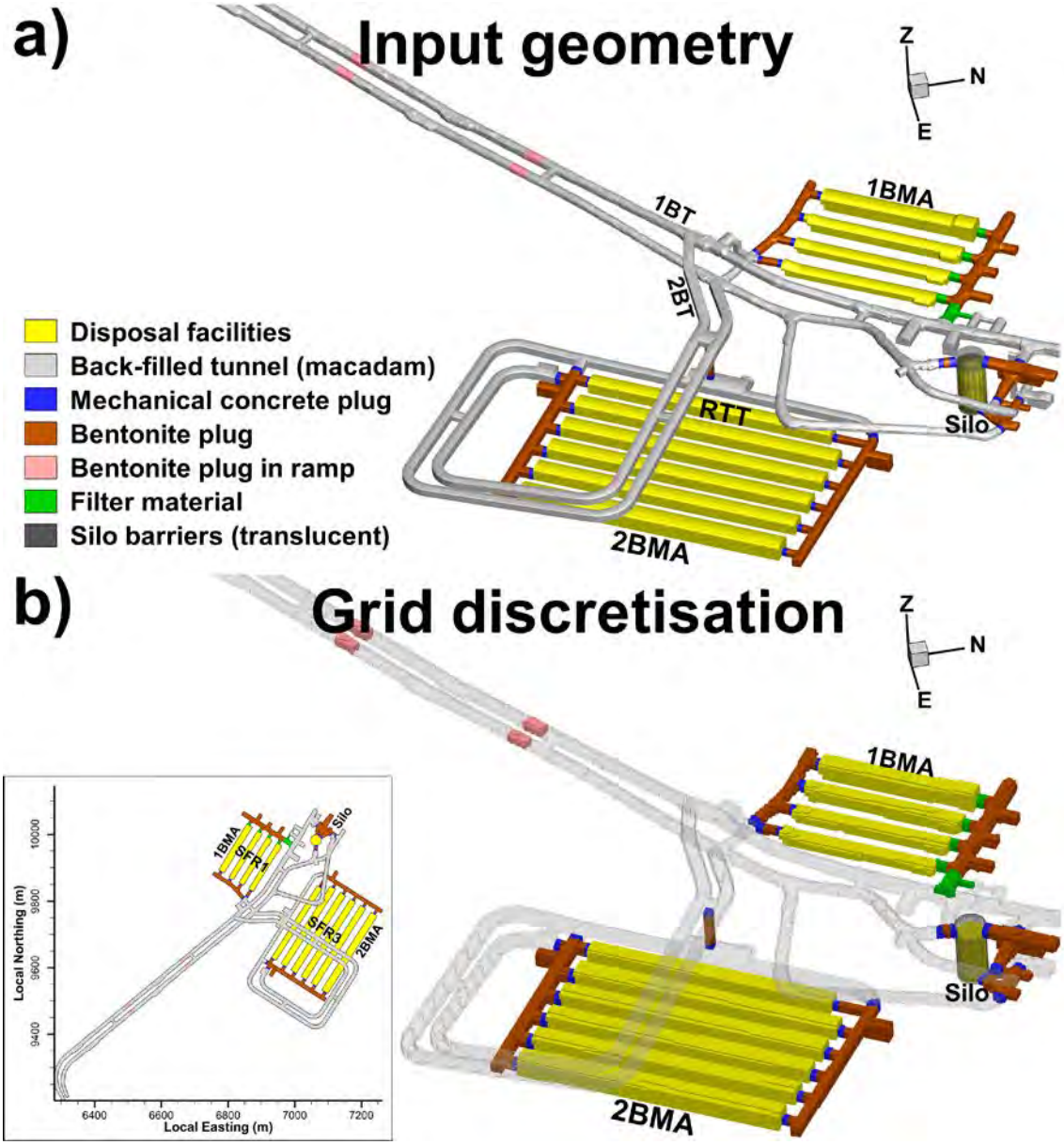

Figure 3-2. *Tunnel geometry in flow simulations; a) input geometry (DarcyTools-object format) and b) discretisation of numerical grid cells. Top-view shows alignment in the horizontal plane (infold). The colour-coding illustrates different functions/materials of the repository elements.*

The hydraulic parameterisation of tunnels varies depending on the functionality in different parts of the repository (e.g. type of backfill/plug material; Figure 3-2). To accommodate defining the different roles in flow simulations, the tunnel geometry has been divided into relevant subunits. Details of the geometric CAD data (Odén and Öhman 2017) are provided in Appendix B. The subdivision of tunnel geometry serves three primary roles in flow simulations:

1. **Grid discretisation:** The model employs local grid refinement to refine the model geometry in areas of particular interest (e.g. the repository tunnel system). The tunnel system affects the repository flow field owing to the hydraulic contrast between its backfill and the excavated host rock mass. This motivates refining the grid cells that represent various parts of the repository, and it has therefore been decided to resolve all tunnel cells by a maximum cell size of 2 m in SR-PSU. Thus, the first application of tunnel-geometry data in the modelling sequence is the identification of grid cells that represent various parts of the repository.
2. **Parameterisation**: The grid cells representing the tunnel system are parameterised according to the backfill or plug material (see Section 4.1.1; Table 4-1). The material properties of backfill/plugs vary between different parts of the repository, which necessitates differentiation between different types of tunnel grid cells.
3. **Calculation of performance measures:** The identification of disposal-room grid cells is key to assessing the performance at the end of simulations. Two types of performance calculations refer directly to disposal-room cells:
   a. **Disposal-room crossflow:** calculated based on flux between cells associated to disposal rooms and adjacent cells located outside.
   b. **Particle-release points:** particle tracking is initiated by releasing particles spatially uniformly over individual disposal rooms. Moreover, the interaction between disposal rooms is evaluated by monitoring particle trajectories that traverse adjacent disposal room.

The identification of different tunnel-cell types is accomplished by means of an inbuilt marking system in DarcyTools, which is practical for later sequences of modelling, as it allows direct access to the marked cell subsets.

3.3 Hydrological conditions at ground surface

3.3.1 Topography (DEM) and regolith layers

The hydrological conditions at ground surface are key to modelling groundwater flow in the shallow bedrock hosting SFR. More specifically, the groundwater table in soil layers (HSD) sets the driving potential that determine hydraulics gradients and groundwater flow in the underlying bedrock. The groundwater table varies locally, depending on net precipitation, local topography, and regolith layering (less strictly referred to as “soil layering”). Thus, the groundwater-flow modelling for SFR relies on a realistic representation of topography and regolith.

Regolith refers to all unconsolidated deposits overlying the bedrock, regardless of origin. It is divided into three types:

1. Quaternary deposits (affected by erosion and sedimentation since the last glaciation),
2. filling material (e.g. the SFR pier is constructed from crushed rock),
3. peat (organic sediment resulting from ingrowth of lakes; Figure 1-2).

Over the time period addressed in SR-PSU, land uplift will transform the setting of the SFR-Forsmark area, from the largely submerged conditions today, characterised by very slow, upward-directed flow, towards an increasingly terrestrial landscape, with horizontal flow predominantly driven by local topography (Sections 1.4 and 2.2.2). During this time, the regolith is affected by landscape-forming processes, starting from marine dynamics (wave erosion, transport and accumulation to the seafloor) and shifting towards lacustrine processes with the gradual emergence above sea

level (i.e. formation and succession of lakes; Brydsten and Strömgren 2013). Two types of regolith models are at hand:

1. the *static* regolith model, developed within SDM Site/SR Site Forsmark, which describes the present conditions, and
2. *dynamic* predictions from the Regolith-Lake Development Model (RLDM; Brydsten and Strömgren 2013), which covers the past and future development of regolith layering.

The RLDM data are the output of a simulation sequence over the latest glaciation cycle (here 8500 BC to 40 000 AD). RLDM focusses on the conceptual dynamics and has not been conditioned to the current state, which results in a discrepancy between the two models at 2000 AD (Figure 3-3a). Thus, for modelling purposes, it can therefore be argued that the static regolith model provides a better representation the regolith layering for the specific time slice 2000 AD. The strength of the dynamic regolith model, on the other hand, is that it allows a coherent description of landscape development, hand in hand with land uplift (Figure 3-3b).

This study addresses the performance of a shallow repository in a transient setting (Section 1.2), which accentuates the necessity of a realistic description of landscape development (i.e. the dynamic regolith model). To ensure consistency in the modelling of the retreating shoreline (i.e. to allow comparing results from 2000 AD versus other time slices without artefacts arising from using data from two conceptually different regolith models) the RLDM data must be consistently used *for all time slices*.

The regolith layers modelled in RLDM data are provided per 500 years (details provided in Appendix A; Table A-1). The regolith layering is interpolated for intermediate time slices, 2100, 2250, and 2750 AD. The computational grid in DarcyTools represents bedrock and therefore a concept of "fixed-bedrock" reference is employed to simplify the modelling of land uplift (Section 3.3.5); the bedrock surface is envisaged as *static* over time, whereas the shoreline retreat is mimicked by a relative displacement of the sea level. This implies that the RLDM data for future stages of land uplift must be re-calculated to the "fixed-bedrock" reference.

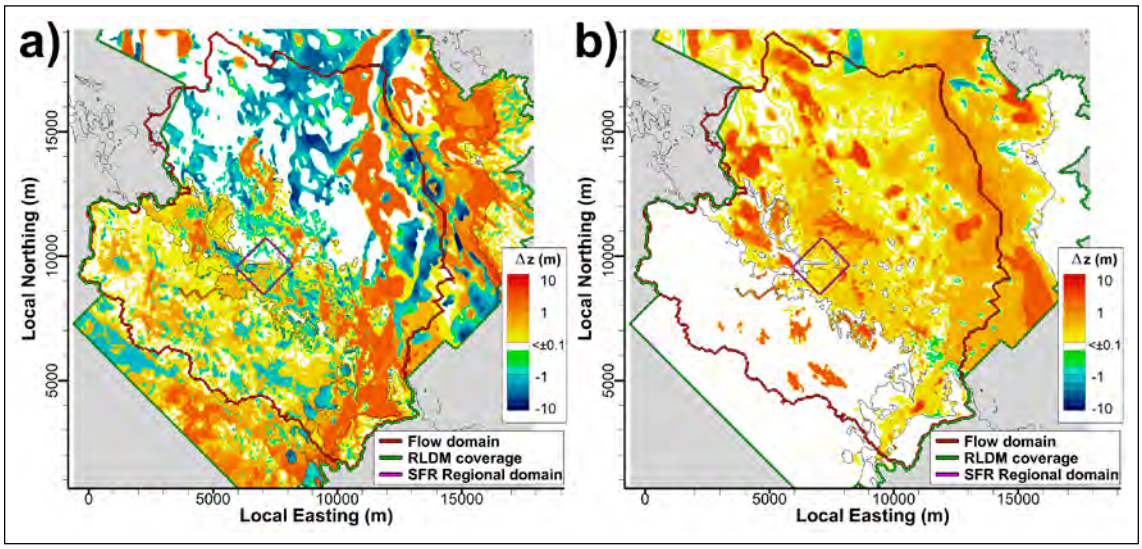

Figure 3-3. *Overview of regolith layers modelled in RLDM; a) topography discrepancy between the static and the dynamic regolith models (2000 AD), and b) modelled change in topography over the time period 2000 AD to 9000 AD. Area outside RLDM coverage shaded in grey.*

The RLDM data have several different roles in modelling. The data are processed differently depending on application (see Section 3.3.2):

1. **Grid generation**: In the flow model, HSD is defined by grid cells between the bedrock surface (constant) and topography (varies over time, as modelled in RLDM). Grid generation requires converting topography data into so-called "DarcyTools objects" (constructed from *.xyz files).
2. **HSD parameterisation**: the different regolith layers are parameterised according to their hydraulic properties (Section 4.5). The RLDM output (ESRI ASCII raster format) are reset according to the fixed-bedrock reference convention, and used directly in the model parameterisation (Section 5.3.1).
3. **Criterion for groundwater table:** the groundwater table in soil serve as the top-boundary condition for groundwater flow (simulated in a so-called "Recharge-phase"; see Section 5.3.2). The groundwater table is constrained by local topography so as not to rise above ground surface, unless it occurs in a local topographical depression. The topography data is therefore "basin-filled" to allow surface water rising to the threshold of local basins.
4. **Prescribe head along rivers:** river cells are prescribed fixed head in flow simulations, according to modelled levels along river trajectories (defined in RLDM). The river levels are modelled based on the levels of lakes, the sea, and the surrounding topography (basin-filled). These river levels are stored in a data file and applied in simulations [SR-PSU_TD18_River_head.in].
5. **Visualisation**: visual confirmation of topography and surface hydrology objects, as well as, production of figures based on *.asc files converted into TecPlot *.plt format.

Model areas outside RLDM coverage (grey-shaded parts of the Flow domain; Figure 3-3) are complemented by topography data from the static regolith model [DEM_xyz_batymetri_20120131.txt].

3.3.2 Processing RLDM data

This section describes the necessary processing of RLDM data to use as input to the DarcyTools modelling. A more detailed description, along with reference to file-management traceability is provided in Appendix A (summarised in Table A-2).

Fixed-bedrock reference

The main objective is to study repository performance in context of model uncertainty and the retreating shoreline. To simplify the numerical simulations in DarcyTools the bedrock surface is employed as a fix reference system for elevation (i.e. at land uplift per 1970, m RHB 70). In this fixed-bedrock reference system, shoreline retreat is modelled by means of a relative sea-level displacement (Näslund 2015); Section 3.3.5).

The regolith data provided from RLDM (Table A-1) are defined in the fixed elevation system RHB70, which implies that the bedrock surface rises gradually with land uplift. To encompass the RLDM data to the DarcyTools setup, the first processing step is therefore to revert the data to the fixed-bedrock reference system, in which the bedrock elevation is constant over time. The regolith elevation is back-calculated by means of land-lift data (Näslund 2015; documentation for traceability in Table A-2).

Constraining groundwater levels by topography (basin-filled)

Surface hydrology has a significant role for simulating the shallow groundwater flow at SFR. The groundwater table is determined by the balance between net precipitation, local infiltration (i.e. recharge to soil and underlying bedrock) and surface runoff. A complication in simulations is that surface runoff is not modelled explicitly in DarcyTools, which implies that areas where the net precipitation exceeds the local infiltration become artificially flooded (i.e. simulated head in the uppermost cell layer rises above ground surface).

This model artefact can be circumvented by constraining the simulated head in the uppermost cell layer (which represents ground surface), such that it does not exceed ground surface. The principles

of modelling the groundwater table in a mixed boundary-condition approach is explained in Sections 5.3.2 and 6.1. As such, the topography, as modelled in RLDM, has a central role in defining the local upper bound for simulated head at ground surface. Note that areas modelled as submerged in RLDM (lakes, rivers, or below sea level) are treated separately (Sections 3.3.3, 3.3.4, and 3.3.5).

The RLDM model addresses the present as well as future lakes in the hydrogeological flow domain (Figure 3-1). However, the extensive model domain contains vast numbers of minor local depressions that are expected to form various types of mires, pools, or even small lakes, but which, for practical reasons, cannot be deterministically modelled in RLDM. Irrespectively, an exception must be introduced to the groundwater criterion: the simulated head within a topographical depression should be allowed to rise to the topographical threshold of the basin (i.e. as opposed to be bounded by the elevation of the actual basin floor). Negligence of doing so implies introduction of unrealistic sink terms that attract particle exit points, and thereby directly affect the simulated performance measures. To accommodate the exception in basins, the topography data is processed to eliminate all local basins and replace them by their basin-threshold levels. This procedure is referred to as "basin-filling", and is performed in two steps: 1) automatized basin-filling (e.g. Figure 3-4), complemented by manual editing in areas of more complex geometry (e.g. Figure 3-5). The procedure as well as the file-management traceability is explained in Appendix A.

Thus, the basin-filled topography is used as the criterion for maximum groundwater level (i.e. the maximum head in a local depression is determined by the *geometric* threshold of the surrounding DEM elevations). Although the basin fill is a substantial improvement for constraining surface head in flow simulations, it does *not guarantee* absence of local depressions, due to inexact matching between RLDM and the DarcyTools grid. The inexact matching is due to:

1. **Discretisation**: The RLDM raster data has a constant resolution of 20 m, while the DarcyTools grid employs local refinement with cell size ranging from 32 m to 8 m. Mapping topography onto small grid cells require interpolation between raster points, while mapping onto larger cells imply averaging raster points.
2. **Coordinate systems:** The DarcyTools grid employs a rotated coordinate system, which implies that it is not aligned with the RLDM data. For example, four corners of a DarcyTools cell may map onto four different topography data, which raises a question on how raster points should be weighed where the ground surface is sloping.

Landscape dynamics in grid discretisation

In the standard DarcyTools procedures, the model top boundary is defined by the uppermost cell layer in the computational grid. Thus, in grid discretisation any grid cells located above the ground surface or seafloor are typically removed (as defined by topography data). However, this study addresses a time period during which the topography is affected by landscape dynamics (Figure 3-3b), which necessitates the use of several, time-specific computational grids. A complication here is that the ECPM upscaling, used to transfer fracture-network properties onto grid parameterisation, is valid only for the underlying grid used in upscaling. Thus, an approach is used which allows representing different changing topography, while still preserving compatibility with fracture upscaling.

The approach is referred to as *cell inactivation*, where:

1. The cells located above the maximum topography (within the time period 2000 to 9000 AD) are *permanently* deleted.
2. The cells located above topography in a particular time slice are *inactivated*, thereby forming a time-specific grid (i.e. these cells remain in the grid, but are isolated from taking part in the flow simulation).

The benefit of this method is that the discretisation of all time-specific grids is identical, which allows re-using the same upscaled ECPM properties for all time slices. The top boundary is defined as the uppermost layer of active cells in the grid (i.e. immediately below a permanently deleted cell or a temporarily inactivated cell). The regolith is defined as all cells in the computational cells that are located above the bedrock surface.

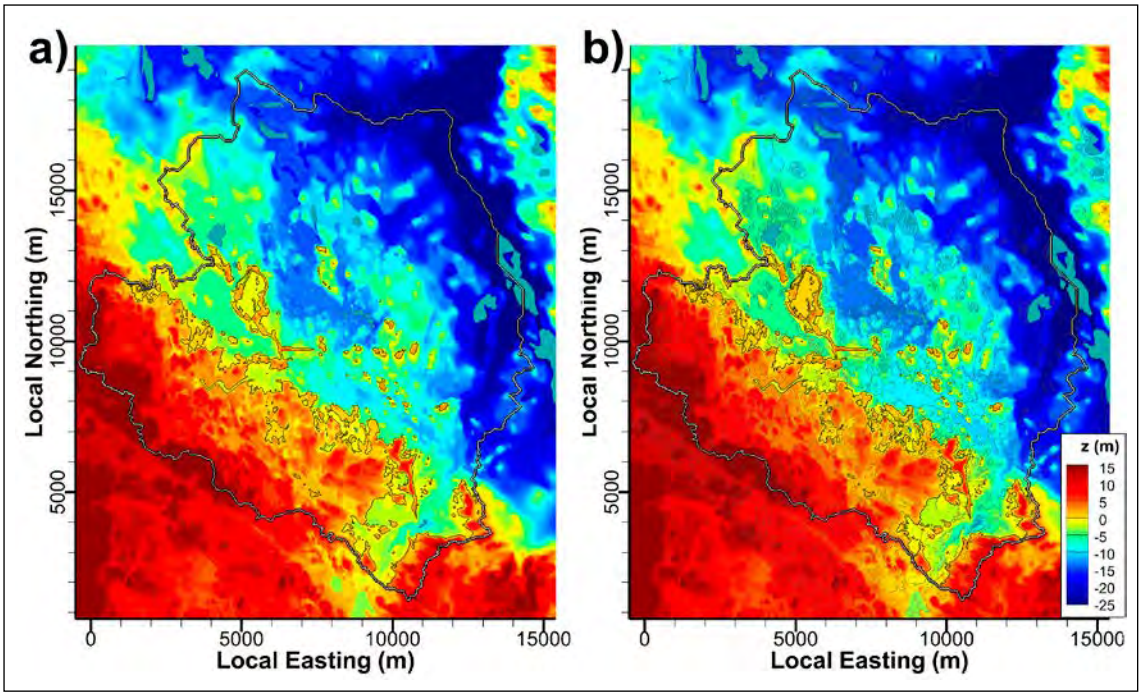

Figure 3-4. *Example of automatized basin filling above sea level; a) original DEM 9000 AD and b) filled DEM, where all topographical basins above sea level 9000 AD have been filled up to the basin threshold. Lakes shown as blue areas.*

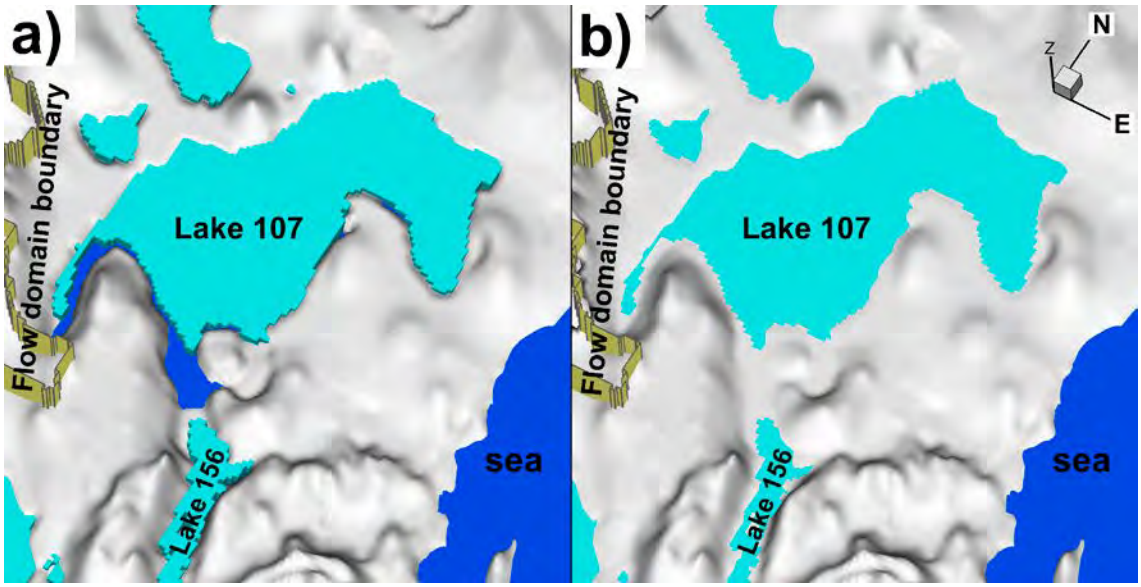

Figure 3-5. *Example of manually filled topographical basins that are partly below sea level (dark blue surface); a) identified depressions near Lake 107, and b) final filled topography.*

3.3.3 Lakes

As described earlier, the groundwater flow in the shallow bedrock at SFR is predominantly controlled by the hydrological conditions at ground surface. In this system, the role of lakes grows continuously, as the hydrogeological conditions eventually mature into a terrestrial setting. Here, the lakes serve as local discharge areas for groundwater flow, which makes them potential exit locations in particle tracking. Thus, the simulation results therefore rely on establishing a realistic description of the lakes in the area, i.e. areal extent as well as water level.

The best description of the hydrological system (lakes, rivers, and regolith layering) is provided by the static regolith model, but as discussed in Section 3.3.1, it is of limited value for describing the dynamic system during future stages of shoreline retreat. Therefore, the modelled lake succession in the area is taken from the RLDM model (areal extent and modelled water level; see Table A-3).

The geometry of lakes (i.e. which varies over time) is defined by means of so-called “DarcyTools objects” (e.g. Figure 3-5). These geometrical objects are used to identify the grid cells that represent lakes in flow simulations. The defined lake cells are identified via a unique DarcyTools cell marker and prescribed fixed head-boundary conditions in the flow simulations, according to the modelled lake thresholds in RLDM (Table A-3). The number of lakes, as well as the spatial extent of individual lakes, varies over time. The time slices studied involve a total of 107 time-specific lake objects (including geometric variants over time). Lake data are also used as fix points in defining water levels along riverbeds (Section 3.3.4). The details of the data management and file conversions is described in Appendix A.

3.3.4 Rivers

Rivers also serve as discharge areas for groundwater flow and their role as potential particle exit locations grows gradually with shoreline retreat. As with the representation of lakes, the RLDM model is judged to provide the best coherent description of future rivers as the seafloor above SFR emerges above sea (Figure 3-1). Analogous to the modelling approach for lakes (Section 3.3.3), the RLDM rivers are mapped onto the DarcyTools grid (by means of so-called “DarcyTools objects”; Table A-4) and prescribed fixed head-boundary condition.

However, unlike the lakes, the river water level varies along its trajectory, which requires a somewhat different modelling procedure (i.e. the specification of head is less straightforward). Prior to simulations, the river head is interpolated along the RLDM trajectories based on the following three conditions: 1) lake thresholds, 2) ground-surface elevation, and 3) the gradient must always slope downstream (details in Appendix A). In the flow simulations, any cell associated to a river can then be prescribed a head value that is consistent with topography data (Table A-4).

3.3.5 Relative sea level displacement in fixed-bedrock reference

The objective of is to study is to analyse the effects of shoreline retreat which arises from the ongoing land uplift. For practical reasons, the DarcyTools simulations employ the bedrock surface as a fix reference for elevation (i.e. land uplift per 1970 AD, expressed in m, RHB 70). In this fixed-bedrock reference system, shoreline retreat is modelled by means of relative sea level displacement (Table 3-2). The relative shore levels are taken from the Global warming climate case (Näslund 2015). The sea level is interpolated for the three time slices introduced in this study, 2100 AD, 2250 AD, and 2750 AD.

Table 3-2. Relative sea level at selected time slices.

Year (AD)	2000	2100	2250	2500	2750	3000	3500	5000	7000	9000
Sea level[1)] (m)	−0.17	−0.75[2)]	−1.63[2)]	−3.08	−4.50[2)]	−5.92	−8.69	−16.6	−26.16	−34.62

[1)] Land uplift is expressed as a relative sea level displacement to the bedrock surface, since 1970 AD (reproduced from Näslund 2015).

[2)] Intermediate time slices introduced to better resolve the early development of shore-line retreat, as compared to Öhman et al. (2014). Interpolated sea level (Appendix D).

4 Model parameterisation

4.1 Tunnel parameterisation

Tunnels are parameterised according to the hydraulic properties of the backfill/plug material that is planned for the various parts of the repository system (Luterkort et al. 2014). The identification of specific backfill/plug material for different tunnel sections (Figure 3-2) is accomplished by means of cell makers in the DarcyTools grid (referred to as Mk in Table 4-1). All general tunnel sections, ramps, and disposal rooms (except the Silo) will be backfilled with macadam. Although the hydraulic conductivity for macadam backfill (i.e. crushed rock) is expected to be on the order $K \approx 10^{-2}$ m/s, it is parameterised as $K = 10^{-5}$ m/s to reduce complications of numerical instability (Figure 4-1). The parameterisation of tunnel plugs and Silo barriers refers to the *intact* plug case (SKB 2014b; Table 4-1). Special attention is given to the Silo, to encompass a realistic representation of the details in its parameterisation and its particle-release locations (Figure 4-3).

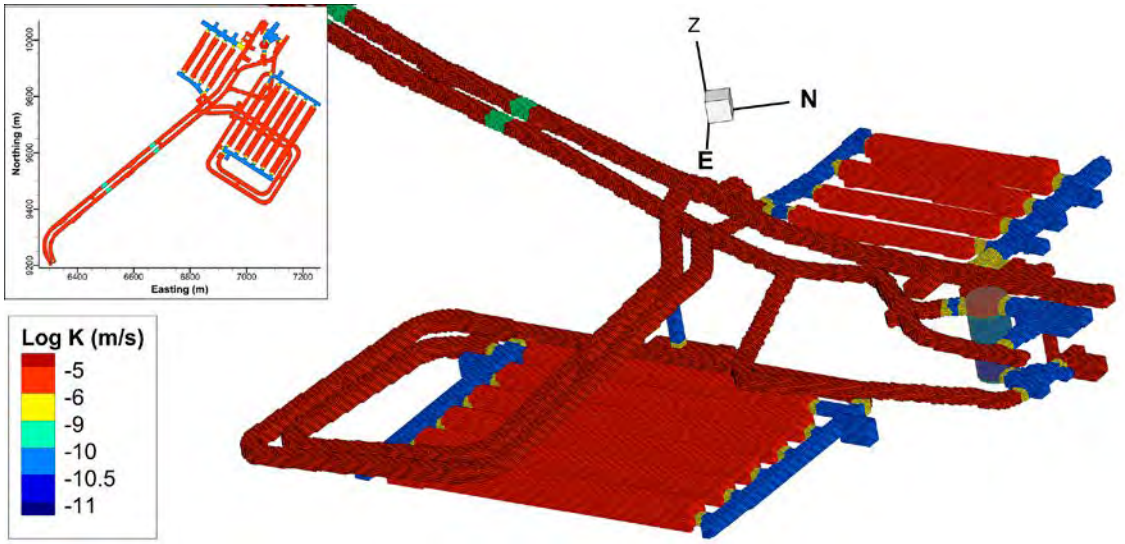

Figure 4-1. *Hydraulic-conductivity parameterisation of the backfilled and plugged repository system (categorisation of tunnel backfill/plug material demonstrated in Figure 3-2).*

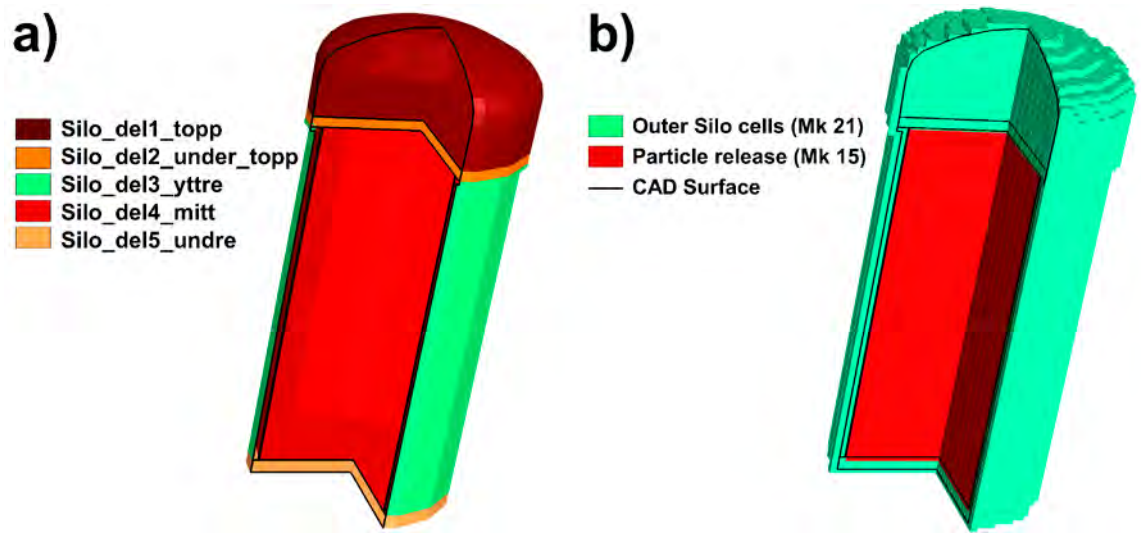

Figure 4-2. *Cell marking of the discretised Silo; a) Silo sub-volumes defined by CAD data (Table B-1), differentiated by colour, and b) defined particle-release location (CAD definitions in black lines).*

In the evaluation of results, particle tracking reflects only retention of the bedrock outside tunnels (Section 5.4.2), and hence the hydraulic properties of tunnel backfill do not, *per se*, affect the particle tracking results (i.e. the backfill has only indirect effects, via its influence on the flow field).

Table 4-1. Tunnel backfill parameterisation (Figure 4-1 and Figure 4-3).

	Mk	Tunnel	Conductivity (m/s)	Description in Swedish (SKB 2014b)
SFR 1	11 12 13 14	1BTF 2BTF 1BLA 1BMA	10^{-5}	Rock vaults, assumed to be backfilled by macadam[1)] (Non-filled, open section of 1BLA not resolved).
	15/21[2)]	Silo interior	5×10^{-9}	Outer concrete cylinder, inner vertical shafts with intervening concrete walls, waste packages and concrete grouting.
	16	1DT, 1BT	10^{-5}	Ramp backfilled with macadam.[1)]
	21[3)]	Silo exterior	10^{-5} 10^{-9} Single-layer walls: $K(z) = 2.1 \times 10^{-10} + 1.6 \times 10^{-12} * \mathbf{z}$	Compacted fill of friction material, e.g. crushed rock or macadam and, at the very top, with cement-stabilized sand. Compacted fill of bentonite/sand mixture (10/90 percentage by weight) at the bottom and top of the silo. Pure bentonite in silo walls, with hydraulic conductivity expressed as function of elevation, z (m RHB70), due to variable degree of self-compaction. In the lower part $K(z) \approx 9 \times 10^{-12}$ m/s and the upper part $K(z) \approx 9 \times 10^{-11}$ m/s (SKB 2014b).
SFR 3	22 23 24 25 26 27	2BLA 3BLA 4BLA 5BLA 2BMA 1BRT	10^{-5}	Rock vaults, assumed to be backfilled by macadam[1)] (Non-filled, open section of BLA caverns not resolved).
	28	1RTT	10^{-5}	Ramp backfilled with macadam[1)]
Intact plugs	30[4)]	Blue	10^{-6}	Mechanical concrete plug (i.e. for mechanical support).
	31	Brown	10^{-10}	Hydraulic tight section with bentonite.
	32[4)]	Green	10^{-6}	Earth-dam plug, consisting of transition material (e.g. 30/70 bentonite crushed rock).
	33	Pink	5×10^{-10}	Plugs in access tunnels, made up of 10 metre long tight hydraulic sections of bentonite surrounded by concrete plugs for mechanical support.

[1)] In reality, the hydraulic conductivity of macadam is initially higher than 10^{-2} m/s. A project decision was taken to assume the lower value 10^{-5} m/s to improve numerical stability in simulations.

[2)] The silo is represented by two DarcyTools cell markers: particles are released from the inner concrete cylinder (Mk = 15), which is enclosed by barriers from which no particles are released (Mk = 21). The value is based on Holmén and Stigsson (2001).

[3)] Conductivity parameterisation of the silo exterior not based on cell marking, but differentiated by geometric bounds based on a combined interpretation of CAD data and SKB 2014b (see Figure 4-3).

[4)] Assumed conductivity value based on a project decision.

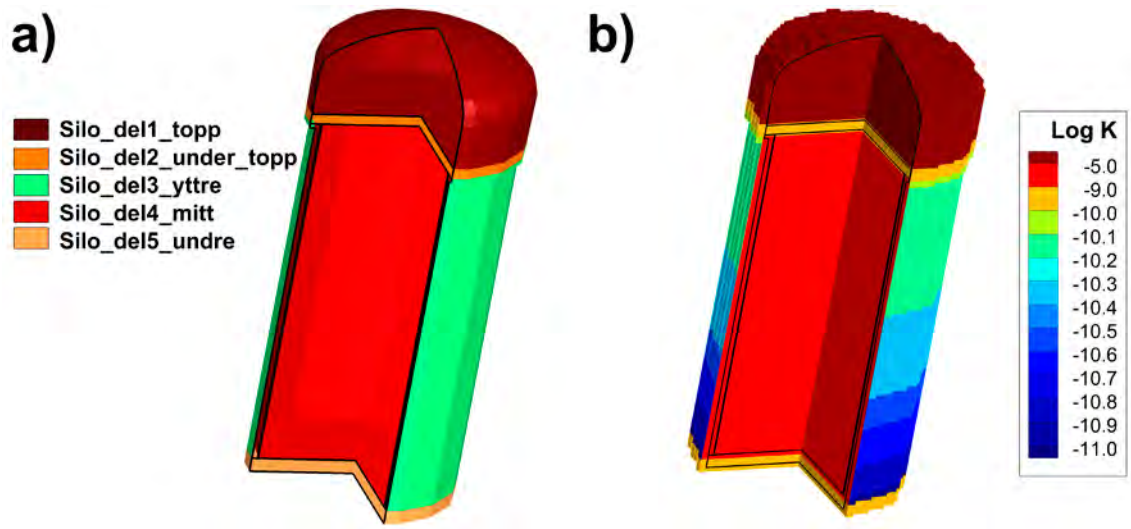

Figure 4-3. *Parameterisation of the Silo; a) Silo sub-volumes defined by CAD data (Table B-1), differentiated by colours, and b) assigned conductivity (CAD definitions in black lines).*

4.2 Parameterisation of bedrock cases

The performance of the groundwater flow model is subject to *heterogeneity* and *conceptual uncertainty* in the bedrock parameterisation. In the groundwater flow model, the bedrock is conceptually divided into two hydraulic domains: HRD and HCD. Heterogeneity is addressed by means of stochastic realisations, while conceptual uncertainties in HCD-parameterisation are addressed by means of variants. The combined effect of uncertainty/heterogeneity in bedrock parameterisation is studied by means of a sensitivity analysis of 30 bedrock cases (Table 2-2). Here, a "bedrock case" refers to the combined parameterisation of both hydraulic domains (Figure A-1).

Moreover, the parameterisation of a bedrock case is merged from two Site-Descriptive Models (as described in Section 3.1.2):

1. The bedrock *inside* the SFR Regional domain is based on variants/realisations of the SDM-PSU model (Section 4.3).
2. The rock mass *outside* this domain is based on variants/realisations of the SDM-Site/SR-Site Forsmark models (Section 4.4).

Combining input data from two models requires special care to avoid overlapping artefacts at the domain interface, along which the two models are being merged, which is explained in detail in Öhman et al. (2013). The regolith (HSD) parameterisation employs a single model, which covers the entire flow-model domain (Section 4.5).

4.3 Bedrock cases inside SFR Regional domain

The "HRD variants" of the SFR Regional domain are combined stochastic realisations of discrete fracture networks (DFN) and Unresolved PDZs (as defined in Öhman et al. 2013; Section 4.3.1). Additional HRD variants include constant hydraulic-conductivity parameterisation, K_{HRD}. The "HCD variants" refer to the parameterisation of deterministic structures, i.e. structures for which the geometry is kept fixed, but where the conceptual parameterisation uncertainties and within-heterogeneity is addressed by means of variants (Section 4.3.2).

SBA structures

Eight so-called Shallow Bedrock Aquifer (SBA) structures were deterministically modelled inside the SFR Regional domain (Öhman et al. 2012). These structures are envisaged as clusters of connected water-bearing fractures, ranging from gently-dipping to horizontal in orientation. As no SBA structures are in direct contact with disposal rooms in SFR 1 or SFR 3, variants of SBA structures are not addressed in the sensitivity analysis. Similar to earlier TDs, all simulations include a fixed SBA variant, in which all 8 structures are included (SBA1 to SBA8). Used file is: [R_Parameterized_SFR_SBA1_to_SBA8], based on parameterisation in Appendix B and H in Öhman et al. (2012).

4.3.1 HRD parameterisation variants

The HRD represents the rock mass domain outside deterministic deformation zones. It is modelled in terms of stochastic realisations of connected discrete fracture networks (DFN) combined with Unresolved PDZs. The latter are conceptually modelled as connected to deformation zones of the Southern and Northern boundary belts (Öhman et al. 2012). The connectivity of the DFN/Unresolved PDZs is coupled in stochastic realisations (i.e. the connected fracture network of RXX, is coupled to the stochastic realisation RXX of Unresolved PDZs). An explanation regarding cut offs applied to delimit the size range of modelled fractures with respect to model domain is provided in Appendix D of Öhman et al. (2014).

Three stochastic HRD realisations are selected to represent the HRD heterogeneity (Table 4-2; Figure 4-4). As part of TD05 (Öhman and Bockgård 2013), realisations R18 and R85 were identified as “optimistic” and “pessimistic”, respectively, for inflow to disposal rooms of SFR 1. R85 was selected as pessimistic, as it had the largest number of fractures intersecting more than one disposal room in SFR 1. Vice-versa, R18 had no fractures that intersect more than one disposal room. Similarly, an additional realisation, R03, was selected to represent a “pessimistic” case for SFR 3. The statistics of the three selected realisations are compared to a larger ensemble of DFN realisations in Figure 4-5 and Figure 4-6. It can be noted that none of the three realisations cover the most transmissive fracture intersections in the DFN ensemble; however, the modelled DFN intercepts are not very representative of true hydrogeological characteristics of the Silo (i.e. the Silo is located in atypically low-conductive rock; Öhman et al. 2012, pp 43–44).

Table 4-2. HRD parameterisation variants.

Variant	Underlying data file	Description
R03	R_SFR_DFN_connected_R03_L26_knwn R_Unresolved_PDZ_R03_knwn	Pessimistic for SFR 3 (4BLA, 5BLA and 2BMA), but also for 1BMA.
R18	R_SFR_DFN_connected_R18_L26_knwn R_Unresolved_PDZ_R18_knwn	Optimistic realisation for SFR 1, used earlier (no large fractures connecting disposal rooms in SFR 1).
R85	R_SFR_DFN_connected_R85_L26_knwn R_Unresolved_PDZ_R85_knwn	Pessimistic realisation for SFR 1, used earlier (large fractures connecting disposal rooms in SFR 1).
C01…C03	Constant parameterisation, $K_{HRD} = 6.5 \times 10^{-9}$ m/s (± one order of magnitude). No file.	Taken from Holmén and Stigsson (2001).

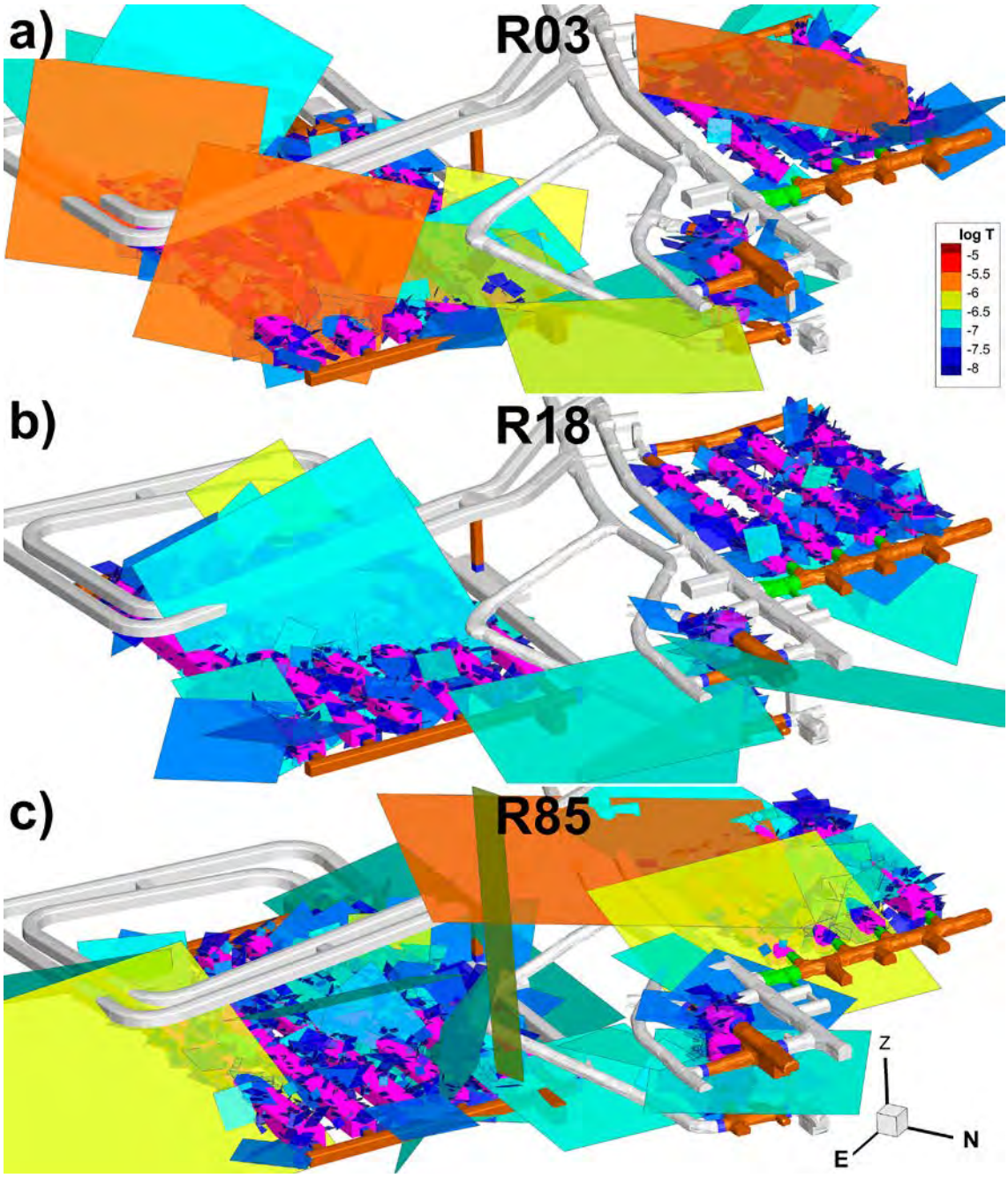

Figure 4-4. *Transmissivity of stochastic fractures intersecting the disposal rooms of SFR 1 and SFR 3; a) realisation R03, b) realisation R18, and c) realisation R85.*

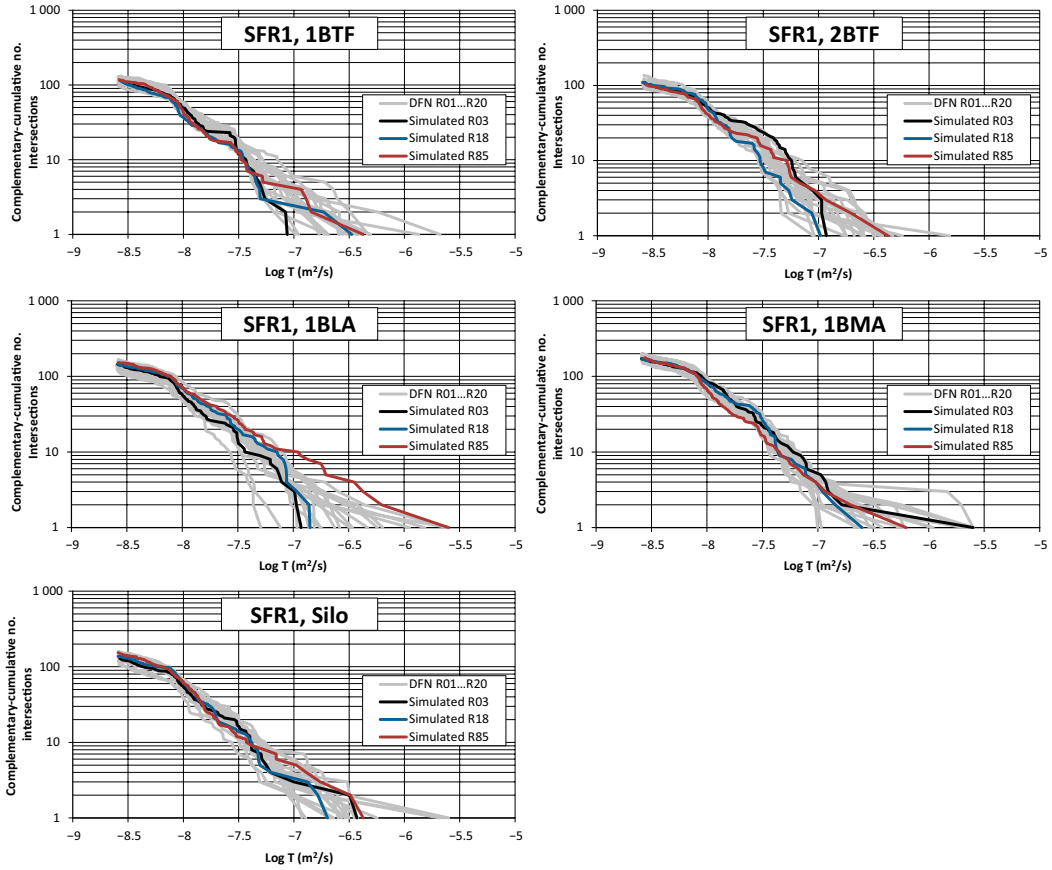

Figure 4-5. *Complementary-cumulative transmissivity distribution of fractures intersecting SFR 1.*

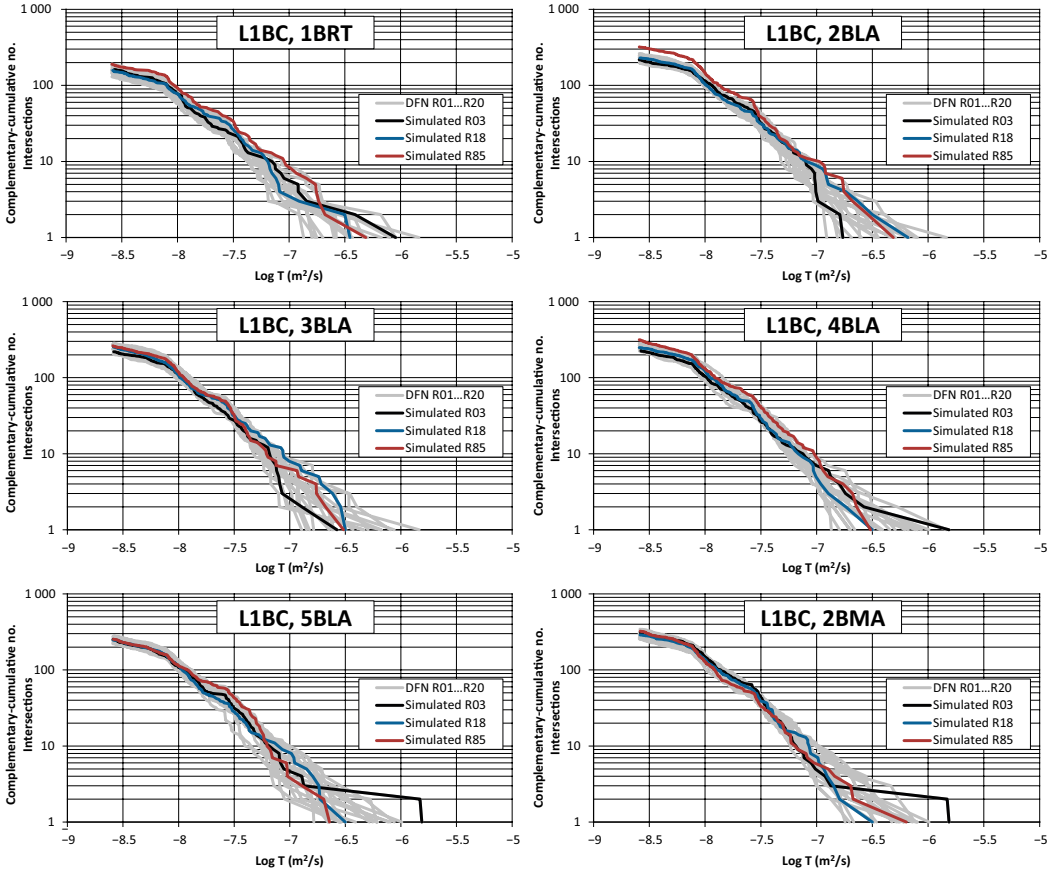

Figure 4-6. *Complementary-cumulative transmissivity distribution for fractures intersecting SFR 3.*

4.3.2 HCD parameterisation concepts

The geometry of the HCDs is taken from the deterministic deformation-zone modelling in SDM-PSU and the parameterisation is based on the conceptual interpretation of borehole data from deformation-zone intercepts (SKB 2013). Thus, the modelling of HCDs are characterised by a general high confidence in geometric description and a comparatively uncertain hydraulic parameterisation. Earlier SR-PSU modelling have therefore focussed on evaluating the sensitivity to parameterisation uncertainty, while keeping the geometry fixed. This study addresses the uncertain extension of six deformation zones north from the SFR Regional domain, in an area identified as the key area for SFR discharge (described in Section 4.4.1).

Of the 40 deformation zones modelled in the SFR Regional model domain, three key structures stand out as the most critical for the SR-PSU assessment. The most critical structure for SFR 1 is: 1) ZFMNNW1209 and the most critical structures for SFR 3 are ZFMWNW0835 and ZFMENE3115.

What makes these structures stand out is their combination of:

1. Direct intersection with disposal rooms, and
2. Uncertain hydraulic parameterisation (which is accentuated by the assumed depth trend).

The SBA structures are not in direct contact to disposal rooms, and hence, they are not varied in model alternatives.

The following aspects are identified as the key uncertainties in transmissivity parameterisation of HCDs (covered by HCD variants in Table 2-2):

1. **Transmissivity variability**: the HCDs are modelled by a base case (homogeneous transmissivity with depth trend, annotated BASE_CASE or HOM in Table 2-2), while the hydraulic heterogeneity is resolved by stochastic realisations R01 and R07 (representing “median” and “pessimistic” tunnel flow, respectively; Öhman 2013a).
2. **Borehole conditioning**: Borehole data (and tunnel grouting) provide local information of deformation-zone intercepts. In particular, the data at hand for conditioning indicate low local transmissivity at key structural intercepts for both SFR 1 (ZFMNNW1209) and the planned extension (ZFMWNW0835 and ZFMENE3115). However, the confidence in borehole conditioning is unclear (i.e. how far the data extrapolation from a borehole intercept is valid). Conditioning is optimistic (due to uncertainty in data extrapolation), while non-conditioned parameterisation is pessimistic (neglects local data).
3. **Depth trend**: Unlike the data support in SDM-Site Forsmark model, the SDM-PSU data set could not support – nor reject – a depth trend in HCD parameterisation (Öhman et al. 2012). It has been found conservative to assume that the HCD depth trend established in SDM-Site Forsmark applies also in the SFR model domain (Öhman et al. 2014). Thus, the sensitivity to depth-trend parameterisation has been sufficiently evaluated and is not included as a component of variability in this sensitivity analysis. Therefore, this study assumes the Forsmark depth trend in HCD parameterisation (i.e. that transmissivity reduces by an order of magnitude over the depth interval k = 232.5 m). As the only exception, bedrock case 15 (Table 2-2) does *not* employ the transmissivity depth trend, as it represents the optimistic case in the repository nearfield simulations (Abarca et al. 2014).
4. **Anisotropy**: SDM-Site Forsmark field investigations provide indications of potentially anisotropic hydraulic properties of the Singö deformation zone (i.e. less transmissive across the structure; e.g. the HFM33 pump test presented in Follin et al. 2007). The Singö deformation zone extends along the current coast line and therefore its transversal hydraulic properties may control the regional-scale flow to SFR (or the Southern boundary belt). This notion has been tested earlier in SR-PSU modelling (e.g. Öhman et al. 2014, Öhman and Odén 2017a).

4.3.3 Selection and implementation of HCD variants

The uncertain aspects described in Section 4.3.2 have been combined to form an ensemble of HCD parameterisation variants in earlier SR-PSU modelling. Of these, six variants (Table 4-3) are selected for the sensitivity analysis in this study (see Table 2-2). The selected HCD variants are prepared

in an input-file format that is accepted by DarcyTools; the details on this processing and name conventions for traceability is presented in Appendix A (Table A-5). Note that the three cases of barrier effects for Singö deformation zone are all derivatives of the base case, and hence not listed in Table 4-3.

Table 4-3. Notation of HCD variants used in Table 2-2.

HCD variant[1)]	Cond.	Depth trend[2)]	Heterogeneity[3)]	Comment
BASE_CASE1	Yes	Yes	None	Used in base case (1). Also in Singö variants.[4)]
nc_DEP_HOM	No	Yes	None	Non-conditioned variant of base case.
nc_NoD_R01	No	No	R01	Only in bedrock case (15): *low* flow.
nc_DEP_R01	No	Yes	R01	Variant of above with depth trend.
nc_DEP_R07	No	Yes	R07	Bedrock case (11): *high* flow.
CD_DEP_R07	Yes	Yes	R07	Conditioned variant of above.

[1)] The filenames deformation-zone input are [Param_SFR_HCD_<HCD variant>] for the 40 deformation zones modelled in SDM-PSU (including minimum extension of the six zones extending north from SFR) and the complementary file [HCD_North_<HCD variant>], which represents the maximum extension of the six zones extending north from SFR (Section 4.4.1).

[2)] Depth trend in HCD transmissivity assumed in the general case, as it is pessimistic in terms of disposal-room flow (parameterised based on Appendix 6 in SKB 2013). As the only exception, nc_NoD_R01 is included to provide the intermediate flow case for nearfield modelling (Abarca et al. 2014).

[3)] Transmissivity variability is modelled as a superimposed random component assumed to follow the log-normal distribution, i.e. Log T + N(0, $\boldsymbol{\sigma}_{HCD}$), where $\boldsymbol{\sigma}_{HCD}$ is taken from SKB (2013, Appendix 6) for the cases with depth trend and without depth trend, respectively. In homogeneous cases, $\boldsymbol{\sigma}_{HCD} = 0$.

[4)] The three Singö cases: CD_Si2_HOM, CD_Si3_HOM, CD_Si4_HOM in Table 2-2 are variants of the input file BASE_CASE1.

The HCD parameterisation concepts are shown for ZFMNNW1209 (Figure 4-7), as earlier SR-PSU simulations has demonstrated its significance for discharge from the four rock caverns of SFR1. The available data for conditioning the deformation-zone parameterisation are boreholes KFR33 and KFR35 and the observed inflow and grouting records from tunnel construction (see Öhman et al. 2013). The base case employs a depth trend in transmissivity and is conditioned by both the borehole and tunnel intercepts (Figure 4-7b); note the elevated transmissivity at the 1BLA intersection (which has been estimated based on the grouting requirements in 1BLA).

Simulations demonstrate that the tunnel-intersection conditioning strongly controls the crossflow through the disposal facilities (i.e. setting fixed hydraulic properties at the tunnel intercept reduces the role of structure's hydraulic heterogeneity outside the intercept). Therefore, to evaluate the effects of heterogeneity most of the heterogeneous cases in this sensitivity analysis are not conditioned (notated "nc" in Table 2-2 and Table 4-3). Heterogeneity is parameterised by superimposing a lognormal-distributed random component. This random component follows $N(0,\sigma_{HCD})$, where σ_{HCD} is the standard deviation of logarithmic transmissivity of an individual HCD, or a group of HCDs (tabulated in SKB 2013, Appendix 6). Extreme values, outside 95 % variability, are rejected and re-sampled. Note that for a given realisation, RXX, the distribution of the random component is identical, regardless of magnitude in σ_{HCD}, conditioning, or imposed depth trend. It can be noted that the parameterisation at the 1BLA and 1BMA intersections stand out with higher transmissivity in both realisations R01 and R07.

Two zones, ZFMWNW0835 and ZFMENE3115, have been identified as particularly significant for the planned extension SFR 3. As described above, the reason for this is their intersection with disposal rooms of SFR3 as well as a large uncertainty in the hydraulic parameterisation (which has been described in Öhman et al. 2014). The uncertainty essentially arises from two deep intercepts (of unrepresentatively long intersection intervals, compared to the true zone thickness), which render anomalously high transmissivity, considering the depth. Since the data exhibit a "reverse depth trend", but are forced into a conceptualisation that assume declining transmissivity at depth (Figure 4-8a and b), and as the result, the structures come out interpreted as highly heterogeneous (i.e. see detailed explanation in Öhman 2013b, Chapter 6).

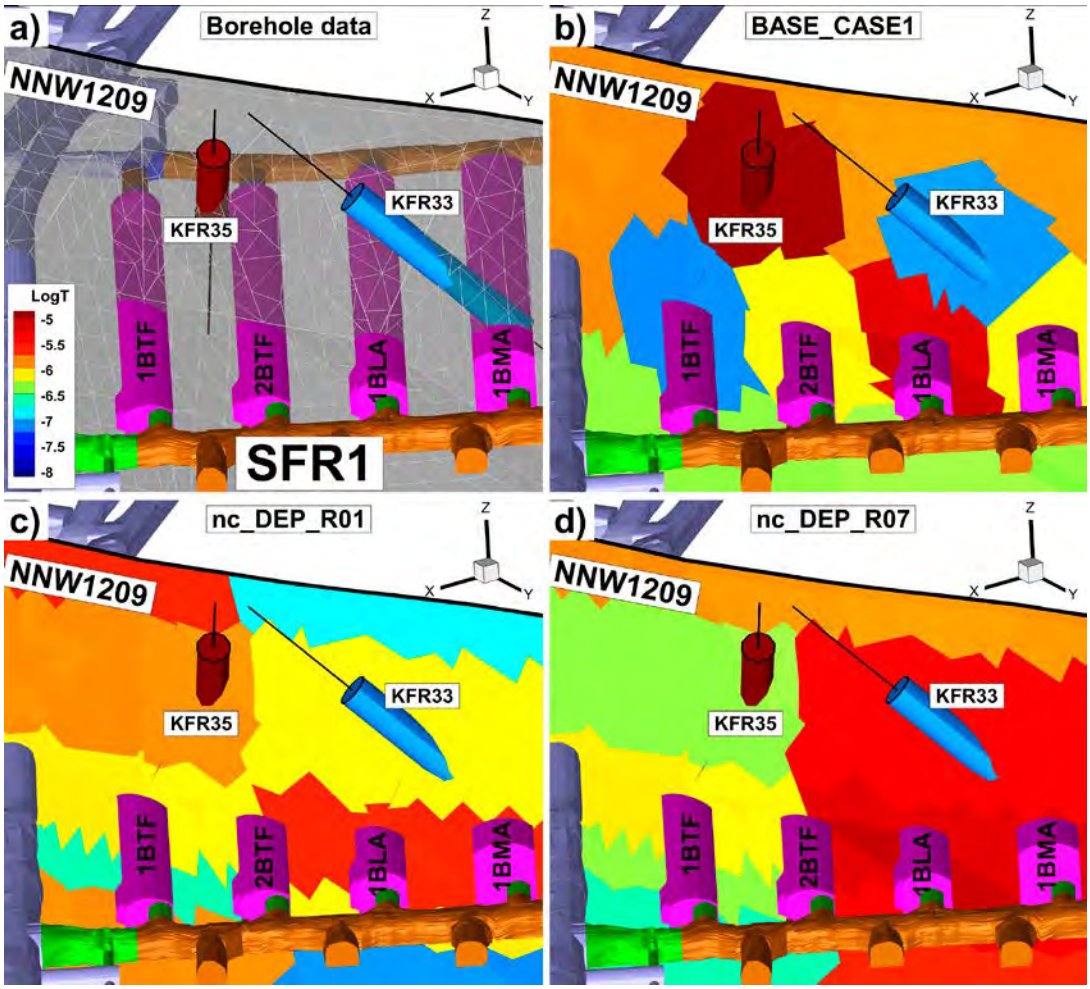

Figure 4-7. *Three parameterisation variants of ZFMNNW1209, which is the key structure for SFR 1 discharge; a) triangulated HCD geometry and borehole-intercept data (cylinders), b) Base case, locally conditioned at borehole and tunnel intercepts, c) non-conditioned heterogeneous realisation R01, and d) non-conditioned realisation R07.*

Thus, the uncertainty relates to how to interpret and weigh the available borehole data, which is manifested by the significant role of local conditioning for simulated disposal-room flow (Figure 4-8c to f). It should be noted that both heterogeneous, non-conditioned, realisations R01 and R07 are associated to high local parameterisation; in fact, the parameterised transmissivity exceeds the underlying borehole data, which is an effect of interpretation in accordance with the depth-trend concept (Figure 4-8).

Alternative parameterisation of the Singö deformation zone

This study addresses the potential barrier effects for transversal flow across the Singö deformation zone, which has also been tested earlier in SR-PSU modelling (e.g. Öhman et al. 2014, Öhman and Odén 2017a). In this approach, a core layer is defined as a third of the deformation zone width, and is then divided into an upper ($z > -245$ m) and lower part ($z \leq -245$ m; Figure 4-9). Three variants of the base case are then defined as (Table 2-2)

- CD_Si2_HOM_DFN_R85_EXT01: The entire core is assumed to be low-conductive (Kupper = Klower = 10^{-9} m/s).
- CD_Si3_HOM_DFN_R85_EXT01: Only the upper part of the core is low-conductive (Kupper = 10^{-9} m/s; Klower = KECPM).
- CD_Si4_HOM_DFN_R85_EXT01: Only the lower part of the core is low-conductive (Kupper = KECPM; Klower = 10^{-9} m/s).

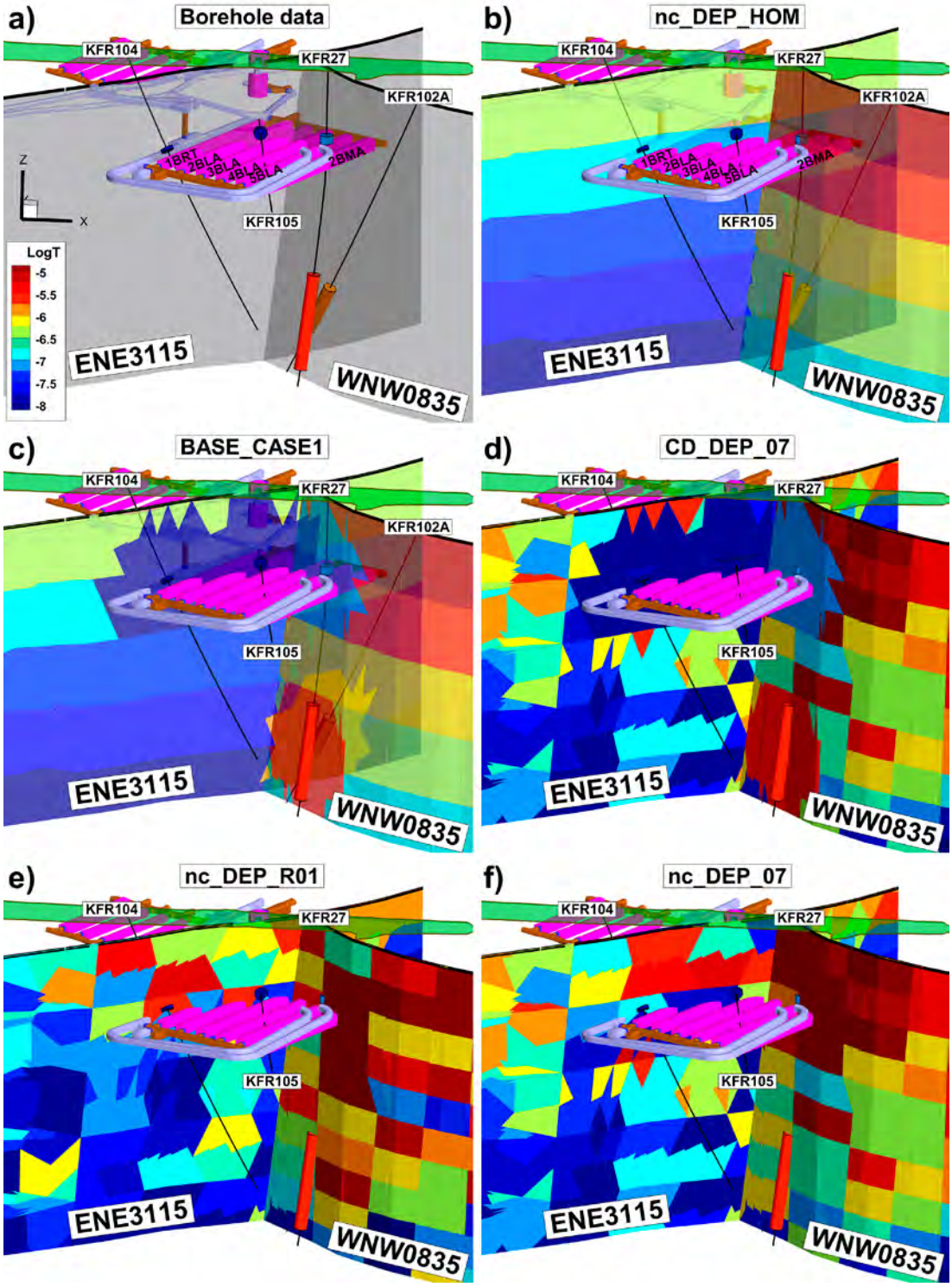

Figure 4-8. *HCD variants of the two key zones for SFR3; a) borehole-intercept data (cylinders), b) homogeneous transmissivity with depth trend, c) borehole-conditioned base case, d) borehole-conditioned realisation R07, e) non-conditioned realisation R01, and f) non-conditioned realisation R07. To enhance visibility, only parts of the SFR3 ramp are shown.*

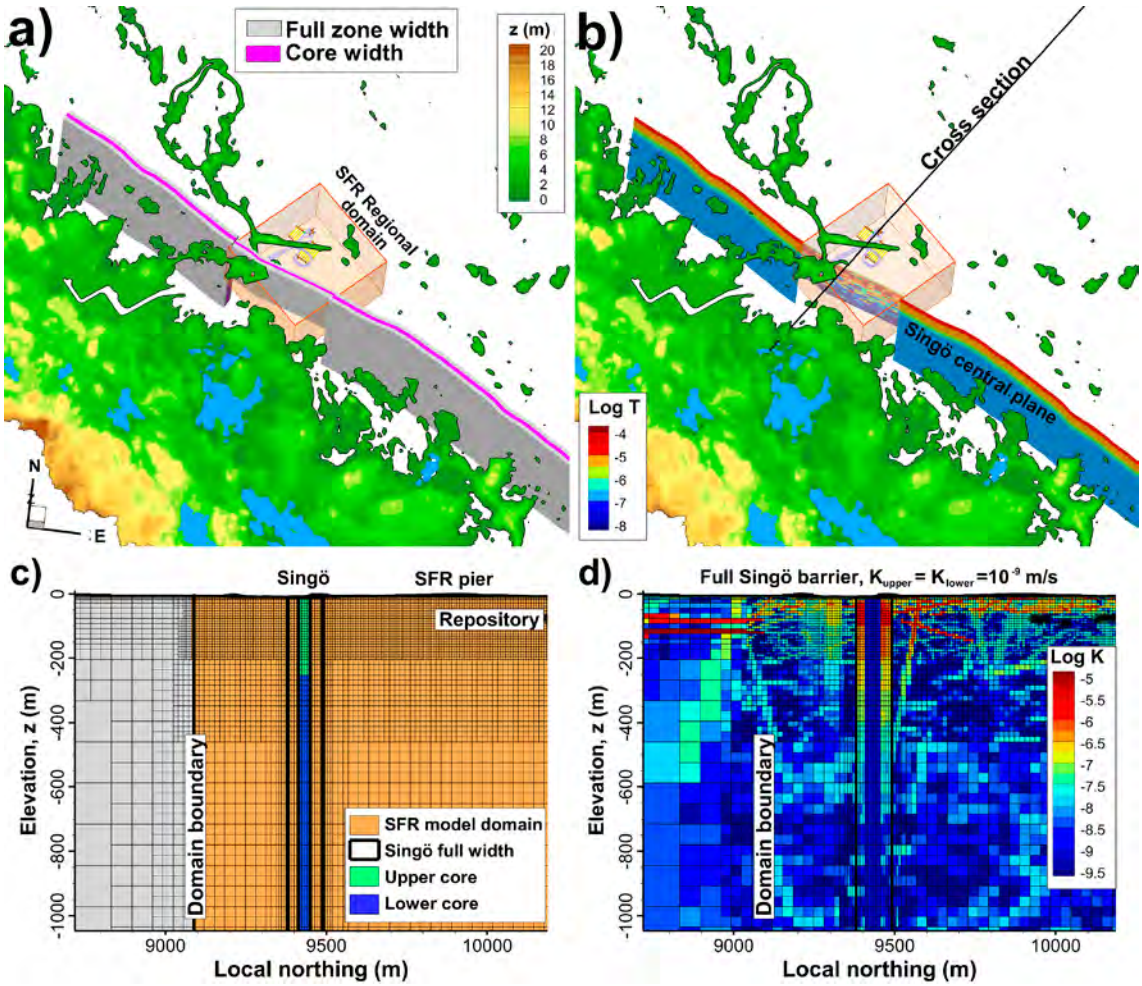

Figure 4-9. *Concept of alternative parameterisation for the Singö deformation zone; a) a core layer is defined as a third of its deformation zone width, b) the core is divided into an upper and lower part, d) the upper and/or lower part are assumed to be low-conductive (variants Si2, Si3, and Si4 in Table 2-2).*

The upper/lower barrier cases are included to evaluate if the full barrier case is pessimistic, or if partial barriers may have larger impacts on repository performance. For example, although the HFM33 pump test (pumping a fracture at c. 200 m depth) indicated poor hydraulic communication across the zone, it is suspected that the SFR drainage system may cause drawdown in the Forsmark area via deeper flow channels. The depth level $z=-245$ to distinguish upper/lower barrier cases was taken based on the lower depth interval of the Repository domain used in DFN modelling (Öhman et al. 2012).

4.4 Bedrock outside SFR Regional domain

The bedrock description outside the SFR Regional domain is taken from the SR-Site/SDM-Site Forsmark model (Figure 4-10; Follin 2008; Joyce et al. 2010), which consists of:

- HCD: deterministically modelled in terms of three components:
  a. Base-case parameterisation of deformation zones (Follin 2008),
  b. sheet joints in the shallow bedrock of the Forsmark lens. These were originally terminated against the Singö deformation zone and therefore partially intersect the SFR model volume (Follin 2008); their original extension is revised so as not to intersect the SFR ramp (Öhman et al. 2013),
  c. six deformation zones defined in SDM-PSU, which are extended north from the SFR Regional domain in two variants (described below).

- HRD: modelled in three variants:
  a. DFN R01: the “static” fracture-network realisation used in Öhman et al. (2014), based on SR-Site’s “Heterogeneity Case” (Joyce et al. 2010),
  b. DFN R02: an anomalous realisation R02, which was found to affect SFR discharge in earlier SR-PSU modelling (Öhman and Odén 2017b).
  c. Constant hydraulic parameterisation, $K_{HRD} = 6.5 \times 10^{-9}$ m/s.

The SR-PSU flow domain exceeds the spatial coverage of the SR-Site Forsmark flow domain (c.f. brown- and grey-shaded areas in Figure 4-10a). A consequence of this, as well as limited data resolution of the current seafloor, is a notable lack of modelled deformation zones in the north-west of the SFR domain (i.e. deterministic structural modelling is strongly correlated to data support, which is manifested by the high number of zones in the Forsmark lens). The SFR discharge occurs in the northern part of the SFR Regional domain significance, and therefore the significance of potential deformation zones in this area is addressed by means of two variants of structures extending north from the SFR Regional domain (Section 4.4.1).

Likewise, DFN realisation R01, which originates from the SR-Site Forsmark model, has been expanded to fully cover the SR-PSU flow domain (Öhman et al. 2014). The alternative HRD variants are described in Section 4.4.2. Moreover, the SR-Site DFN realisation lacks full DFN coverage above z = 0 m elevation, which causes an artificially low hydraulic conductivity in bedrock above c. z = −10 m elevation with implications to bedrock recharge in the elevated parts of the Forsmark inland. To compensate this, a minimum bedrock conductivity of 3×10^{-8} m/s is assigned above z = −10 m elevation (see Table 4-4). The model files covering the HCD and HRD outside the SFR Regional domain are listed in Appendix A (Table A-6).

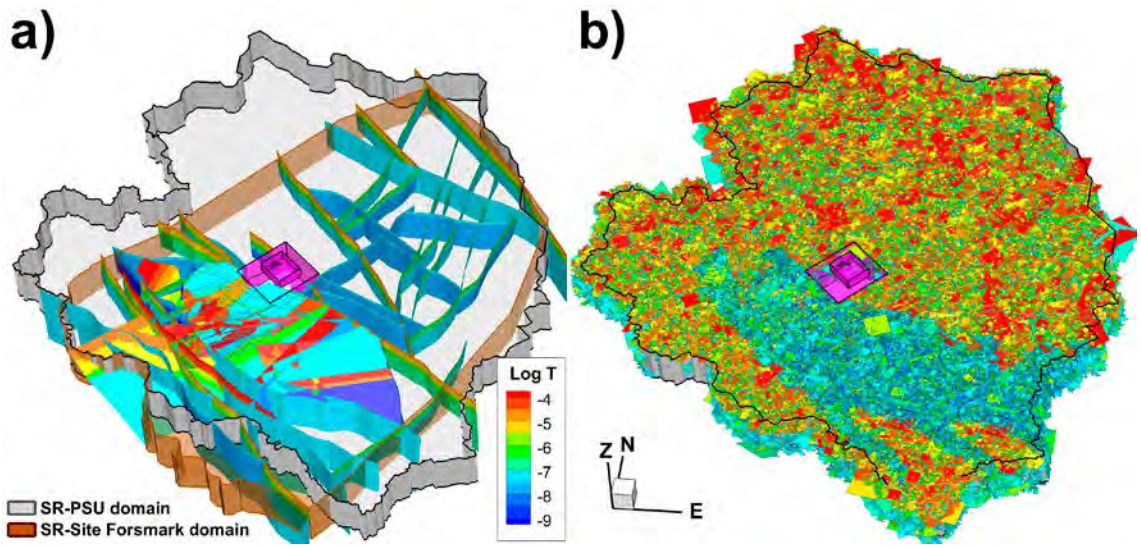

Figure 4-10. *Model components outside SFR Regional domain; a) deterministic HCDs consisting of parameterised deformation zones and sheet joints and b) stochastic HRD, represented by fracture-network realisation R01, based on SR-Site’s “Heterogeneity Case” (Joyce et al. 2010).*

4.4.1 HCD variants

Six zones (ZFMNNE3266, ZFMNNE3265, ZFMNNE3264, ZFMNS3154, ZFMNNW3113, and ZFMNNW0999) were defined in SDM-PSU and terminated against the north-eastern boundary of the SFR Regional domain. This termination was *not* based on geological merits, but instead due to modelling principles, as the scope of the SDM-PSU model is limited to the SFR Regional domain. However, these zones are not included in the SDM-Site Forsmark model (Figure 4-10a), and to avoid artefacts related to conceptual model boundaries (artificial terminations) in particle tracking, five of them were extended outside the SFR Regional domain (pink lines in Figure 4-11a). However, simulation results (Öhman et al. 2014) indicate that the uncertain extension of these zones potentially affect the modelled discharge locations of SFR (Figure 4-11a) and therefore, an alternative extension is explored in the sensitivity analysis (Figure 4-11b). Note that this alternative extension is hypothetic and schematic (i.e. not underpinned by data) and its purpose is to evaluate the significance of the potential extension of these zones.

The three parameterisation variants are shown for the extended geometry (Figure 4-12). Of the six extended structures, ZFMNS3154 is identified as the potentially most significant for particle transport, due to its:

1. more critical location within the discharge area for SFR, and
2. comparatively higher transmissivity parameterisation.

Analysis of upscaled ECPM translations demonstrates how the hydraulic role of the geometrically extended structures depend on the HRD parameterisation (Figure 4-13). In other words, the geometric extension of ZFMNS3154 may affect particle transport significantly in a low-conductive setting (c.f. Figure 4-13b and c), whereas may have a subordinate role in a highly conductive setting (Figure 4-13d).

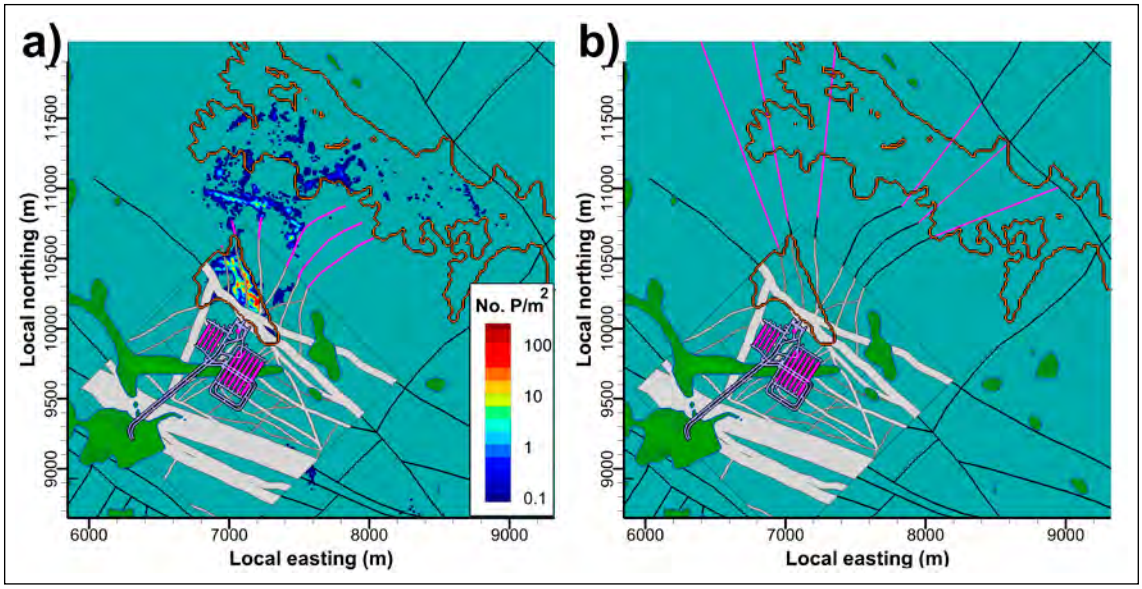

Figure 4-11. *Uncertain deformation-zone extension in SDM-PSU that may affect discharge locations; a) current extension outside SFR Regional domain (pink lines) and particle tracking exit locations (contoured; Öhman et al. 2014) and b) hypothetical further extension north (pink lines). Orange lines outline the two key biosphere objects for SFR discharge (157_2 and 116; see Figure 2-2).*

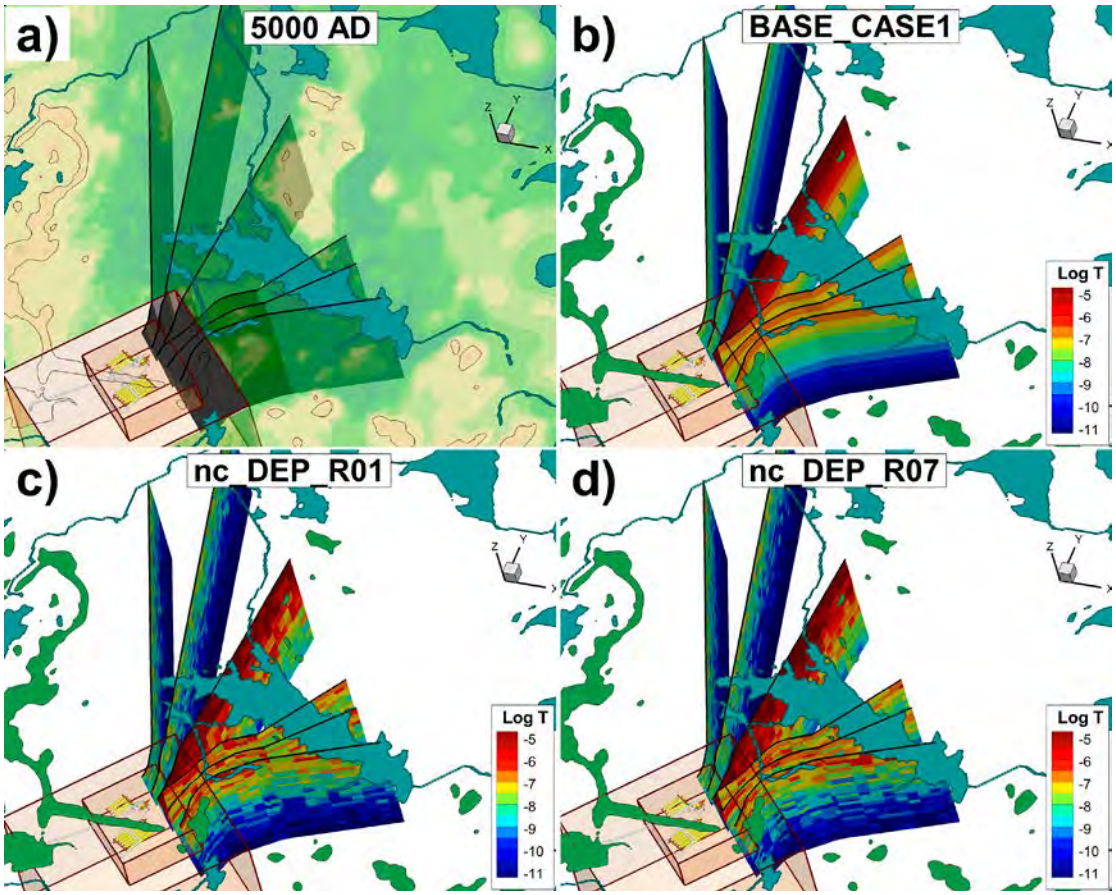

Figure 4-12. *Parameterisation of the six deformation zones extended north from the SFR Regional domain; a) structural extrapolation in context of landscape at 5000 AD, b) homogeneous base case, c) heterogeneous R01 and d) heterogeneous R07.*

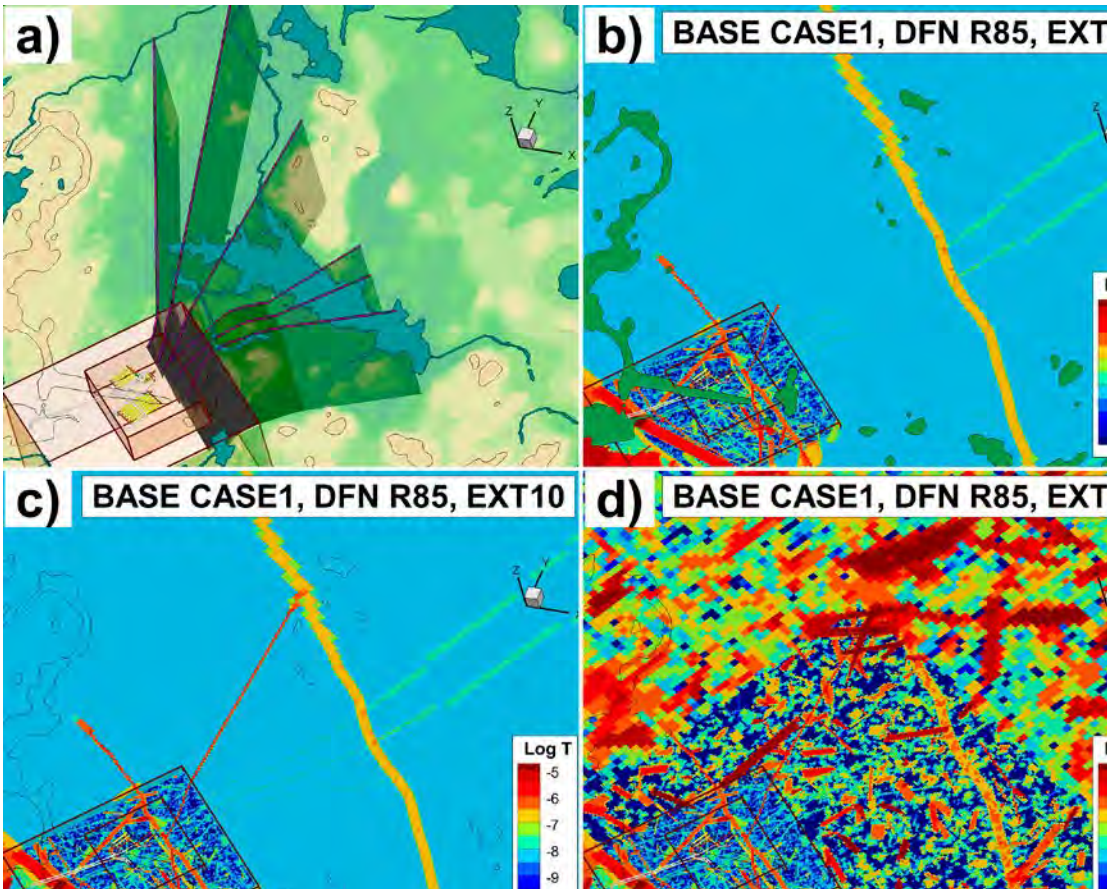

Figure 4-13. *Significance of HCD extension north from SFR relative to HRD parameterisation outside the SFR Regional domain; a) maximum extrapolation of six HCDs with uncertain extension in context of landscape at 5000 AD, b) minimum HCD extension with homogeneous HRD, c) maximum HCD extension with homogeneous HRD and d) maximum HCD extension with heterogeneous DFN R02.*

4.4.2 HRD variants

The repository performance is generally understood to depend on bedrock properties in the nearfield (i.e. local structures and local fracture network), and therefore earlier analyses have primarily focussed on the parameterisation of the bedrock inside the SFR Regional domain (Figure 3-1). However, simulation results have demonstrated that, under particular circumstances, the hydraulic heterogeneity modelled outside the SFR Regional domain may divert particle transport towards downstream biosphere objects (Öhman and Odén 2017b). The reason for this is that two stochastic DFN realisations are merged over the SFR Regional-domain boundary (the "varied" SDM-PSU realisations and the "static" SR-Site Forsmark realisation) and this merging has an overlap related to fracture size. In other words, large stochastic fractures generated outside the SFR Regional domain may extend several hundred meters into the SFR domain (e.g. red fracture in Figure 4-14b).

This study therefore includes an anomalous DFN realisation, R02, that was identified for its impact on particle-exit locations (Öhman and Odén 2017b). The principles for generating DFN R02 can be summarised as follows (details provided in Table A-6, Appendix A):

1. The peripheral parts of the flow domain are described by SR-Site's heterogeneity case (i.e. identical to realisation R01; Figure 4-15a).
2. All fractures inside a "DFN generation volume", downstream from SFR, are deleted from SR-Site's heterogeneity case (grey in Figure 4-15b).
3. The realisation R02 is generated inside the "DFN generation volume". Non-connected fractures, which are not part of the flowing fracture network, are removed (i.e. as fracture-network upscaling for DarcyTools simulation refers to the subset of flowing fractures). A so-called "connectivity fringe" is temporarily used in the geometrical connectivity analysis to ensure that DFN connectivity is not affected by merging over domain boundaries (pink in Figure 4-15b; details in Öhman and Odén 2017b).
4. Realisation R02 is merged with the surrounding SR-Site's heterogeneity case.

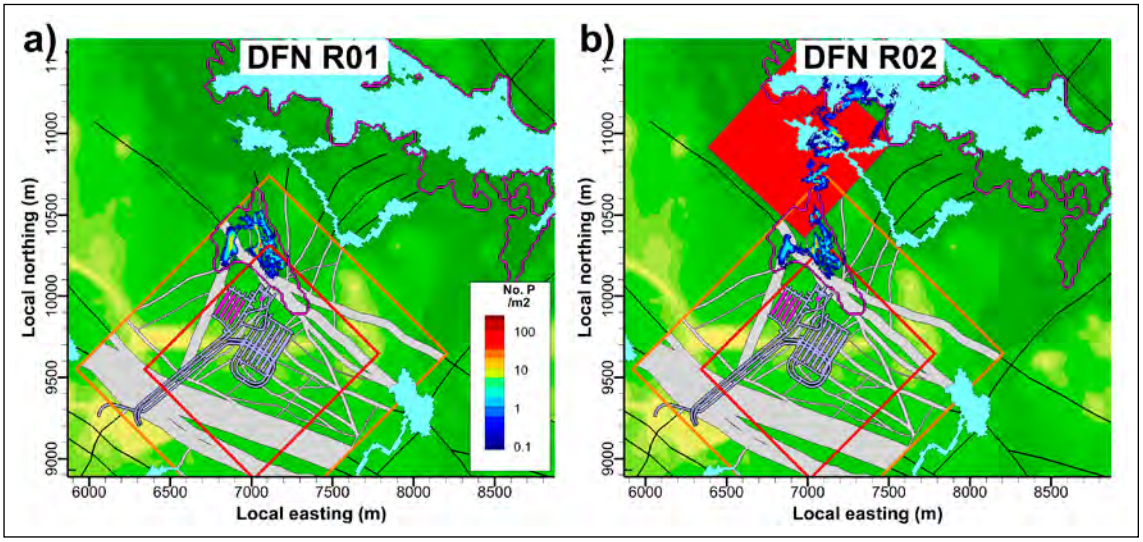

Figure 4-14. *Simulated particle-exit locations for two stochastic DFN realisations outside the SFR Regional domain; a) DFN R01, originating from SR-Site's heterogeneity case (used as the static realisation in Öhman et al. 2014) and b) DFN R02, an anomalous realisation diverting SFR discharge towards the downstream lake object 116 (Öhman and Odén 2017b).*

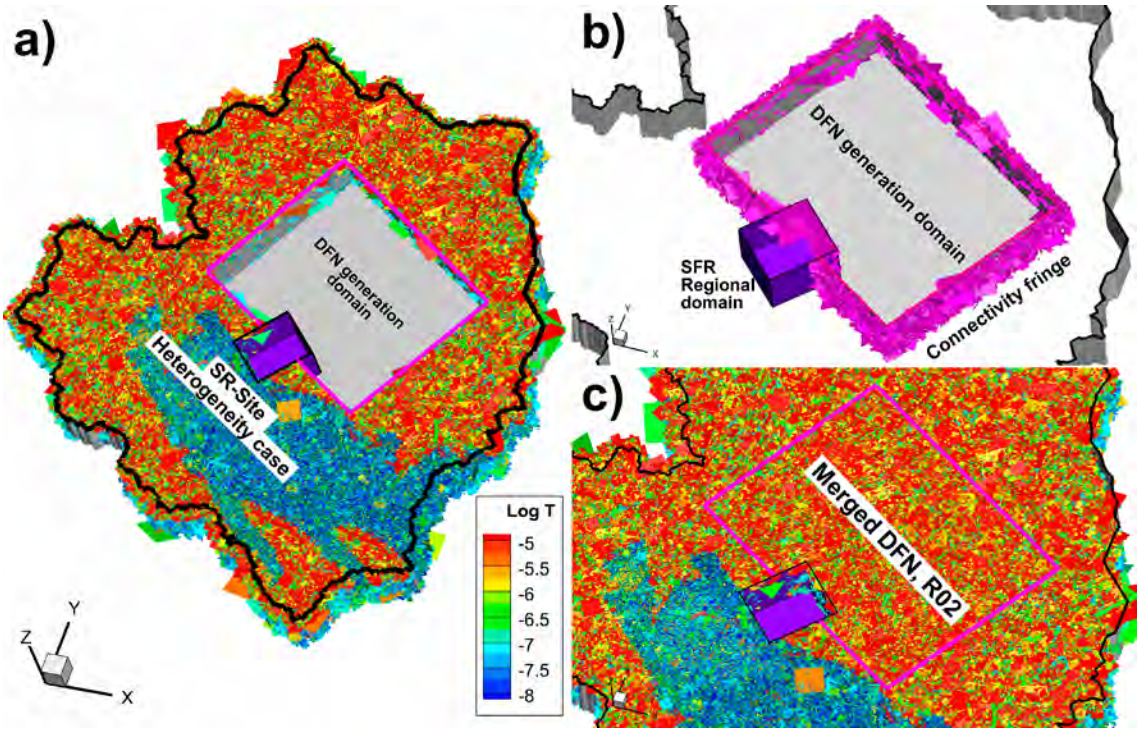

Figure 4-15. *Principle for merging DFN realisations outside the SFR Regional domain (purple); a) static DFN parameterisation, b) fracture-generation domain (grey) and connectivity fringe (pink), and c) merged realisation, DFN R02.*

4.5 HSD parameterisation

Groundwater flow in the shallow host rock of SFR is driven by the groundwater table in the overlying HSD. The groundwater table is determined by the flux balance between net precipitation, infiltration and runoff, and therefore varies locally, depending on topography, regolith depth, and the hydraulic conductivity of the soil. In other words, the HSD parameterisation determines how well the groundwater table follows the ground-surface topography. Permeable regolith layers (e.g. till, glaciofluvial material and the coarse fill material of the pier; Table 4-4) is expected to hold a smooth groundwater table, which is relatively independent from topographical variation compared to that in less permeable materials (e.g. lacustrine/marine postglacial deposits and glacial clay). Earlier studies have demonstrated that less permeable materials uphold the groundwater table closer to ground surface, but still do not limit the recharge to the underlying bedrock (Öhman and Odén 2017b).

Moreover, the potential discharge areas of SFR (i.e. particle-exit locations) vary somewhat over the time span addressed in SR-PSU, from the submerged seafloor during the early stages of shoreline retreat, to local depressions in the terrain (such as lakes and wetlands), during the later simulation sequence. In other words, the SFR discharge is associated to areas that are or have been subject to lacustrine/marine accumulation of low-conductive postglacial clay (Table 4-4).

The hydraulic-conductivity parameterisation of HSD (i.e. RLDM regolith layers) is taken from the SR-Site/SDM-Site Forsmark model (Bosson et al. 2010). The HSD porosity has been assumed to be equal to specific yield (Table 4-4); however, in practice neither porosity, nor specific yield, are used in simulations, as:

1. The mass-balance calculation in DarcyTools simulations refers to cell-averaged flow, which can be expressed in terms of either Darcy flow, Q (m3/s; volumetric flow rate), or Darcy flux, q (m/s; i.e. flow rate per unit area). Thus, the actual fluid velocity is not being solved for *per se* in the DarcyTools flow simulations.

2. The fracture-flow velocity is only calculated during the evaluation of advective travel time for particles. However, all evaluated performance measures refer to bedrock retention only (Section 1.3), and therefore both porosity and flow-wetted surface area are nullified in HSD to eliminate the risk of accidental contribution to accumulated transit time or F-quotient during particle tracking.

Table 4-4. HSD hydraulic conductivity of regolith layers (Table 2-3 in Bosson et al. 2010).

Regolith layer	K_h (m/s)	K_v (m/s)	Porosity[4] (–)	Layer definition (Table A-1)
Peat[1]	3.0×10^{-7}	3.0×10^{-7}	0.2	From <lpgd> to <Filled_pdem[1]>
Lacustrine accumulation of post-glacial deposits	1.5×10^{-8}	1.5×10^{-8}	0.05	From <mpgd> to <lpgd>
Marine accumulation of post-glacial deposits	1.5×10^{-8}	1.5×10^{-8}	0.03	From <gkl> to <mpgd>
Glacial clay	1.5×10^{-8}	1.5×10^{-8}	0.03	From <fill> to <gkl>
Filling[2]	1.5×10^{-4}	1.5×10^{-4}	0.2	From <glfl> to <fill>. Special handling of the SFR pier[2]
Glaciofluvial material	1.5×10^{-4}	1.5×10^{-4}	0.2	From <till> to <glfl>
Till	7.5×10^{-6}	7.5×10^{-7}	0.05	From <bedr> to <till>
Upper bedrock[3]	$\geq3.0\times10^{-8}$	$\geq3.0\times10^{-8}$	$\geq1.0\times10^{-5}$	Thin soil coverage (soil depth < 4.0 m) and elevated bedrock (z > −10 m).

[1] Note that the upper surface of peat refers to the basin-filled DEM (Section 3.3.2), which implies that local basins are assumed to be peat-filled, or at least filled with a relatively high-conductive material.

[2] Special attention is given to the SFR pier. To avoid artefacts in the determination of the surface head in the Pier, the "conductivity of fill" is expanded 2 grid cells, horizontally (2 × 8 m). Below an elevation of z = −3 m, a layer of till is assumed to underlie the filled areas around the SFR pier [SR-PSU_TD18_Model_parameterisation.f].

[3] A minimum bedrock conductivity of 3×10^{-8} m/s is assigned in two cases: 1) at thin soil coverage (soil depth < 4 m), and above an elevation of −10 m (this is to compensate that DFN coverage above z = 0 m, is unavailable outside the SFR Regional domain, Section 4.4).

[4] HSD porosity set equal to 0.0 in particle tracking to avoid unintentional contribution to performance measures of the bedrock.

An overview of the modelled HSD in the relevant area for SFR discharge (i.e. termination points in particle-tracking) is provided in Figure 4-16. The following should be noted in this visualisation:

1. The following landmarks are provided for spatial reference of the visualised area:
   a. SFR Regional domain (orange lines),
   b. present land above sea (green shaded; c.f. Figure 3-1), and
   c. key biosphere objects (157_2 and 116; white outline).
2. Lakes and rivers are not included in the figure (c.f. Figure 3-1).
3. The visualisation employs the "fixed-bedrock" elevation reference, where the bedrock elevation is envisaged as static over time (Section 3.3.5).
4. The filling material of the constructed SFR pier is not shown here (see closeup of model implementation of the pier in Figure 4-18).
5. The "filled peat layer" (Figure 4-16e and f) includes two components:
   a. peat, as modelled in RLDM, and
   b. basin-filling of local depressions (performed exclusively for controlling the groundwater table in DarcyTools simulations; Section 3.3.2).

The first regolith layer on top of the bedrock surface is till. Till is modelled as wide-spread over the area and with thicknesses typically ranging from a few meters to 10 m (Figure 4-16b). Moreover, till is modelled as static over time (i.e. assumed to not be affected by erosion). Glaciofluvial deposits occur within the model domain, but with negligible role in simulations due to their remote location. The SFR pier is constructed from rock blast, which is assumed to have hydraulic properties equivalent to the glaciofluvial deposits. Owing to its central location, atop of SFR, the parameterisation of the pier (or more precisely, its modelling uncertainties) has a central role in flow simulations (see separate discussions below). The pier itself is not understood to hold groundwater notably higher

than its surroundings, and therefore its impact on the flow around SFR is expected to be small (irrespectively of the complications in modelling mentioned below).

The till layer is covered by three low-conductive layers (glacial clay and postglacial deposits from lacustrine/marine accumulation; Table 4-4). These three layers occur in a patched appearance, associated to re-distribution of wave erosion (e.g. sheltered basins in the seafloor; Figure 4-16c and d). Minor changes over time can be noted for these low-conductive layers, with the most notable changes north of the SFR pier (Figure 4-16d).

The uppermost regolith layer is peat. This layer is basin-filled to allow the groundwater level to exceed ground surface locally in topographical depressions; this implies that all potential wetlands are assigned the same properties as peat (Table 4-4).

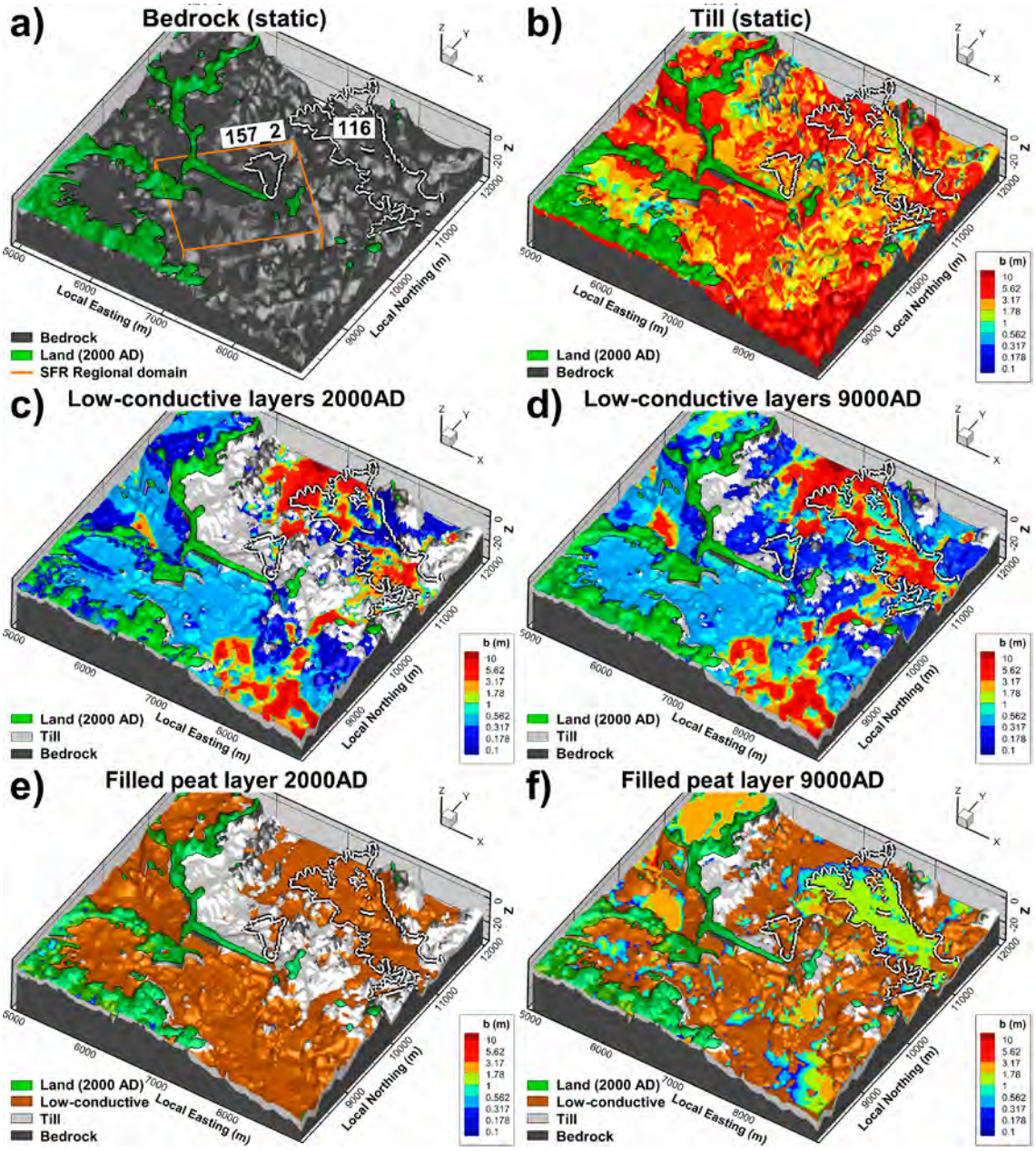

Figure 4-16. *Regolith thickness, b (m), in the SFR near field; a) bedrock surface (dark grey), b) static till layer (contoured), c) current distribution of low-conductive layers (submerged), d) future distribution of low-conductive sediments (terrestrial), as well as, e) and f) modelled peat (contoured thickness atop of brown-shaded low-conductive sediments). The SFR Regional domain (orange lines), biosphere objects 157_2 and 116 (white lines), and current land above sea (green shade) included for reference.*

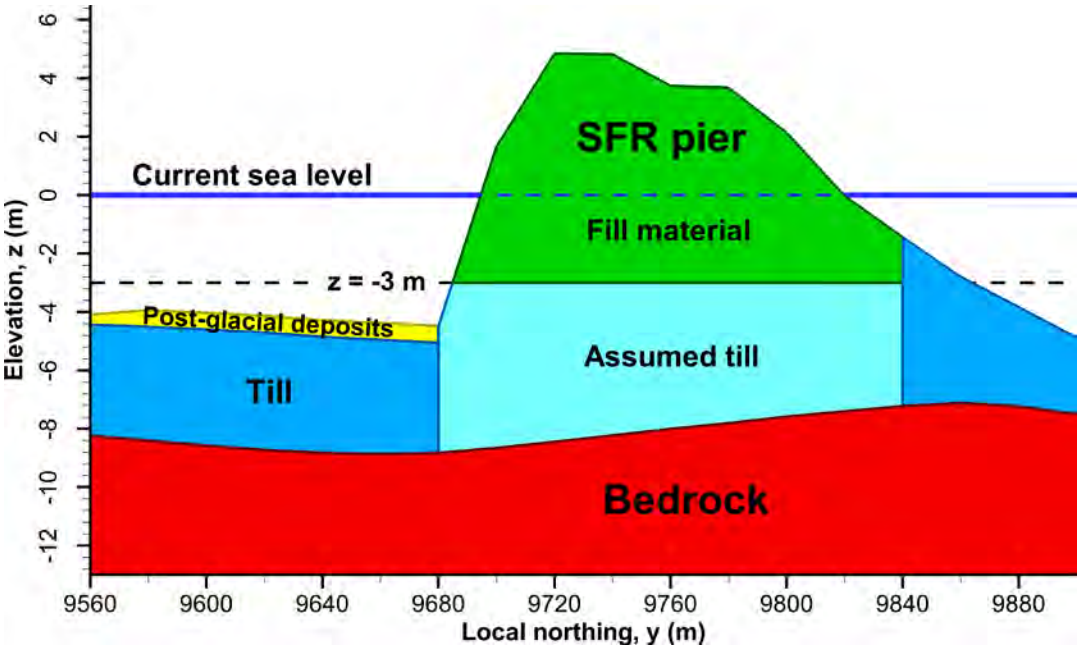

Figure 4-17. *Cross section of modelled pier composition (local easting x = 6600 m). An underlying till layer is assumed below the elevation z = −3 m. Note vertical exaggeration and see numerical implementation in Figure 4-18.*

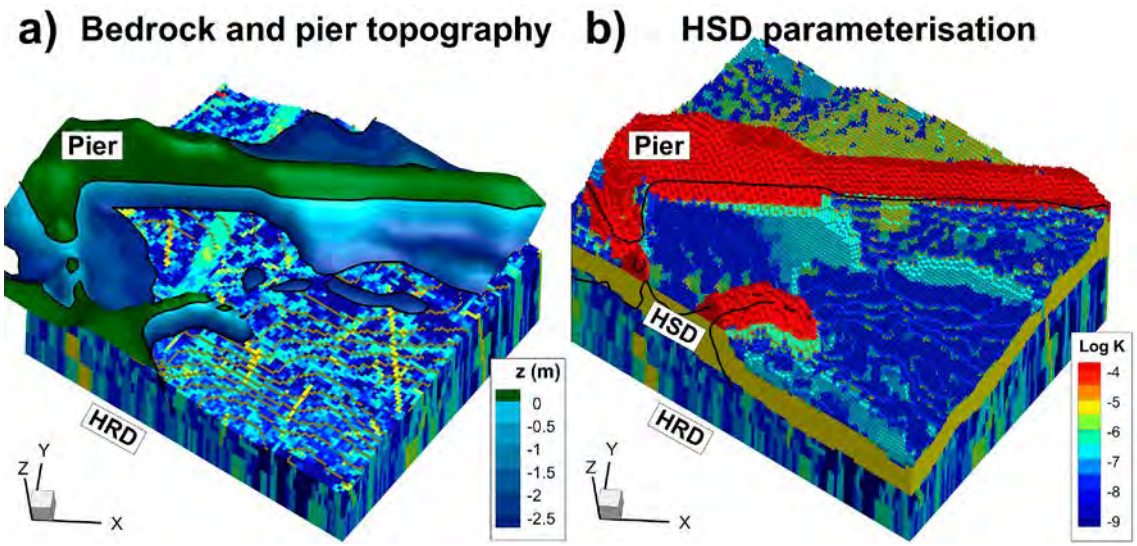

Figure 4-18. *Parameterisation of the SFR pier; a) relief of the pier (contoured by elevation, z) and the underlying bedrock (contoured by ECPM conductivity), b) pier parameterisation: $K_{fill} = 1.5 \times 10^{-4}$ m/s for $z \geq -3$ m (contoured red), and the assumed underlying till-layer for $z < -3$ m (contoured orange). Note also the thin uppermost layer of postglacial clay, $K_{clay} = 1.5 \times 10^{-8}$ m/s (contoured blue), south of the pier.*

The SFR pier; parameterisation and groundwater table

The wave-breaking pier on top of SFR was constructed from blast rock that was excavated during the repository construction. The model representation of the pier is given special attention in simulations, as it has been recognised as a key uncertainty during later stages of shoreline retreat. The prominent role of the SFR pier in flow simulations is due to a combination of the following three aspects:

1. **Hydrogeological role:** The pier has a central location, c. 60 m above the repository, and extends on top of a submerged ridge of natural sediments, which may serve as a potential local water divide during later stages of shore-line retreat. Although the influence of the pier may be limited to its immediate surroundings, its impact on repository performance is accentuated by the proximity the repository.
2. **Hydrogeological contrasts:** Compared to its surroundings (presently submerged below the sea), the pier stands out as a marked topographical anomaly of highly permeable material (parameterised as $K_{fill} = 1.5 \times 10^{-4}$ m/s; Table 4-4). Although its permeable material does not appear to hold groundwater, the combination of topographical and hydraulic contrasts poses a challenge for simulating realistic groundwater levels during future stages of shoreline retreat.
3. **Uncertain material composition:** the material composition of the pier is not fully clear below the current sea level (i.e. if the pier was constructed on bare bedrock, or if it was constructed on top natural sediments). This implies uncertainties regarding its hydraulic contact with the underlying bedrock, as well as its potential role as a local water divide during future stages of shoreline.

The monitored groundwater levels in the pier cannot be differentiated from the sea level. This confirms the very low hydraulic gradients that can be expected in highly permeable material (sand, gravel, and blocks) and these present-day conditions suggest that the pier is unlikely to serve as a local water divide. However, comparatively less is known about the material composition at depth (i.e. if the pier was constructed on bare bedrock, or if it was constructed on top natural sediments). Drilling notes taken during the PSU investigations support the existence of a *till layer* below the rock-blast material (see Öhman et al. 2014). Based on consideration to the surrounding deposits, it was decided to assume a till layer below an elevation of $z = -3$ m (Figure 4-17).

Although till is modelled as rather permeable, $K_H = 7.5 \times 10^{-6}$ m/s and $K_V = 7.5 \times 10^{-7}$ m/s, it is considerably less permeable than fill material, $K_{fill} = 1.5 \times 10^{-4}$ m/s, and provides a more realistic description of the contact between the pier and the bedrock surface that control the local groundwater table during later stages of shore line retreat (Figure 4-18). It should also be noted that the pores of the coarse construction material may gradually fill up over time (e.g. due to sedimentation or soil formation), and may successively approach till in material properties.

5 Simulation sequence

5.1 Grid generation

The DarcyTools computational grid is generated by means of an inbuilt module GridGen, which facilitates unstructured gridding that enables local refinement (e.g. near ground surface and tunnel geometry). The discretization sequence is carried out via a structure of commands specified in the standardised Compact Input File on xml-format (Svensson et al. 2010). Each discretisation command consists of a geometric reference (i.e. DarcyTools objects in Chapter 3) combined with either: 1) a specification on local maximum cell side length, and/or 2) classification of grid subdomains by means of a cell marker ID. Cell-marker IDs have a key role in subsequent modelling; for example, they are used in property assignment, boundary conditions, and particle release points. All details on grid discretisation are given in Appendix A3 (Table A-7).

Cell-inactivation principle

In the standard DarcyTools approach, the model top boundary is defined by removal of grid cells above ground surface (i.e. as defined by a DEM). During time span addressed in SR-PSU, the topography alters due to landscape dynamics, which is modelled in terms time slices that represent nine stages of shoreline retreat. Covering the time aspect by the standard "cell-removal approach" is very inefficient. The reason is that the upscaling of ECPM properties (Section 5.2) is valid for a unique grid discretisation, only, which would imply that ECPM conversion of all bedrock cases must be repeated for each of the nine time slices (time consuming and complex file management). Instead, a so-called *cell-inactivation* method is employed, that controls the topography alteration by means of cell marking, but within the framework of a *static* grid discretisation. The benefit of the static discretisation is that full compatibility is maintained between time-specific grids and ECPM properties. In principle, only time-invariant geometries are used in discretisation, while both time-variant and static geometries are used in classification of cell markers (e.g. Mk 999 = cell inactivation).

5.2 ECPM upscaling

DarcyTools employs a Continuum Porous-Medium (CPM) representation of geological media (Svensson et al. 2010), in which the hydraulic properties of a flowing fracture network are approximated by those of a porous medium. DarcyTools allows transferring fracture-network characteristics onto its computational grid by means of geometric upscaling. The upscaled properties are referred to as Equivalent Continuous Porous Medium (ECPM) properties. As the ECPM approach is based on an underlying stochastic DFN model, the resulting ECPM properties are also stochastic. Geometric up-scaling does not always ensure *hydraulic* consistency between the complex heterogeneity of the underlying flowing fracture network and the approximated ECPM. Thus, "Equivalent" implies a fine resolution of the computational grid to be valid.

DarcyTools employs a *staggered* grid arrangement with ECPM properties which are derived from geometric upscaling of a fracture network over local control volumes (Svensson et al. 2010). This staggered grid involves *scalar* properties, defined at cell centres (e.g. porosity and flow-wetted surface area), and so-called *tensor* properties, stored at cell walls (e.g. conductivity). In other words, scalar and tensor ECPM properties do not represent identical control volumes, but are offset by half a grid cell.

A consequence of the staggered grid arrangement is that each step in the cell-jump particle tracking approach involves *one* cross-cell flow, but *two* grid-cell porosities and fws-values (Section 5.4.2). The ECPM conversion relies on several approximations:

- all fractures[1] inside a cell-wall control volume contribute to advection,
- the advection takes place over their full fracture surface area,
- porosity of fractures below the fracture-size truncation is negligible for flow.

Kinematic porosity and transport aperture

Kinematic porosity refers to the fractional void volume of the flowing fracture system (i.e. as opposed to the immobile porosity). It is a critical parameter for relating simulated flow over cells to fluid velocity and ultimately determining advective travel time of tracked particles. Unfortunately, the parameter is difficult to measure in field. The DarcyTools upscaling algorithm (GEHYCO; Svensson et al. 2010) offers the translation of fracture apertures into cell-averaged kinematic porosity (i.e. an ECPM entity). Aperture refers to the fracture void opening; it is an uncertain parameter: known to vary over the fracture plane and not readily assessable from field data. Different so-called equivalent fracture apertures (i.e. representative values) have been suggested for describing specific processes being studied (e.g. hydraulic, mechanic, and transport apertures). The results of Äspö Task Force 6c (Dershowitz et al. 2003) have suggested an empirical relation for transport aperture, e_t, that is assumed to be representative for modelling solute transport in fractures:

$$e_t = 0.46\sqrt{T}, \tag{5-1}$$

, where T is the fracture transmissivity (m^2/s). This relation was also used as a starting point for model calibration in SDM-Site Forsmark (Follin 2008). In SR-PSU, the kinematic porosity is upscaled from the underlying stochastic fracture networks, where the transport aperture of fractures is calculated according to Eq. (5-1), with a minimum porosity value set to 10^{-5} [–]. Performance measures are only calculated for the bedrock; therefore, both porosity and fws are nullified in tunnel backfill and in overlying sediments when particle tracking is performed.

All the details on the management of model files and naming conventions during ECPM conversion are presented in Appendix A3 (Table A-8).

5.3 Flow simulations

DarcyTools has primarily been developed for the site-scale modelling of groundwater flow in deep rock. As such, the hydrological flow balance at ground surface, such as runoff, is not modelled in detail. Consequently, a model artefact of local excess head may occur at ground surface, if net precipitation exceeds local recharge (i.e. local excess head defined as exceeding topography). Two methods, which both have their merits and drawbacks, are commonly applied to circumvent this model artefact:

1. Prescribed-head condition at the model top boundary (e.g. assume $H = z_{topography}$).
2. Free-groundwater table (inbuilt DarcyTools algorithm).

The prescribed-head approach is numerically convenient, as it sets the groundwater table directly from the topography. However, a limitation of the approach is that it *assumes* a constant depth to the groundwater table, without consideration to the local hydrogeological conditions. Thus, the approach does not differentiate between the areas that are expected to be saturated (e.g. discharge areas) and other areas that are expected to be unsaturated (e.g. local topographical peaks and glaciofluvial deposits). This approach is therefore less appropriate in SR-PSU, as the model representation of SFR pier has proved to be of particular significance for model performance (Section 4.5).

[1] More precisely, only fractures within a specified size interval are included; minimum fracture side length ranges from 2 to 16 m, depending on fracture set and depth domain. Furthermore, only the hydraulically connected subset of the fracture network is modelled, details provided in TD05 (Öhman and Bockgård 2013).

The alternative to use the inbuilt free-groundwater algorithm in DarcyTools, on the other hand, provides a smooth groundwater table, where the groundwater depth varies with local hydrological conditions. This groundwater table is determined locally by the flow balance between net precipitation, infiltration, and a rudimentarily modelled surface runoff (i.e. the latter being mimicked by a fictive hydraulic parameterisation of the uppermost 20 m of the soil/bedrock. The method has been calibrated to apply for the present-day hydrological conditions and specifically to simulate the deep bedrock flow in SDM-Site Forsmark. The drawbacks for application in SR-PSU are:

1. during later stages of shoreline retreat, the algorithm renders unrealistic submerged areas (Öhman 2010; i.e. groundwater standing above ground surface). The reason for this is that the DarcyTools algorithm solves the groundwater table from a delicate flux balance, driven by hydrological conditions, which are poorly known in areas that are currently below sea (such as lake thresholds and the network of rivers and streams). Moreover, the fictive HSD parameterisation is calibrated for the present-day hydrological conditions in the Forsmark area (i.e. applies for a specific constellation of topography, lakes, and rivers). Thus, the parameterisation is not necessarily generic for future stages of land uplift (i.e. not automatically valid for the areas that are currently below sea, but will gradually emerge above sea).
2. the generalised fictive parameterisation of the uppermost 20 m is not very appropriate for modelling flow in the shallow bedrock at SFR.
   a. Firstly, the introduction of a fictive parameterisation over the uppermost 20 m has a substantial impact on simulation output (i.e. performance measures of bedrock retention), as the bedrock coverage over the repository is only c. 50 m, with an overlying 5 m till layer.
   b. Secondly, the fictive parameterisation does neither differentiate between soil and underlying bedrock (i.e. does not resolve local soil depth), nor does it resolve the local occurrence of regolith layers with specific hydraulic properties (i.e. the man-made pier, and occurrence of clay layers).

Instead, a hybrid approach is suggested, where the two boundary-condition types “flux” and “fixed head” are combined in a preceding “Recharge phase” to simulate realistic head for the model top boundary (allowing unsaturated areas, but not excess head). The top-boundary head is then applied as a fixed-head boundary condition in subsequent steady state simulations, in order to establish a well-converged flow solution. The flow simulations are managed in three steps (i.e. sequence c) in Figure A-1):

1. Final setup of the model parameterisation (Section 5.3.1).
2. Solve a realistic top-boundary condition in a so-called “Recharge phase” (Section 5.3.2).
3. Apply the top-boundary condition in a so-called “Steady-state phase” to obtain a high-convergent flow solution.

The automatized execution of flow simulations and its traceable management of input and output data files are described in Appendix A3.

5.3.1 Finalising model setup

The final model setup (i.e. property assignment in the computational grid) is performed by means of the DarcyTools module PropGen (Svensson et al. 2010), as compiled from the customized source code [SR-PSU_TD18_Model_parameterisation.f]. PropGen has the following key functions:

1. Finalise the hydraulic-domain parameterisation. Input data on bedrock ECPM conductivity (HRD and HCD in Table A-8) and HSD conductivity (Table 4-4) are merged and converted into permeability (i.e. the operational unit in DarcyTools). Any bedrock conductivity below 10^{-10} m/s are re-set to a minimum value of 3×10^{-11} m/s. Inactive cells (marked as 999), are assigned cell-wall conductivities $K_{inactive} = 10^{-20}$ m/s (Section 4.5).
2. Identify tunnel and tunnel-plug cells, based on cell markers (Table 4-1), and implement as permeability (i.e. over-writing “bedrock values”).

3. Calculate cell porosity, *n*, defined as sum of intersectional fracture void volume per cell volume, i.e. fracture volume is based on fracture area and transport aperture in Eq. (5-1). A minimum porosity of 10^{-5} [–] is applied.
4. Output is also exported in TecPlot format for visual verifications (e.g. Figure 4-1 and Figure 4-3).

The principles for numerical implementation of HSD parameterisation and the automatized management of input and output data files are described in Appendix A3 (Table A-9).

Numerical implementation inactive cells

The modelling procedure employs a *cell inactivation method*, to be able to represent topographical changes between different time slices with a single grid. Grid cells above the basin filled DEM for a given time slice are defined by setting the DarcyTools cell marker to 999. Two measures are taken to isolate these cells from taking part in the flow solution: 1) an extremely low conductivity value is assigned to all cell walls, $K_{inactive} = 10^{-20}$ m/s, and 2) an arbitrary fixed-head boundary condition is prescribed to the cells, i.e. H = 0.0 m. In effect, the cells marked 999 are isolated from the flow solution. The benefit is that the cells are not permanently deleted, but can be re-activated for modelling a different time slice. Special care must be taken to inactivated cells in recharge calculations.

5.3.2 Determining top-boundary condition in a recharge phase

The top boundary is defined as the uppermost layer of *active cells* in the grid (i.e. immediately below either permanently deleted or temporarily inactivated cells). The purpose of this initial "recharge phase" is to establish a realistic top-boundary condition for the subsequent steady-state simulation (i.e. head in surface-layer cells). As such, the recharge phase has two primary targets:

1. constrain unrealistic excess head (i.e. head exceeding ground surface, as defined by the DEM),
2. allow unsaturation, for example, in local topographical peaks. Two such examples with particular significance for the local flow field in SR-PSU are: 1) the SFR pier and 2) islets east of the pier.

The determination of head in the model top boundary is primarily based on the following four key components:

1. Fixed head in the surface-water areas that are defined in RLDM (Table 5-1).
2. Spatially variable recharge, locally ranging from 0 to full net precipitation, P-PET = 160 mm/yr.
3. Maximum-head criterion in surface-layer cells, determined by local topography, and
4. Local HSD conductivity.

Table 5-1. Fixed head in pre-defined surface-water areas.

Surface-water	Identification	Prescribed head, H (m, elevation)
1. Seafloor	Uppermost cell layer below relative sea level (Table 3-2)	$z_{sea\ level}$ (Table 3-2)
2. Lakes	cell markers (Table A-3)	$z_{lake\ threshold}$ (Table A-3)
3. Rivers	cell marker Mk = 102	[SR-PSU_TD18_River_head.in][1)]

[1)] The input file [SR-PSU_TD18_River_head.in] contains river-trajectory nodes (x,y) and estimated riverbed head for each time slice (Section 3.3.4). Prescribed head for river cells are interpolated based on the nearest two river-trajectory nodes.

Maximum-head criterion in surface-layer cells

Excess head in ground-surface cells is defined as head exceeding the local topography. It should be noted that the DEMs modelled in RLDM [pdem<time slice>.asc] contain local depressions that are below the scale for defining lakes. These depressions may hold surface water, e.g. minor lakes, wet lands, pools, or be peat-filled. Irrespectively of which, it can be argued that the head criterion should not relate to the elevation in local depressions, but by the geometric *threshold* surrounding depression. Therefore, the "excess head" in top-boundary cells is defined as $H - z_{DEM}$ (m, elevation in fixed-bedrock reference), where z_{DEM} refers to the local basin-filled DEM elevation (Section 3.3.2). The local z_{DEM} for ground-surface cells is determined from [Filled_pdem<time slice>_Fixed_bedrock.asc], i.e. after a step of back-rotating and translating cell coordinates into the RT90 coordinate system. This mapping between RLDM and DarcyTools is inexact due to combined effect of: 1) discretisation differences and 2) coordinate-system rotation. Although the basin-fill is a substantial improvement, the inexact matching implies that a complete absence of local depressions cannot be guaranteed in groundwater flow simulations.

Ground-surface head oscillates between iterations, due to: 1) step-wise adjustments in local recharge, and 2) resulting non-stationary flow solution. Therefore, an "excess-head tolerance" was introduced, which declines as a function of iterations (Figure 5-1). After 44 iterations, this tolerance levels out to a constant 0.25 m, which is judged to reflect the combined errors from: 1) RLDM modelling and 2) the inexact mapping between DarcyTools and RLDM. For ground-surface cells exceeding the tolerance, the boundary-condition type is switched from "flux" to "fixed head", where $H = z_{DEM}$ (m, elevation). The resulting ground-surface head after 100 iterations are used to specify fixed head in the subsequent steady-state phase.

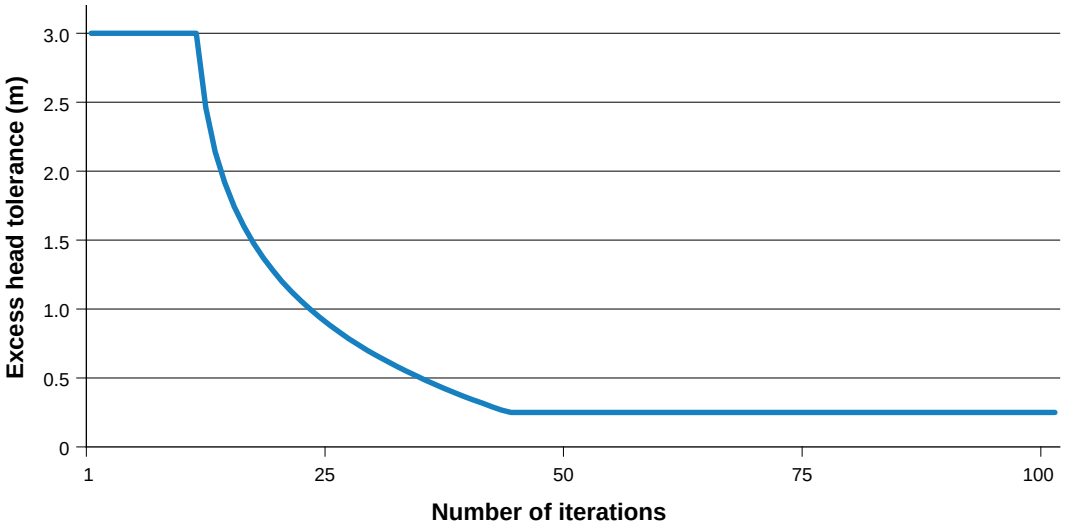

Figure 5-1. *Tolerance in simulated excess head of ground-surface cells in the recharge phase.*

Conceptualisation of local recharge

The flow domain has a generally flat topography (Figure 3-1), particularly in areas that are currently below sea. Therefore, large areas are expected to be saturated with large runoff components (i.e. in addition to the pre-defined open-water types in Table 5-1). Surface runoff is controlled by surface-hydrology components below the resolution scale of the DarcyTools model setup (e.g. small brooks and overland flow); in other words, geometric details with high hydraulic contrasts, that cannot be realistically represented in a model that primarily targets bedrock and future conditions. Consequently, neglecting the runoff component leads to local excess head where net precipitation exceeds local recharge (i.e. local excess head defined as exceeding topography). Excess head is an unrealistic model artefact, which implies exaggerating local gradients and flow, as well as, distorting the particle-tracking exit locations. Two means are therefore taken to deplete artificial excess head in surface-layer cells:

1. Local recharge is envisaged as [net precipitation - runoff]. In cells with excess head, the local recharge is therefore reduced, sequentially by iterations, from a maximum of P-PET = 160 mm/yr to a minimum of 0.0 mm/yr. The reduction is done on a cell-specific basis.
2. Excess head larger than the tolerance (Figure 5-1) changes the boundary condition of the individual cell from “flux type” to “fixed-head type”.

The automatized transfer of input and output data files between the two phases during the flow simulations is described in Appendix A3 (Table A-10 and Table A-11 for the recharge and steady-state phases, respectively).

5.4 Post process

The performance measures (Section 1.3) are calculated by means of post-processing of flow solutions. This is conducted by means of the DarcyTools module PropGen, as compiled from customized Fortran codes (see Table A-12 and Table A-13). The post-processing is executed in batches, in which the traceability between input and output data is automatized.

Two types of performance measures (Section 1.3) are analysed:

1. analysis of the simulated flow field (Section 5.4.1) provides cross-flow, head, and hydraulic gradients in disposal rooms, as well as, bedrock re/discharge in biosphere objects.
2. Bedrock retention properties, L_r, F_r, and $t_{w,r}$, as well as, disposal-room interactions, are determined by means of particle tracking (Section 5.4.2).

5.4.1 Flow-field analysis

The flow-field post processing has two objectives:

1. Calculate cross flow over disposal rooms as a performance measure, and
2. Calculate bedrock re/discharge in biosphere objects for inter-code comparison with the Biosphere modelling.

Cross flow refers to the total flow over a predefined cross-sectional area in the computational grid. This area is the interface between a subunit of interest, *i*, (e.g. a tunnel section or bedrock surface) and surrounding, arbitrary grid cells, *j*. For example, this *ij*-interface may refer to a tunnel wall between tunnel cells identified by marking, Mk = *i* (Table 4-1), and surrounding bedrock/plugs with grid-cell marking Mk = $j \neq i$ (i.e. *j* may include several cell markers). Four components of the cross flow can be determined over the *ij*-interface:

1. total inflow to subunit *i*, ΣQ_{ij+}
2. total outflow from subunit *i*, ΣQ_{ij-}
3. total outflow from surrounding grid cells *j*, ΣQ_{ji-}
4. total inflow to surrounding grid cells *j*, ΣQ_{ji+}

By symmetry, $\Sigma Q_{ij+} = -\Sigma Q_{ji-}$ and $\Sigma Q_{ij-} = -\Sigma Q_{ji+}$. Furthermore, mass balance in a well-converged flow solution holds that, if no sink or source terms are present in subunit *i*, $\Sigma Q_{ij+} = \Sigma Q_{ji+} = |\Sigma Q_{ij-}| = |\Sigma Q_{ji-}|$. As the exception, due to an inbuilt error in the DarcyTools pressure correction between cells of different sizes (Öhman et al. 2013c) the tunnel flow of 2BMA must be based on *bedrock cells*.

In order to reduce local "corner-flow" effects, the cross-flow calculation is performed on so-called "cell-net flow basis". Here, "corner flow" refers to cells with more than one cell-wall flows, of opposite direction, over the *ij* interface (e.g. may occur in tunnel corners and along the curved silo walls). In other words, "corner flows" are envisaged as typical discretisation artefacts that should not be included in the net flow over the subunit *i*. The cell-net flow for a cell with marker Mk = *i* is defined as,

$$Q_{ij}^{cell,net} = \sum_{n} Q_{ij}^{wall}, i \neq j. \qquad (5\text{-}2)$$

, where Q_{ij}^{wall} is the cell-wall flows from the grid cell (Mk = *i*) to *n* ambient grid cells (Mk = j ≠ *i*). The total cross flow over subunit *i* is then calculated as the sum of *positive* cell-net flows, ΣQ_{ij+}, and the sum of *negative* cell-net flows, ΣQ_{ij-}, for all cells with marker Mk = *i*. The cell marking defining disposal rooms and bedrock/HSD interface in the computational grid is presented in Table A-7.

The management of input and output data files during the automatized calculations of disposal-room flow is described in Appendix A4 (Table A-12).

5.4.2 Particle tracking

DarcyTools facilitates two inbuilt particle-tracking methods: 1) stream-line routing and 2) the so-called cell-jump method (Svensson et al. 2010). Unfortunately, the inbuilt particle-tracking methods are not very feasible due to the extensive demands of SR-PSU (involving multiple model setups and large numbers of particles released). Instead, particle tracking is performed as a post process applied to a steady-state flow field (i.e. outside the DarcyTools flow solver).

There are reasons for using a standalone post process:

1. Rapid execution time (processing steady-state solutions reduces particle tracking to a geometric problem, circumventing the computational demanding (and time consuming!) iterative time-stepping within the DarcyTools solver. The post-processor algorithm also allows simultaneous processing in parallel working folders).
2. Flexibility: the code can easily be adapted to meet the various needs within the SR-PSU project (customize definition of performance measures, target specific issues, etc).
3. File management: Output can be customized to meet the particular demands within the SR-PSU project (e.g. apply file-naming conventions, condense output to reduce file sizes, export in defined delivery structures, user-specified TecPlot output, etc).

In principle, the used algorithm [SR-PSU_Td18_p-track_random_deplete_loops.f] is very similar to the so-called "DarcyTools to MARFA interface" used in SR-Site Forsmark. It is based on the cell-jump method, where particles (i.e. discretisation of water volumes) traverse the computational grid on a cell-to-cell basis, according to inter-nodal flow between cells. The method assumes complete mixing of water in all cells, which implies a stochastic component in the routing of particle trajectories. A drawback of the method is that unfavourable conditions exaggerates the dispersion (i.e. non-alignment between the grid geometry and the flow direction forces the particle trajectories into a zig-zag pattern).

Particle-tracking principles and performance measures

A particle trajectory represents the advective flow path of a discretised water volume through the bedrock. The purpose of particle tracking is to quantify cumulative bedrock retention properties along an ensemble of trajectories. The evaluation targets only the retention properties in bedrock, and therefore no properties of tunnel-backfill or HSD are included in the performance measures.

Particles are released uniformly within disposal rooms (i.e. evenly distributed over cells identified as disposal rooms via cell markers, Table A-13). However, the "release point" is defined as the tunnel-wall passage (i.e. or put in other words, the bedrock entry point). A proportionality exists between density of particle-release points and tunnel-wall flux. Particle trajectories are terminated at the bedrock surface, where the "exit point" is defined by the cell wall between a bedrock cell and a HSD cell.

The probability, P_{ij}, of navigating from cell *i* to cell *j* is assumed to be proportional to the flow in that direction, Q_{ij}, where a *sign-criterion* applies to Q_{ij}, depending on the *direction* of particle tracking:

$$P_{ij} = \frac{Q_{ij}}{\sum Q_{ij}}. \qquad (5\text{-}3)$$

Particle tracking can be performed in two directions: in *forward* tracking, only outward-directed flows are included in Eq. (5-3), whereas in *backward* tracking only includes inward-directed flows.

The performance measures L_r, F_r, and $t_{w,r}$ (Section 1.3), are determined as cumulative bedrock properties for particle trajectories (i.e. from bedrock entry to bedrock exit). The underlying equations for accumulating these bedrock properties along a particle trajectory are presented below.

The total path length of particle trajectories, L_r (m), is calculated as the sum of distances between the centre points of passed cell walls. Note that cell-wall centre coordinates are used in the path-length calculation, as opposed to cell-centre coordinates. The purpose of using cell-wall centre coordinates is to allow for diagonal "corner cutting" through cells (i.e. to some extent reducing the overestimation due to rectilinear nature of particle jumps).

Likewise, the advective travel time of a flow path, $t_{w,r}$ (y), is determined as the sum of travel times for each discrete particle step along the trajectory. The discrete travel time, t_{ij}, taken to move from the centre of cell *i* to the centre of cell *j*, is assumed to be:

$$t_{ij} = \frac{n_i V_i + n_j V_j}{2Q_{ij}}, \qquad (5\text{-}4)$$

, where *n* is cell porosity and *V* is cell volume (i.e. the product *nV* is the cell volumetric water content). The factor 2 in the denominator reflects that only *half* of the cell volumetric water contents, $n_i V_i$ and $n_j V_j$, are involved in the inter-nodal flow Q_{ij}.

Analogously, the cumulative flow-related transport resistance, F_r (y/m), or F-quotient, is also determined as the summed bedrock properties for discrete particle jumps. The transport resistance for each discrete jump, from cell centre *i* to cell centre *j*, F_{ij}, is assumed to be:

$$F_{ij} = a_w t = \frac{fws_i + fws_j}{2Q_{ij}}, \qquad (5\text{-}5)$$

, where a_w is flow-wetted fracture surface area per volume of water and *fws* is the flow-wetted fracture surface areas in cells *i* and *j*, respectively (based on Svensson et al. 2010 and MARFA interface). Calculated performance measures only reflect the bedrock; therefore, both porosity and *fws* are nullified in tunnel backfill and in overlying sediments.

The management of input and output data files during the automatized particle-tracking analysis is described in Appendix A4 (Table A-13).

6 Results

6.1 Simulation of the top-boundary condition

This section demonstrates the first phase of the groundwater flow simulations, where the top-boundary condition is determined (i.e. the preceding "Recharge phase" Section 5.3.2). Owing to the automatized execution approach (Section 5.3), all bedrock cases are simulated under the same premises (convergence criteria, number of iterations, etc.). As an example, the top-boundary condition of the base case (BASE_CASE1_DFN_R85_EXT01) are presented for the first six time slices (2000 AD to 3000 AD). The figures follow the same format as was used in Öhman et al. (2014) to facilitate comparison against earlier results.

Topography and shoreline retreat

The shoreline retreat in the SFR near-field is shown for the six selected time slices (Figure 6-1). Note that all elevations are expressed in the so-called fixed-bedrock reference system, where the sea level is envisaged as declining, relatively to a static bedrock surface (Section 3.3.5). Pre-defined surface water areas in RLDM (lakes and rivers) are shown as blue-grey surfaces. During simulations, the simulated head is monitored below two topographical peaks (one in the pier and the other in an islet, east of the pier; grey points in Figure 6-1). The numerical convergence and the simulated turnover from submerged to terrestrial conditions can then be evaluated at these monitoring points (Figure 6-5, Figure 6-6, and Figure 6-7).

Local recharge and fixed head

The recharge is allowed to vary locally (0 to 160 mm/yr; contoured in Figure 6-2), but switched to "fixed-head" conditions where the simulated head in ground-surface cells exceeds its tolerance (Figure 5-1), even for a zero recharge (pink cells in Figure 6-2). The simulated recharge has a rather patchy pattern of "binary character" (i.e. distinct recharge and discharge subareas). For example, the coarse material in the SFR pier infiltrates the maximum recharge (dark red in Figure 6-2), while the marine deposits emerging above sea level at 2500 AD to 3000 AD infiltrates little recharge (blue areas in Figure 6-2).

The fixed-head conditions tend to occur: 1) along the coast line, 2) along topographical depressions (i.e. typical discharge areas), and 3) in low-conductive sediments (c.f. Figure 4-16).

Relative ground-surface head

The simulated ground-surface conditions are demonstrated in terms of "relative head" (Figure 6-3). This relative head is expressed as ground-surface head relative to local ground surface, $H - z_{DEM}$ (m, elevation in fixed-bedrock reference), where z_{DEM} refers to the local basin-filled DEM elevation (Section 3.3.2). In other words, this measure demonstrates the difference between the *applied boundary condition* (i.e. simulated head) versus the simpler boundary condition assuming $H = z_{DEM}$ (discussed in Section 5.3). *Less strictly speaking*, this relative head can be envisaged as an approximate measure of groundwater depth (i.e. this analogy requires that the vertical hydraulic gradients are negligible).

Low relative head (contoured blue) signifies areas with deep groundwater table. For example, this occurs at local topographical peaks and particularly so if the material is highly conductive (i.e. such as the SFR pier and its surrounding fill; Figure 6-1). Vice versa, high relative head (contoured red) indicate saturated areas, where groundwater table is at or close to the ground surface (i.e. Figure 6-1). This occurs in topographical depressions and/or in the presence of low-conductive deposits (Figure 4-16).

Top-boundary head

In general, the simulated head at ground surface has a smoother appearance, as compared to topography (e.g. islets east of the pier; c.f. Figure 6-1 and Figure 6-4). Owing to spatial contrasts in HSD-conductivity (Figure 4-16), the ground-surface head does not necessarily follow topography variations intimately (Figure 6-4). For example, the high-conductive fill material renders an even head pattern in the pier (i.e. low horizontal gradient). Notably, at 2000 AD, the maximum head inside the pier is only one centimetre above sea level, while during later stages of shoreline retreat its head (groundwater table) becomes controlled by the surrounding elevation of low-conductive sediments in all directions (Figure 6-7). Isolated local peaks in head are noted in a few small islets that emerge out of the sea at c. 3000 AD. These islets are not assigned fixed-head (Figure 6-2), but reflect the recharge-simulation result of low-conductive outcropping bedrock (i.e. depending on the underlying DFN realisation).

Monitored performance

As an example of model performance, the simulated head at two points below topographical peaks is monitored during the simulation progress (Figure 6-5, Figure 6-6 and Figure 6-7). The lateral positions of these monitoring points are shown as grey points in Figure 6-1 to Figure 6-4, and their elevations are $z=-7$ m in the pier (i.e. in the assumed till; Figure 4-17), and $z=-4$ m in the islet east of the pier (i.e. in the bedrock).

The overall convergence of the flow solution is evaluated in terms of the root-mean-square error in the head solution (i.e. standard DarcyTools output). After the initial recharge phase, run in 100 iterations, the subsequent steady-state phase is run for 25 iterations, which improves the convergence by c. 4 orders of magnitude (e.g. Figure 6-5a). This convergence is considered to provide sufficient accuracy for the later post-processing (Section 5.4). As the exception, bedrock case 6, with high constant K_{HRD}, required more than 25 steady-state iterations to provide a satisfactory mass-balance error for the silo (Section 6.2).

At 2000 AD, the head in the pier stabilises rapidly to c. 1.5 cm above sea level (Figure 6-5b). At later stages, the head in the pier is still rising at the end of the recharge phase (Figure 6-6f), after which it stabilises rapidly – with only minor changes – in the steady state phase. This suggests that a higher head could have been obtained in the pier if only the recharge phase would have been prolonged by additional iterations. However, this notion must be considered in context of three model uncertainties:

1. Uncertainties regarding material properties in the SFR pier are discussed in Section 4.5. For example, the significance of potential natural deposits below the fill material is expected to outweigh the observed uncertainty regarding the groundwater level in the SFR pier.
2. The combination of variable cell size in a rotated model-coordinate system causes an ambiguity in the mapping between DarcyTools grid cells and the ground-surface level, as modelled in RLDM. This uncertainty has been judged to correspond to a 0.25 m tolerance in the ground-surface head criterion (Section 5.3.2), which can be taken as an approximate estimate of the level of accuracy in the determined groundwater level.
3. The mixed boundary condition is a novelty in DarcyTools modelling, and as such it has not yet reached its full potential. A limitation in the current implementation is that the change in boundary-condition type is, as yet, permanent (i.e. one-way switch from flux to prescribed head). A consequence of this is that numerical oscillations tend to successively “trap” ground-surface cells into the prescribed-head condition, which in turn causes an artificial gradual rise in groundwater level with iterations. Hence it is motivated to interrupt the recharge phase before reaching a fully stationary appearance. Based on judgment of simulation results (Figure 6-1 to Figure 6-4) and convergence appearance (Figure 6-5 and Figure 6-6), it was decided to run the recharge phase for 100 iterations.

The monitored points also demonstrate the turnover in flow regime that occurs during the period 2500 AD to 3500 AD (Figure 6-7):

1. During the early time slices, up to 2500 AD, the simulated head at the two points intimately follows the retreating sea, which is indicative of “submerged conditions” (i.e. land uplift has

not yet reached its full effect on bedrock flow; flow is still driven by the regional-scale gradient between the Forsmark inland and the sea).

2. the transition occurs during 2500 AD to 3500 AD, which is manifested by the simulated head at the two monitoring points falling off from the retreating sea (i.e. parts of the SFR pier are starting to hold groundwater above the sea level, which forms local hydraulic gradients).
3. the flow field gradually matures into stationarity (i.e. terrestrial conditions, where the bedrock flow at SFR depths become fully driven by the hydraulic gradients of the local groundwater table, and is no longer affected by further shoreline retreat).

The same succession is also observed in the analysis of tunnel flow over time (Section 6.2).

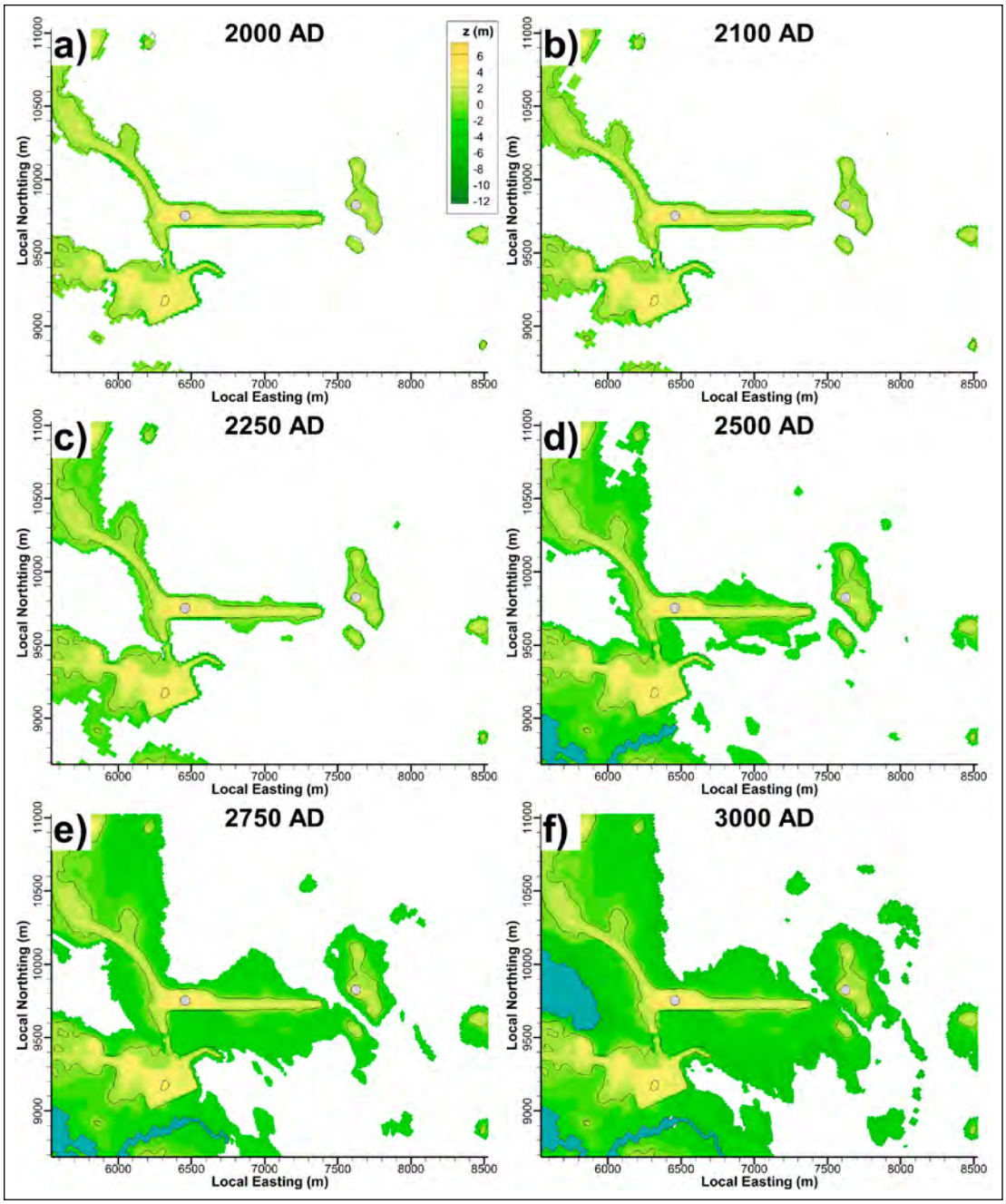

Figure 6-1. *Elevation of ground-surface cells expressed in the fixed-bedrock reference (Section 3.3.5) showing the retreating sea. Pre-defined surface water shown as blue-grey surfaces. Head is monitored below topographical peaks in the pier and in an islet east of the pier (grey points).*

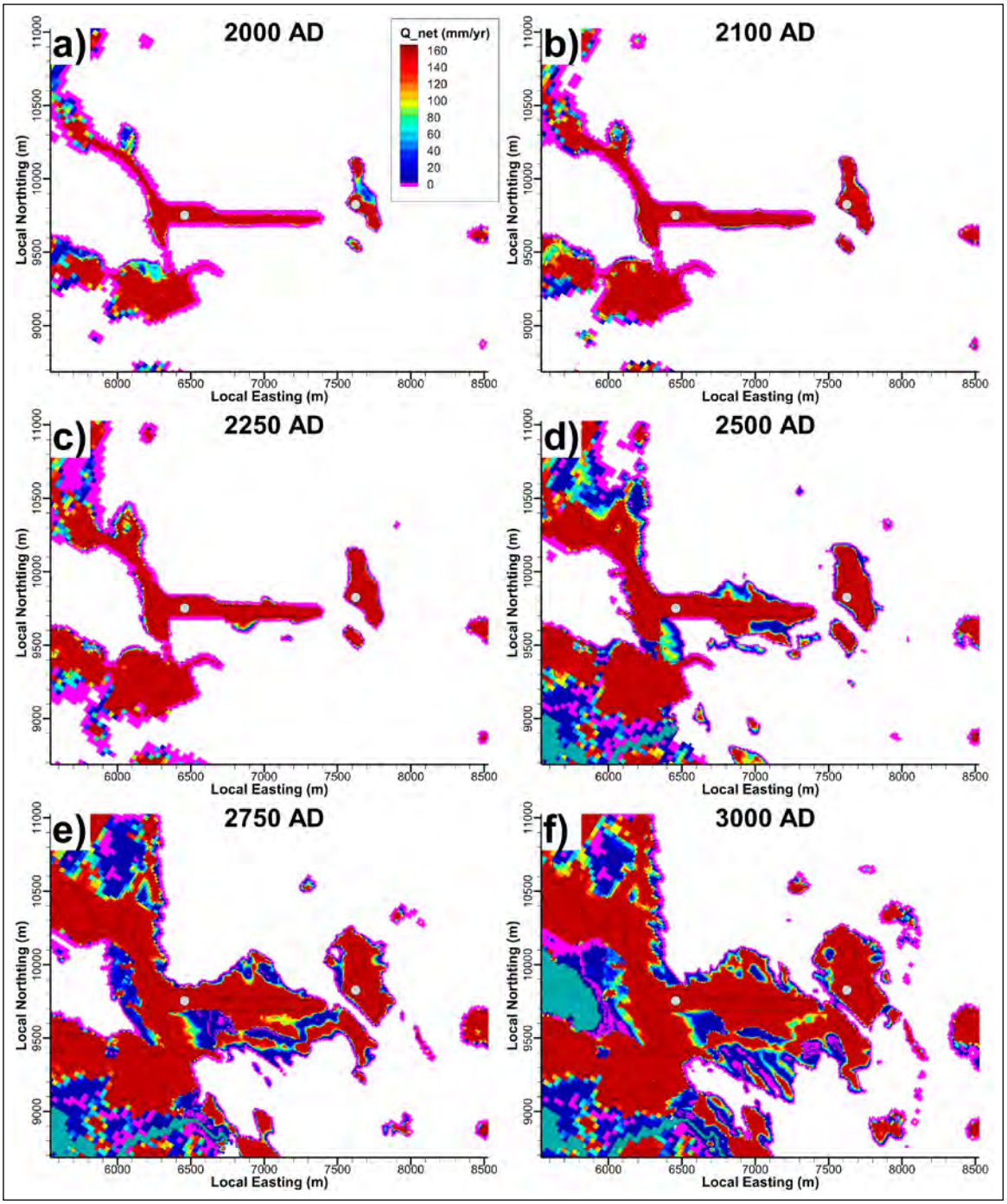

Figure 6-2. *Simulated local recharge in the base case for early time slices (fixed-head cells in pink). Head monitored below topographical peaks in the pier and in an islet east of the pier (grey points).*

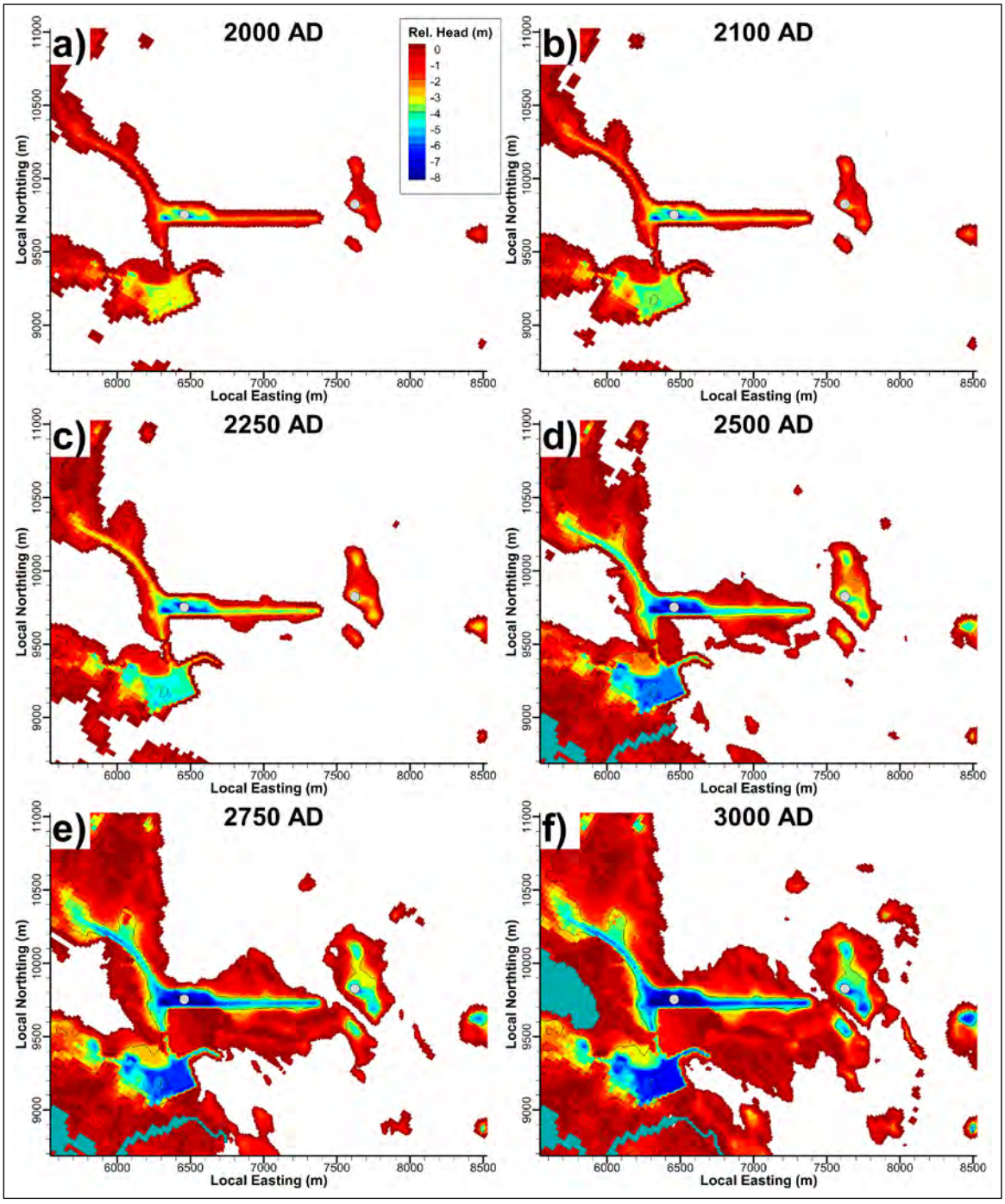

Figure 6-3. *Simulated relative ground-surface head, $H - z_{DEM}$ (m), in the base case for early time slices. This relative head is expressed as head in the uppermost active cell layer, relative to local elevation of ground surface. Pre-defined surface water shown as blue-grey surfaces. Head monitored below topographical peaks in the pier and in an islet east of the pier (grey points).*

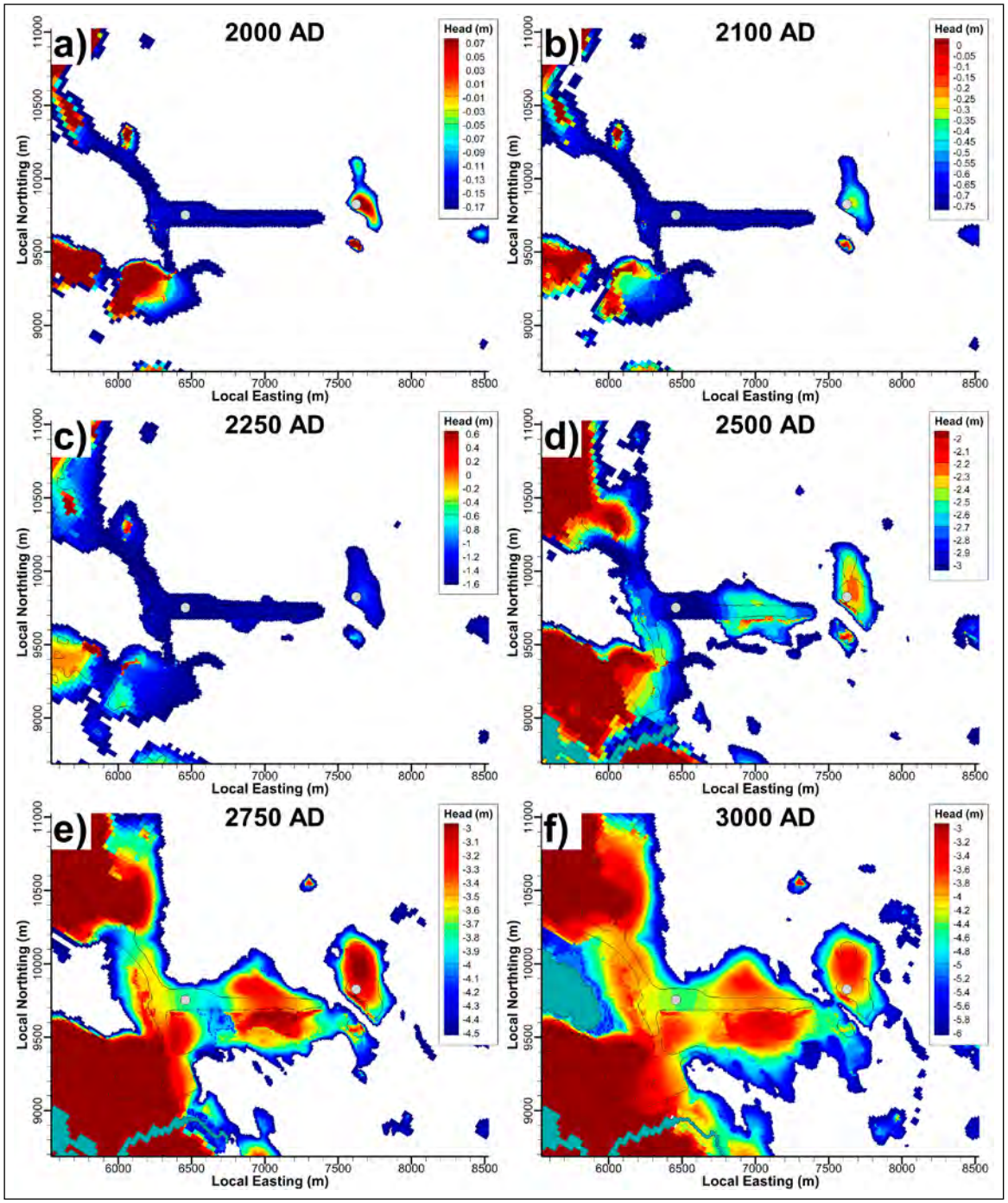

Figure 6-4. *Simulated ground-surface head in the base case for studied time slices. Head is expressed in the fixed-bedrock reference (Section 3.3.5). Pre-defined surface water shown as blue-grey surfaces. Head monitored below topographical peaks in the pier and in an islet east of the pier (grey points).*

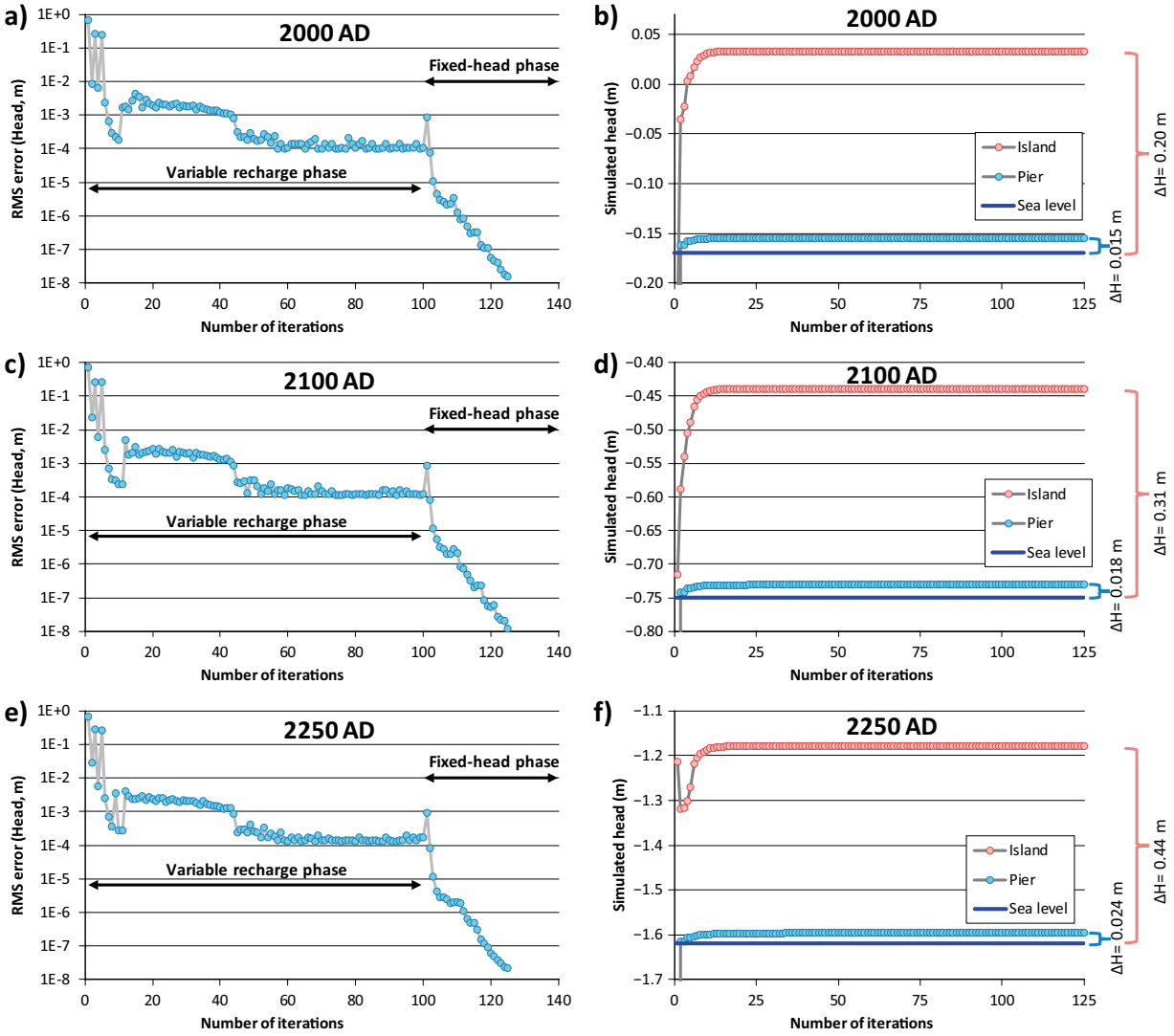

Figure 6-5. *Summary of the two flow-simulation phases for BASE_CASE_1_DFN_R85_EXT01; flow-solution convergence and monitored head at two points (location indicated by grey points in Figure 6-1 to Figure 6-4). Extracted data from the history files in Table A-11.*

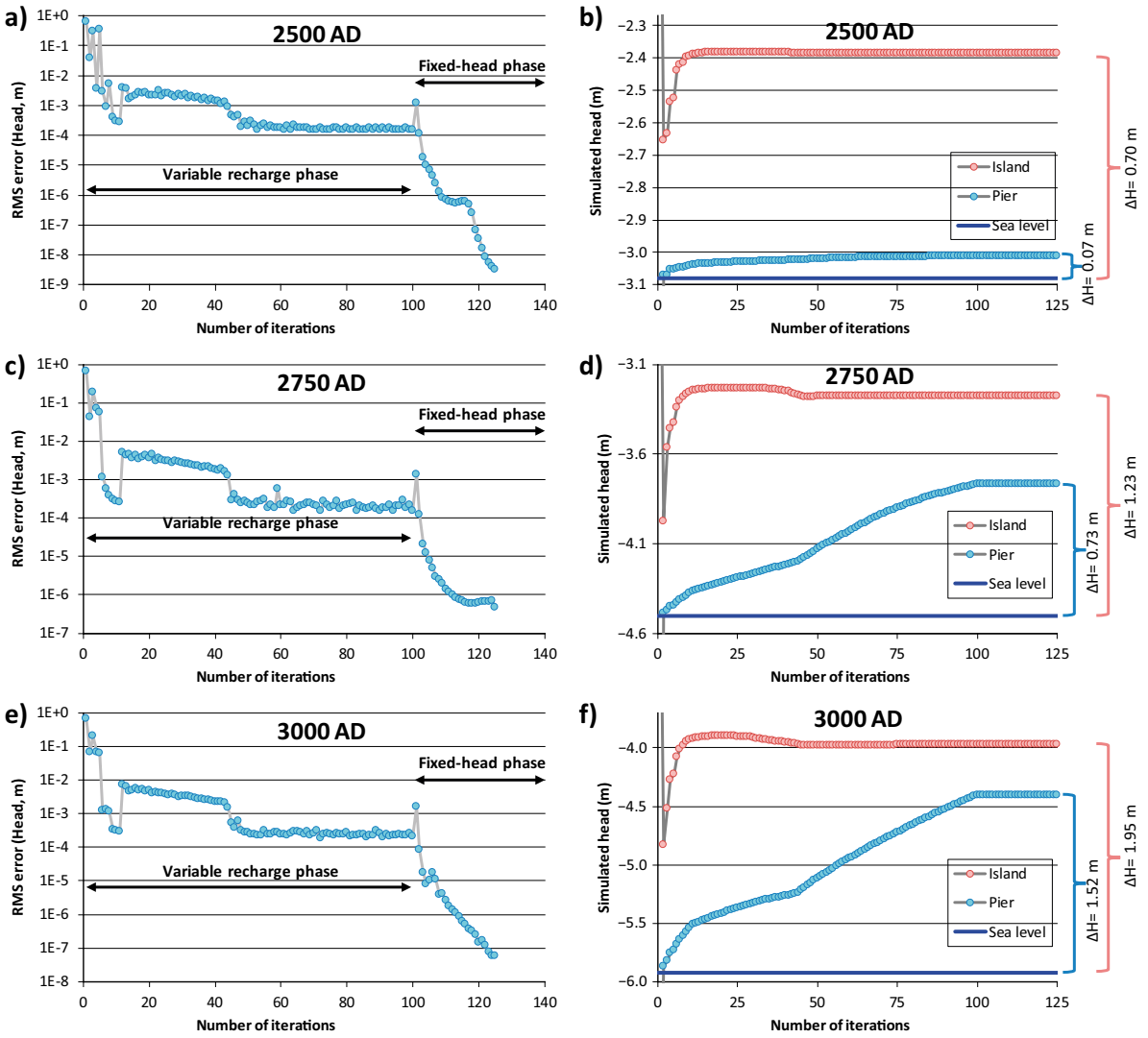

Figure 6-6. *Summary of the two flow-simulation phases for BASE_CASE_1_DFN_R85_EXT01; flow-solution convergence and monitored head at two points (location indicated by grey points in Figure 6-1 to Figure 6-4). Extracted data from the history files in Table A-11.*

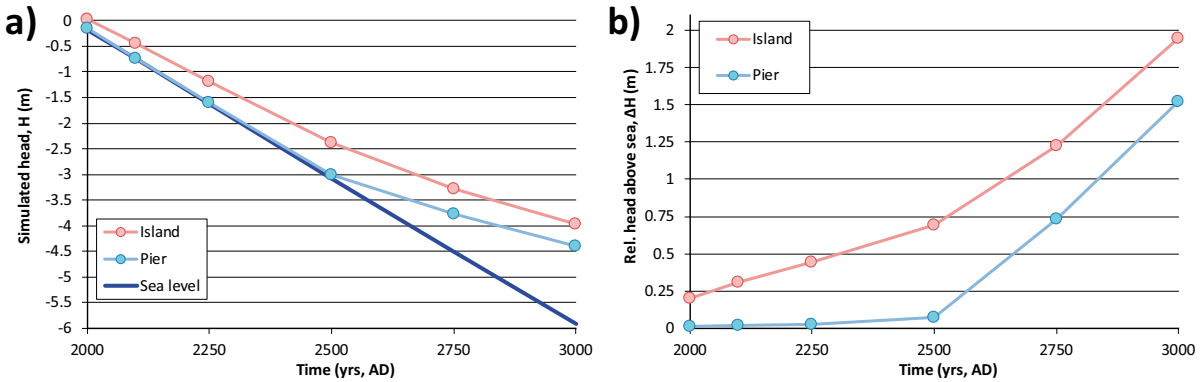

Figure 6-7. *Simulated head over time at two points below topographical peaks: the SFR pier and in an islet east of the pier (grey points in Figure 6-1); a) head expressed in the fix-bedrock reference, H (m), and b) relative head above sea, ΔH (m).*

6.2 Cross flow in disposal rooms

6.2.1 Mass balance in flow calculation

Cross flow over disposal rooms are evaluated for all bedrock cases and all time slices (i.e. 30 bedrock cases × 9 time slices × 11 disposal rooms = 2 970 tunnel flows). A relative mass-balance error in disposal-room cross flow can be determined as: $(\Sigma Q_{ij+} - |\Sigma Q_{ij-}|)/\Sigma Q_{ij+}$, see Eq. (5-2). Overall, the relative error is generally very low, with a maximum of 1 % (Figure 6-8). The largest relative errors (> 0.1 %) are associated to the disposal rooms of SFR3 during the low flow at early stages of shoreline retreat (Figure 6-9).

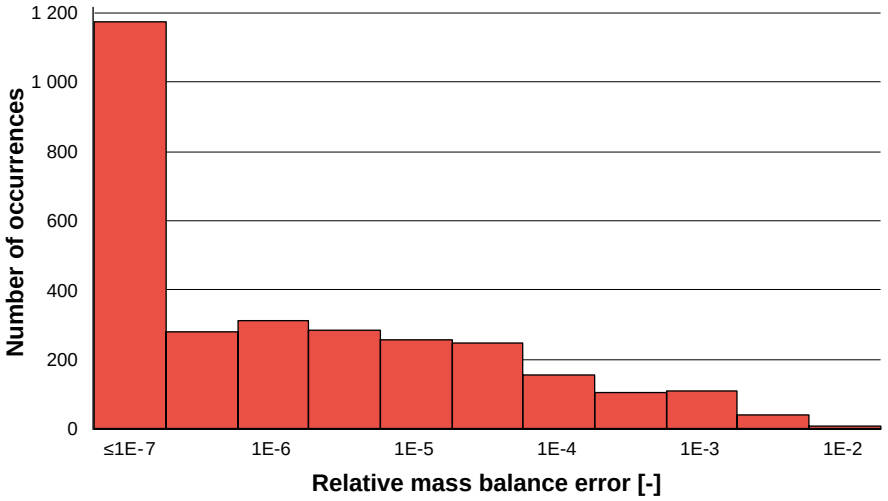

Figure 6-8. *Distribution of mass balance error for 2 970 evaluated tunnel flows.*

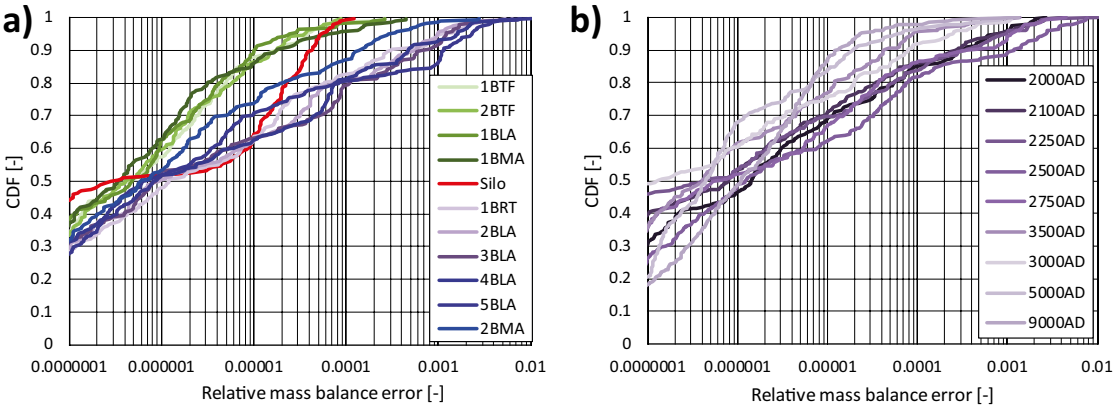

Figure 6-9. *Cumulative distribution of mass balance error; a) per disposal room and b) per time slice.*

6.2.2 Overview of simulation results

The range of simulated disposal-room cross flow among the bedrock cases can be illustrated by means of box-whisker plots. The grey-shaded box covers 50 % of the simulated cross flows (first to third quartiles) and the median bedrock case is shown by a black line (Figure 6-10). The whiskers indicate the bedrock cases with minimum and maximum flow, respectively. Most of the bedrock cases are associated to minor variation in tunnel flow (small boxes compared to whiskers); the maximum variation (i.e. whiskers) reflects cases with constant K_{HRD} (Section 6.2.4). Owing to the bentonite-sealed walls of the Silo, its cross flow through is considerably lower than it is over other disposal rooms.

The disposal-room cross flow increases during the early of stages shoreline retreat, to reach approximately stationary conditions at c. 3500 AD to 5000 AD (Figure 6-11 and Figure 6-12). From the time slice of c. 3000 AD, 1BLA and 1BMA stand out with higher cross flows; this is probably related to their intersection with deformation zone ZFMNNW1209 (formerly referred to as Zone 6). Among the SFR 3 disposal rooms, 2BMA stands out with higher cross flows, particularly at early time slices. The disposal rooms 4BLA, 5BLA, and 2BMA exhibit comparatively larger interquartile variability than 1BRT, 2BLA, and 3BLA at the later stages of shoreline retreat (Figure 6-12a-c); the reason for this is that the former (rock caverns 4BLA, 5BLA, and 2BMA) are subject to the parameterisation uncertainty of conditioning intercepts of ZFMWNW0835 (see Figure 4-8).

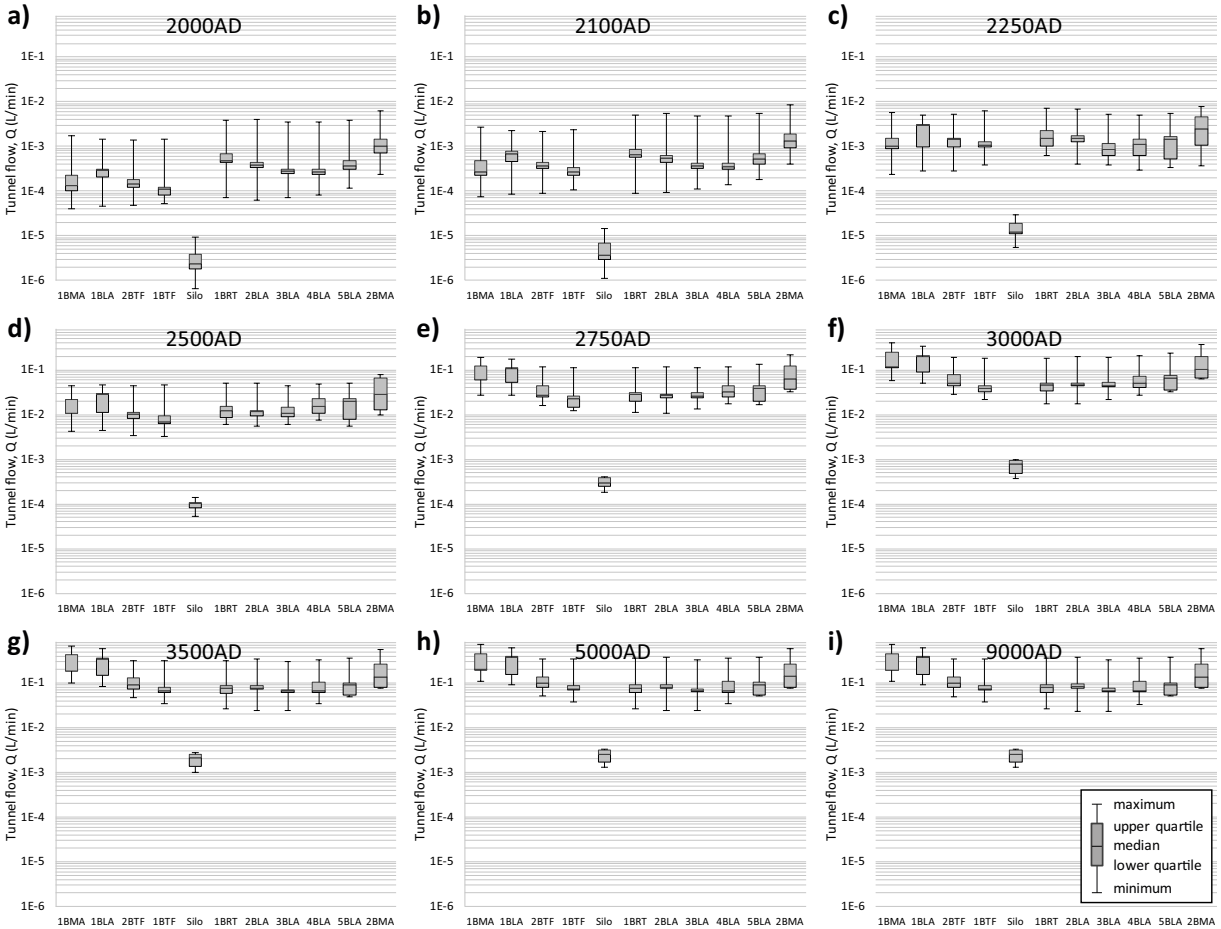

Figure 6-10. *Box-whisker plots of the distribution of simulated disposal-room cross flow in the sensitivity study of 30 bedrock cases (Table 2-2). Distributions of individual disposal rooms are compared, and the progress over time is shown for 6 time slices (Table 2-1). The low cross flow through the Silo is resolved in Figure 6-11.*

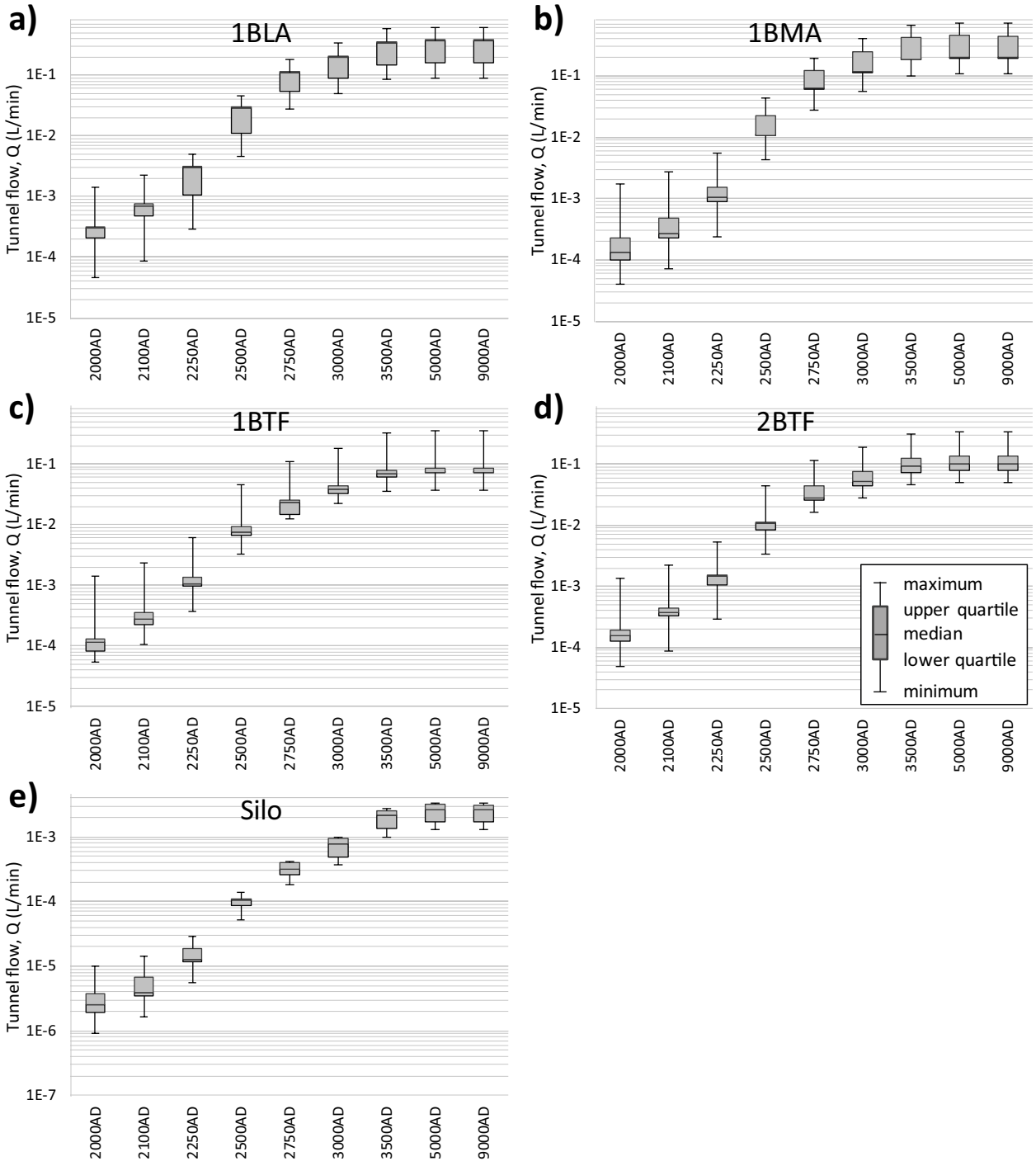

Figure 6-11. *Simulated disposal-room cross flow in SFR1 over time (9 time slices); variability of 30 bedrock cases (Table 2-2) demonstrated by box-whiskers.*

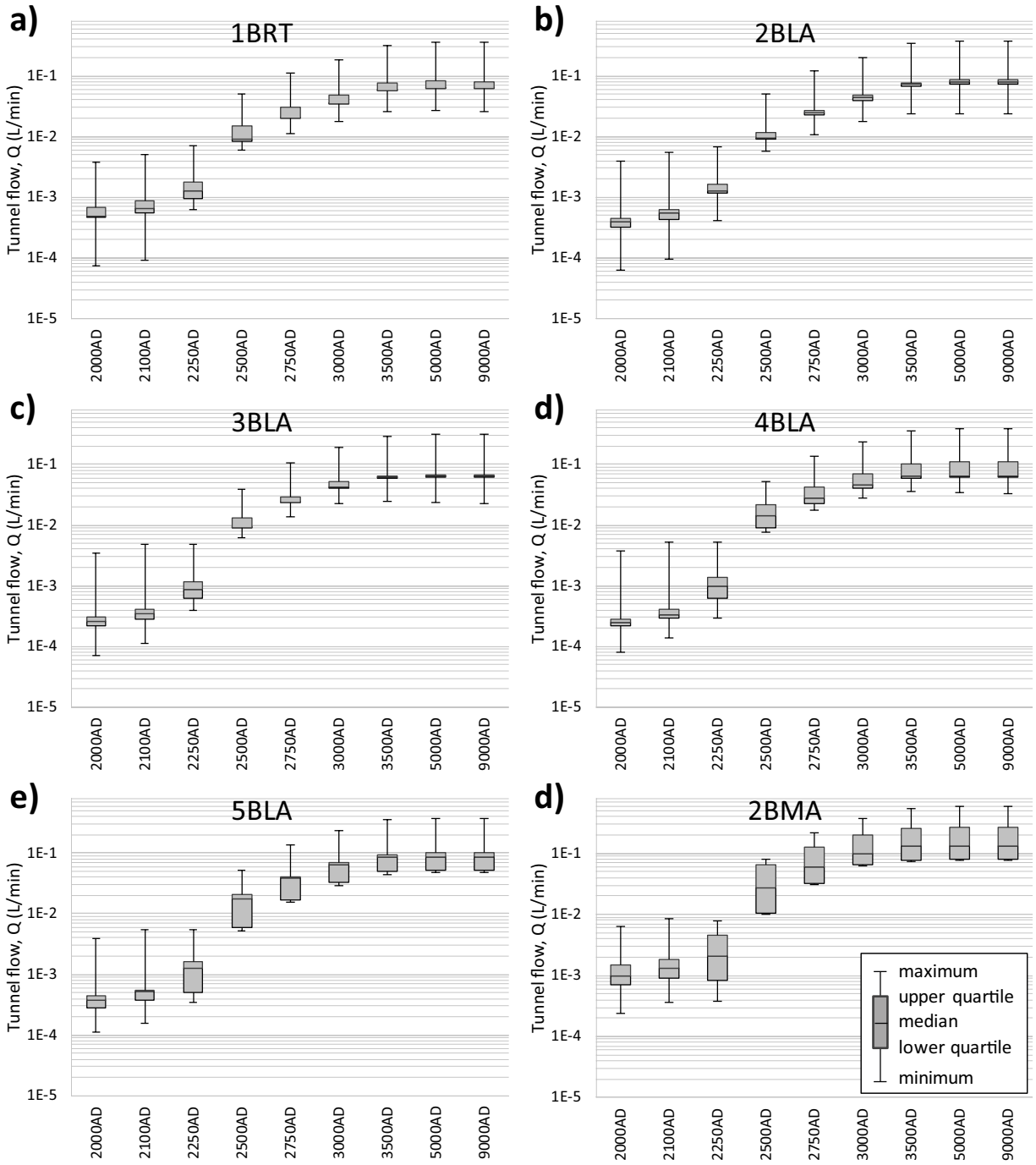

Figure 6-12. *Simulated disposal-room cross flow in SFR3 over time (9 time slices); variability of 30 bedrock cases (Table 2-2) demonstrated by box-whiskers.*

Sensitivity to bedrock parameterisation

The significance of different components in bedrock parameterisation are evaluated by comparing the simulated disposal-room crossflows in terms of a relative-ranking concept. This approach is partly based on the analysis in TD11 (Öhman et al. 2014), where each simulated disposal-room crossflow is assigned a percentile based on the rank within its population of 30 bedrock cases per each time slice (percentile = 1 – rank/n + 0.5/n, for n = 30). The ranking and percentile assignment is specific for each disposal room, which means that for a given simulated model setup (i.e. bedrock case and time slice) 11 different flow percentiles are calculated.

To provide an overview of the sensitivity to different bedrock-parameterisation components, in terms of disposal-room flow, these 11 individual values are lumped into an average percentile over the repository (Table 6-1). However, it should be noted that this average percentile does not resolve the internal variability between disposal rooms (i.e. exceptionally low and high individual disposal-room flows may balance out for a given model setup, appearing as an "average" bedrock parameterisation in terms of the average flow percentile). It should also be noted that average flow rank may change over time; for example, the Singö-barrier cases 19 and 20 only rank as low disposal-room flow during the early stages of shoreline retreat, whereas the low rank for case 15 (i.e. selected as the low-flow representative bedrock case) appears at c. 2250 AD. Note also that the cases of constant HRD parameterisation inside the SFR Regional domain (i.e. C01, C02, and C03 in cases 6, 7, 8) rank as low-, intermediate-, and high-flow cases.

Table 6-1. Average flow percentile[1)] for bedrock cases.

		Time slice (AD)								
No.	Bedrock case	2000	2100	2250	2500	2750	3000	3500	5000	9000
1*	BASE_CASE1_DFN_R85_EXT1	0.40	0.42	0.36	0.39	0.41	0.41	0.38	0.30	0.37
2	BASE_CASE1_DFN_R85_EXT02	0.33	0.35	0.33	0.32	0.34	0.29	0.28	0.48	0.48
3	BASE_CASE1_DFN_R85_EXT11	0.36	0.38	0.33	0.42	0.33	0.32	0.45	0.28	0.41
4	BASE_CASE1_DFN_R85_EXT12	0.30	0.31	0.33	0.36	0.33	0.25	0.30	0.44	0.47
5	nc_Si1_HOM_HRD_C02_EXT01	0.81	0.76	0.51	0.39	0.36	0.33	0.40	0.39	0.38
6	nc_Si1_R01_HRD_C01_EXT01	0.03	0.03	0.10	0.13	0.11	0.12	0.11	0.11	0.11
7	nc_Si1_R01_HRD_C02_EXT01	0.76	0.70	0.44	0.43	0.41	0.40	0.40	0.38	0.38
8	nc_Si1_R01_HRD_C03_EXT01	0.98	0.98	0.98	0.98	0.93	0.91	0.91	0.91	0.91
9	nc_Si1_R01_DFN_R03_EXT02	0.27	0.24	0.43	0.45	0.50	0.54	0.46	0.49	0.47
10	nc_Si1_R01_DFN_R03_EXT01	0.31	0.28	0.43	0.49	0.53	0.57	0.51	0.45	0.47
11*	nc_DEP_R07_DFN_R85_EXT1	0.72	0.73	0.76	0.71	0.71	0.75	0.73	0.69	0.66
12	nc_Si1_R07_HRD_C02_EXT01	0.90	0.87	0.76	0.64	0.56	0.50	0.56	0.54	0.53
13	CD_Si1_R07_DFN_R85_EXT01	0.45	0.50	0.57	0.60	0.67	0.63	0.67	0.69	0.70
14	nc_Si1_R01_DFN_R85_EXT01	0.41	0.44	0.60	0.63	0.64	0.68	0.66	0.61	0.58
15*	nc_NoD_R01_DFN_R18_EXT1	0.57	0.58	0.22	0.19	0.21	0.22	0.22	0.22	0.22
16	nc_Si1_R07_DFN_R85_EXT02	0.64	0.65	0.75	0.68	0.64	0.66	0.62	0.73	0.71
17	nc_Si1_R07_DFN_R18_EXT02	0.39	0.37	0.38	0.56	0.59	0.57	0.49	0.49	0.48
18	nc_Si1_R07_DFN_R03_EXT02	0.52	0.42	0.59	0.64	0.62	0.57	0.59	0.62	0.61
19	CD_Si2_HOM_DFN_R85_EXT01	0.07	0.10	0.28	0.46	0.48	0.43	0.52	0.49	0.50
20	CD_Si3_HOM_DFN_R85_EXT01	0.13	0.16	0.27	0.45	0.43	0.40	0.54	0.38	0.27
21	CD_Si4_HOM_DFN_R85_EXT01	0.34	0.36	0.35	0.46	0.47	0.35	0.41	0.37	0.29
22	nc_Si1_R07_DFN_R85_EXT11	0.68	0.68	0.75	0.75	0.67	0.70	0.69	0.66	0.71
23	nc_Si1_R07_DFN_R85_EXT12	0.57	0.65	0.78	0.78	0.74	0.73	0.73	0.76	0.77
24	nc_Si1_R01_DFN_R85_EXT11	0.37	0.41	0.61	0.66	0.62	0.67	0.62	0.58	0.61
25	nc_Si1_R01_DFN_R85_EXT12	0.33	0.37	0.61	0.59	0.64	0.62	0.56	0.53	0.53
26	BASE_CASE1_DFN_R85_EXT00	0.58	0.57	0.43	0.33	0.38	0.54	0.41	0.60	0.59
27	BASE_CASE1_DFN_R85_EXT10	0.56	0.56	0.40	0.27	0.29	0.43	0.23	0.41	0.50
28	nc_Si1_HOM_HRD_C02_EXT00	0.93	0.88	0.64	0.42	0.47	0.49	0.47	0.43	0.42
29	nc_Si1_HOM_HRD_C02_EXT10	0.90	0.84	0.61	0.45	0.47	0.46	0.51	0.52	0.53
30	BASE_CASE1_DFN_R85_EXT01	0.39	0.42	0.39	0.38	0.43	0.45	0.53	0.47	0.33

* Bedrock cases 1, 11, and 15 are referred to as the representative cases (i.e. base case and its bounding cases). These are identical to those used in (Öhman et al. 2014). The output of these three cases will be delivered to the Comsol near-field simulations, and are therefore executed separately. Neither of these three cases involve variants of Singö, and hence their second sub string (char4:6) refers to the usage of depth trend (DEP = yes, NoD = No).

[1)] Colour-coded to enhance the relative ranking of different bedrock cases in terms of disposal-room flow (i.e. blue = low, white = intermediate, and red = high).

6.2.3 Comparison against earlier results

Representative bedrock cases

The impact of the updated plugging/backfill and the layout of the SFR3 extension, L2.6 (Section 3.2), can be evaluated by comparing the simulated disposal-room cross flows against an earlier study (e.g. Öhman et al. 2014). The present simulation results are compared to those of TD11, based on the three representative bedrock cases 1, 11, and 15 (Table 2-2) and six time slices (c.f. lines and dots in Figure 6-13).

Overall the TD11 disposal-room flows are consistently reproduced, which means that, as implemented in the model, the updated plugging/backfill and layout of SFR3 generally has minor impact on modelling results. Detailed inspection reveals a minor increase in simulated disposal-room flow. The largest increases in simulated flow are associated to:

- time slice 2500 AD: this time slice is identified as the transition period between submerged and terrestrial conditions, at which the results are sensitive to ground-surface conditions.
- 1BRT (and, to a lesser extent, all five disposal rooms of SFR1): this finding is in line with expectations. The layout revisions for SFR3 primarily concerns the access tunnel for 1BRT (i.e. its hydraulic connection to ground surface, which is now shared with the disposal rooms of SFR1).

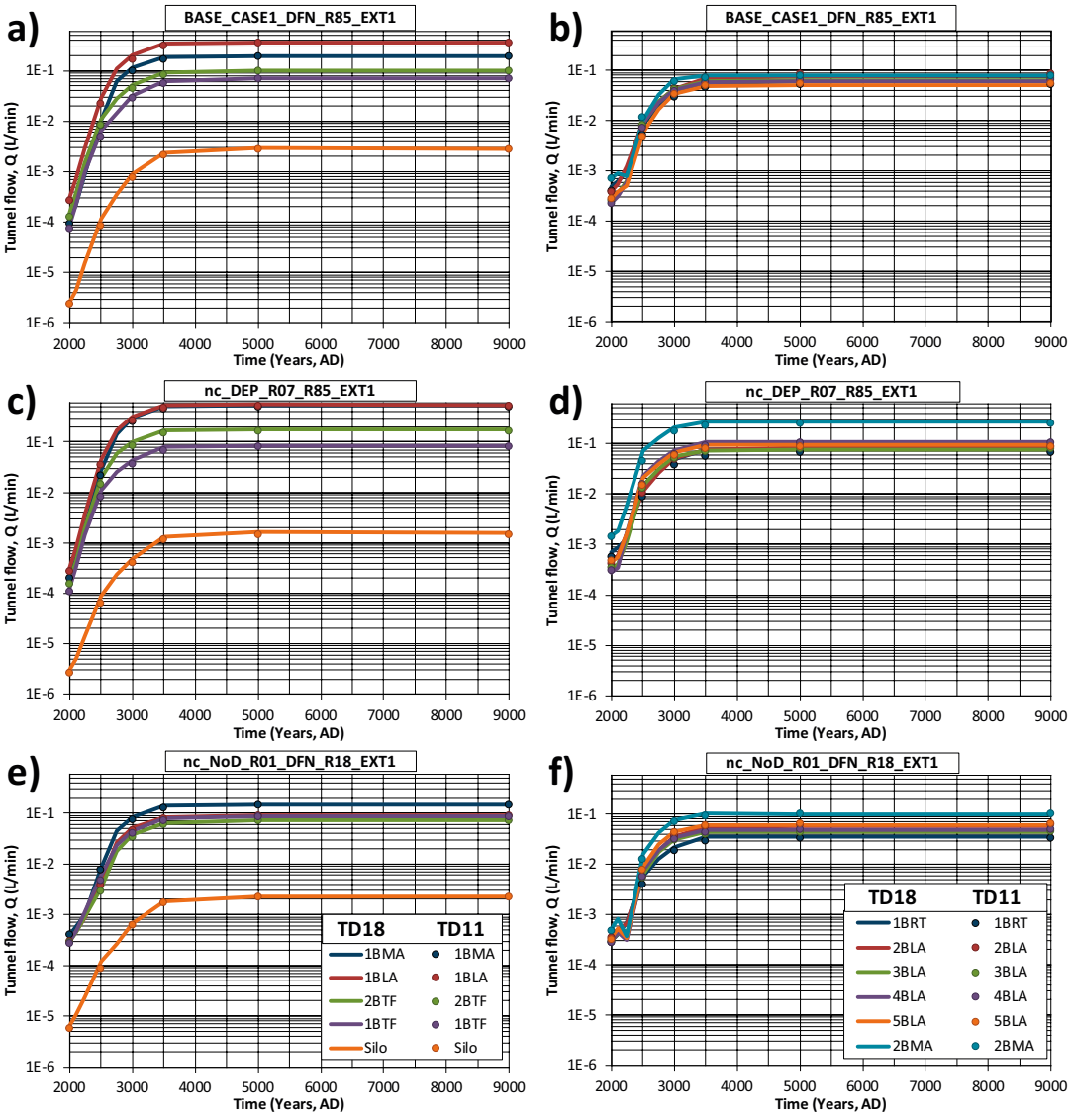

Figure 6-13. *Present simulated disposal-room cross flows (TD18; lines) compared to earlier simulation results (TD11; dots). The comparison involves three bedrock cases (the representative cases 1, 11, and 15; Table 2-2) and six time slices.*

Comparison between full bedrock case ensembles

The simulated disposal-room crossflows are also compared against the earlier results in terms of the full bedrock case ensembles (i.e. all 30 bedrock cases in the present study, against the 17 cases in TD11). In this comparison, it should be noted that the objective in TD11 was to screen a plausible setup of realistic bedrock parameterisations, in order to define three representative bedrock cases, while the present study targets more extreme parameterisation cases, including those identified as anomalous in earlier SR-PSU modelling. Thus, the span of the previous simulation results are not expected to be reproduced in this study. For example, the span between the minimum/maximum values in present study widely exceed those of the previous study (i.e. the comparatively long whiskers in TD18; Figure 6-14 to Figure 6-16); these minimum/maximum values are associated to the constant hydraulic conductivity K_{HRD} cases (i.e. not data-based cases; see also Section 6.2.4).

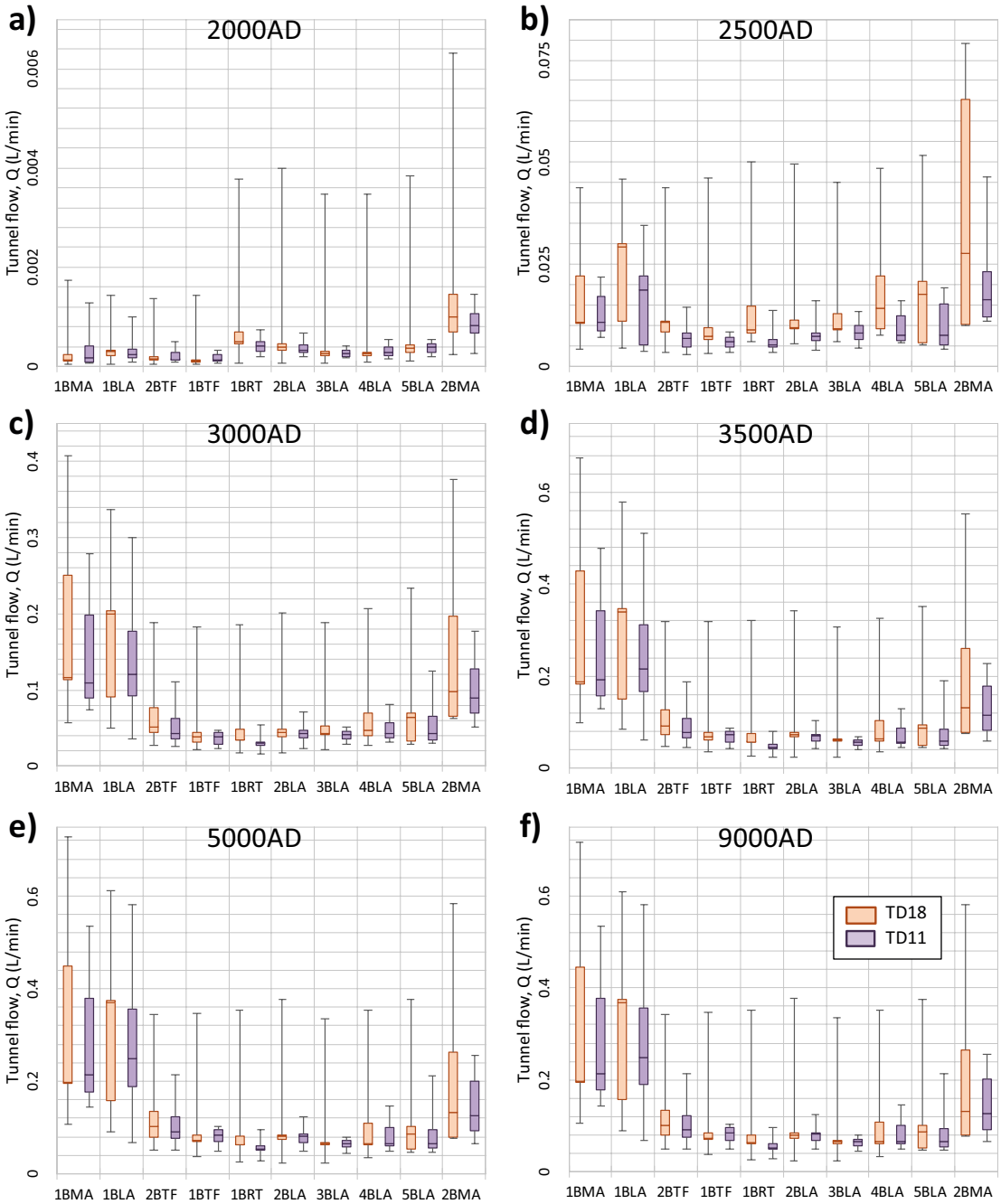

Figure 6-14. *Simulated disposal-room cross flow (TD18; orange) compared to results from earlier study (TD11; purple). Linear scaling on y-axis.*

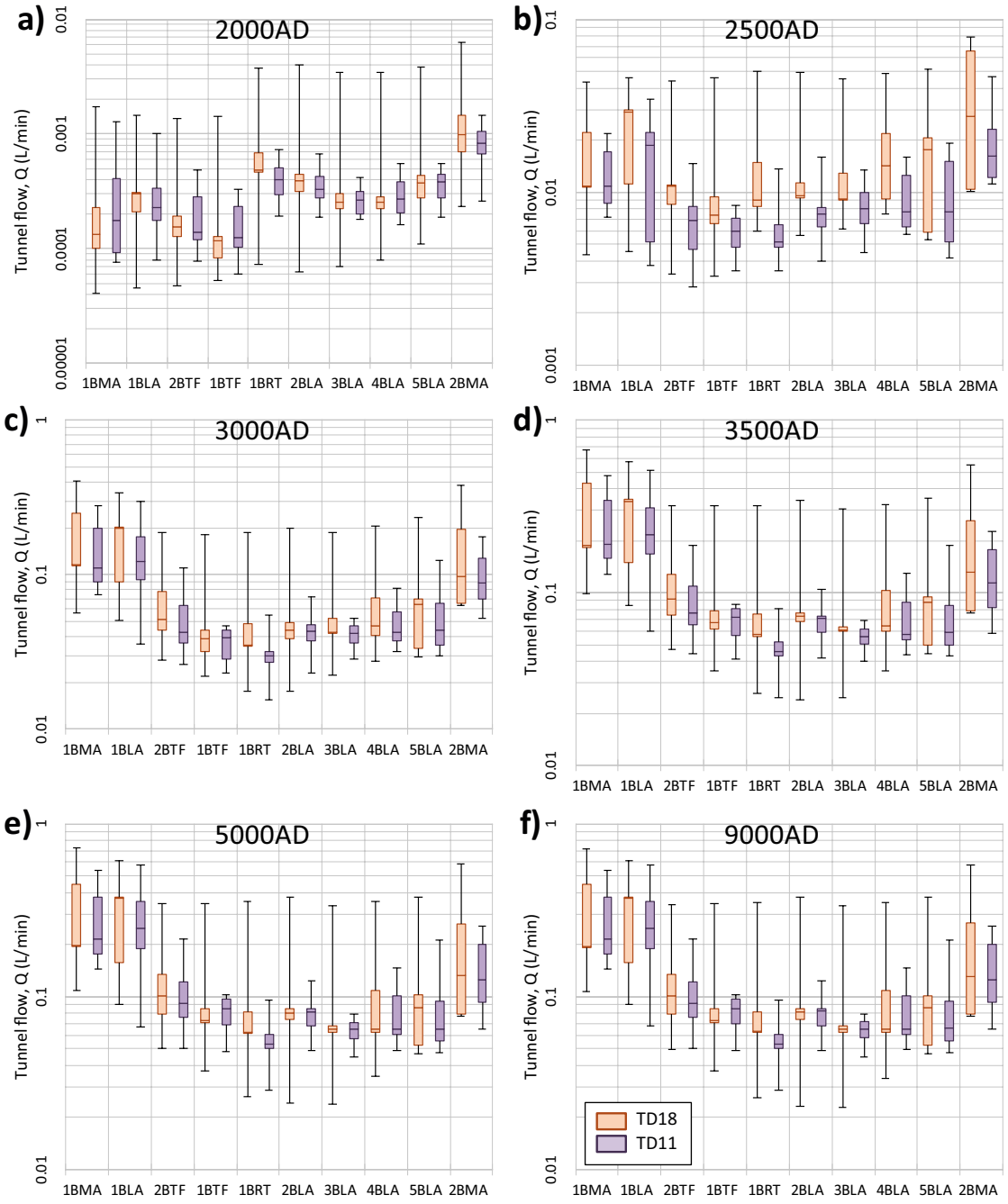

Figure 6-15. *Simulated disposal-room cross flow (TD18; orange) compared to results from earlier study (TD11; purple). Logarithmic scaling on y-axis.*

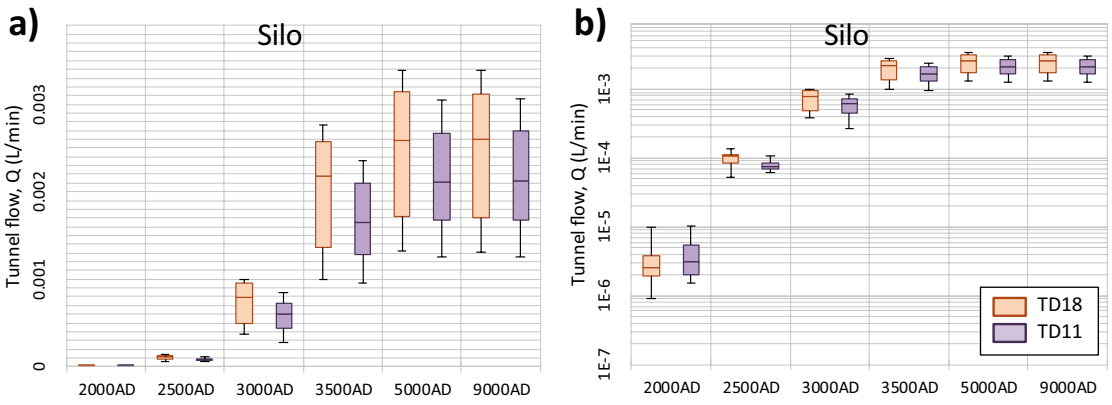

Figure 6-16. *Simulated cross flow for the Silo (present study; orange) compared to results from earlier study (TD11; purple); a) linear scaling on y-axis and b) logarithmic scaling.*

6.2.4 Range of variability and bounding cases

Three bedrock cases, 1, 11, and 15, were identified as bounding cases, representative for covering a realistic range of the uncertainty/heterogeneity in bedrock parameterisation (Öhman et al. 2014; marked by yellow shading in Table 2-2). These were selected based on a ranking system of simulated flow through the 11 disposal rooms in SFR 1 and SFR 3 (Öhman et al. 2014). Notably, the bounding cases were not selected to cover the present-day flow regime, as the simulated tunnel crossflows 2000 AD reflect vertical flow, which substantially deviates from that primarily addressed in long-term safety assessment; therefore, the 2000 AD simulation output were excluded from the ranking system (Öhman et al. 2014).

The deviating flow regime during the early stages of shoreline retreat is also observed in the present sensitivity analysis (Figure 6-17). During the submerged conditions (before 2250 AD), the disposal-room flow is upward-directed, driven by regional-scale flow that discharges to the seafloor; this flow regime is comparatively sensitive to bedrock parameterisation, and the selected bedrock cases 11 and 15 are clearly not representative of the variability in simulation results. After 2250 AD, the flow regime stabilises owing to a growing component of horizontal flow, as the ridge of natural sediments below the pier gradually emerges above sea. From c. 2250 AD the three selected bedrock cases can be regarded to represent the variability in simulated average flow through disposal rooms (c.f. blue lines enclosing several grey lines). The bounding cases of constant hydraulic conductivity, C01 and C03 (i.e. cases 6 and 8 in Table 2-2), stand out clearly against the other bedrock cases. Note that the heterogeneous bedrock cases (i.e. DFN realisations) exhibit a larger internal variability between the individual disposal rooms, which is not manifested in the average flow shown in Figure 6-17.

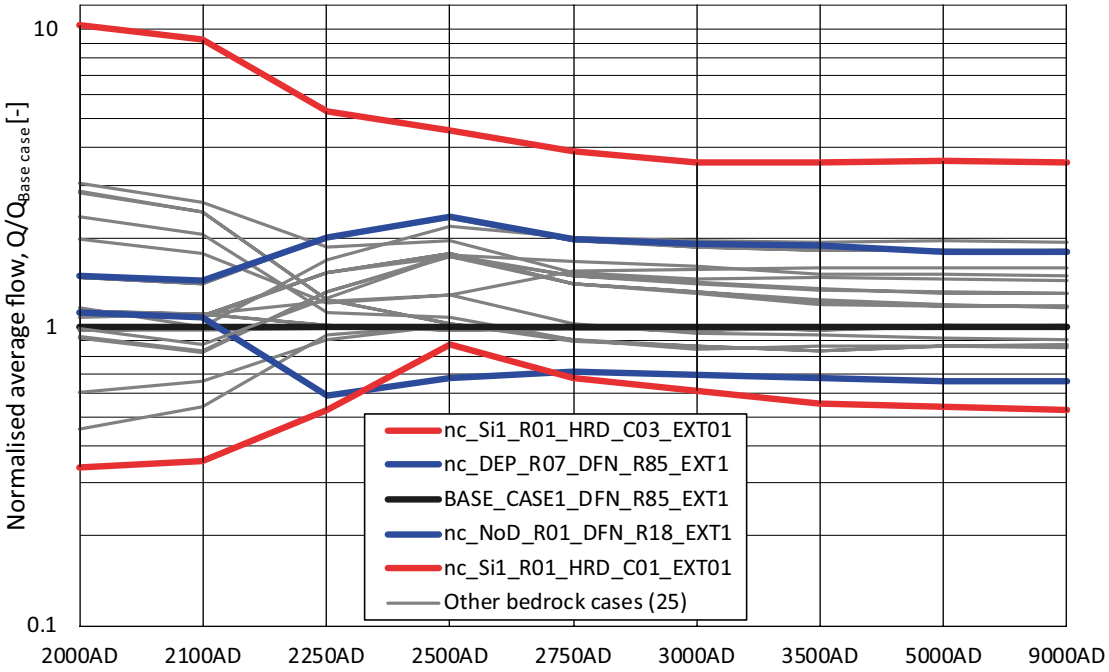

Figure 6-17. *Range of variability in average simulated disposal-room cross flow for 30 bedrock cases (Table 2-2) with time. The average disposal-room cross flow is normalised by the base case (black line). Bounding cases in the previous sensitivity study (Öhman et al. 2014; blue lines) compared against the bounding cases of constant hydraulic conductivity, C01 and C03 (red lines).*

6.2.5 Anisotropy in bedrock parameterisation

The cases C01 to C03 do not only represent constant hydraulic conductivity but also isotropic parameterisation, as compared to the DFN approach, which has a marked horizontal transmissive fracture component. The significance of anisotropy in the DFN model can be evaluated by comparing cases C01 to C03 (i.e. cases 6, 7, and 8) against the corresponding bedrock case with DFN R85 (i.e. case 14). Here, case C02 employs the effective rock-mass conductivity estimated by Holmén and Stigsson (2001) ($K_{HRD} = 6.5 \times 10^{-9}$ m/s), while C01 is simply set to a factor of 10 higher, and C03 to a factor 10 lower. The case C02 is therefore expected to be comparable with the DFN case (although not necessarily for the post-closure flow regime, and not specifically for R85), while the two other cases lack data basis, and are only intended to test the relative significance between HRD and HCD for repository performance.

The following is noted regarding the simulated disposal-room crossflows for the cases C01 to C03 relative to the corresponding for DFN realisation R85, $Q_{[constant\ KHRD]}/Q_{DFN\ R85}$ (Figure 6-18 and Figure 6-19):

- For several disposal rooms, the relative flow for case C02 is close to 1.0, which indicates a reasonable consistency between the effective value calibrated to tunnel inflow (Holmén and Stigsson 2001) and the DFN model based on borehole data (i.e. at least realisation R85). There are however exceptions, for example, the relative flow in 1BLA, which is considerably below 1.0 for C02.
- On average, case C01 exceeds R85 (and C02) by a factor of 4–5, while C03 is only a factor 2–5 lower than R85 (and C02). Both factors are considerably below that elaborated in HRD parameterisation (i.e. a factor of 10), which signifies that a large component in tunnel flow is associated to deformation zones (i.e. which are not varied in this comparison).

- The significance of DFN anisotropy for disposal-room flow is manifested during the transition period, as the flow regime changes from submerged to terrestrial. On average, the isotropic parameterisation cases, C01 to C03, typically result in relatively higher flows during the first period, 2000 AD to 2500 AD (i.e. dominated by vertical flow), as compared to the later regime when the horizontal flow component dominates.
- Notably, the case C02 renders somewhat higher flow through the Silo, as compared to case C03, which has a higher HRD parameterisation (Figure 6-18e). The reason for the deviant behaviour in Silo crossflow is its low-conductive barriers (e.g. its concrete cylinder, $K = 5 \times 10^{-9}$ m/s; Figure 4-3), which is on par with C02. Thus, increasing the hydraulic conductivity of the surrounding rock mass bypasses the flow (due to reduced gradients).

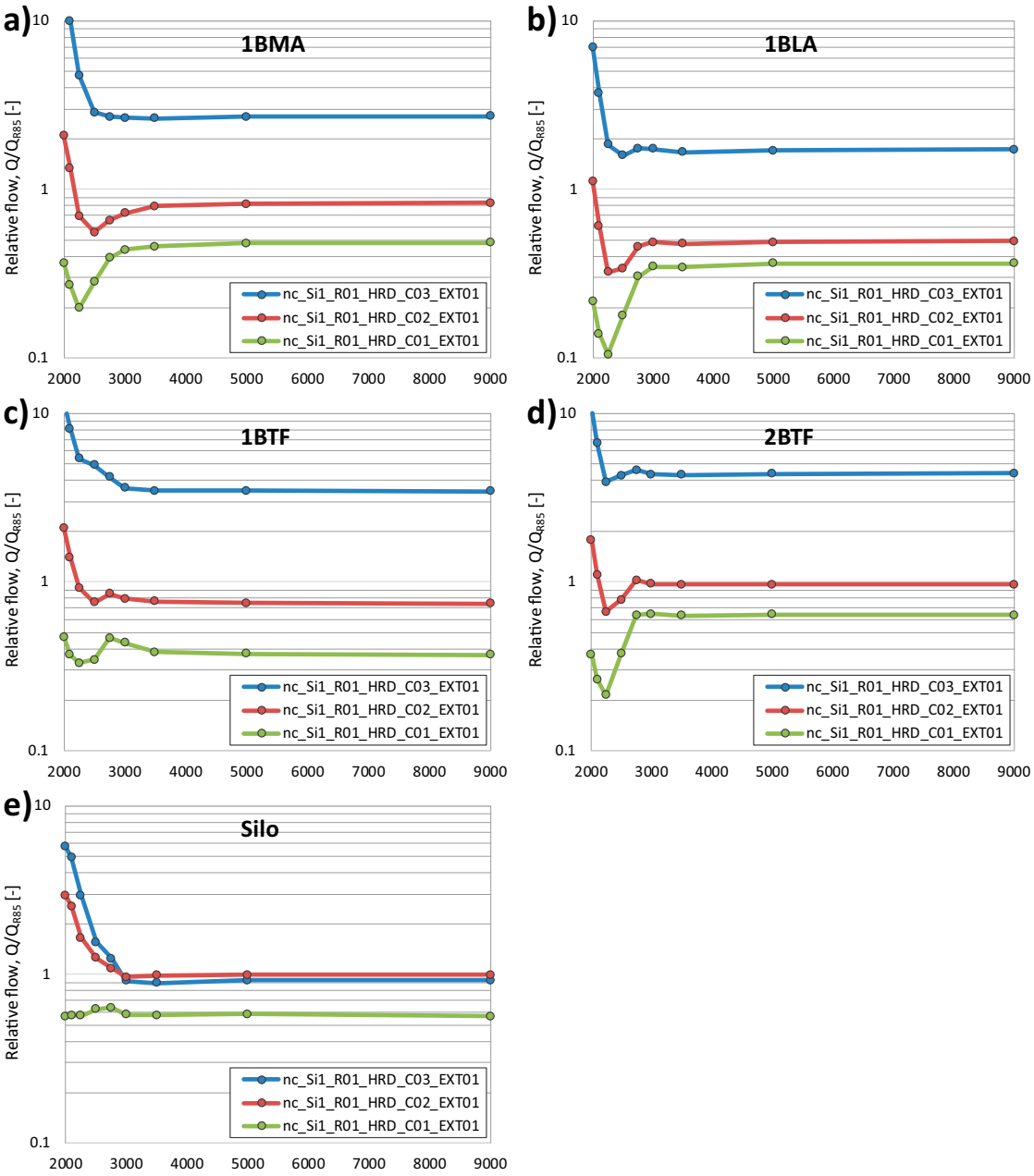

Figure 6-18. *Significance of anisotropic bedrock parameterisation for disposal-room flow in the transient hydrogeological setting at SFR. Tunnel flow for constant, isotropic hydraulic-conductivity parameterisation (cases C01, C02, and C03) relative to DFN realisation R85 (i.e. case 14: nc_Si1_R01_DFN_85_EXT01) over time.*

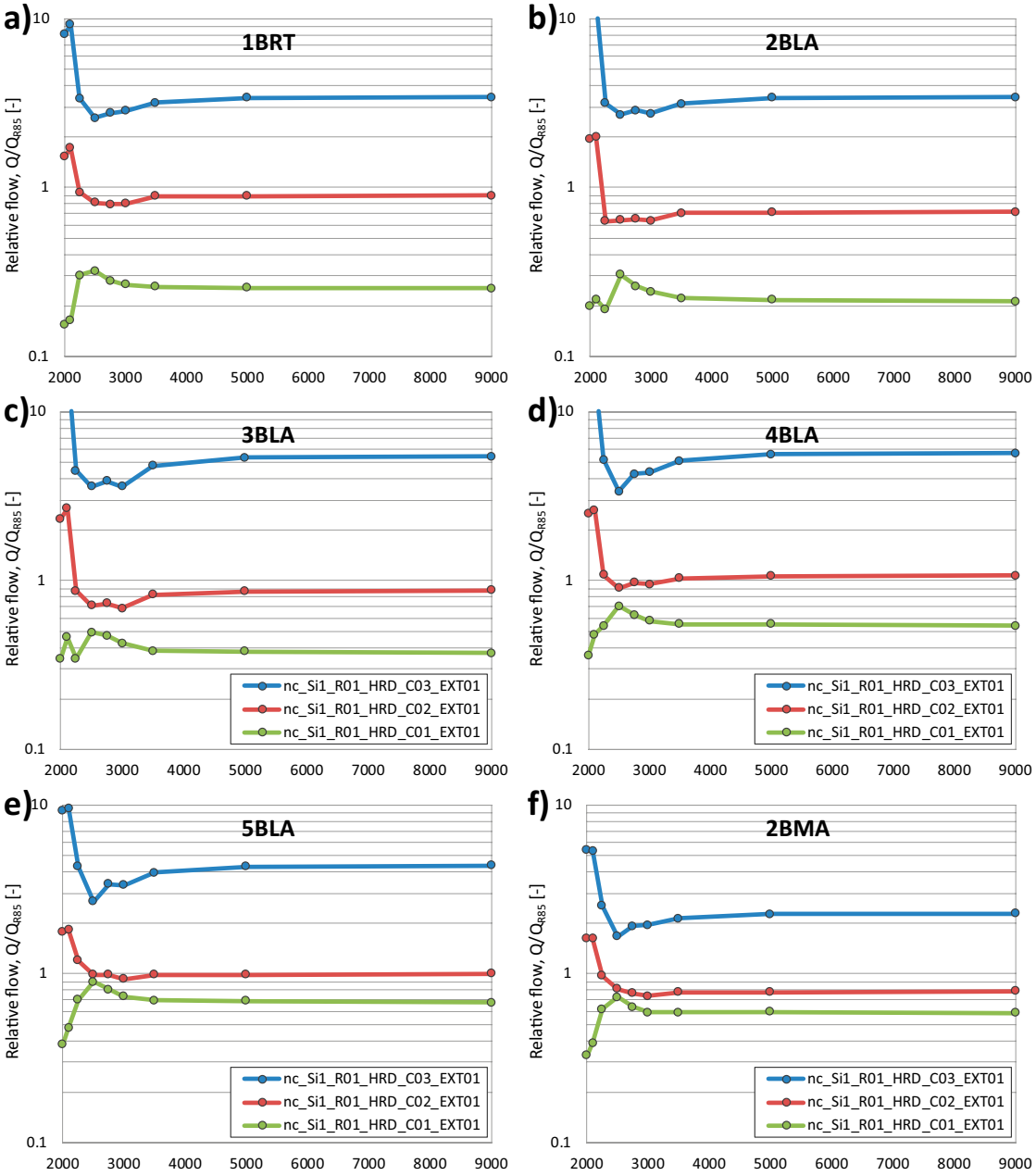

Figure 6-19. *Significance of DFN bedrock parameterisation for disposal-room flow in the transient hydrogeological setting at SFR. Tunnel flow for constant, isotropic hydraulic-conductivity parameterisation (cases C01, C02, and C03) relative to DFN realisation R85 (i.e. case 14: nc_Si1_R01_DFN_85_EXT01) over time.*

6.2.6 Sensitivity to Singö-barrier variants

The effect of the Singö deformation zone acting as a barrier for transversal regional-scale flow is evaluated by comparing disposal-room crossflow for cases 19, 20, and 21 (Table 2-2) versus the base case (i.e. case 30). A barrier for transversal flow is implemented in the core of the Singö deformation zone, defined as $K_{core} = 10^{-9}$ m/s over a third of its full width, in three parameterisation variants (Section 4.3.3):

- Case 19: Barrier implemented over the entire core (CD_Si2_HOM_DFN_R85_EXT01).
- Case 20: Barrier limited to upper part ($z > -245$ m; CD_Si3_HOM_DFN_R85_EXT01).
- Case 21: Barrier limited to lower part ($z \leq -245$ m; CD_Si4_HOM_DFN_R85_EXT01).

The effects are evaluated as relative flow between the Singö-barrier cases and the base case, $Q_{Singö\ barrier}/Q_{Base\ case}$ (Figure 6-20 and Figure 6-21). The largest effects are found in the early time slices, up to 2500 AD, during the submerged period when the flow in the SFR host rock is driven by the regional-scale flow. The effects of the Singö barrier vanish over time as the flow regime matures into terrestrial conditions, driven by the local-scale topography of the emerging ridge, on which the SFR pier has been constructed. The crossflows in SFR3 are comparatively more sensitive to the Singö barrier case (Figure 6-20b), as its deeper location makes it more subject to regional-scale flow passing Singö deformation zone. Notably, the 2BMA crossflow stands out at 2250 AD, where the barrier case renders higher flow than the base case does (c. 45 % higher; Figure 6-20b). However, this anomaly should not be overinterpreted, as the 2BMA crossflow is undergoing a strong transition at this stage, where the cross flow increases an order of magnitude (Figure 6-12d).

Limiting the barrier implementation to the upper part ($z > -245$ m; case 20) has the same type of effects, but they are less pronounced (i.e. the same pattern, but of less magnitude), whereas implementing the barrier in the lower part ($z \leq -245$ m; case 21) has no notable effect on disposal-room cross flows (i.e. on the order 1 %; not shown). The reason for this is probably that the role of Singö deformation zone declines at depth due to the assumed depth trend in HCD parameterisation; at depth, the Singö ECPM parameterisation is on par with the assumed barrier parameterisation (see Figure 4-9d).

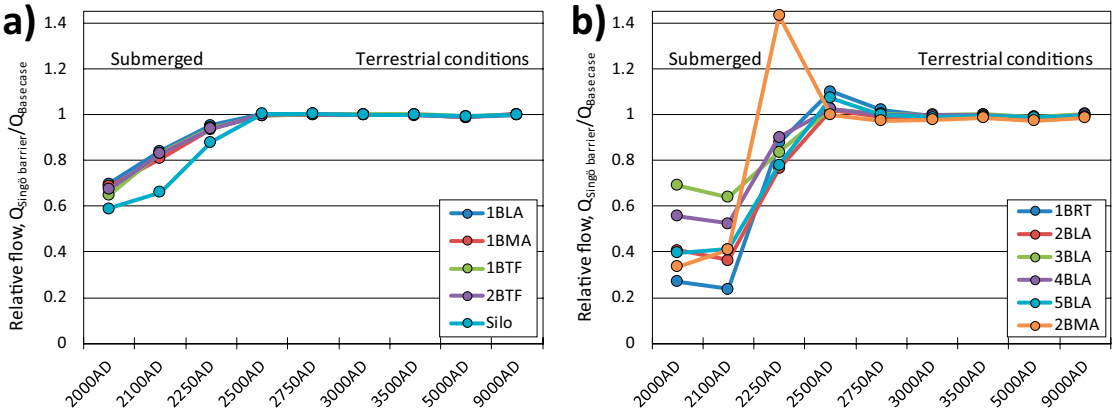

Figure 6-20. *Effect of implementing a barrier over the entire core of the Singö deformation zone, evaluated in terms of disposal-room flow relative to the base case (i.e. case 19, CD_Si2_HOM_DFN_R85_EXT01, compared to the base case, 30).*

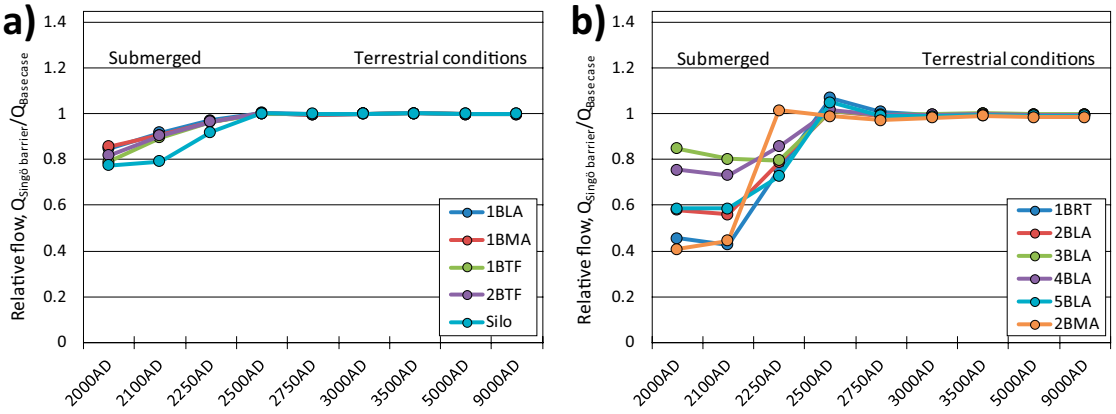

Figure 6-21. *Effect of implementing a barrier in the upper part of the Singö deformation zone, evaluated in terms of disposal-room flow relative to the base case (i.e. case 20, CD_Si3_HOM_DFN_R85_EXT01, compared to the base case, 30).*

6.2.7 Sensitivity to parameterisation outside SFR Regional domain

The bedrock parameterisation variants outside the SFR Regional domain address the HCD extension north from SFR and three alternative HRD parameterisations (Table 2-1). All six variants are combined with the base-case HCD parameterisation (EXT00, EXT01, EXT02, EXT10, EXT11, and EXT12; cases 26, 30, 2, 27, 3, and 4 in Table 2-2). Analysis demonstrates that:

- the HCD extension north from SFR has no effect on disposal-room cross flow.
- DFN realisation R01 (i.e. EXT01 and EXT11) and DFN realisation R02 (i.e. EXT02 and EXT12) render identical disposal-room crossflows.
- Constant HRD parameterisation (i.e. KHRD = 6.5×10^{-9} m/s; EXT00 and EXT10) increases disposal-room cross flow by c. 30 % during the first stages of land uplift (i.e. similar to findings in Section 6.2.5).

In summary, the disposal-room crossflow is not particularly sensitive to bedrock parameterisation of outside the SFR Regional domain.

6.3 Particle tracking

Recharge and discharge locations for flow across disposal rooms are simulated by means of particle tracking. The recharge/discharge refers to flow across the bedrock surface (i.e. the interface between bedrock and overlying HSD). The spatial distribution of these locations is quantified in terms of areal density, number of particles/m^2, based on 1 000 000 particles released uniformly within the disposal rooms of SFR 1 and SFR 3, respectively. Recharge flow paths are determined by means of *backward* particle tracking, with the disposal rooms as the starting point (i.e. only including *upstream* flow components in Eq. (5-3)). Analogously, discharge locations (or, "exit locations") are determined by means of *forward* particle tracking, with the disposal rooms as the starting point (i.e. only including *downstream* flow components in Eq. (5-3)).

The starting point of trajectories is defined at the tunnel-wall passage, and the termination point of trajectories (i.e. "recharge location" or "discharge location", depending on direction of particle tracking) is defined at the bedrock/HSD interface passage.

6.3.1 Recharge locations

Recharge locations refer to the point of origin for recharging flow paths and tend to occur at topographical peaks, as well as, hydraulic conduits in the bedrock. The recharge locations for SFR 1 and SFR 3 are analysed in terms of areal density, No. particles/m^2, for the base case bedrock parameterisation (case 30; Figure 6-22 and Figure 6-23, respectively). The transition in recharge over time is analysed for six selected time slices and compared to the results of TD11 (Öhman et al. 2014).

At the present shoreline (time slice 2000 AD), the main area for simulated recharge occurs near the shore of the Forsmark mainland (i.e. just north of Lake Bolundsfjärden; not from the constructed pier above SFR). Recharge also occurs up to 5 km inland from the coast, in the elevated region that forms the outer boundary of the flow model domain (c.f. Figure 3-1). The recharge locations of SFR 1 and SFR 3 are more or less identical (c.f. Figure 6-22a and Figure 6-23a).

By the time slice 2500 AD, natural sediments have emerged above sea level on both sides along the pier (land uplift per 500 years is approximately 3 m; Section 3.3.5). This relatively modest change in coast line causes a distinct turnover in the local flow regime around SFR (c.f. head solution in Figure 6-4b), which shifts the simulated recharge location from the Forsmark coast to the SFR pier (Figure 6-22b and Figure 6-23b). This transition, from regional-scale flow to a local topography-driven flow cell, is studied in more detail below in context of addressing the parameterisation uncertainty for flow across the Singö deformation zone.

From the time slice 3000 AD and onwards, the simulated pattern in recharge locations stabilises to more or less stationary. The dominant recharge to SFR 1 occurs via ZFMNNW1209 (formerly Zone 6; Figure 6-22d; note logarithmic scaling of density), although a minor contribution also comes from the elevated sediments, south of the SFR pier. In comparison, SFR 3 involves deeper and longer flow

paths, which displaces the recharge towards the elevated sediments, south of the SFR pier. The deformation zones in this area are interpreted as less transmissive, and hence the recharge locations for SFR 3 are comparatively less correlated to deformation-zone intercepts than those for SFR 1. However, the thin zone ZFMWNW8042 can be identified as a major recharge location for SFR 3 (Figure 6-23d), which has a very similar transmissivity parameterisation to ZFMNNW1209.

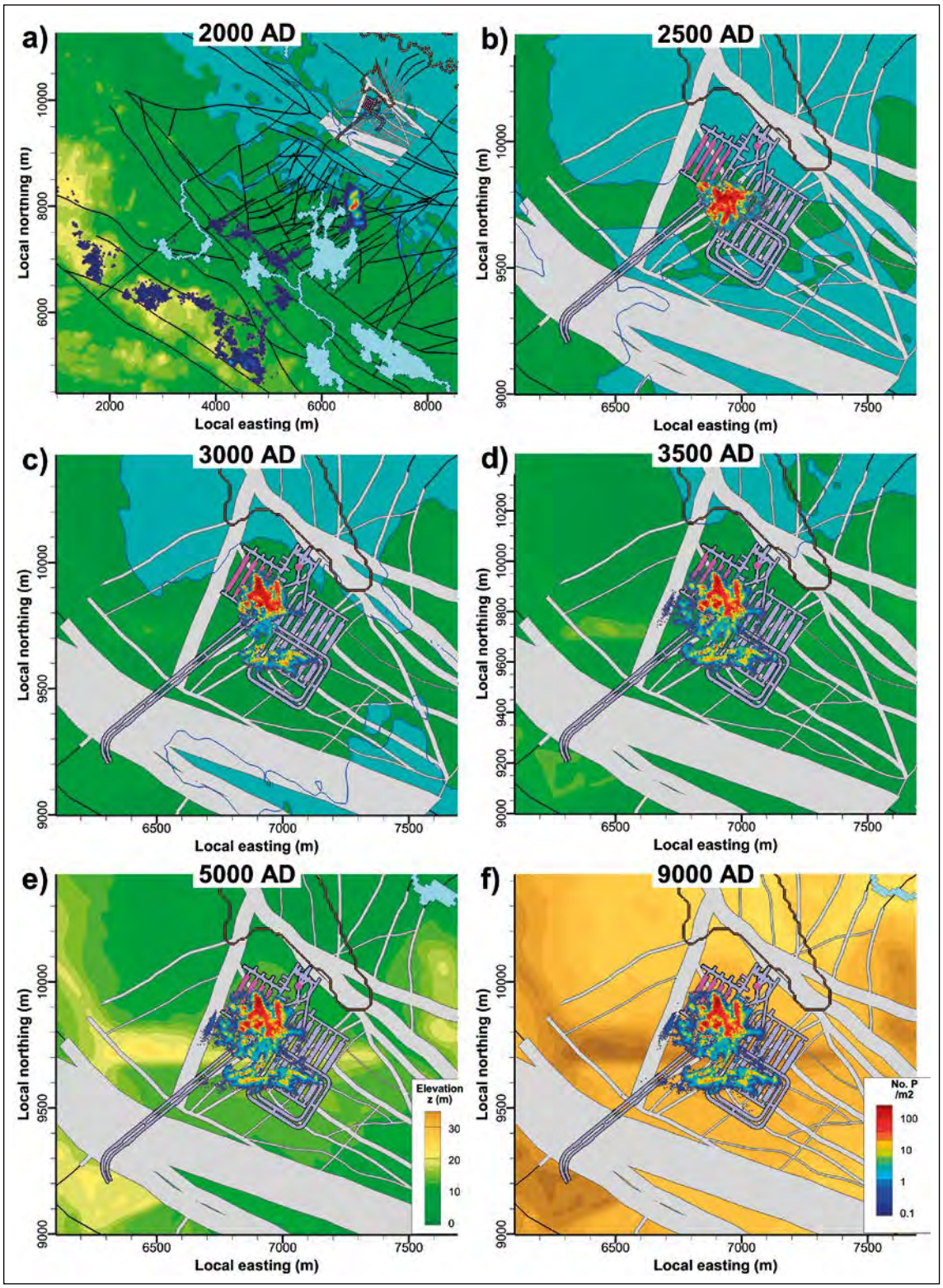

Figure 6-22. *Density of recharge locations for SFR1 disposal rooms over time for base case [BASE_CASE1_DFN_R85_EXT01].*

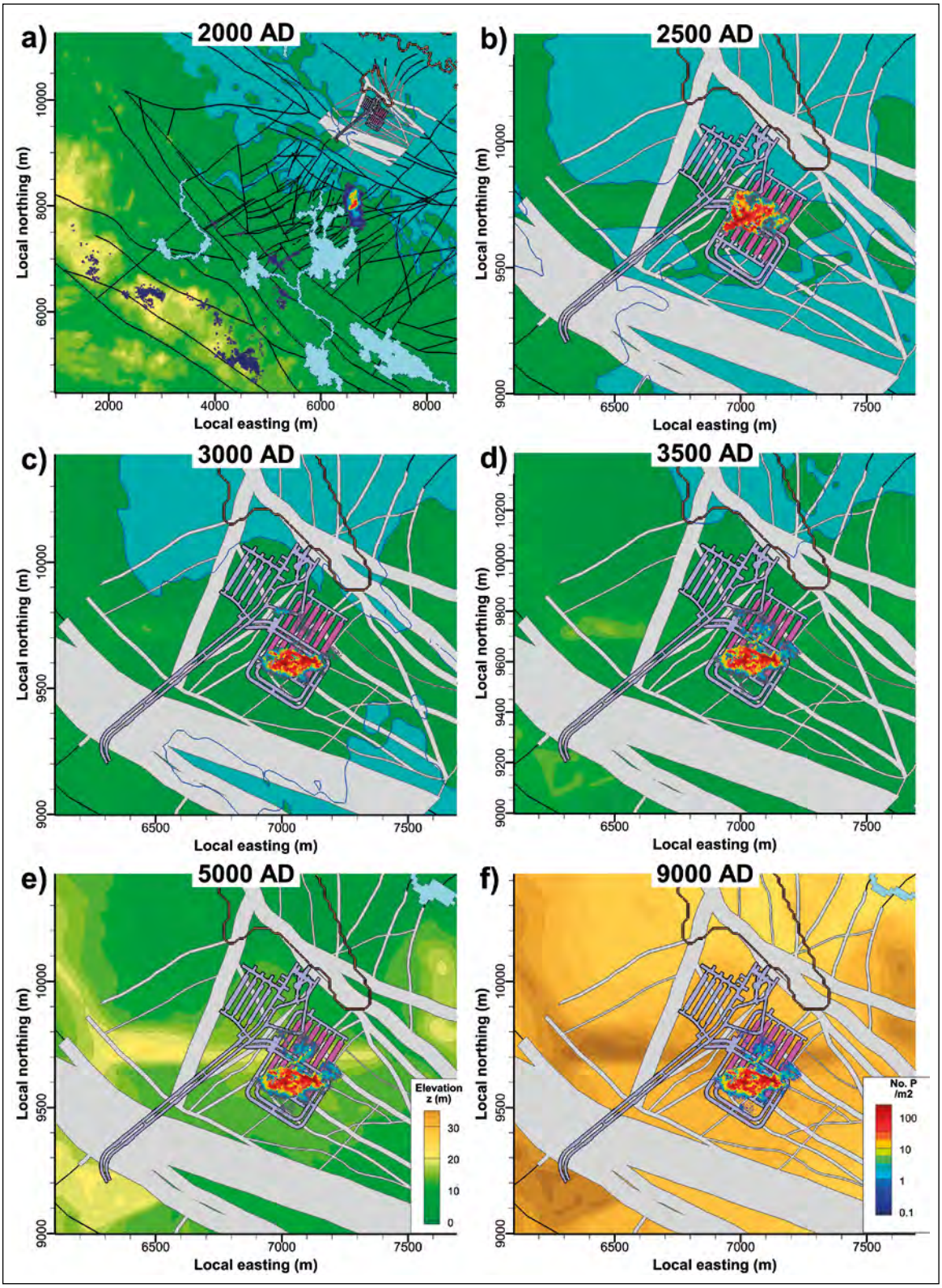

Figure 6-23. *Density of recharge locations for SFR3 disposal rooms over time for base case [BASE_CASE1_DFN_R85_EXT01].*

Sensitivity to Singö-barrier variants

During the early post-closure phase, the flow regime in the SFR host rock is controlled by a delicate balance between two gradients: the regional-scale gradient and the counter-acting groundwater table of the pier and the natural ridge that gradually emerges above SFR. Both of these gradients are weak, and entail parameterisation uncertainties (e.g. material properties in the deeper parts of the pier, which is currently below water), which causes uncertainty in simulated flow.

The sensitivity to hypothesised barrier effects in Singö deformation zone for recharge during the early stages of land uplift is evaluated by comparing the simulated recharge for cases 19, 20, and 21 (Table 2-2) versus the base case (i.e. case 30). The two bounding cases are: the base case (30), which employs the standard ECPM parameterisation without any barrier, versus case 19, where a barrier is implemented in the core of the Singö deformation zone, defined as $K_{core} = 10^{-9}$ m/s (Section 4.3.3). Intermediate variants are case 20 and case 21:

- Case 19: Barrier implemented over the entire core (CD_Si2_HOM_DFN_R85_EXT01).
- Case 20: Barrier limited to upper part (z >−245 m; CD_Si3_HOM_DFN_R85_EXT01).
- Case 21: Barrier limited to lower part (z ≤ −245 m; CD_Si4_HOM_DFN_R85_EXT01).

Analysis of disposal-room crossflow demonstrates that the case of maximum barrier effects (i.e. case 19) reduces the crossflow by 30 % to 70 % under the present-day conditions, although the sensitivity to Singö deformation-zone parameterisation declines with land uplift and becomes negligible by c. 2500 AD (Section 6.2.6). In addition to the confirmed reduction in flow rate, analysis of recharge flow paths to SFR1 and SFR3 demonstrates that a Singö barrier particularly reduces the fraction of flow that crosses the zone (i.e. difference between light grey and orange bars in in Figure 6-24; also density of inland recharge locations in Figure 6-25 and Figure 6-26).

In the base-case parameterisation, almost all recharge to SFR1 and SFR3 crosses the Singö deformation zone at 2000 AD (light grey bars > 99.5 % in Figure 6-24); only minor recharge occurs north of Singö (< 0.5 %; Figure 6-25a and b). The full Singö barrier (Si2; case 19), reduces the recharge across the zone by c. 10 % to SFR1 and 0.6 % to (orange bars in Figure 6-24); this is due to increased recharge from the SFR pier and the islet to the east of the pier (< 0.5 %; Figure 6-25c and d).

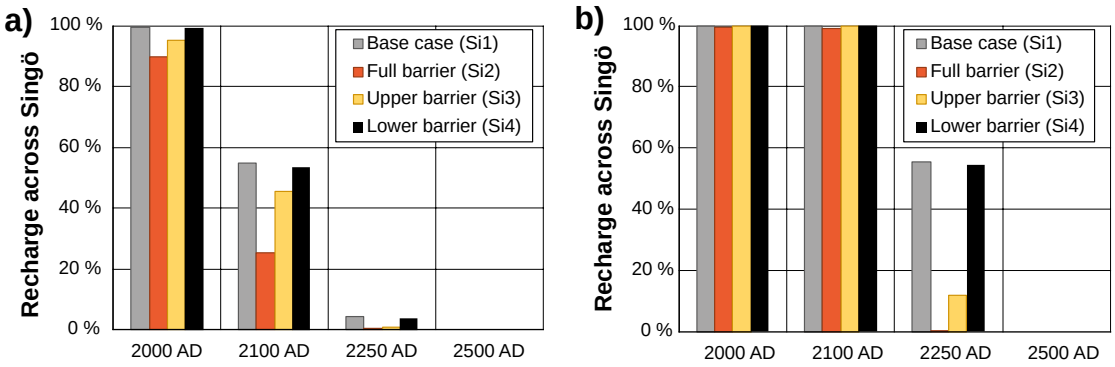

Figure 6-24. *Fraction of SFR recharge flow that crosses the Singö deformation zone depending on barrier implementation for transversal flow; a) recharge to SFR1 disposal rooms and b) recharge to SFR3 disposal rooms.*

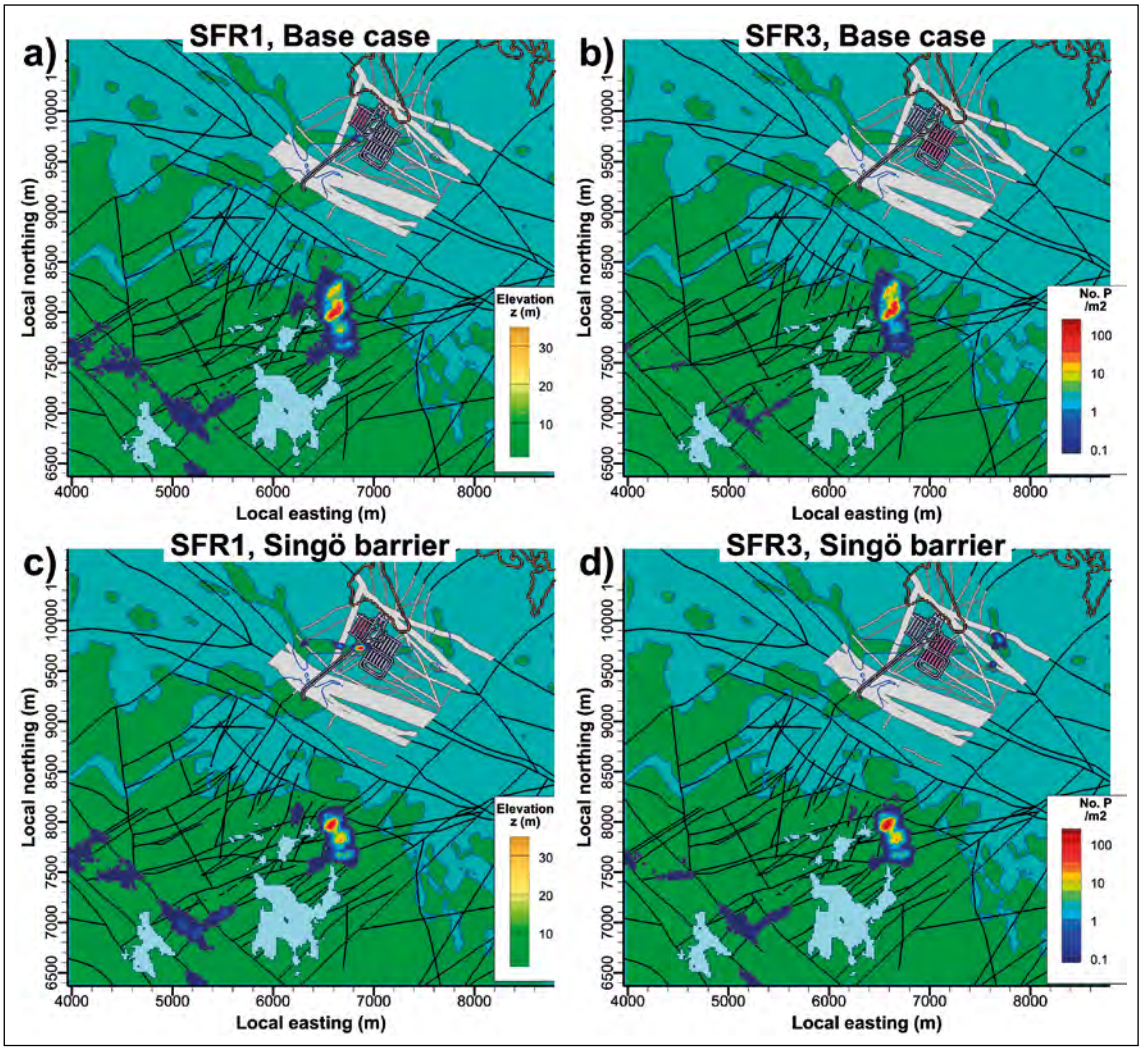

Figure 6-25. *Recharge locations for SFR disposal facilities, 2000 AD, subject to implementation of a barrier for flow across the Singö deformation zone. Simulation results for two parameterisation variants compared: a) and b) base case (case 30), versus c) and d) the full Singö barrier case (case 19).*

The recharge to SFR originates from two distinct areas on either side of the Singö deformation zone (Figure 6-26):

1. the “Forsmark inland” during the earliest stages of land uplift (just north of Lake Bolundsfjärden, but south of Singö deformation zone),
2. the SFR pier, including the underlying ridge of natural sediments (i.e. north of the Singö deformation zone).

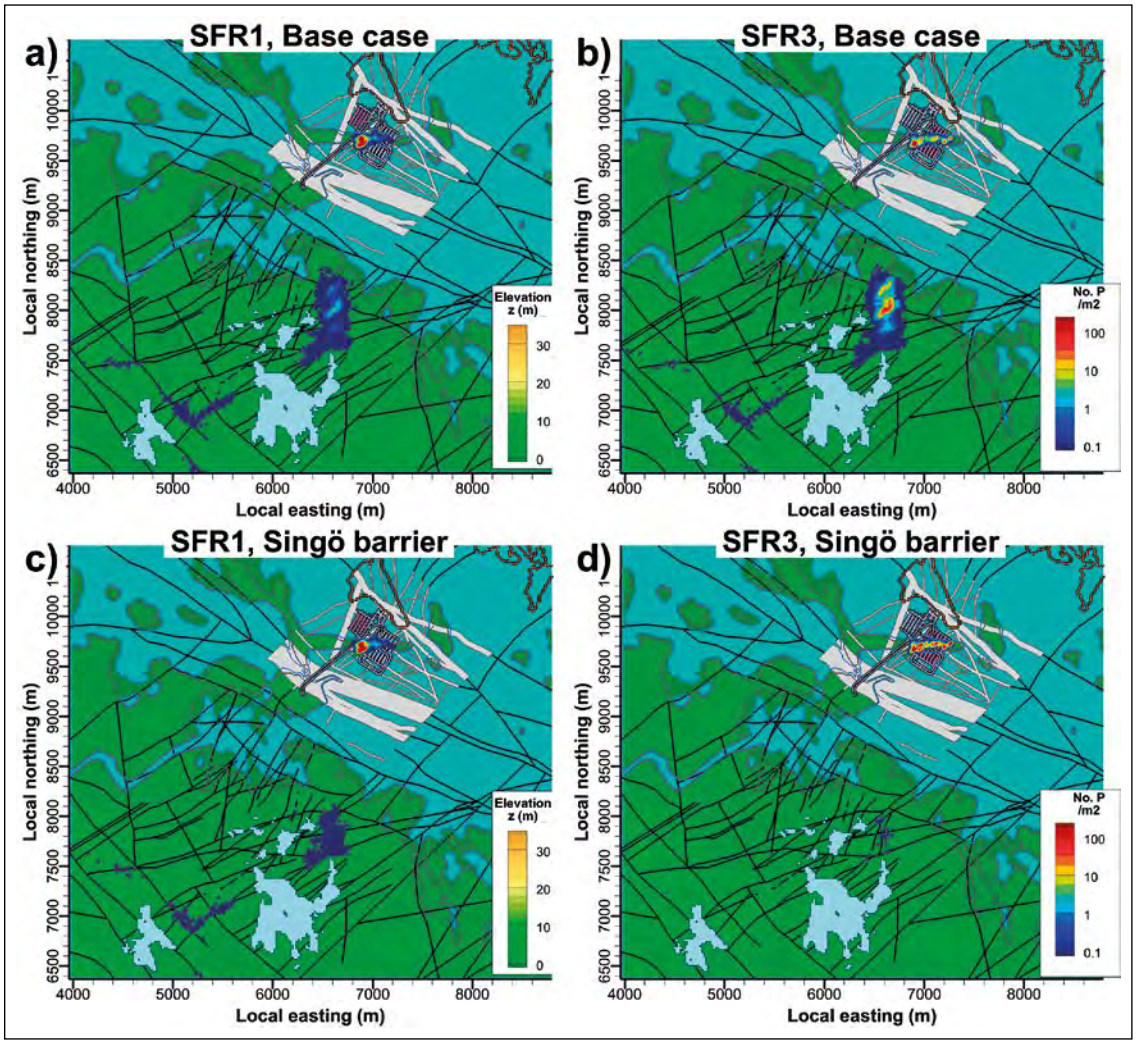

Figure 6-26. *Recharge locations for SFR disposal facilities, 2250 AD, subject to implementation of a barrier for flow across the Singö deformation zone. Simulation results for two parameterisation variants compared: a) and b) base case (case 30), versus c) and d) the full Singö barrier case (case 19).*

The distinction of recharge areas appears as a rather "bimodal" length distribution of recharging flow paths (Figure 6-27 and Figure 6-28). The transition in recharge locations occurs earlier for the shallower SFR1 (c. 2100 AD), as compared to the deeper SFR 3 (c. 2250 AD). The Singö barrier cases (full barrier and upper barrier; Si2 and Si3) promotes this transition, while the base-case parameterisation and the deep barrier delays the "transition into terrestrial conditions".

By 2500 AD, all the recharge to SFR is, irrespectively of Singö deformation-zone parameterisation, fully re-located to the nearfield above the facility (i.e. the natural ridge, on which the pier has been built). However, it must be kept in mind that this re-localisation of SFR recharge does not imply that the regional-scale flow across the Singö zone ceases (irrespectively of barrier assumption), nor that its influence on the flow through SFR disposal rooms has fully ceased (Figure 6-29).

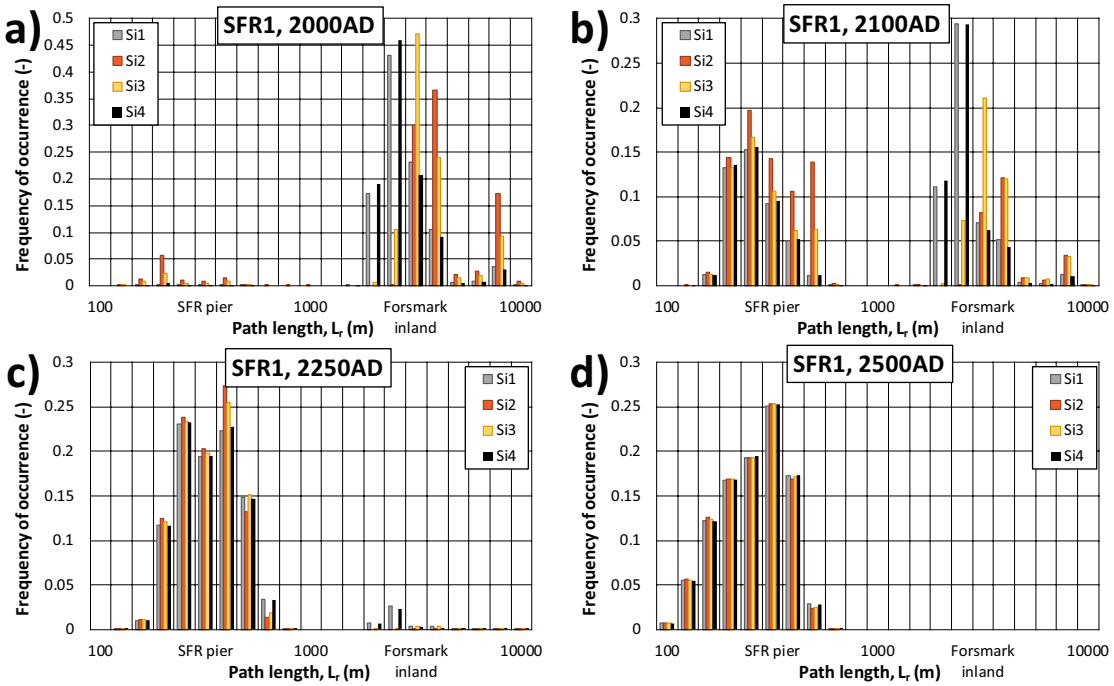

Figure 6-27. *Recharge path length for SFR 1 depending on Singö deformation-zone parameterisation. Alternatives Si1 to Si4 refer to bedrock cases 30, 19, 20, and 21 (Table 2-2).*

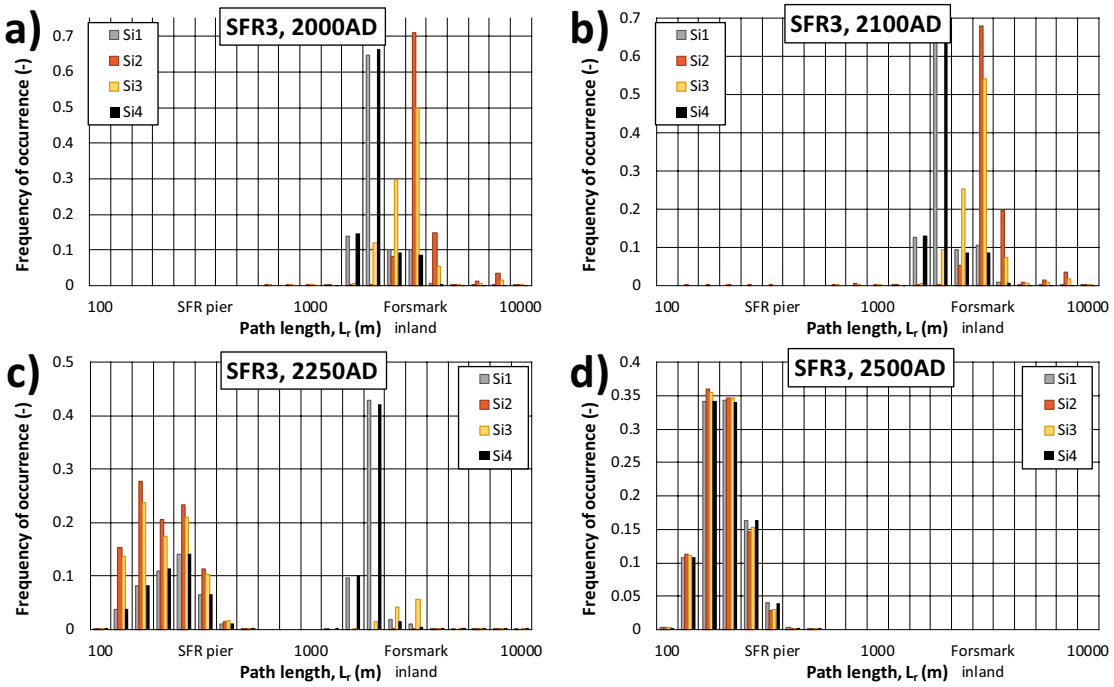

Figure 6-28. *Recharge path length for SFR 3 depending on Singö deformation-zone parameterisation. Alternatives Si1 to Si4 refer to bedrock cases 30, 19, 20, and 21 (Table 2-2).*

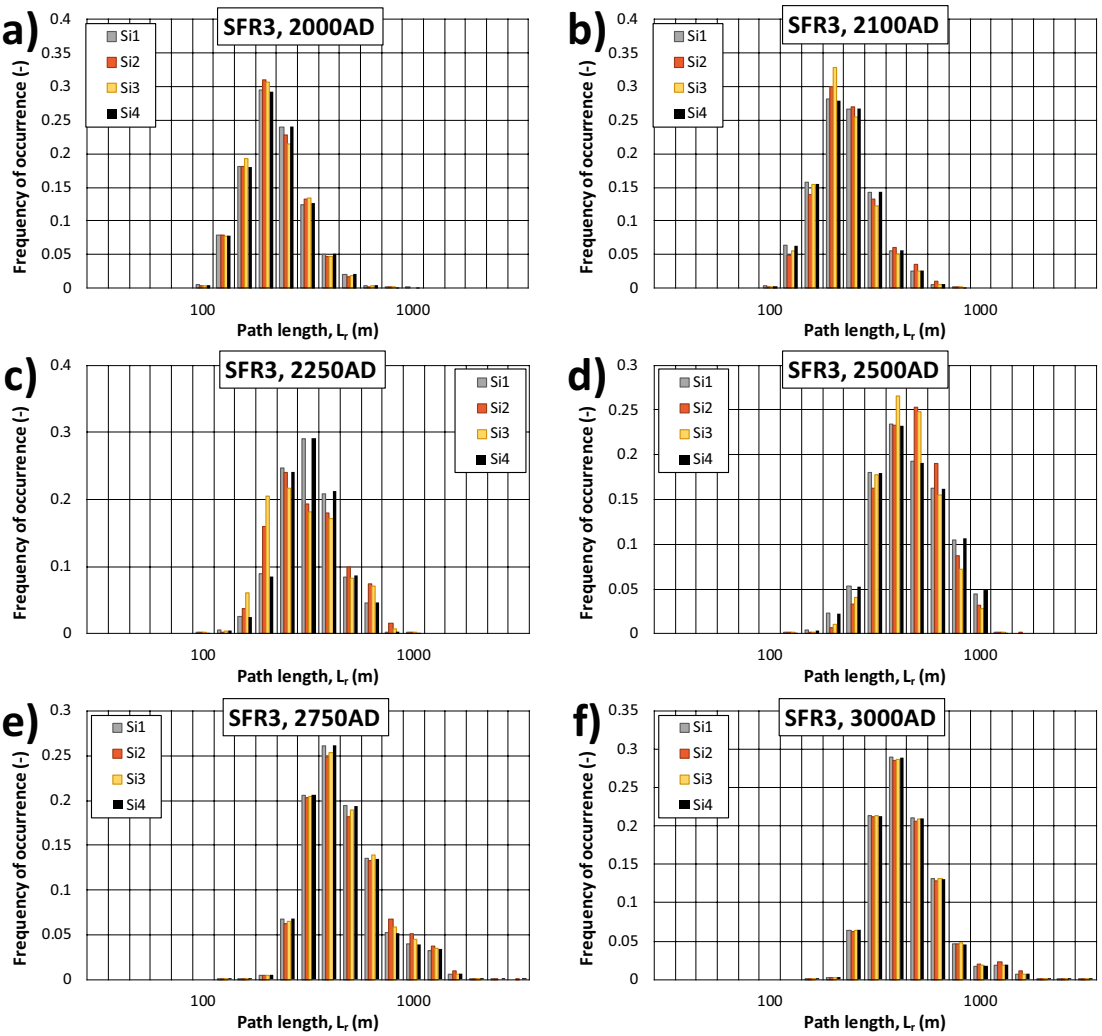

Figure 6-29. *Discharge path length for SFR 3 depending on Singö deformation-zone parameterisation. Alternatives Si1 to Si4 refer to bedrock cases 30, 19, 20, and 21 (Table 2-2).*

6.3.2 Exit locations

The spatial distributions of discharge locations (or "exit locations") are evaluated analogously to the recharge locations (Section 6.3.1). The patterns in discharge locations of SFR 1 and SFR 3 are compared over time, in terms of the six selected time slices (Figure 6-30 and Figure 6-31). A couple of characteristics can be noted:

Shoreline displacement successively forces the exit locations further away from the release points. Before the time slice 3500 AD, exit locations are essentially below the cost line. The flow regime changes from upward-directed, under early time slices, to increasingly horizontal, during later time slices.

The density of exit locations is strongly correlated to ground intercepts of deformation zones (most likely, also transmissive stochastic DFN fractures). The dominant discharge path for SFR 1 is ZFMNNW1209 (Zone 6) during time slices 2000 to 2500 AD, after which ZFMNNE0869 and ZFMNW0805A/B dominates during time slices 3000 to 3500 AD. The pattern of exit locations from SFR 1 appears stationary between time slices 5000 and 9000 AD and in essence, all particles discharge to biosphere object 157_2 (e.g. Figure 6-30).

During early stages, SFR 3 has exit locations both north and south of the SFR pier. As the horizontal component in the flow regime successively grows, the exit locations are driven north, towards ZFMNW0805A/B and ZFMNS3154. Most particles discharge into biosphere object 157_2, although owing to its deeper location, a lesser amount of particles discharge into biosphere objects 27 and 31 (i.e. related to biosphere object 116, which is also referred to as Charlie's lake).

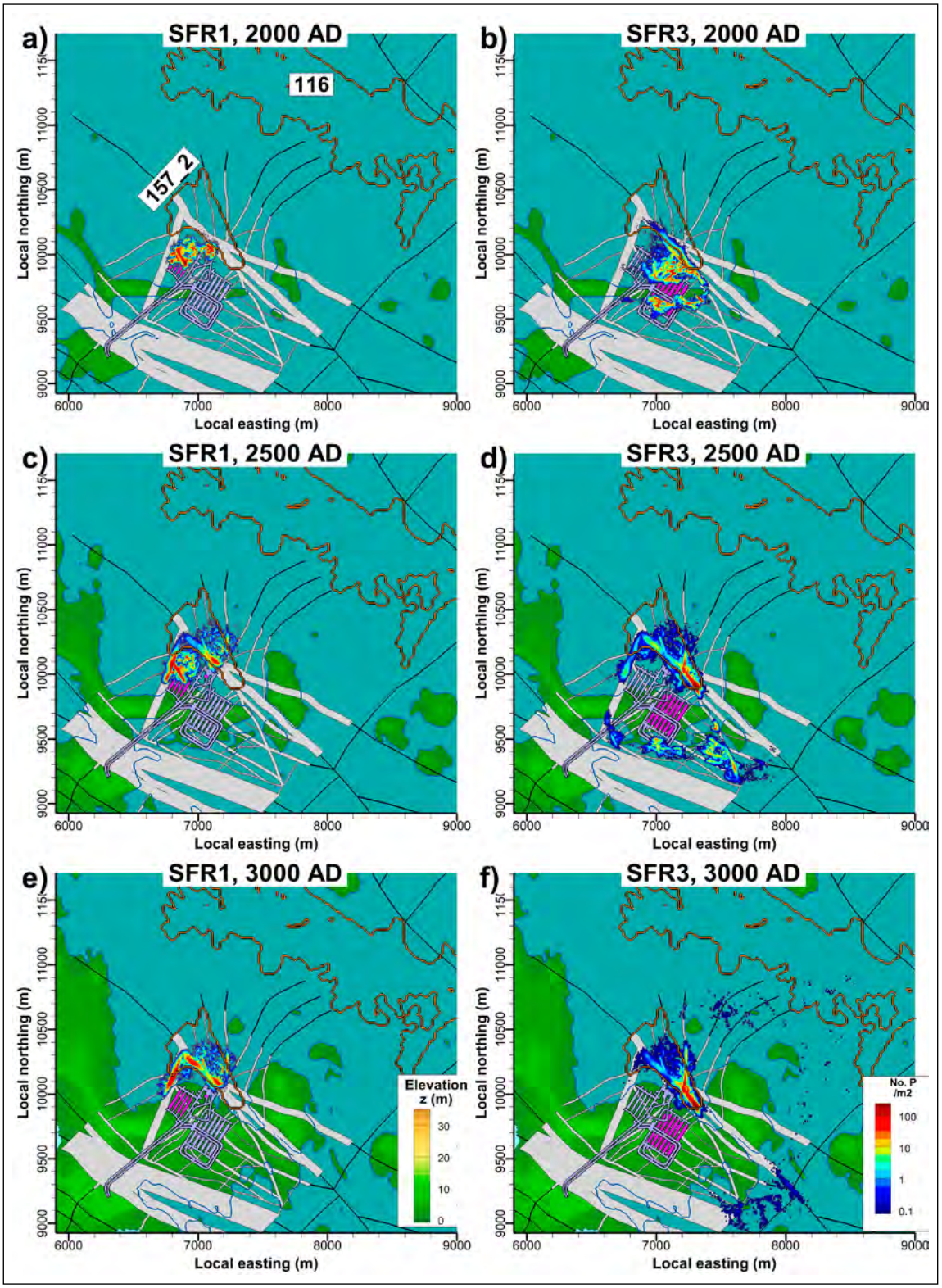

Figure 6-30. *Early exit locations from disposal rooms in SFR 1 (pink shade; left) and SFR 3 (pink shade; right), [BASE_CASE1_DFN_R85_EXT01], time slices 2000 to 3000 AD. Biosphere object IDs 116 and 157_2 included for reference (lines).*

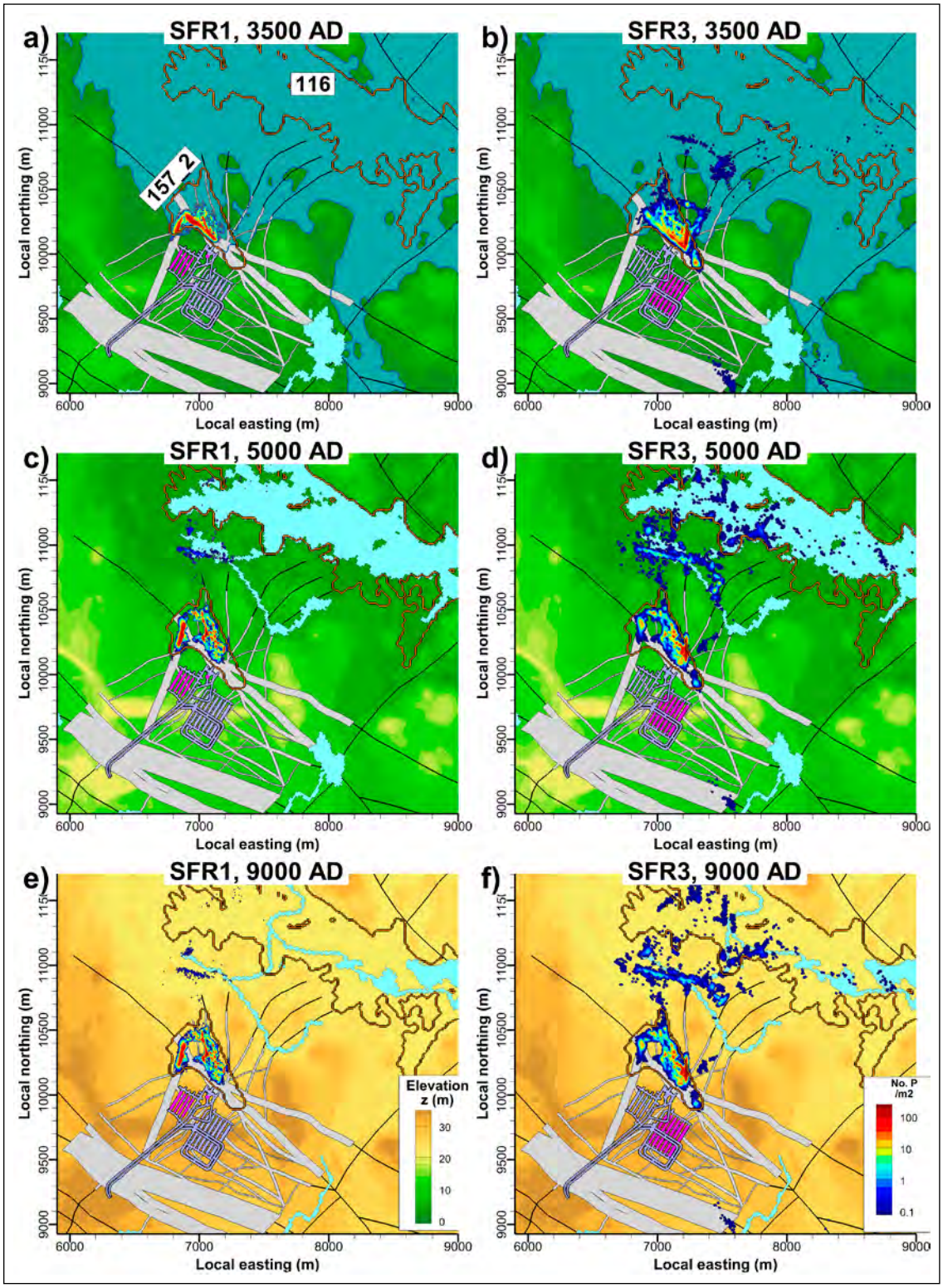

Figure 6-31. *Late exit locations from disposal rooms in SFR 1 (pink shade; left) and SFR 3 (pink shade; right), [BASE_CASE1_DFN_R85_EXT01], time slices 3500 to 9000 AD. Biosphere object IDs 116 and 157_2 included for reference (white lines).*

Parameterisation variants outside the SFR Regional domain

Particle exit locations mainly occur within the nearest biosphere object 157_2, but also outside the SFR Regional domain (Table 6-2). The sensitivity to bedrock parameterisation outside the SFR Regional domain is evaluated by comparing bedrock cases with identical parameterisation inside the SFR Regional domain (i.e. here BASE_CASE1_DFN_R85), but with alternative parameterisation outside the SFR Regional domain (cases 2, 3, 4, 26, 27, 30 in Table 2-2). The parameterisation variants outside the SFR Regional domain are denoted EXT followed by one integer representing the extension of 6 zones North from SFR (0 for minimum or 1 for maximum), and another integer for the HRD parameterisation: 0 for constant K_{HRD}, 1 for DFN realisation R01, and 2 for DFN realisation R02.

The exit locations are classified in terms of seven biosphere objects (Table 6-2). However, the DarcyTools particle tracking terminates at the bedrock surface and therefore all particles do not necessarily reach a biosphere object (i.e. the transport from the bedrock surface to the biosphere object is modelled separately in SR-PSU Biosphere). As the result, some particle exit locations become classified as "outside" biosphere objects. Visual inspection suggests that the particles classified as "outside" should be associated to the downstream objects 157_1 or 116 (Figure 6-32f and Figure 6-33f).

Table 6-2. Particle exit locations depending on parameterisation outside the SFR Regional domain.

Bedrock case[1)]			Biosphere object (Figure 2-2)						
	HCD	HRD	157_2	157_1	116	159	121_1	121_2	Outside
SFR1									
EXT00	Min	Constant	99.96 %	0.001 %					0.04 %
EXT01	Min	DFN R01	99.69 %	0.22 %	0.01 %				0.08 %
EXT02	Min	DFN R02	52.59 %	23.46 %	5.69 %				18.26 %
EXT10	Ext.	Constant	99.94 %	0.01 %					0.05 %
EXT11	Ext.	DFN R01	99.50 %	0.40 %	0.01 %				0.09 %
EXT12	Ext.	DFN R02	50.25 %	23.37 %	5.35 %				21.03 %
SFR3									
EXT00	Min	Constant	92.53 %	0.76 %	1.46 %	0.01 %	< 0.001 %	0.01 %	5.23 %
EXT01	Min	DFN R01	89.30 %	2.94 %	0.72 %	0.57 %	0.001 %	0.01 %	6.46 %
EXT02	Min	DFN R02	67.44 %	8.98 %	11.73 %	0.003 %	< 0.001 %	0.004 %	11.84 %
EXT10	Ext.	Constant	90.41 %	0.87 %	2.14 %	0.002 %	0.001 %	0.01 %	6.58 %
EXT11	Ext.	DFN R01	86.86 %	3.45 %	2.12 %	0.39 %	< 0.001 %	0.01 %	7.19 %
EXT12	Ext.	DFN R02	66.23 %	8.07 %	12.32 %	0.002 %	< 0.001 %	0.01 %	13.37 %

[1)] All bedrock cases employ the base-case parameterisation inside the SFR Regional domain (cases 2, 3, 4, 26, 27, 30 in Table 2-2). The parameterisation variants for HRD and HCD outside the SFR Regional domain are denoted EXT followed by one integer for HCD extension of 6 zones North from SFR (0 for minimum or 1 for maximum), and one integer for HRD parameterisation: 0 for constant K_{HRD}, 1 for DFN realisation R01, and 2 for DFN realisation R02.

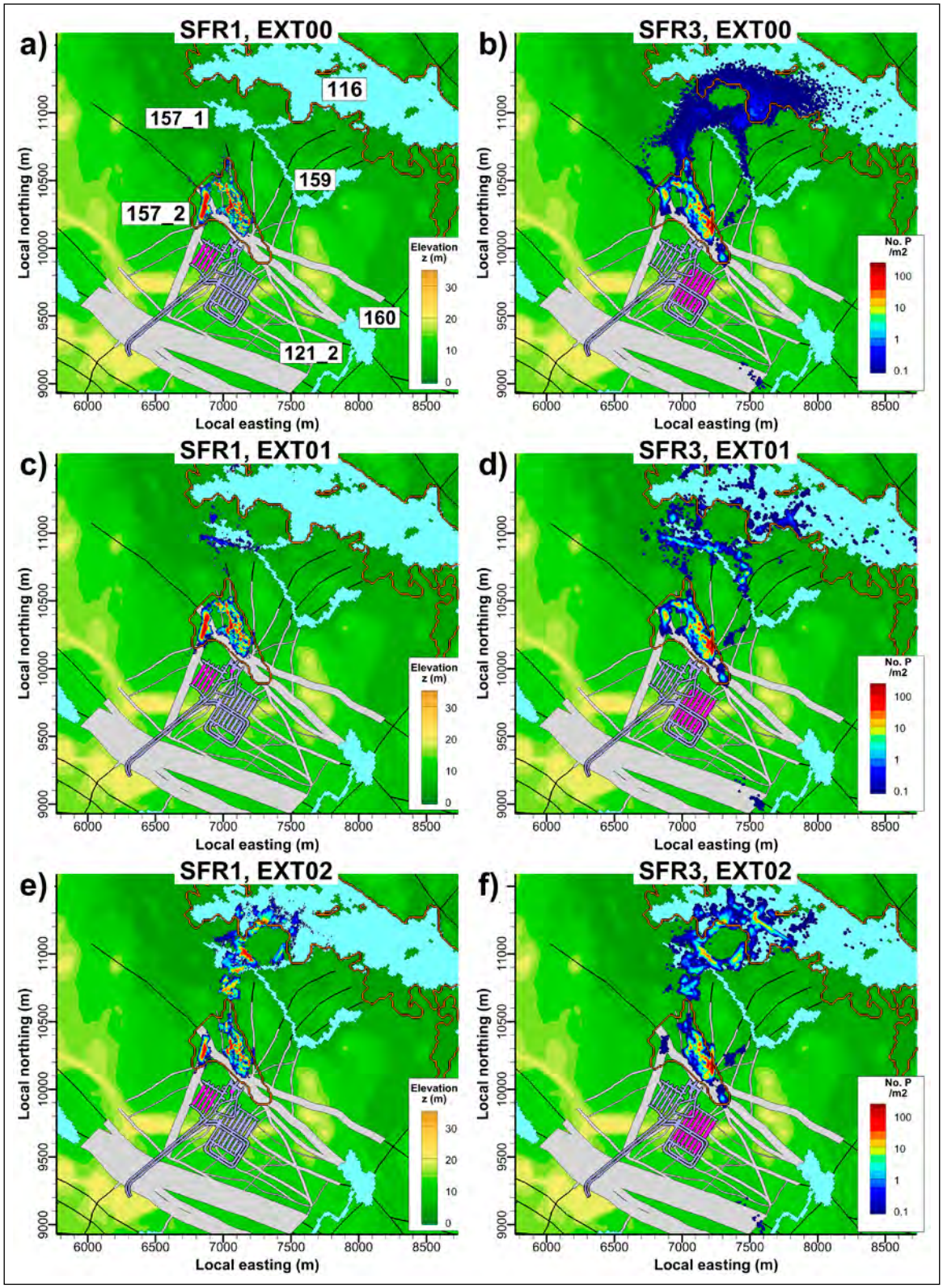

Figure 6-32. *Sensitivity to HRD parameterisation outside SFR Regional domain for exit locations during terrestrial conditions ([BASE_CASE1_DFN_R85], 5000 AD) from SFR1 (pink shaded; lefts) and SFR 3 (pink shade; right); a) and b) constant HRD parameterisation, c) and d) DFR realisation R01, and e) and f) DFR realisation R02. Biosphere object IDs 116 and 157_2 included for reference (orange lines).*

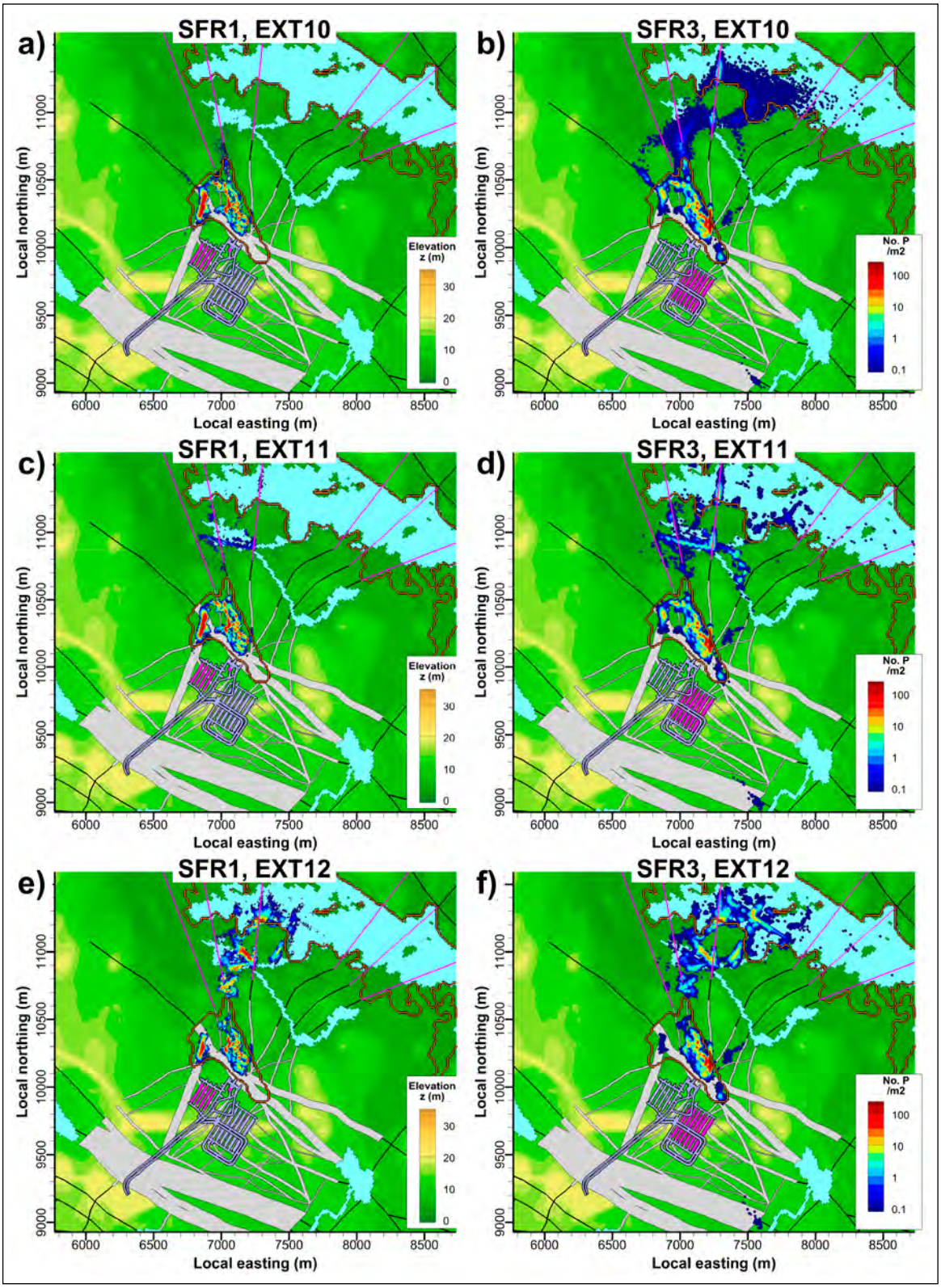

Figure 6-33. *Sensitivity to HRD parameterisation outside SFR Regional domain for exit locations during terrestrial conditions ([BASE_CASE1_DFN_R85], 5000 AD) from SFR1 (pink shaded; lefts) and SFR 3 (pink shade; right); a) and b) constant HRD parameterisation, c) and d) DFR realisation R01, and e) and f) DFR realisation R02. Biosphere object IDs 116 and 157_2 included for reference (orange lines).*

6.3.3 Performance measure statistics (Q, F_r, $t_{w,r}$, and L_r)

This section demonstrates the temporal component in simulated performance measures, based on the three bedrock cases that were selected as representative for the variability in simulation results in TD11 (Öhman et al. 2014). The focus here is the impact of the changing flow regime over time, which is resolved by steady-state simulations at nine selected stages of shore-line retreat (i.e. time slices, Table 2-1). The dynamic flow regime – gradually developing from the present-day submerged conditions to terrestrial conditions towards the later phase – is manifested as a transition in performance measures presented. This transition is resolved both on discrete time-slice basis (e.g. Figure 6-34a and b) and on the continuous time scale (e.g. Figure 6-34c and d). For a given time point, the performance measures are presented as median values (dots e.g. in Figure 6-34), and the range of variability among the three representative bedrock cases (error bars, e.g. in Figure 6-34).

This transient pattern in performance measures related to the changing flow regime is observed both in disposal-room cross flow (Figure 6-34) and in particle tracking (Figure 6-35 to Figure 6-37). Here, the measures Fr, tw,r, and Lr have been determined by means of forward tracking of 100 000 particles released in each of the 11 disposal rooms of SFR 1 and SFR 3, but only for the three selected bedrock cases (Section 6.2.4). The output of each particle-tracking simulation is a distribution of performance measures (i.e. $3 \times 11 \times 100\,000$), but in order to simplify the presentation only the medians are studied. The largest and lowest median values among these three Bedrock cases are shown as error bars in Figure 6-35 to Figure 6-37, whereas the middle median value is indicated by a dot. Examples of the corresponding underlying distributions are presented in Sections 6.3.4 to 6.3.6 (although not resolved at the individual disposal-room level).

The transient patterns in simulation results varies somewhat between disposal rooms and the type of performance measures. In general, the conditions approach stationarity at around 3500 AD to 5000 AD. However, the transition in performance measures of SFR3 is delayed a few hundred years compared to those of SFR1 (only minor changes occur for SFR3 during the first hundred years). The delay is due to the deeper location of SFR3, as the regional-scale flow component prevails longer at depth. SFR 3 also has systematically longer path lengths, advective travel times, and higher flow-related transport resistance, which is – at least partly – due to its generally lower flows and deeper location.

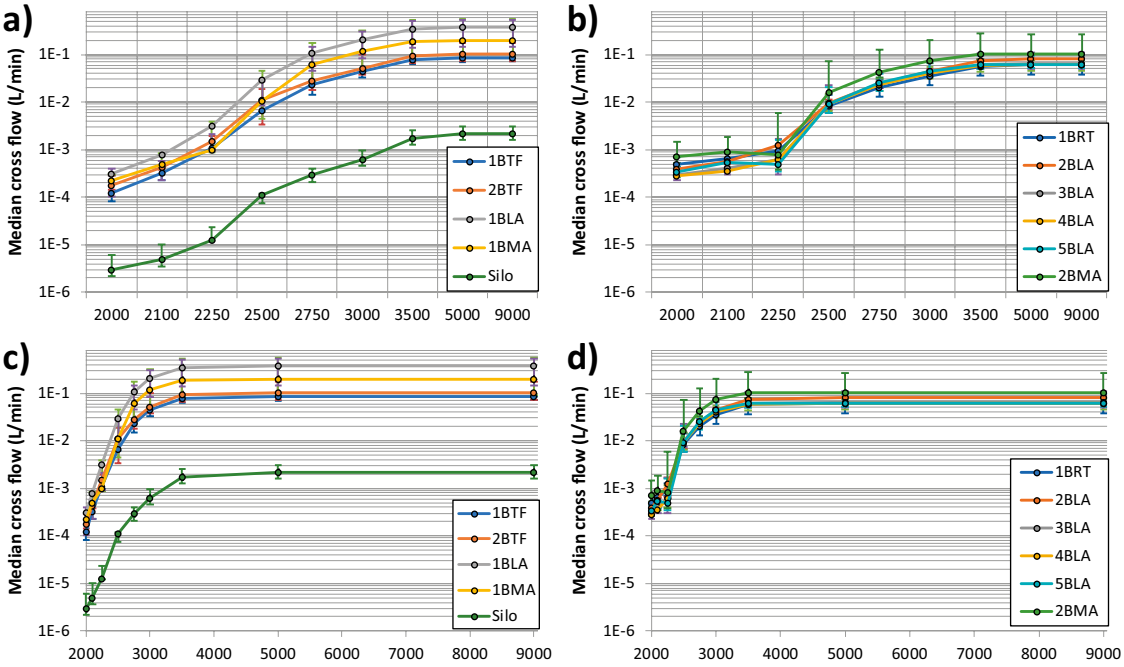

Figure 6-34. *Disposal-room cross flow (Q); a) and b) plotted for the different time slices and b) plotted against time. Dots indicate median of the three representative bedrock cases (1, 15, and 11), and bars indicate the observed variability (c.f. Figure 6-10 to Figure 6-12 in Section 6.2.2).*

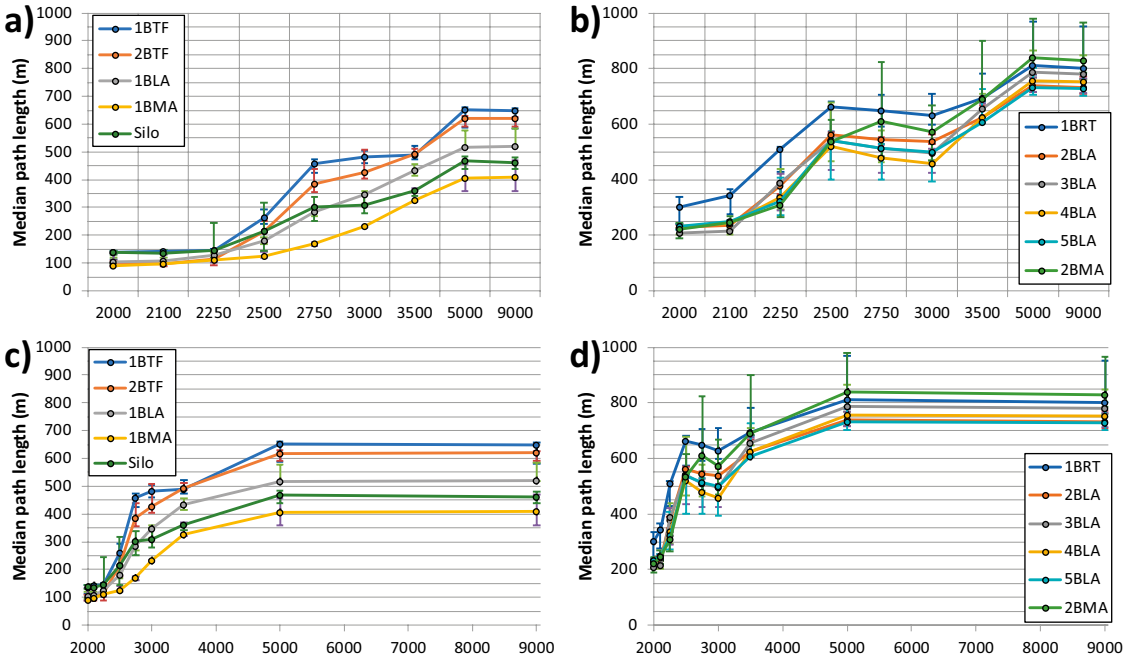

Figure 6-35. *Median path length (L_r) for trajectories from disposal rooms; a) and b) plotted for the different time slices and b) plotted against time. Dots indicate median of the three representative bedrock cases (1, 15, and 11), and bars indicate the observed variability.*

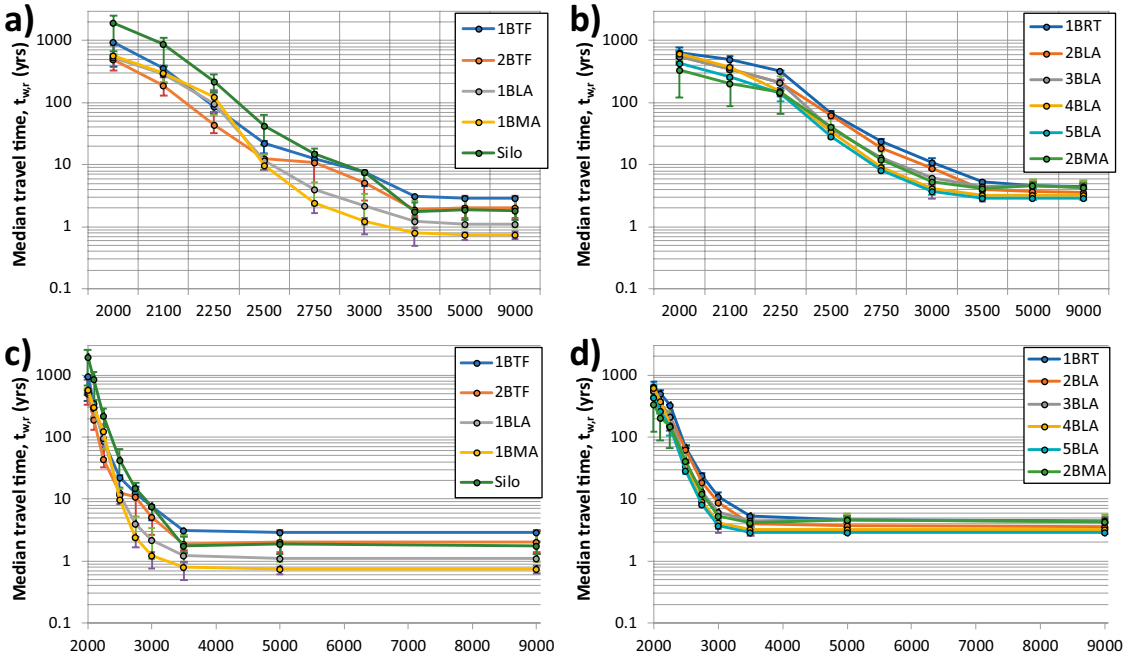

Figure 6-36. *Median advective travel times ($t_{w,r}$) for trajectories from disposal rooms; a) and b) plotted for the different time slices and b) plotted against time. Dots indicate median of the three representative bedrock cases (1, 15, and 11), and bars indicate the observed variability.*

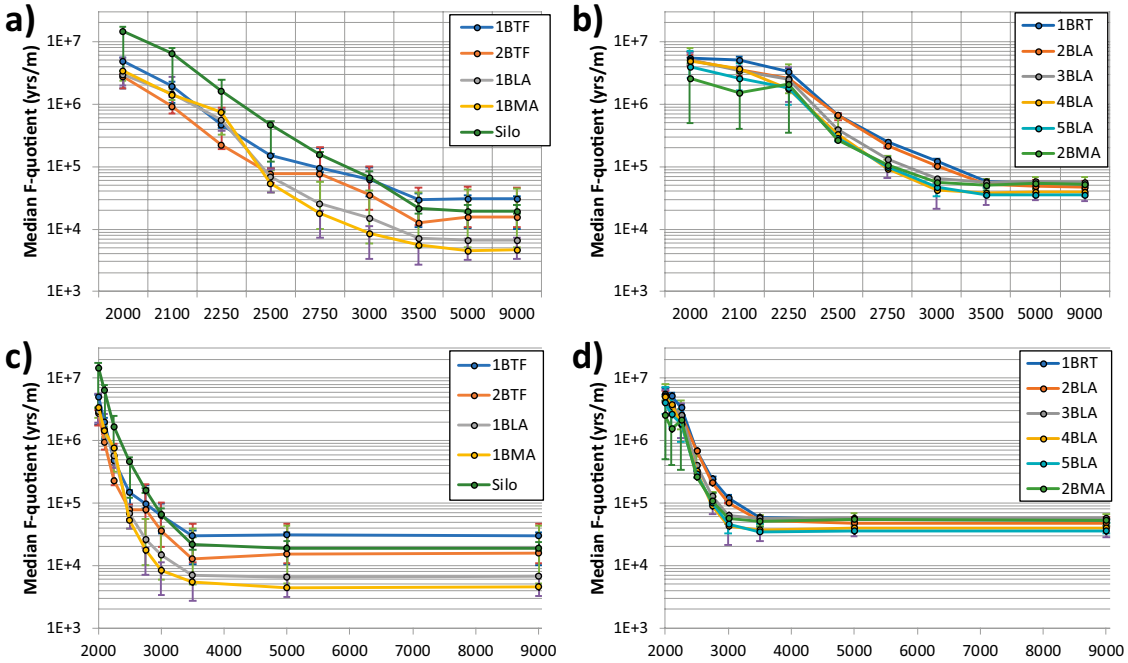

Figure 6-37. *Median flow-related transport resistance (F_r) for trajectories from disposal rooms; a) and b) plotted for the different time slices and b) plotted against time. Dots indicate median of the three representative bedrock cases (1, 15, and 11), and bars indicate the observed variability.*

6.3.4 Flow-related transport resistance

The flow-related transport resistance, F_r, for particles starting in SFR 1 and SFR 3, respectively, is studied for the three selected representative bedrock cases (Section 6.2.4) and for all nine time slices (Figure 6-38 to Figure 6-40). During the submerged conditions at 2000 AD, the flow-related transport resistance is high, c. 10^7 y/m, and the difference between SFR 1 and SFR 3 is small, compared to future time slices. The transport resistance decreases as the flow increases with the ongoing shoreline retreat, but appears to reach stationary values at around 5000 AD. The particle trajectories from SFR 3 tends to have higher transport resistance (Table 6-3), which is probably due to its deeper location and lower flows. The differences between the three bedrock cases are fairly small.

Table 6-3. Flow-related transport resistance percentiles (5 %, 50 %, and 95 %), F_r (y/m), at selected time slices.

Bedrock case	Source	2000 AD			3000 AD			5000 AD		
		5 %	50 %	95 %	5 %	50 %	95 %	5 %	50 %	95 %
1	SFR 1	8.3E+5	6.4E+6	3.2E+7	4.7E+3	3.0E+4	1.8E+5	3.0E+3	9.2E+3	5.7E+4
	SFR 3	9.4E+5	6.2E+6	2.6E+7	1.2E+4	6.6E+4	4.5E+5	1.1E+4	4.5E+4	3.2E+5
15	SFR 1	9.2E+5	2.4E+6	9.7E+6	5.7E+3	4.9E+4	3.3E+5	3.3E+3	2.1E+4	1.4E+5
	SFR 3	1.2E+6	4.4E+6	1.9E+7	1.5E+4	7.5E+4	6.4E+5	1.2E+4	5.7E+4	3.1E+5
11	SFR 1	7.4E+5	5.3E+6	2.9E+7	1.7E+3	2.0E+4	2.1E+5	1.3E+3	1.1E+4	9.5E+4
	SFR 3	3.2E+5	3.9E+6	2.7E+7	9.0E+3	6.8E+4	1.1E+6	8.0E+3	4.3E+4	7.0E+5

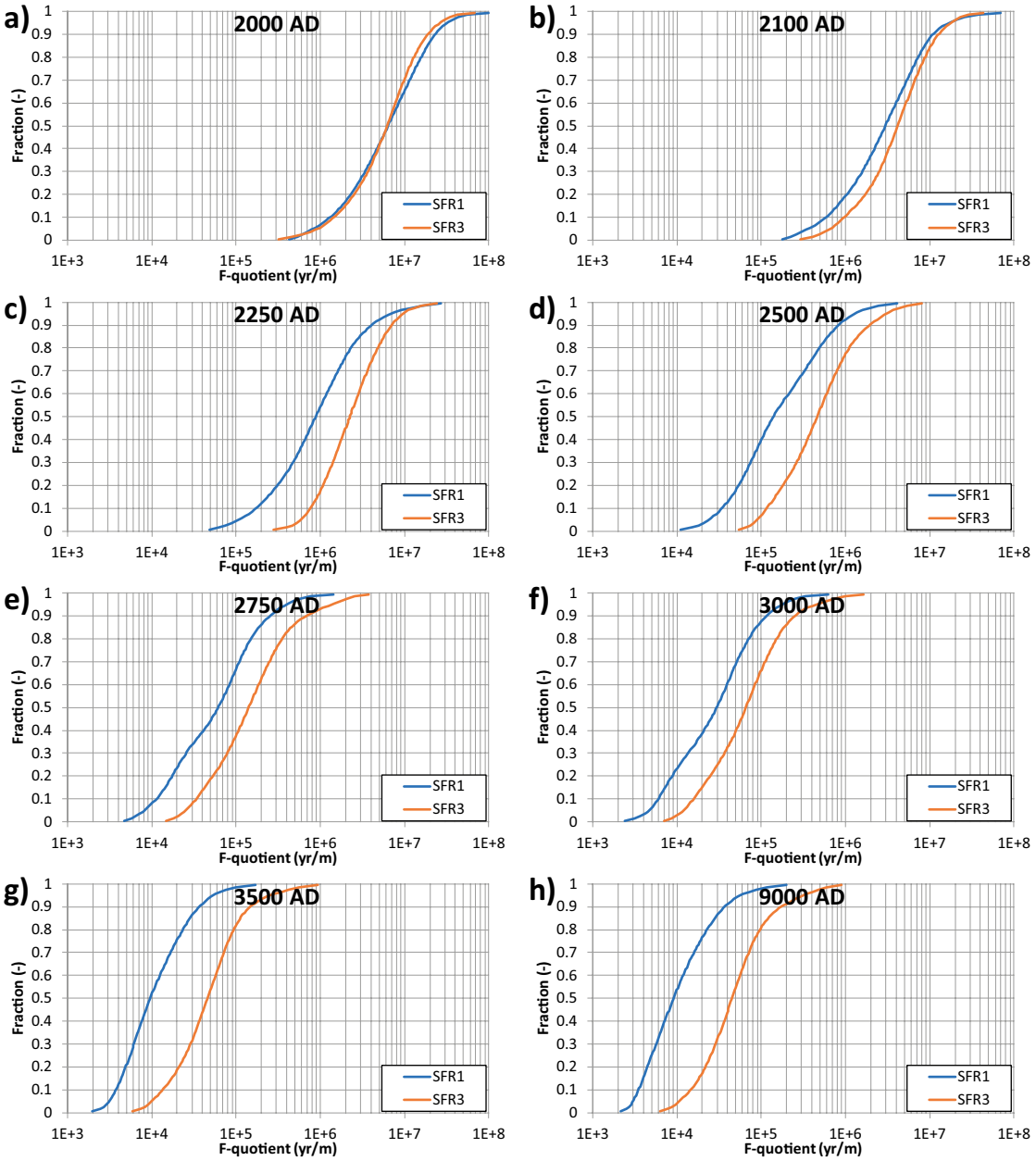

Figure 6-38. *Flow-related transport resistance, F_r (yr/m), with time, base case [BASE_CASE1_DFN_R85_EXT1].*

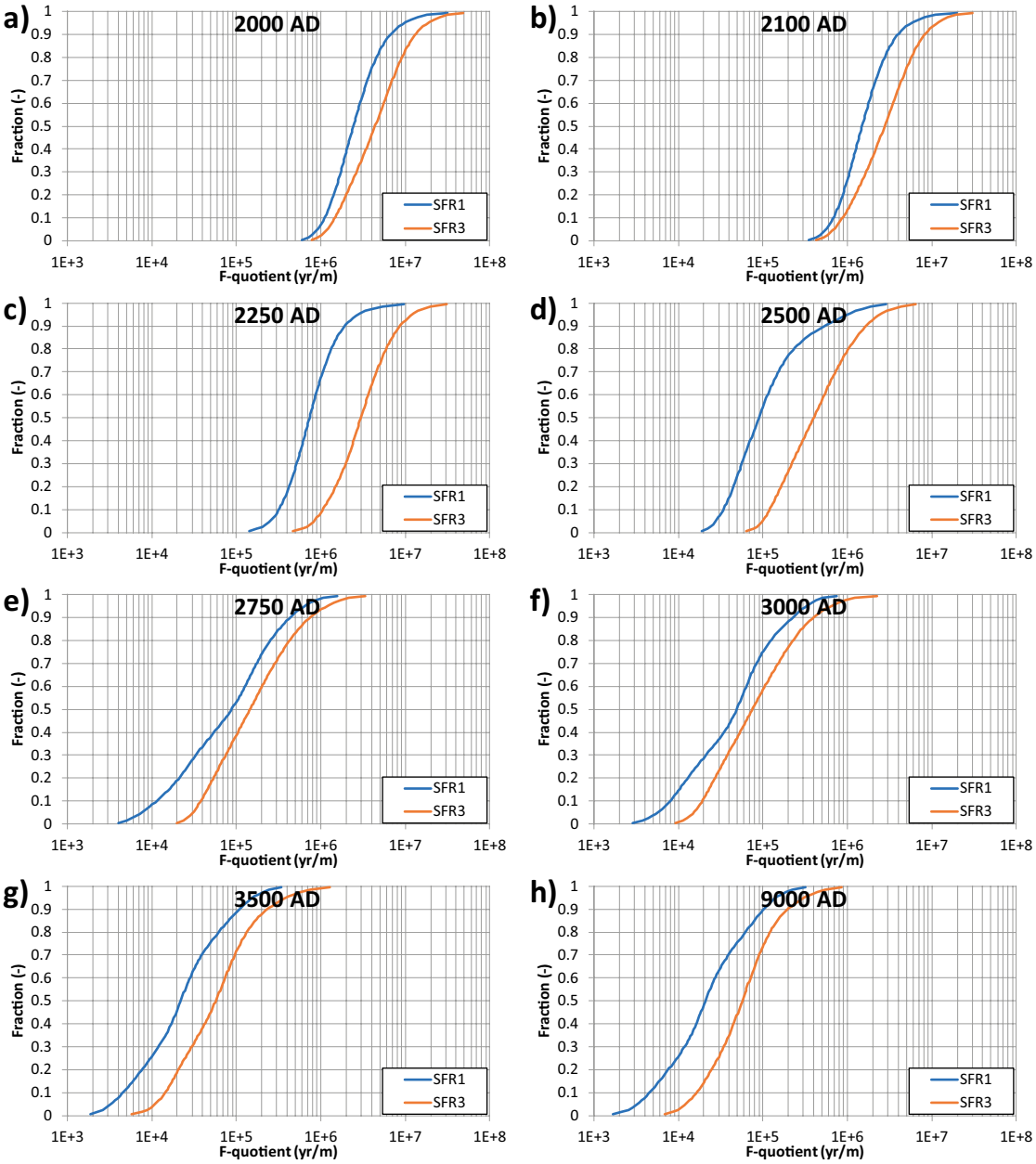

Figure 6-39. *Flow-related transport resistance, F_r (yr/m), with time, case 15 [nc_NoD_R01_DFN_R18_EXT1].*

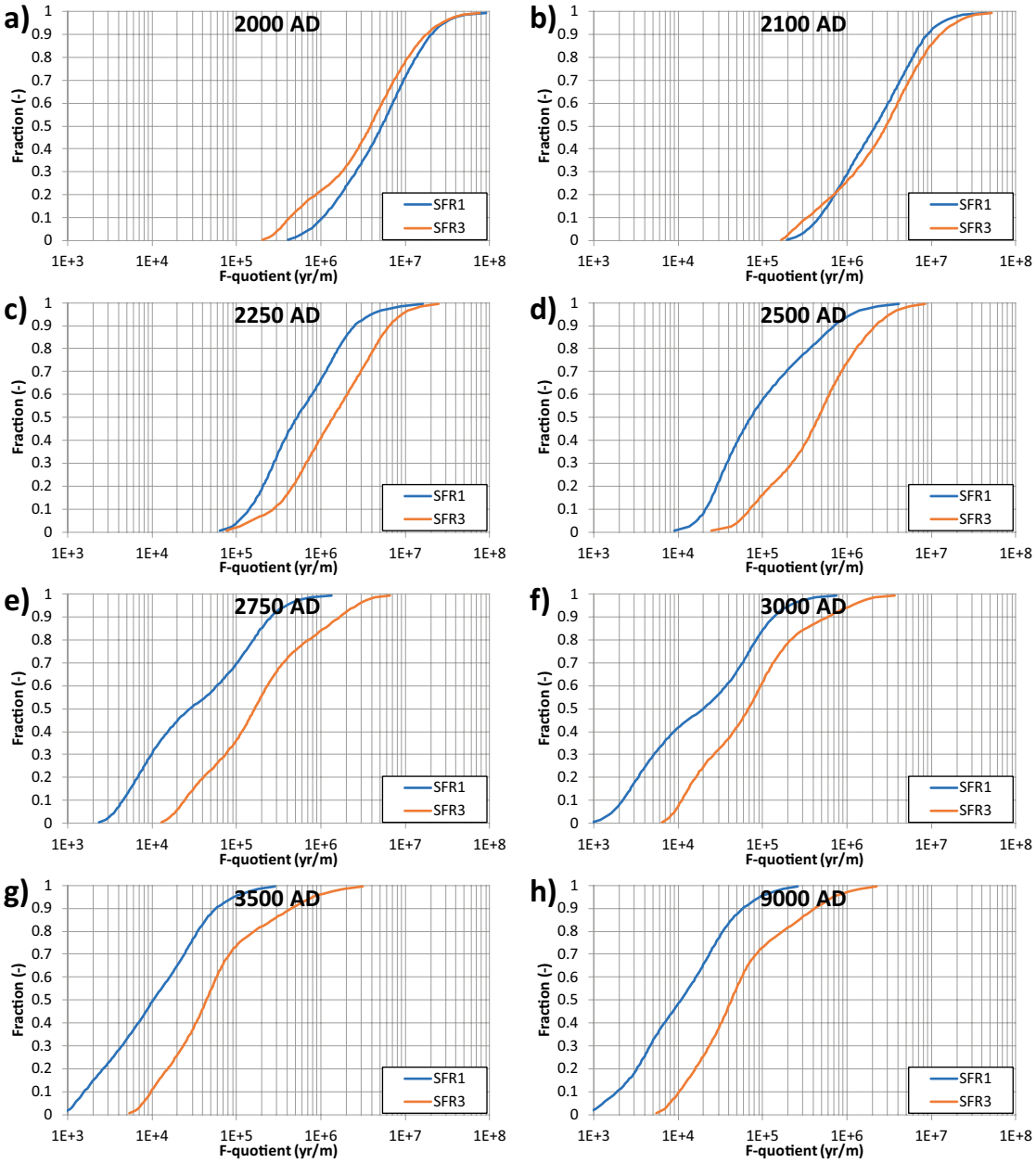

Figure 6-40. *Flow-related transport resistance, F_r (yr/m), with time, case 11 [nc_DEP_R07_DFN_R85_EXT1].*

6.3.5 Advective travel time

The advective travel time, $t_{w,r}$, for particles starting in SFR 1 and SFR 3, respectively, is studied for the three selected representative bedrock cases (Section 6.2.4) and for all nine time slices (Figure 6-41 to Figure 6-43). At 2000 AD, the travel times are long, c. 100 to 1 000 years, and the difference between SFR 1 and SFR 3 is small, compared to future time slices. Notably, SFR 1 has the longest travel times at 2000 AD (see detailed analysis in Appendix C of Öhman et al. 2014), whereas the travel times from SFR 3 are consistently longer at later time slices (Table 6-4). The differences between the three bedrock cases are fairly small.

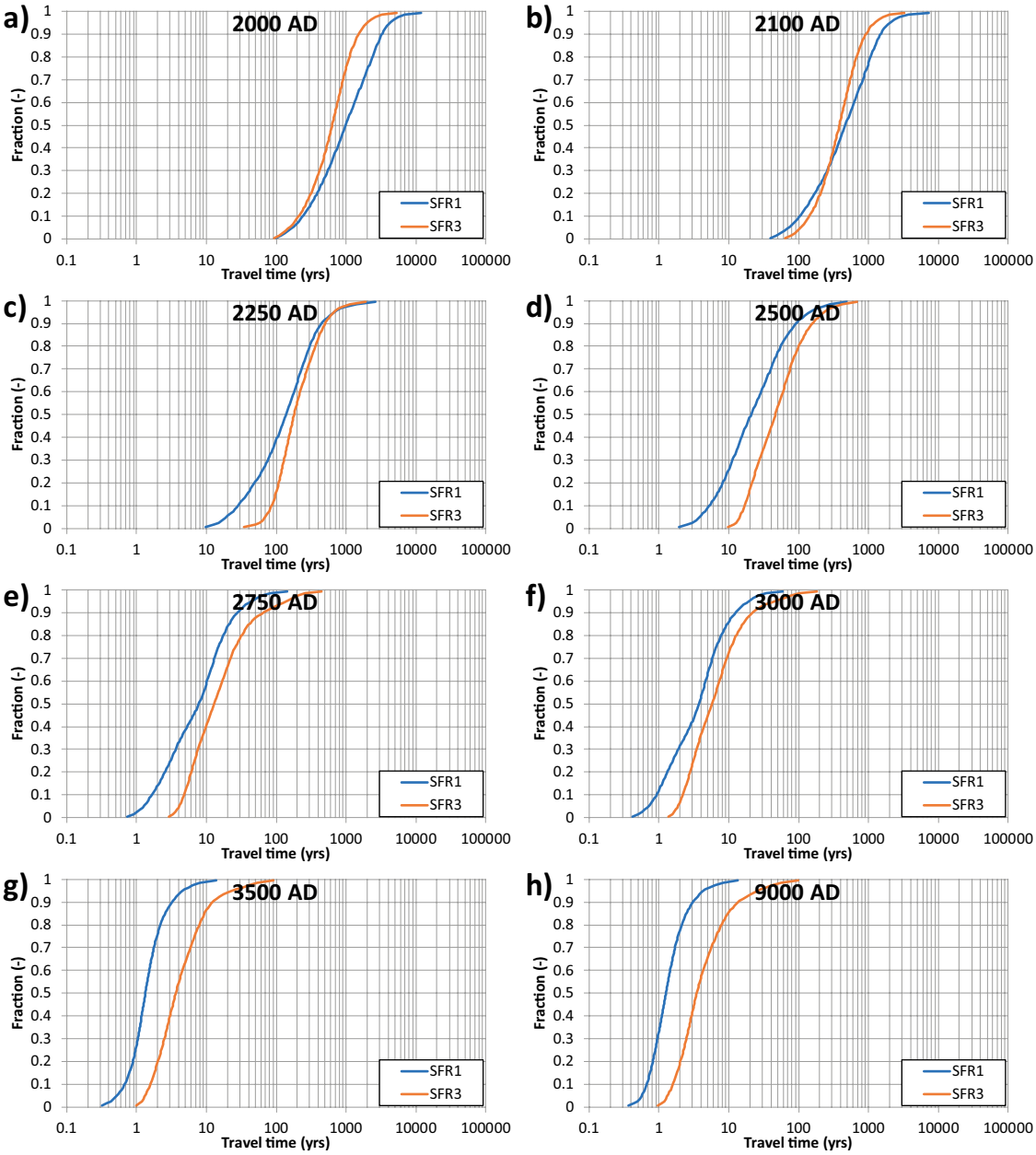

Figure 6-41. *Advective travel time, $t_{w,r}$ (yrs), with time, base case 1 [BASE_CASE1_DFN_R85_EXT1].*

Table 6-4. Travel-time percentiles (5 %, 50 %, and 95 %), $t_{w,r}$ (y), at selected time slices.

Bedrock case	Source	2000 AD			3000 AD			9000 AD		
		5 %	50 %	95 %	5 %	50 %	95 %	5 %	50 %	95 %
1	SFR 1	169	985	4207	1	4	19	1	1	4
	SFR 3	154	629	1997	2	6	45	1	3	26
15	SFR 1	203	523	1487	1	4	22	0	2	9
	SFR 3	175	440	1424	2	6	83	1	5	32
11	SFR 1	153	850	3741	0	3	19	0	1	6
	SFR 3	81	490	1942	2	6	117	1	4	74

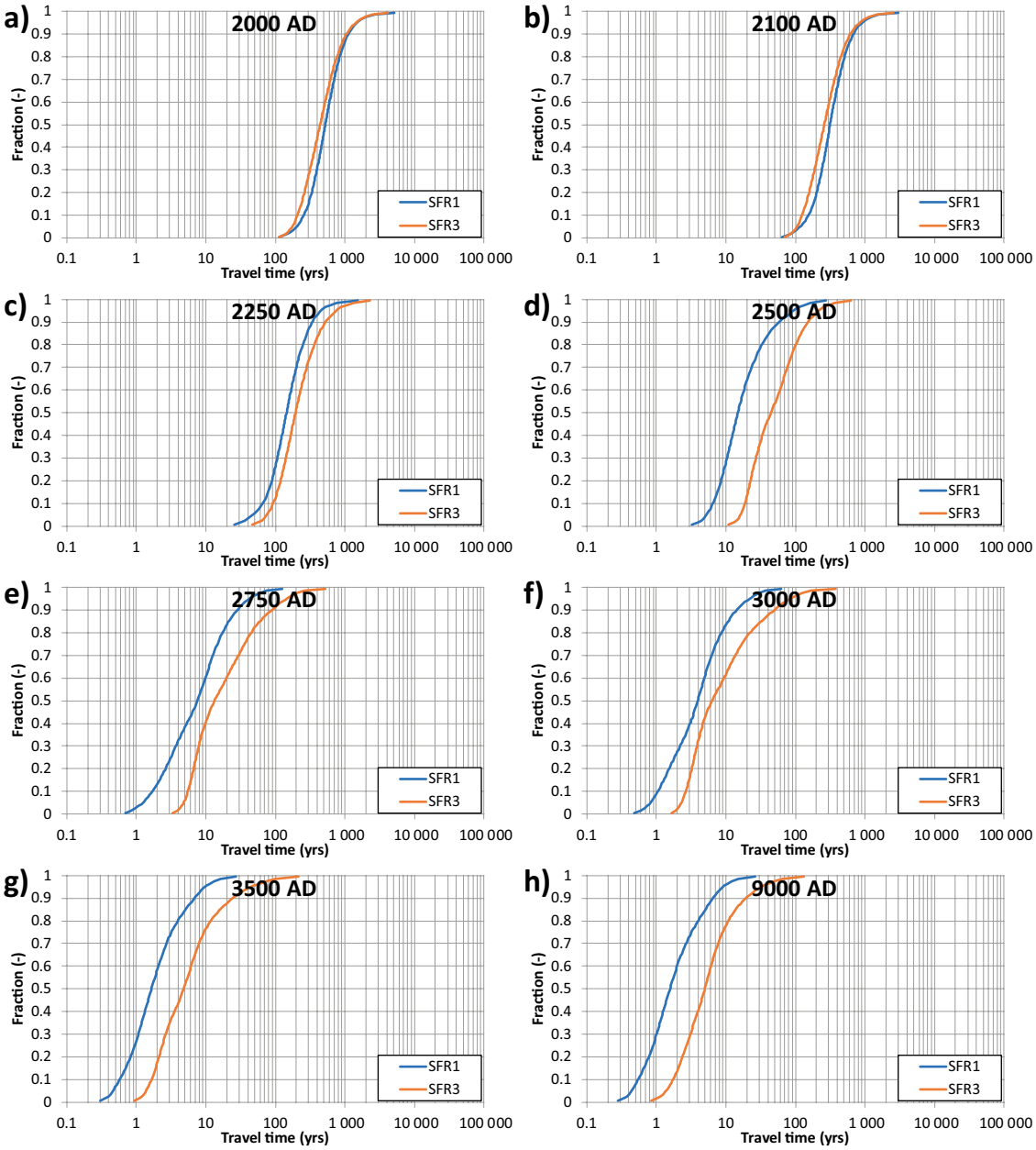

Figure 6-42. *Advective travel time, $t_{w,r}$ (yrs), with time, case 15 [nc_NoD_R01_DFN_R18_EXT1].*

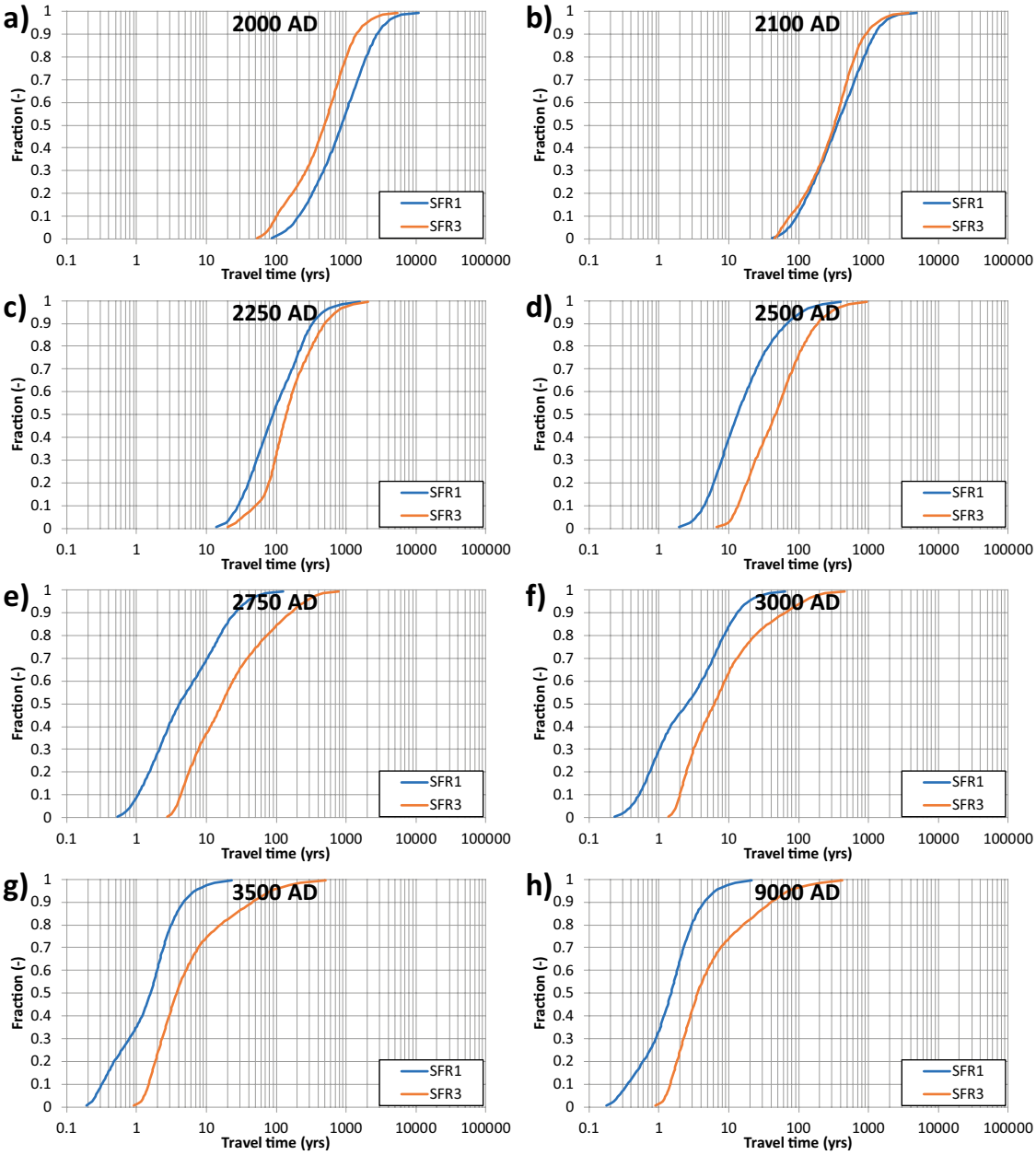

Figure 6-43. *Advective travel time, $t_{w,r}$ (yrs), with time, case 11 [nc_DEP_R07_DFN_R85_EXT1].*

6.3.6 Path length

The path length, L_r, for particles starting in SFR 1 and SFR 3, respectively, is studied for the three selected representative bedrock cases (Section 6.2.4) and for all nine time slices (Figure 6-44 to Figure 6-46). The shortest path lengths are found in the upward-directed flow regime at 2000 AD. Over time, the path lengths increase owing to the changing flow regime (can be seen in e.g. Figure 6-30 and Figure 6-31). The path lengths are consistently longer from SFR 3 than from SFR 1 (Table 6-5), which is due to its deeper location, as well as, the fact that a lesser fraction of particles exit in biosphere object 157_2 (Figure 6-30 and Figure 6-31). The differences between the three bedrock cases are fairly small.

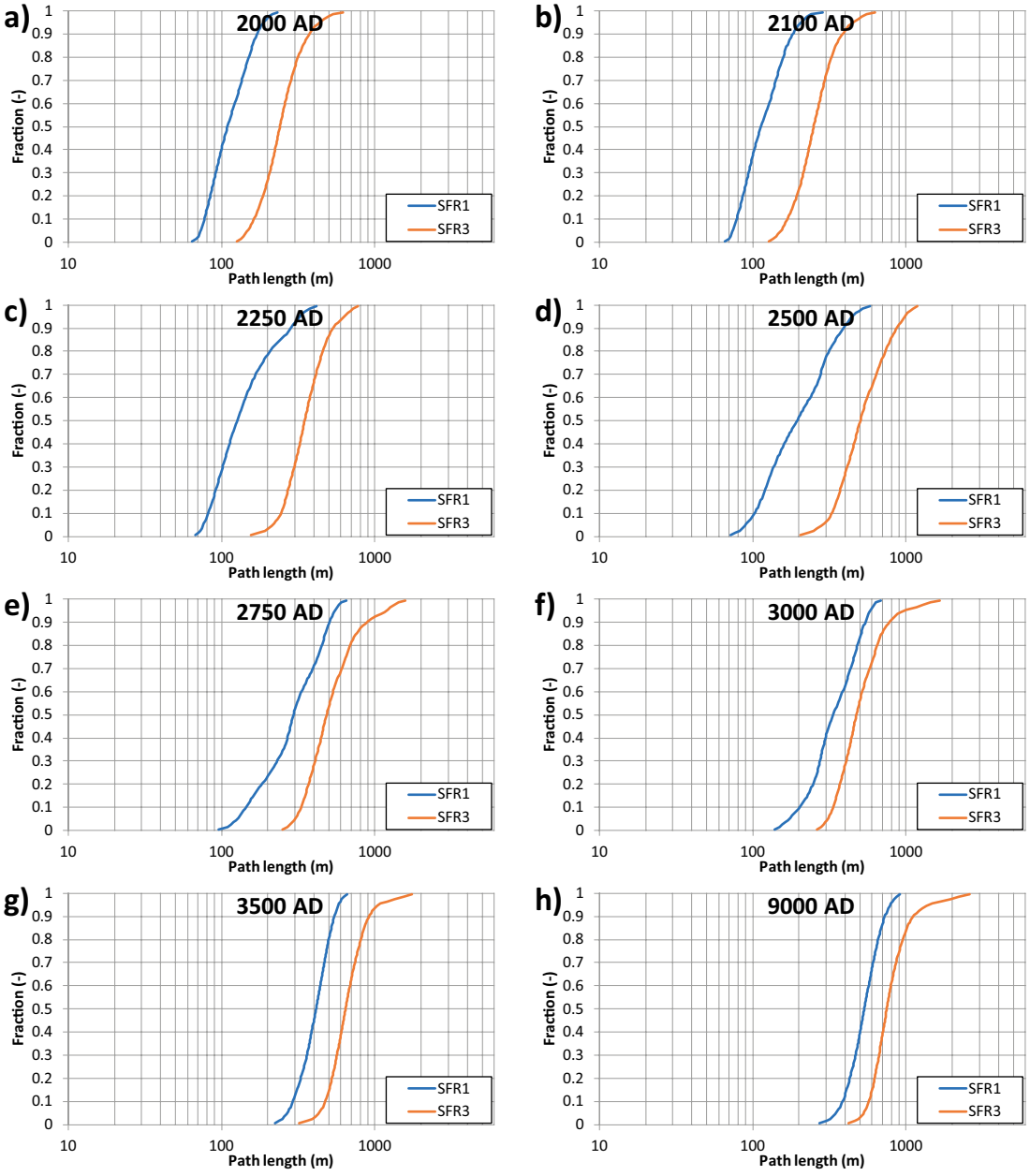

Figure 6-44. *Path length, L_r (m), with time, base case 1 [BASE_CASE1_DFN_R85_EXT1].*

Table 6-5. Path-length percentiles (5 %, 50 %, and 95 %), L_r (m), at selected time slices.

Bedrock case	Source	2000 AD			3000 AD			9000 AD		
		5 %	50 %	95 %	5 %	50 %	95 %	5 %	50 %	95 %
1	SFR 1	73	109	187	172	335	583	349	534	789
	SFR 3	148	240	434	307	474	968	530	748	1423
15	SFR 1	84	125	194	179	342	625	323	453	803
	SFR 3	151	220	352	325	535	1804	503	772	1610
11	SFR 1	71	109	199	172	303	537	327	512	814
	SFR 3	145	226	411	310	551	1603	530	848	2362

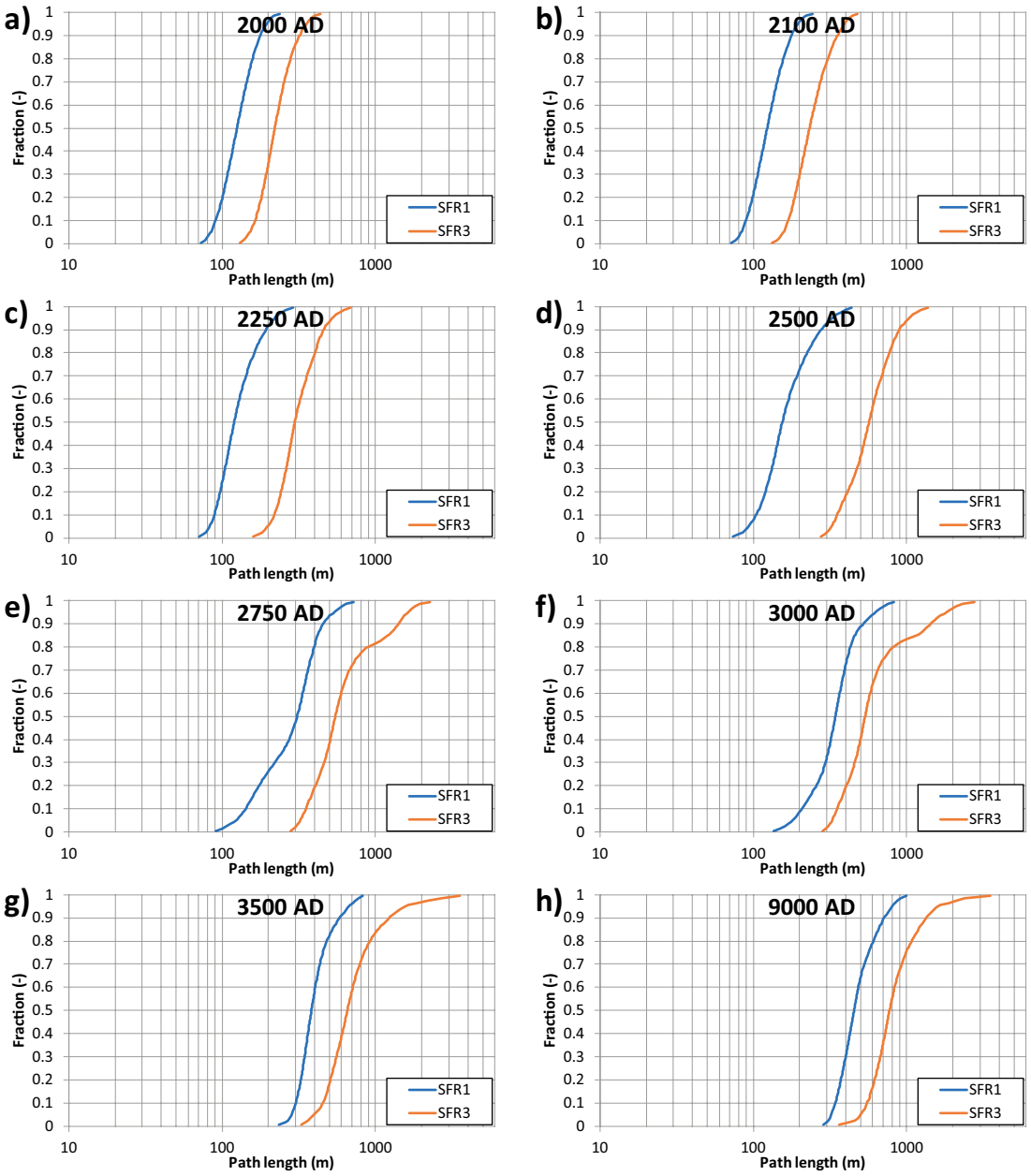

Figure 6-45. *Path length, L_r (m), with time, bedrock case 15 [nc_NoD_R01_DFN_R18_EXT1].*

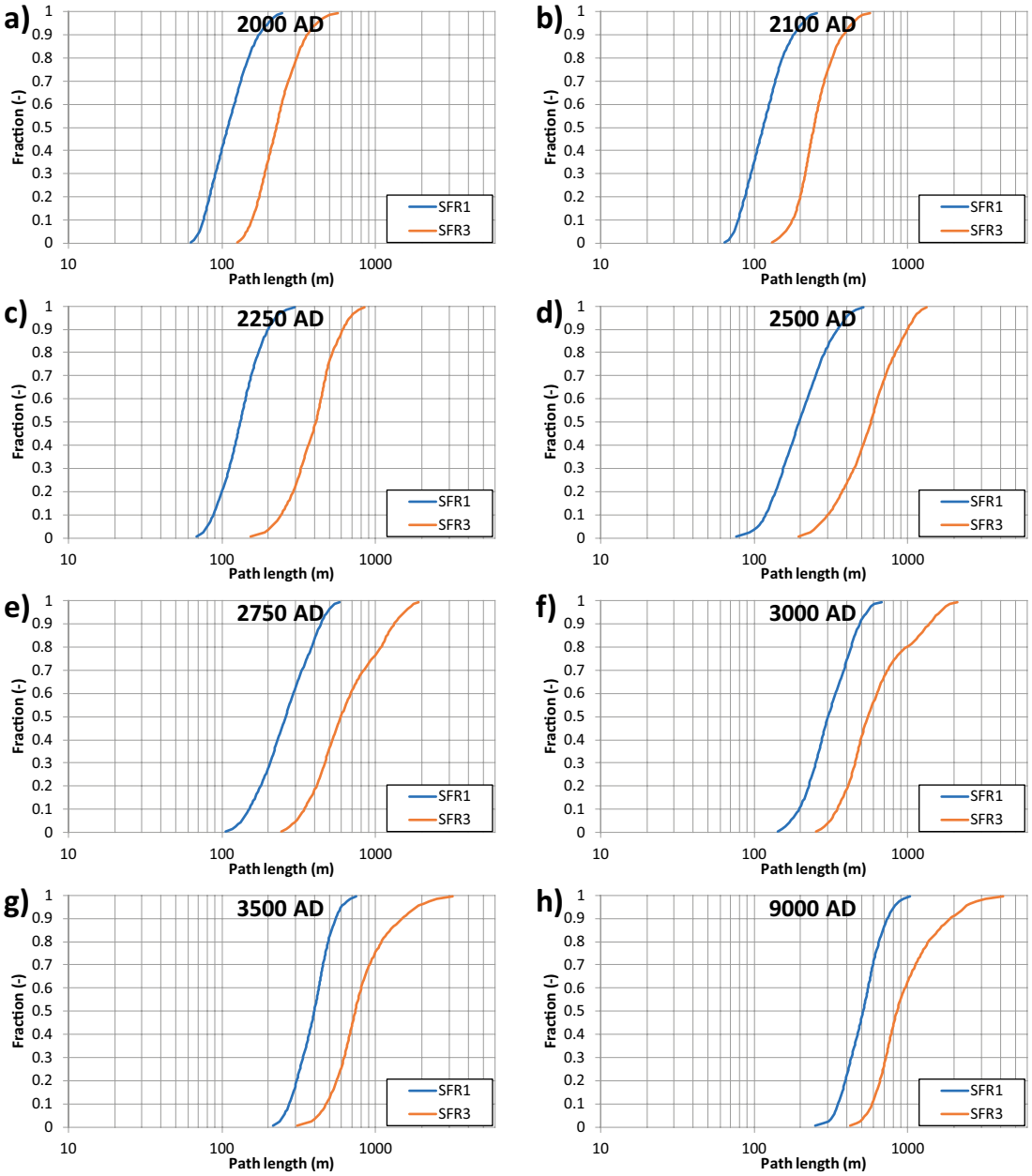

Figure 6-46. *Path length, L_r (m), with time, bedrock case 11 [nc_DEP_R07_DFN_R85_EXT1].*

7 Summary and conclusions

As a part of the license application for the expansion of SFR, the radiological safety for the entire repository after closure is assessed (SR-PSAR). Two different climate conditions are studied in SR-PSAR, temperate and periglacial conditions (Odén et al. 2014). The SR-PSU project has studied various issues/uncertainties in the hydrogeological modelling of SFR, addressed in studies defined in terms of so-called Task Descriptions (TDs). This present report summarises the methodology, setup, and results of the groundwater flow modelling, which represents the final modelling stage under temperate conditions.

The groundwater flow model, developed in SDM-PSU (SKB 2013), is used to assess performance measures for the existing repository (SFR 1) and its planned extension (SFR 3). The combined effects of bedrock heterogeneity, parameterisation uncertainty, and the transient flow regime on performance measures are assessed in a sensitivity analysis. The sensitivity analysis consists of 30 so-called Bedrock cases (model-parameterisation variants), which are studied as steady state solutions under selected time slices. The time slices cover nine representative stages of shoreline retreat, where particular emphasis is paid to the early stages of shoreline retreat (Table 2-1).

The primary outcomes of the sensitivity analysis are:

1. a demonstration of the dynamic hydrogeological setting under temperate climate conditions, and
2. performance measures delivered to users within SR-PSAR.

Performance measures

The key performance measures (output) from the groundwater flow modelling are:

- Disposal-room cross flow, Q (m^3/s).
- Particle exit location at the bedrock/regolith interface.
- Flow-related transport resistance along bedrock flow paths, Fr (y/m).
- Advective travel times along bedrock flow paths, tw,r (y).

A performance measure of supporting character is:

- Length of bedrock flow paths, Lr (m).

The particle-tracking results for each bedrock case and time slice have been exported to different users with SR-PSU.

Characteristics of the hydrogeological setting

The local parameterisation of deformation zones that intersect disposal rooms has been identified as a key uncertainty for the evaluation of cross flows through the disposal rooms. The three most critical deformation zones are identified as:

- ZFMNNW1209: formerly referred to as Zone 6. The zone intersects all four rock vaults of SFR 1. In the base case, its parameterisation is conditioned at tunnel intercepts based on estimated grouting requirements. Hence, the conditioning of this zone is a main uncertainty in the analysis (Figure 4-7).
- ZFMWNW0835 and ZFMENE3115: both intersecting 3 rock vaults in SFR 3 (Figure 4-8). Previous hydrogeological modelling in SR-PSU has identified the key uncertainty in the parameterisation of these zones to be amplified by the assumed depth trend (see Öhman et al. 2014). The objective of the sensitivity analysis is to provide upper estimates of the sensitivity to bedrock parameterisation uncertainty, and therefore it was decided to assume depth-trend in HCD transmissivity in all bedrock cases (i.e. except in the low-flow case 15).

The results demonstrate the understanding of post-closure repository performance under present-day hydrogeological conditions, as well as, how these are predicted to change during future stages of shoreline retreat. The altering flow regime is addressed by comparing steady-state flow solutions at selected stages of shoreline retreat, referred to as "time slices". The current flow regime is characterised as modest and upward-directed. As the hydrostatic pressure underneath the Baltic Sea retreats further away from SFR, the flow regime becomes successively governed by local topography, and grows with an increasingly horizontal component. The flow regime around SFR approaches stationarity at c. 3500 to 5000 AD (i.e. largely unaffected by further shoreline withdrawal).

This transient character of the hydrogeological setting is reflected in all studied performance measures. For example, the cross flow through disposal rooms, Q, increases during the early stages of shoreline displacement, to reach approximately stationary conditions at 3500 to 5000 AD (Figure 6-34). Another example is the migration of repository-discharge areas, i.e. locations where the discharging groundwater from the repository reaches ground surface. Up to c. 3500 AD, the discharge areas are displaced by the retreating Baltic Sea shoreline (Figure 6-30), but remain more or less static in the 5000 AD and 9000 AD time slices (Figure 6-31). This pattern in successively relocating discharge areas is also observed in terms of increasing particle-trajectory lengths, L_r, up to c. 5000 AD (Figure 6-35). As the horizontal component in the flow field grows stronger, the advective travel time, $t_{w,r}$, and flow-related transport resistance, F_r, decrease (Figure 6-36 and Figure 6-37), which signifies that, in the determination of these performance measures, the significance of increasing flows outweighs the increasing path lengths. Similarly, the change in $t_{w,r}$ and F_r between the 5000 AD and 9000 AD time slices is negligible.

Performance of SFR 1

The existing SFR 1 exhibits somewhat higher range of variability in simulated disposal-room cross flow, which is related to its sensitivity to the parameterisation of ZFMNNW1209 (i.e. the observed variability is high for 1BLA and 1BMA, although this is specific to the HCD realisations studied; instead the variability should be interpreted as generic, applying to all four rock caverns). The SFR discharge is associated to deformation-zone intercepts and are somewhat displace by the retreating shoreline. The key recipient for SFR 1 discharge forms at around 3750 AD (biosphere object 157_2; Figure 2-3). Under specific premises (exemplified by DFN realisation R02 outside the SFR Regional domain) may divert discharge to lake object 116 (Table 6-2). With the exception of the particular flow regime under current, submerged conditions, the existing disposal facility SFR 1 has consistently poorer performance compared to the planned extension SFR 3.

Performance of SFR 3

During the early stages, SFR 3 has exit locations both north and south of the SFR pier, but as the horizontal component in flow successively grows, the exit locations are driven north. Most particles from SFR 3 discharge into biosphere object 157_2, although owing to its deeper location, a smaller number of particles discharge to biosphere objects related to biosphere object 116. The deeper location of SFR 3 renders systematically longer path lengths, longer advective travel times, and higher flow-related transport resistance, as compared to SFR 1.

Representative Bedrock cases

Based on a statistical ranking analysis of simulation results, three bedrock cases were selected as representative for covering the range in observed cross flow through disposal rooms in TD11 (Öhman et al. 2014). The results of these three representative bedrock cases compare well to the earlier results obtained in TD11 (Section 6.2.3), and the flow solutions have been exported to the near-field modelling team (Abarca et al. 2014). The span of simulated disposal-room flow in the representative cases is less than varying the bedrock parameterisation by an order of magnitude (Figure 6-17). The three selected cases 1, 11, and 15 are still considered to be representative of the span in tunnel flow arising from uncertainty in bedrock parameterisation.

Specific hydrogeological issues

The key recipient for SFR 1 discharge forms at around 3750 AD (biosphere object 157_2; Figure 2-3). Simulations demonstrate that – under specific premises – the DFN parameterisation outside the SFR Regional domain may divert a substantial amount of discharge to lake object 116 (c. 50 %; Table 6-2). Geometric/statistical analysis of multiple stochastic DFN realisations demonstrate that that the particular DFN realisation is anomalous (i.e. the hydrogeological traits of R02 are anomalous in context of a larger ensemble; Öhman and Odén 2017b). Nevertheless, this case demonstrates that the SFR performance is subject to bedrock properties outside the characterised domain in the PSU Site-Descriptive Model (SKB 2013).

The existence of deformation zones in the SFR discharge area, just north of the SFR Regional domain, has been identified as a hydrogeological uncertainty (Figure 4-11). Simulations demonstrate that elaborating the extension of six deformation zones north from the SFR model domain has minor effect on performance (Table 6-2).

The hydrogeological character of the Singö deformation zone has been identified as another uncertainty that may affect the balance between regional-scale flow and local-scale flow driven by the emerging seafloor sediments and thereby control flow in the SFR host rock during early stages of shoreline retreat. Simulations demonstrate that implementing a barrier for transversal flow ($K = 10^{-9}$ m/s) may reduce disposal-room flow by 30 % to 70 % during the first 100 years or so, but that the effects become negligible after c. 2500 AD.

References

SKB's (Svensk Kärnbränslehantering AB) publications can be found at www.skb.com/publications. SKBdoc documents will be submitted upon request to document@skb.se.

Abarca E, Idiart A, de Vries L-M, Silva O, Molinero J, von Schenck H, 2014. Flow modelling on the repository scale for the safety assessment SR-PSU. SKB TR-13-08, Svensk Kärnbränslehantering AB.

Bosson E, Sassner M, Sabel U, Gustafsson L-G, 2010. Modelling present and future hydrology and solute transport at Forsmark. SR-Site Biosphere. SKB R-10-02, Svensk Kärnbränslehantering AB.

Brydsten L, Strömgren M, 2013. Landscape development in the Forsmark area from the past into the future (8500 BC to 40 000 AD). SKB R-13-27, Svensk Kärnbränslehantering AB.

Curtis P, Markström I, Petersson J, Triumf C-A, Isaksson H, Mattsson H, 2011. Site investigation SFR. Bedrock geology. SKB R-10-49, Svensk Kärnbränslehantering AB.

Dershowitz W, Winberg A, Hermanson J, Byegård J, Tullborg E-L, Andersson P, Mazurek M, 2003. Äspö Hard Rock Laboratory. Äspö Task Force on modelling of groundwater flow and transport of solutes. Task 6c. A semi-synthetic model of block scale conductive structures at the Äspö HRL. SKB IPR-03-13, Svensk Kärnbränslehantering AB.

Follin S, 2008. Bedrock hydrogeology Forsmark. Site descriptive modelling, SDM-Site Forsmark. SKB R-08-95, Svensk Kärnbränslehantering AB.

Follin S, Johansson P-O, Hartley L, Jackson P, Roberts D, Marsic N, 2007. Hydrogeological conceptual model development and numerical modelling using CONNECTFLOW, Forsmark modelling stage 2.2. SKB R-07-49, Svensk Kärnbränslehantering AB.

Holmén J G, Stigsson M, 2001. Modelling of future hydrogeological conditions at SFR. SKB R-01-02, Svensk Kärnbränslehantering AB.

Joyce S, Simpson T, Hartley L, Applegate D, Hoek J, Jackson P, Swan D, Marsic N, Follin S, 2010. Groundwater flow modelling of periods with temperate climate conditions – Forsmark. SKB R-09-20, Svensk Kärnbränslehantering AB.

Luterkort D, Nyblad B, Wimelius H, Pettersson A, Aghili B, 2014. SFR förslutningsplan. SKBdoc 1358612 ver 1.0, Svensk Kärnbränslehantering AB.

Näslund J-O, 2015. Shore level data Forsmark Global warming SR-PSU. SKBdoc 1359616 ver 2.0, Svensk Kärnbränslehantering AB.

Odén M, 2017. SR-PSU: Task description TD18. Temperate simulations PSAR SR-PSU. SKBdoc 1616010 ver 1.0,Svensk Kärnbränslehantering AB.

Odén M, Öhman J, 2017. SR-PSU SFR geometrier för DarcyTools. SKBdoc 1611280 ver 1.0, Svensk Kärnbränslehantering AB.

Odén M, Follin S, Öhman J, Vidstrand P, 2014. SR-PSU Bedrock hydrogeology. Groundwater flow modelling methodology, setup and results. SKB R-13-25, Svensk Kärnbränslehantering AB.

SKB, 2008. Geovetenskapligt undersökningsprogram för utbyggnad av SFR. SKB R-08-67, Svensk Kärnbränslehantering AB. (In Swedish.)

SKB, 2013. Site description of the SFR area at Forsmark at completion of the site investigation phase. SDM-PSU Forsmark. SKB TR-11-04, Svensk Kärnbränslehantering AB.

SKB, 2014a. Climate and climate related issues for the safety assessment SR-PSU. SKB TR-13-05, Svensk Kärnbränslehantering AB.

SKB, 2014b. Initial state report for the safety assessment SR-PSU. SKB TR-14-02, Svensk Kärnbränslehantering AB.

Svensson U, Ferry M, Kuylenstierna H-O, 2010. DarcyTools version 3.4 – Concepts, methods and equations. SKB R-07-38, Svensk Kärnbränslehantering AB.

Svensson U, Follin S, 2010. Groundwater flow modelling of the excavation and operational phases – Forsmark. SKB R-09-19, Svensk Kärnbränslehantering AB.

Werner K, Sassner M, Johansson E, 2013. Hydrology and near-surface hydrogeology at Forsmark – synthesis for the SR-PSU project. SR-PSU Biosphere. SKB R-13-19, Svensk Kärnbränslehantering AB.

Öhman J, 2010. Site investigation SFR. Hydrogeologic modelling of SFR v 0.1. Influence of the ridge on the flow fields for different target volumes. SKB R-09-43, Svensk Kärnbränslehantering AB.

Öhman J, 2013a. TD08- SFR3 effect on the performance of the existing SFR. SKBdoc 1395214 ver 2.0, Svensk Kärnbränslehantering AB.

Öhman J, 2013b. TD10- SFR3 adaptation to hydrogeological conditions. SKBdoc 1395215 ver 1.0, Svensk Kärnbränslehantering AB.

Öhman J, 2013c. Detailed study of nbgrad. SKBdoc 1396127 ver 1.0, Svensk Kärnbränslehantering AB.

Öhman J, Bockgård N, 2013. TD05 – Effects in ECPM translation. SKBdoc 1395200 ver 1.0, Svensk Kärnbränslehantering AB.

Öhman J, Odén M, 2017a. TD14 **–** Complementary simulation cases in support of SR-PSU. SKBdoc 1496921 ver 1.0, Svensk Kärnbränslehantering AB.

Öhman J, Odén M, 2017b. TD15 Complementary simulation cases in support of SR-PSU. SKBdoc 1578373 ver 1.0, Svensk Kärnbränslehantering AB.

Öhman J, Odén M, 2017c. TD16 – Effect of connecting RTT to existing access tunnel. SKBdoc 1581260 ver 1.0, Svensk Kärnbränslehantering AB.

Öhman J, Vidstrand P, 2014. SR-PSU Bedrock hydrogeology. TD12 – Water-supply wells in rock. SKB P-14-05, Svensk Kärnbränslehantering AB.

Öhman J, Bockgård N, Follin S, 2012. Site investigation SFR. Bedrock hydrogeology. SKB R-11-03, Svensk Kärnbränslehantering AB.

Öhman J, Follin S, Odén M, 2013. Site investigation SFR. Bedrock hydrogeology – Groundwater flow modelling. SKB R-11-10, Svensk Kärnbränslehantering AB.

Öhman J, Follin S, Odén M, 2014. SR-PSU Hydrogeological modelling. TD11 – Temperate climate conditions. SKB P-14-04, Svensk Kärnbränslehantering AB.

Appendix A

Modelling sequence and traceability in data management

The different steps in the modelling approach are presented in general terms in Chapters 3, 4, and 5 of the main report. This appendix provides the details of the execution of simulations, with focus on traceability in handling of all input and output; not only at each given execution step, but also in the transfer between different steps in the modelling sequence. An overview of the modelling sequence, which is broken down into four separate file-management routines, is presented in Appendix A1.

As the conceptual framework and principles of the modelling approach is presented in the main report, this appendix focuses on the numerical execution of the modelling sequence. That is: file-name conventions of all input and output data and codes used to manage traceability in the throughout the different steps of the simulation sequence. This is broken down into three subsections:

- Preparation of input data, file conversion, and parameterisation (Appendix A2).
- Model setup and execution of the flow simulations (Appendix A3).
- Post-processing to extract results (Appendix A4).

The reader is referred to the main report for a more comprehensive exposé on the rationale and context of the different execution steps.

A1 Overview of modelling sequence

As explained in Section 1.2, a total of 270 model setups are addressed (i.e. the combinations of 30 bedrock cases, and 9 stages of shoreline retreat). In the automatized execution of these model setups, each is defined by the combination of two variables <Bedrock case> and <time slice> (i.e. Table 2-1 and Table 2-2 in the main report). Here the brackets, < >, and colour marking are used to denote the variables of the sensitivity analysis, and have a key role for the traceability in data management. Even a single model setup is complex, involving multiple input files that are being processed in several steps (Figure A-1). There are (at least) three reasons to apply automatized data-file management in the modelling sequence:

- Minimisation of data-handling related errors: automatizing ensures that: 1) all model setups are consistently handled (i.e. all model setups are treated the same way), and 2) application of input files is consistent with the specified <Bedrock case>/ <time slice>case (i.e. follows specifications in Table 2-1 and Table 2-2).
- Traceability: automatizing provides traceable data management via the source codes, and also maintains a strict traceability between sequences by means of case-specific filenames for intermediate input and output (i.e. all I/O filenames are tagged by relevant specification to <Bedrock case> and/or <time slice>). No output can be fully processed until all its underlying intermediate input components have been pre-processed (e.g. DFN realisations, HCD fracture files, ECPM upscaling, etc.).
- Time efficiency: automatizing allows: 1) parallel processing in different working directories and 2) continuous processing over weeks, day and night.

Consequently, data file management is automatized as far as possible. The modelling sequence is divided into four main sequences (Figure A-1), which are handled by file-managing routines to maintain traceability between input and output:

a. **Data for grid preparation:** The computational grid itself is generated by the DarcyTools module GridGen. The geometric input data to control the grid generation are managed by a range of customized tools (see footnotes to Figure A-1).
b. **ECPM upscaling:** The ECPM upscaling (conversion from fracture/deformation-zone properties to grid-cell properties of an Equivalent Continuum Porous Medium) is performed by the DarcyTools module FracGen. The automatized execution and management of input and output is controlled by [SR-PSU_TD18_Manage_ECPM.f90], see Section 5.2.
c. **Final model setup and flow simulation:** The model parameterisation is setup by the customized DarcyTools module PropGen, and flow is simulated by the DarcyTools solver. The automatized execution of these is managed by [Td18_Manage_DT_runs.f90], see Section 5.3.
d. **Post processing:** flow-field analysis, managed by [SR-PSU_TD18_GET_flows.f90] (Section 5.4.1), and particle tracking, managed by [SR-PSU_Td18_p-track_random_deplete_loops.f] (Section 5.4.2).

The file-managing routines are controlled by manually constructed input files, in which the list of bedrock cases (Table 2-2) and time slices (Table 2-1) are specified. Their purpose is to monitor and manage the parallel processing in different working directories, while maintaining strict traceability between input and output. The file managing codes typically operate in the following sequence:

1. Read the list of model setups to execute in the input text file [List_of_model_setups_for_DTS.txt], which contains the list of <Bedrock case> and/or <time slice> from Table 2-2.
2. Write and execute a DOS-command batch file (*.bat) that copies all required input files into the current working folder.
3. Check that all necessary input files exist in the local working directory.
4. Write the necessary DarcyTools input (i.e. construct the “cif.xml” file), but also specify information on the data set in either of two types of control files: [ECPM_setup.txt] and [DTS_setup.txt] (footnotes 15) and 16) in Figure A-1).
5. Execute relevant DarcyTools module (FracGen, PropGen, or DTS). Within the DTS module, the file [DTS_setup.txt] is used to tag <Bedrock case> and <time slice> to all output data filenames. It is also used, for example to prescribe the sea level for the specified <time slice>.
6. Write and execute a DOS-command batch file (*.bat) that creates a local folder into which all relevant output and input data are copied.
7. Steps 3–6 may be repeated, but at the end mark the current <Bedrock case> / <time slice> as “DONE” and proceed to the next in sequence (return to Step 1).

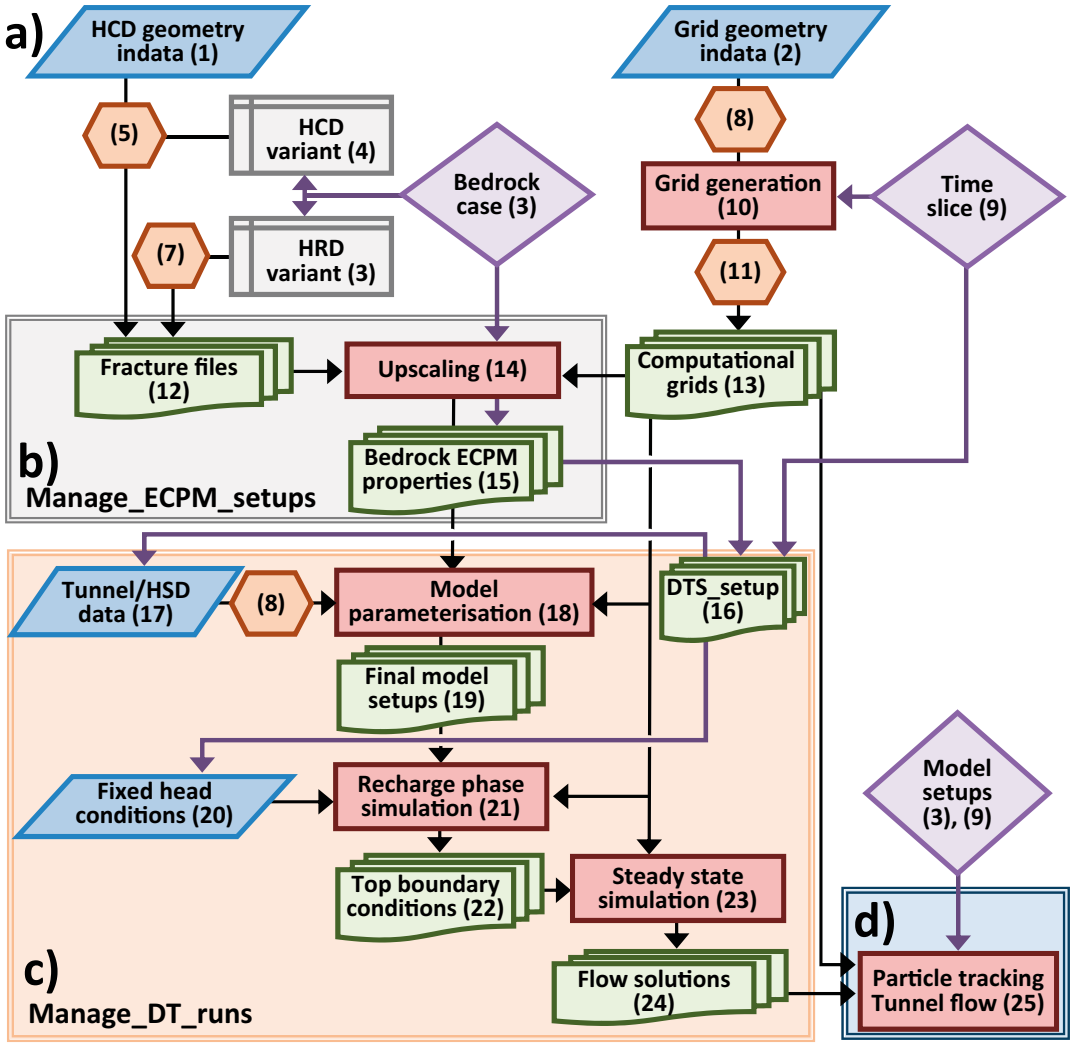

Figure A-1. *Model execution structure consisting of four sequences; a) data and grid preparation, b) upscaling ECPM properties, c) model-setup finalisation and flow simulation, and d) post processing.*

1. **HCD geometry in the SFR Regional domain**; the geometry is taken from the geological model (Curtis et al. 2011), [SFR_DZ_MASTER_v1.0.DT], but six lineaments have been extended north from the SFR Regional domain (Figure 4-11a; [SFR DZ MASTER v1.0-hydro_extensions. xml]). This study considers an alternative extension (Figure 4-11b; [SR-PSU_TD18_Extended_ Lineaments.DT]).
2. **Geometric data for grid discretisation**; Geometry of model domains, regolith layers, lakes, rivers, tunnels, and tunnel plugs are described in Chapter 3.
3. **Defined bedrock cases**; The sensitivity analysis involves 30 bedrock cases (Table 2-2; i.e. parameterisation variants). A <Bedrock case> consists of: a) a HCD parameterisation variant (<HCD variant>; Section 4.3.2) and b) a HRD variant (or realization, RXX; Section 4.3.1). Traceability and consistent management of the specified bedrock cases (i.e. file transfer between modelling sequences) is provided by two control files: [ECPM_setup.txt] (footnote 15) and [DTS_setup.txt] (footnote 16).
4. **HCD variant**; the internal heterogeneity and conceptual uncertainty in HCD parameterisation inside the SFR Regional domain is addressed by HCD parameterisation variants (Section 4.3.2). Six <HCD variant> are selected for analysis (Table 4-3).
5. **HCD parameterisation:** A selection of 6 HCD-parameterisation variants is applied to deterministically modelled deformation zones inside SFR Regional domain using Fortran code [Assign_SFR_HCDs heterogeneity_TD11.f]. Sequence described in Table A-5. Output is in DarcyTools "known-fracture" format: [R_Param_SFR_<HCD variant>], where <HCD variant> is specified in (3).
6. **HRD variants**; the heterogeneity in the rock mass outside deformation zones is addressed by HRD variants. Three stochastic coupled realisations of DFN and Unresolved PDZs inside SFR Regional domain (R03, R18, and R85) are studied in the sensitivity analysis (Table 4-2).
7. **File preparation**; Parameterisation, generation, and removal of isolated fractures follows the procedure described in Öhman et al. (2013) (summarized in Section 4.3.1). All files are converted into DarcyTools "known-fracture" format and rotated into the model coordinate system, as described in Öhman et al. (2013). Used files: [R_SFR_DFN_connected_RXX_L26_knwn] and [R_Unresolved_PDZ_RXX_knwn], for HRD variants XX = 03, 18 and 85.
8. **File preparation**; All delivered geometry data, e.g. tunnel data (stl), topography and bedrock surface DEMs (xyz), lakes and rivers (GIS shape) are converted into DT "object"-format and rotated into the model coordinate system (details in Chapter 3).
9. **Time slices**; Model performance is evaluated at 9 stages of shoreline retreat, defined as <time slice> in Table 2-1. In the modelling sequence, <time slice> controls: a) *cell marking* of inactive cells, topography, lakes, and rivers in grid generation (10), b) RLDM regolith layering in *HSD parameterisation* (18), and c) *fixed-head criteria* during recharge phase simulations (20). <time slice> is tagged in the control file [DTS_setup.txt] (16) to ensure consistent file management.
10. **Grid generation**; One grid per time slice is generated [xyz_<time slice>_L26] by means of the DarcyTools module GridGen (Section 5.1). Notably, the discretisation is *static*, to facilitate time-independent compatibility in upscaled ECPM properties, while cell marking is *time dependent* to reflect the modelled dynamics in RLDM (shore line, DEM, lakes, and rivers; Brydsten and Strömgren 2013). Grid generation commands are traceable via the standardised Compact Input File [SR-PSU_TD18_cif_GGN_<time slice>.xml] and [SR-PSU_TD18_GGN_<time slice>_ L26.log], where <time slice> is specified in (9).
11. **Grid modification**: Identified inconsistencies in the computational grid are edited via the DarcyTools module PropGen, compiled from: [SR-PSU_TD18_GRID_RE-write.f] (Section 5.1).
12. **Fracture files**; The bedrock parameterisation in the flow model (HRD and HCD) is defined based on an underlying set of fracture files. These fracture files are prepared in the standard DarcyTools "known-fracture" format for the subsequent step of upscaling into ECPM properties (14). The sensitivity analysis of bedrock parameterisation primarily addresses: 1) the uncertainty and heterogeneity *inside* the SFR Regional domain (Section 4.2), but also 2) parameterisation combinations *outside* the SFR Regional domain, referred to as "EXTXX" in Table 2-2, see Section 4.4.

13. **Computational grids**; Nine DarcyTools grids are generated, with *time-dependent* cell marking to reflect the landscape dynamics modelled in RLDM (Brydsten and Strömgren 2013), but with *static* discretisation for time-independent compatibility with upscaled ECPM properties. Used files: [xyz_<time slice>_L26], where <time slice> is specified in (9).

14. **Upscaling bedrock ECPM properties**; The ECPM properties for a given <Bedrock case>, (3), are upscaled from fracture files by means of the DarcyTools module FracGen (GEHYCO algorithm). Traceability between input (12) and output (15) is provided via automatized file-management, using the Fortran code [SR-PSU_TD18_Manage_ECPM.f90] (details in Section 5.2).

15. **Bedrock ECPM properties;** In DarcyTools, hydraulic fracture properties are approximated by those of a porous medium and referred to as Equivalent Continuous Porous Medium (ECPM) properties. Upscaled bedrock ECPM properties (conductivity, free fracture volume, and flow-wetted surface area), define the hydraulic domains HCD and HRD in the final model setup (18). File management and applied filename conventions for ECPM-upscaling input/output are described in Table A-8. A control file is generated and stored along with data output files [ECPM_setup.txt].

16. **DTS_setup.txt;** control file defining model setup, combined from [ECPM_setup.txt] (15) and specified <time slice> in (9). Used to ensure traceability and consistency in file-management, between parameterisation (14) and final model output (25), and also to maintain name conventions for output files.

17. **HSD and tunnel data**; The final model setup (18) requires geometric and hydraulic data for the parameterisation of HSD and tunnels (described in Chapter 3). The control file [DTS_setup.txt] in (16) defines the grid and RLDM data for a specific <time slice>.

18. **Model parameterisation;** The final model setup for subsequent flow simulations, (21) and (23), is merged from three sub-domains: 1) the bedrock (HCD and HRD) is assigned ECPM properties (15), 2) HSD is parameterised based on RLDM regolith layering for <time slice> (Table 4-4), and 3) tunnel backfill parameterisation (i.e. assuming intact tunnel plugs; Table 4-1). Minimum values are also applied for conductivity and porosity. Performed by means of the DarcyTools module PropGen, compiled from: [SR-PSU_TD18_Model_parameterisation.f]. <time slice> is specified in [DTS_setup.txt], (16).

19. **Final model parameterisation**; The final model parameterisation for a given <Bedrock case>, (3), defines all three hydraulic domains HCD, HRD, and HSD (also includes tunnel backfill parameterisation). The grid parameterisation consists of the properties: permeability, porosity, and flow-wetted surface area, which are employed in flow simulations, (21) and (23), and post processing, (25). File management and applied filename conventions for input/output are described in Table A-9.

20. **Prescribed-head conditions**; Rivers, lakes, and the seafloor are assigned fixed head based on RLDM data for the <time slice>, specified in control file [DTS_setup.txt], (16). A so-called basin-filled DEM for the specific <time slice> is used as a criterion for maximum head in top-layer grid cells; described in Section 5.3.2.

21. **Recharge phase simulation**; The top-boundary condition for the subsequent steady-state phase, (23), is determined in this preceding simulation. Head in the ground-surface layer is simulated by a principle of combining locally variable recharge and maximum-head conditions, (20). Key outputs are: 1) the solved top-boundary condition, and 2) visualisation for verifications (Table A-10). Simulation premises traceable via [SR-PSU_TD18_DTS_RECHARGE.f].

22. **Top boundary condition**; Input/output of the recharge-phase simulation are documented in Table A-10. [<Bedrock case>_<time slice>_rstslv] is used as a fixed-head boundary condition for the top layer of grid cells in the subsequent steady state simulation, (23).

23. **Steady state simulation**; Based on the fixed-head condition for the model top boundary, the flow solution is progressed to better convergence. Simulation premises traceable via [SR-PSU_TD18_DTS_Steady_state.f] and the DarcyTools Compact Input File: [<Bedrock case>_<time slice>_cif.xml].

24. **Flow solutions**; Input/output of the steady-state simulation are documented in Table A-11. The two key outputs are: [<Bedrock case>_<time slice>_Flow_solution.dat], used in post processing, (25) , and [<Bedrock case>_<time slice>_rstslv], delivered to Comsol near-field simulations.

25. **Post processing**; Performance measures are extracted from the flow solutions (24): tunnel cross flows are extracted with [SR-PSU_TD18_GET_flows.f90], and particle tracking is executed by [SR-PSU_Td18_p-track_random_deplete_loops.f]. Input/output of particle tracking is documented in Table A-13, following the [DTS_setup.txt] convention, (16), (described in more detail in [TD11_Exit_locations_2013-01-15__READ_ME_____.txt]).

A2 Preparation of input model files

This section provides details on the preparation of geometric data used to control the top boundary of the model (regolith layers, lakes, and rivers), but also bedrock parameterisation. The inventory of tunnel geometry data is rather extensive, and therefore presented separately in Appendix B. The preparation of early intermediate time slices (2100 AD, 2250 AD, and 2750 AD), as well as a consistency check of all ground-surface data, is provided in Appendix D.

Regolith-layer geometry (results of RLDM modelling)

The top boundary of the flow model is defined by the regolith, which consists of three components: 1) Quaternary deposits, 2) filling material, and 3) peat. The regolith layering changes over time, according to the Regolith-Lake Development Model (RLDM; Brydsten and Strömgren 2013). Modelled regolith-layer data have been delivered to DarcyTools modelling per every 500 years (as defined in terms of upper-surface elevation; Table A-1). Altogether nine stages of shoreline retreat are studied in the DarcyTools simulations (<time slice> in Table 2-1); of these, three early time slices are interpolated (Appendix D). The RLDM data require pre-processing to serve as input in the DarcyTools simulations (Table A-2).

Table A-1. Regolith data files delivered from RLDM.

Filenames[1)]	Description	Usage
pdem<time slice>.asc pdem<time slice>.xyz	Upper peat surface elevation (m). Peat starts to form −500 AD. This layer is therefore missing in earlier time steps.	HSD parameterisation Point data used for basin filling, defining lake/river objects, grid generation
lpgd<time slice>.asc	The upper surface of lacustrine accumulation of postglacial deposits, elevation (m). Lacustrine accumulation begins 1500 AD. This layer is therefore missing in earlier time steps.	HSD parameterisation
mpgd<time slice>.asc	The upper surface of marine accumulation of post glacial deposits, elevation (m). The same layer is used from 7000 AD to 55 000 AD	HSD parameterisation
gkl<time slice>.asc	The upper surface of glacial clay, elevation (m). The same layer is used from 7000 AD to 55 000 AD	HSD parameterisation
fill<time slice>.asc	The upper surface of filling, elevation (m). This layer is used for all time steps.	HSD parameterisation
glfl<time slice>.asc	The upper glaciofluvial-material surface elevation (m). Thickness is constant during all time steps.	HSD parameterisation
till<time slice>.asc	The upper till surface elevation (m). Thickness is constant during all time steps.	HSD parameterisation
bedr<time slice>.asc bedr<time slice>.xyz	The upper bedrock surface, level in the height system RH 70 (m). The level has been corrected for all layers from −8000 AD to 55 000 AD using the Sea shoreline curve for the reference scenario.	HSD parameterisation Point data not used[2)]

[1)] The RLDM data are provided for the following selected <time slice>: 2000 AD, 2500 AD, 3000 AD, 3500 AD, 5000 AD, and 9000 AD. Three early time slices (2100 AD, 2250 AD, and 2750 AD) are interpolated (Appendix D). Extensions *.asc are in GIS raster format, while *.xyz is in point-data ASCII format.

[2)] Owing to the “fixed-bedrock” convention used, the bedrock surface is modelled as static. The bedrock surface is therefore defined by the original definition in the static regolith model [bedrock_up_v2_2000 AD.xyz], GIS #12_08.

Conversion to fixed-bedrock format

One of the main objectives is to study transient effects during future stages of shoreline retreat. The land uplift, arising from post-glacial rebound, is accounted for in all regolith data (Table A-1). However, the DarcyTools simulations employ a fix bedrock-reference system for elevation (i.e. at land uplift per 1970, m RHB 70), in which shoreline retreat is modelled by means of relative sea level displacement (Näslund 2015; Section 3.3.5).

The first step in processing RLDM data is therefore to back-calculate its elevation into the fixed-bedrock reference system, in which the bedrock is static over time. This is accomplished by means of a Fortran code [Future_HSD_data_to_fixed_Bedrock_format.f90], which for traceability, adds the suffix "_Fixed_bedrock" to the RLDM data filenames (Table A-2).

Basin filling the uppermost RLDM layer (i.e. "DEM") to control surface head

Surface runoff is not modelled explicitly in DarcyTools. Consequently, excess ground-surface head may occur locally where net precipitation exceeds recharge (i.e. head locally exceeding topography). This model artefact is circumvented by iteratively controlling that the simulated head in the uppermost cell layer in the model does not exceed ground surface; the principles of this modelling approach is explained in detail in Sections 5.3.2 and 6.1. As such, the uppermost RLDM layer, also referred to as "basin-filled DEM", has a central role in defining the local upper bound for simulated head at ground surface. Note that areas modelled as submerged in RLDM (lakes, rivers, or below sea level) are treated separately (Sections 3.3.3, 3.3.4, and 3.3.5).

However, the landscape dynamics modelling (RLDM) only resolves wetlands exceeding a certain scale, and consequently, the DEM contains local depressions below the scale for deterministic RLDM modelling. Such depressions may be peat-filled or hold surface water, e.g. minor lakes, wetlands, or pools. Irrespectively of which, it can be argued that the criterion for simulated head in depressions should be determined by the basin threshold rather than the elevation of the actual basin floor (i.e. the basin threshold is the maximum water level, if entirely water filled). In other words, a necessary preparatory step for implementation as a head criterion in simulations is to process the topography data such that all local basins are eliminated and replaced by basin-threshold levels. This procedure is referred to as "basin-filling", and is explained below.

One filled DEM is prepared for each time slice [Filled_pdem<time slice>_Fixed_bedrock.asc], by filling local topographical depressions until reaching the surrounding geometric threshold. During this process, elevations in areas deterministically modelled as submerged are kept fixed (i.e. lakes, rivers, or below sea level). Thus, the final basin-filled DEMs slope towards: 1) the sea, 2) a lake with specified threshold (RLDM), or 3) a modelled river. The basin-fill is conducted in three steps (Table A-2):

1. Automatized filling [Basin_fill_DEMs.f90], millimetre by millimetre, of topographical basins above sea level for a given <time slice> (Figure 3-4). To avoid unmotivated filling along the seafloor, basins below sea level are not altered. Basins extending partly below sea level are handled manually, in a second step, as it is difficult to determine if their geometric thresholds are above sea level based on algorithms.
2. Manual filling [Manual_Basin_fill_DEMs_adjustments.f90] of remaining basins that are identified by visual inspection as isolated from the sea for a given <time slice>. Isolated basins are partly below sea level, but have a geometric threshold above sea level (Figure 3-5). The purpose is to avoid erroneous identification of local inland sea-cells in simulations, which otherwise may render inaccurate particle exit locations. The SFR tunnel entry is an example of a basin partly below sea level. For example, known lake levels are used as thresholds for the 2000 AD <time slice>.
3. The basin-filled DEMs are exported into GIS raster format, by means of the Fortran code [Create_Upper_DEM_ASC.f90].

The basin filled DEM is used as a criterion for maximum local groundwater level (i.e. the maximum head in a local depression is determined by the *geometric* threshold of the surrounding DEM elevations). An evaluation of the consistency between the basin-filled DEM, rivers and lakes is presented in Appendix D.

Although the basin-fill is a substantial improvement for constraining surface head in flow simulations, it does *not guarantee* absence of local depressions, due to inexact mapping between RLDM raster and the DarcyTools grid. The inexact mapping is due to: 1) discretisation differences (e.g. the DarcyTools grid has variable refinement) and 2) coordinate-system differences (e.g. the DarcyTools grid has a rotated coordinate system).

Constructing DarcyTools objects to implement HSD in grid generation

In the standard DarcyTools procedure, the model top boundary is defined by removal of grid cells above topography (i.e. as defined by a DEM DarcyTools object). This study addresses several stages of shoreline retreat (time slices), during which the topography alters due to landscape dynamics. The altering topography is honoured by using time-specific computational grids [xyz_<time slice>_L26], where the model top boundary is defined by [R_Filled_pdem<time slice>_Fixed_bedrock.dat]. For time efficiency, a *cell inactivation* method is used, where:

1. cells are *permanently* deleted, if located above the maximum DEM elevation, determined over the time period 2000 to 9000 AD, [R_MAX_Filled_DEM_2000 AD_to_9000 AD(onlyRLDM).dat].
2. cells are *inactivated* in the time-specific grid, if located above the DEM for the particular <time slice>, determined by [R_Filled_pdem<time slice>_Fixed_bedrock.dat].

The benefit of this method is that the discretisation of all time-specific grids is identical, which allows re-using the same upscaled ECPM properties for all time slices (i.e. ECPM upscaling is a time-consuming step that is only valid for a specific grid discretisation). The top boundary is defined as the uppermost layer of active cells in the grid (i.e. immediately below a permanently deleted cell or a temporarily inactivated cell). The regolith is defined as above computational cells above the bedrock surface [R_bedrock_up_v2_2000 AD.dat]. This file is the original data source for bedrock surface (GIS #12_08; [bedrock_up_v2_2000 AD.xyz]), defined in the static regolith model. Due to the "fixed-bedrock" reference convention, all bedrock surface data are identical (apart from negligible round-off errors).

Table A-2. RLDM data processing in 3 steps.

Purpose [input]	**Execution code [output]**
1. Conform to DarcyTools elevation reference system	
Convert regolith layer elevations (Table A-1) into fixed-bedrock format. [*.asc], [*.xyz]	Future_HSD_data_to_fixed_Bedrock_format.f90 (adds suffix *"_Fixed_bedrock") [*_Fixed_bedrock.asc], [*_Fixed_bedrock.xyz]
2. Basin fill uppermost regolith layer (i.e. "DEM")	
Fill local topographical basins above sea level [pdem*_Fixed_bedrock.xyz]	Basin_fill_DEMs.f90 (adds prefix "Filled_"*) [Filled_pdem*_Fixed_bedrock.xyz] [Filled_pdem*_Fixed_bedrock.plt]
Fill local topographical basins below sea level. [Filled_pdem*_Fixed_bedrock.xyz]	Manual_Basin_fill_DEMs_adjustments.f90 (replaces files "Filled_"*) [Filled_pdem*_Fixed_bedrock.xyz] [Filled_pdem*_Fixed_bedrock.plt]
File-format conversion to GIS raster format. [Filled_pdem*_Fixed_bedrock.xyz]	Create_Upper_DEM_ASC.f90 (extension *".asc") [Filled_pdem*_Fixed_bedrock.asc]
3. DarcyTools objects in grid generation	
Construct DarcyTools object defining topography and bedrock surface [Filled_pdem*_Fixed_bedrock.xyz] [bedrock_up_v2_2000 AD.xyz]	DEM_to_DT_object.f (extensions *".dat", *".plt") [Filled_pdem*_Fixed_bedrock.dat], [Filled_pdem*_Fixed_bedrock.plt] [bedrock_up_v2_2000 AD.dat], [bedrock_up_v2_2000 AD.plt]
Construct a universal DarcyTools object, defining maximum RLDM topography 2000 AD to 9000 AD [Filled_pdem*_Fixed_bedrock.xyz]	DEM_Maximum_Z.f (extensions *".dat", *".plt") [MAX_Filled_DEM_2000 AD_to_9000 AD(onlyRLDM).dat] [MAX_DEM.plt]
Rotate DarcyTools objects into local model coordinate system [Filled_pdem*_Fixed_bedrock.dat], [bedrock_up_v2_2000 AD.dat], [MAX_Filled_DEM_2000 AD_to_9000 AD(onlyRLDM).dat]	Rotate_DT_objects.f90 (adds prefix "R_"*) [R_Filled_pdem*_Fixed_bedrock.dat], [R_bedrock_up_v2_2000 AD.dat], [R_MAX_Filled_DEM_2000 AD_to_9000 AD(onlyRLDM).dat]

Transferring RLDM lake geometry into "DarcyTools object"-format

Implementation of geometric data in the DarcyTools grid generation requires that data are converted into the so-called "DarcyTools object" file format. Therefore, time-specific DarcyTools objects representing lakes at a given time slice are constructed, in the following 4 steps:

1. RLDM lake vector shapes (lakes_<time slice>.shp) and RLDM topography point data (pdem<time slice>_Fixed_bedrock.xyz) are joined in ArcGIS. Topographical points (x,y,z) falling inside, and on the border of, a lake vector object are exported as a text file, under the name [Lake_<Lake ID>_<time slice>.txt]. All lakes for a given <time slice> is stored in a separate working directory, which also includes a directory list [List_of_LAKES.txt], containing the filenames and threshold data for all lakes.
2. Lake data [Lake_<Lake ID>_<time slice>.txt] are transformed into watertight 3D CAD volumes [Lake_<Lake ID>_<time slice>.stl], enclosing each lake water volume. The conversion is made by the code [Make_Lakes.F90], which extrudes the volume between the bottom and the surface of a lake. The extrusion is facilitated by duplicating a unit CAD cuboid [Box_Template.txt], which locally is vertically bounded by the bottom (i.e. local RLDM topography) and the surface (i.e. the specified threshold) of a lake. The CAD objects are also translated from their original RT90 coordinate system by [−1626000., −6692000.].
3. By means of the DarcyTools module OGN, CAD volumes [Lake_<Lake ID>_<time slice>.stl] are then converted into so-called "DarcyTools objects" [Lake_<Lake ID>_<time slice>.dat] and Tecplot output [Lake<Lake ID>.plt]. The conversion is a standard DarcyTools procedure. The TecPlot output facilitates 3D visualisation and verification against topographical depressions in the RLDM DEMs.
4. Finally, lake objects [Lake_<Lake ID>_<time slice>.dat] are rotated into the local DarcyTools coordinate system [R_Lake_<Lake ID>_<time slice>.dat] by means of the Fortran code [Rotate_DT_objects.f90]. Pivot point in local coordinate system: [6400. 9200.], rotation angle: 32.58816946°.

These time-specific, individual lake objects [R_Lake_<Lake ID>_<time slice>.dat] are only used to define lake cells in the computational grid. Lakes for the intermediate early time slices, 2100 AD, 2250 AD, and 2750 AD are interpreted from the lake succession sequence (Appendix D). Grid refinement of lake is controlled by a joined, time-independent DarcyTools object [R_MAX_EXTENSION_ALL_LAKES.dat], which confines the maximal extension of all lakes (horizontally and vertically) for all time slices. This object is constructed parallel to the preparation of time-specific, individual lake objects, described above. The purpose of time-independent grid refinement (i.e. refining) is time efficiency, as ECPM conversion becomes compatible with all grids (motivated in Section 3.3.2).

Table A-3. Prescribed head for lake cells, identified by DarcyTools cell markers.

		DarcyTools marker, for <time slice>								
Lake ID	Lake level (m)	2000	2100	2250	2500	2750	3000	3500	5000	9000
107	−6.24							158	189	214
108	−15.23								188	
110	−6.05							157		
114	−33.49									215
116	−14.24								187	216
117	−5.72							156	186	
118	−5.13						136	155	185	
120	−2.6				123	123	135	154	184	
121	−10.42								183	
123	−10.91								182	
124	0.48	103	103	103	122	122	134	153		
125	0.4	104								
126	−12.24								181	
129	5.82	105	105	105	121	121	133	152		
132	3.66	106	106	106	120	120	132	151		
134	−1.35			119	119	119	131	150	180	217
136	0.42	107	107	107	118	118	130	149	179	
142	1.82	108	108	108	117	117	129	148		
144	0.41	109	109	109	116	116	128	147		
146	−13.87								178	218
148	0.56	110	110	110	115	115	127	146	177	
149	5.32	111	111	111	114	114	126	145	176	
150	−8.22							144	175	219
151	−16.83									220
152	−15.41								174	221
153	−8.29							143	173	
154	−15.36								172	222
155	−6.6							142	171	
156	−6.06							141	170	223
157	−13.99								169	
159	−11.84								168	
160	−7.09							140	167	
163	−16.19								166	224
164	−20.19									225
165	−18.62									226
166	−16.2								165	227
167	−16.99									228
170	−10.14								164	229
173	−10.53								163	230
175	−10.06								162	
176	−4.95						125	139	161	
177	−8.73								160	
178	−7.59							138		
179*	−1.67*				113	113	124	137	159	
180	−20.34									231
184	−24.24									232

* Lake 179 is the Biotest lake. It is prescribed sea-level head before 2500 AD.

Transferring RLDM river data to DarcyTools

Rivers (streams and brooks) are treated as prescribed head-boundary conditions in the flow model (Section 3.3.4). Similarly to the representation of lakes, the "river cells" are implemented in the computational grid by means of so-called "DarcyTools objects" (Table A-4). In the flow simulations, any cell identified as a river (i.e. all river cells are marked by the identification number 102) is prescribed a head value that is linearly interpolated between the nearest two points in an input text file [SR-PSU_TD18_River_head.in] (Table A-4). Riverbed head is not provided in RLDM data, but is estimated according to principles described below.

DarcyTools objects representing rivers at different time slices are constructed, in 4 steps:

1. RLDM river data are prepared for DarcyTools modelling by combining river data (GIS vector format) with topography data (GIS raster format). To facilitate this joint analysis, the river nodes are exported into a text file (vattendrag_SDEADM.UMEU_FM_GEO_10171.txt. This river-node list is organised in such a way that the corresponding element list of river-segments is straight-forward to manually construct [Connectivity_list.dat]. The modelled river geometry in RLDM is "stationary" (rivers do not meander or vanish over time). Therefore, the nodal data, exported at "maximal river extension" (i.e. a late stage of shoreline retreat, t > 9000 AD), represent the river geometry at any given <time slice>, provided the nodes below sea level are inactivated in the subsequent flow simulations.
2. Two corrections are made to [Connectivity_list.dat]: 1) junctions between river branches are forced to occur at the nearest common river node, and 2) river starting locations (i.e. origin point of tributaries) are harmonized with topography data (i.e. a few river nodes that are inconsistent with raster topography data are removed).
3. The local riverbed head is interpolated for each <time slice> and stored in a condensed input file for flow simulations [SR-PSU_TD18_River_head.in] (see Table A-4). In this interpolation, three types of river nodes are treated as deterministic, fixed values:
   a. the starting point of river tributaries (taken as local topography elevation),
   b. river nodes inside lakes (i.e. any node falling inside [Lake_<Lake ID>_<time slice>.txt] is assigned head equal to lake threshold, Table A-3),
   c. river segments below sea level are temporarily set equal to sea level, but are later inactivated in the subsequent flow simulations.

Remaining river nodes are treated as flexible points and are interpolated by iterations [Interpolate_River_Head.f90], until:

   a. head variability along the riverbed is smoothened out, such that the river gradient is directed towards the sea, and
   b. difference between river head and local RLDM topography is minimized (node topography elevation extracted from [pdem<time slice>_Fixed_bedrock.xyz]).

4. For the grid generation, watertight 3D CAD volumes [Filled_Streams_<time slice>_z25.stl] are constructed based on the node list and the element list. This conversion is made by the code [Make_Rivers.F90], which extrudes a 5 m wide channel, extending from below the local estimated riverbed head (H(x,y) -1 m) to a fixed elevation of 25 m (note that any part extending above ground surface is eliminated in the grid generation). The CAD objects are also translated from their original RT90 coordinate system by [−1626000., −6692000.].
5. Next, the DarcyTools module OGN, is used to convert the CAD volumes [Filled_Streams_<time slice>_z25.stl] into so-called "DarcyTools objects" [Filled_Streams_<time slice>_z25.dat] and Tecplot output [Filled_Streams_<time slice>_z25.plt]. This conversion is a standard DarcyTools procedure. The TecPlot output facilitates 3D visualisation and verification against RLDM topography.
6. Finally, the river objects [Filled_Streams_<time slice>_z25.dat] are rotated into the local DarcyTools coordinate system [R_Filled_Streams_<time slice>_z25.dat] by means of the Fortran code [Rotate_DT_objects.f90]. Pivot point in local coordinate system: [6400. 9200.], rotation angle: 32.58816946°.

Table A-4. Input data files used to prescribe head in rivers.

Input file	Description
R_Filled_Streams_<time slice>_z25.dat	Geometric DarcyTools object used in grid generation to define river cells above sea level at <time slice>. All river cells are given the cell marker 102.
SR-PSU_TD18_River_head.in	Input text file used to prescribe fixed head along riverbeds in flow simulations. Local riverbed head is estimated for 4 821 points (x,y,H) along river trajectories. (x,y) are in local rotated model coordinates. H is available in 9 columns, one for each <time slice>. The prescribed head for a riverbed cell is linearly interpolated between the two nearest points.

Input files for bedrock parameterisation

As described earlier, the DarcyTools' method for bedrock parameterisation has two key steps:

1. definition of parameterised structural input data (consisting of deterministic structures, HCD, and stochastic fractures, HRD), followed by
2. the geometric upscaling which converts the properties of the parameterised discrete structures into Equivalent Continuum Porosity Medium (ECPM) properties

This section describes the generation of parameterised structural input data in the data formats that are accepted by DarcyTools.

A categorical approach for merging the bedrock parameterisation of two hydrogeological models (SDM PSU and SDM Site Forsmark) was employed in the preceding sensitivity analysis (Öhman et al. 2014):

1. the bedrock parameterisation of SDM PSU was applied inside the SFR Regional domain, while
2. the bedrock parameterisation of SR-Site/SDM-Site Forsmark (Table A-6) was applied outside the SFR Regional domain.

The sensitivity analysis of parameterisation uncertainty was strictly limited to the SFR Regional domain (i.e. the sub-volume defined in SDM-PSU).

The current study still focuses on the parameterisation of the SFR nearfield, but also including a few variants for the bedrock outside the SFR Regional domain that have been identified as affecting repository performance in earlier SR-PSU studies. For example, this study addresses two variants of HCD geometry north from the SFR Regional domain (six structures with uncertain extension), as well as HRD parameterisation variants outside the SFR Regional domain. Thus, the distinction of model sub-volumes inside/outside the SFR Regional domain has a less clear-cut role in the current sensitivity analysis.

The basic principle in established SKB methodology for flow simulations is that the HCD geometry is assumed to be known, and kept fixed static in bedrock cases, whereas the transmissivity parameterisation is elaborated in terms of stochastic realisations and/or conceptual models (i.e. various aspects of uncertainty; Table 4-3). The current study is delimited to address the parameterisation uncertainty of the 40 deformation zones defined in SDM-PSU; the parameterisation of the deformation zones define in SDM-Site Forsmark is not varied in this study.

HCD geometry (SDM-PSU)

In addition to analysing the uncertainty in HCD parameterisation, this study addresses the uncertainty of deformation-zone extension in the area associated to SFR discharge during terrestrial conditions (i.e. the area covered by lake 116; Section 4.4.1). The uncertainty of structural extension in this area (deformation zones NNW3113, NNW0999, NS3154, NNE3266, NNE3265, and NNE3264) arises due to lack of definition geological modelling outside the SFR Regional domain (Section 4.4).

The two variants are defined for the six zones of uncertain extension outside the SFR Regional domain (Figure 4-11; notation in Table 2-2):

- EXT0 (Figure 4-11a): minimum extension of the six uncertain HCDs [SFR DZ MASTER v1.0.DT]. This geometry is combined from the geological model v.1.0 [SKBdoc 1244246 SFR_DZ_MASTER_v1.0] and [SFR DZ MASTER v1.0-hydro_extensions].
- EXT1 (Figure 4-11b): maximum extension of the six HCDs. The geometry of these cases is defined by the combination of [SFR DZ MASTER v1.0.DT] and [SR-PSU_TD18_Extended_Lineaments.DT].

In all bedrock cases the HCD geometry of deformation zones and sheet joints are taken from SR-Site Forsmark ([861006_DZ_PFM_REG_v22_SJ.dt] and [081006_sheet_joints_v5.ifz].

Table A-6) and kept fixed in the sensitivity analysis. The merging of HCD geometry across the SFR Regional domain boundary is explained below.

HCD parameterisation (SDM-PSU)

Two types of data are used in the parameterisation of the 40 deformation zones defined in Curtis et al. (2011):

1. effective HCD transmissivity (SKB 2013, Appendix 6). Compiled in the input file [DZ_data.dat].
2. conditional values at borehole intercepts (Öhman et al. 2013, Table A-2). Compiled in the input file [Conditional_DZ_data.dat].

All parameterisation variants of the HCD inside the SFR Regional domain (Table 4-3) were generated in the preceding sensitivity analysis, TD11 (Öhman et al. 2014). The input data files were prepared in the so-called DarcyTools "known-fracture format" by means of a customised Fortran code [Assign_SFR_HCDs heterogeneity_TD11.f]. For traceability the code employs a hard-coded file-naming convention [Param_SFR_HCD_<HCD variant>] (Table A-5). A variant of this code [Assign_HCDs_North_from_SFR.f] was used to parameterise the extended geometry (marked pink in Figure 4-11b), with output [HCD_North_<HCD variant>].

Table A-5. Implementation of selected HCD variants.

Purpose [input]	**Execution [output]**
1. Define structural geometry of the 6 extended HCDs	
Triangulate the minimum extension (defined in RVS) [SFR DZ MASTER v1.0-hydro_extensions.xml] Define and triangulate the maximum extension	RVS_info.bat [LINEAMENT_EXTENSIONS.DT] [SR PSU_TD18_Extended_Lineaments.DT]
Combine the default extension of the 6 HCDs with geological model v.1.0 (Curtis et al. 2011) [SKBdoc 1244246 SFR_DZ_MASTER_v1.0.xml] [LINEAMENT_EXTENSIONS.DT]	RVS_info.bat Manual merging in text editor [SFR DZ MASTER v1.0.DT]
2. Parameterise HCD variants	
Generate HCD variants in DarcyTools "known-fracture" format, by combining: 1. structural geometry [SFR DZ MASTER v1.0.DT] (+ [SR PSU_TD18_Extended_Lineaments.DT]) 2. tabulated effective transmissivity [DZ_data.dat] 3. tabulated conditional data [Conditional_DZ_data.dat] 4. tabulated inverse cumulative normal distribution [Norm_dist.dat]	[Assign_SFR_HCDs heterogeneity_TD11.f] [Assign_HCDs_North_from_SFR.f] Export fracture files with prefix "Param_SFR_" and "HCD_North_" For DarcyTools (known-fracture format) and TecPlot (.plt; e.g. Figure 4-12)
3. Rotation	
Rotate DarcyTools known-fracture files into local model coordinate system [Param_SFR_<HCD variant>] [HCD_North_<HCD variant>]	Rotate_DT_objects.f90 (adds prefix "R_"*) [R_Param_SFR_<HCD variant>] [R_HCD_North_<HCD variant>]

Merging hydrogeological models to cover the area outside the SFR

The bedrock parameterisation of SDM-PSU is complemented by that of SR-Site Forsmark to cover the peripheral parts outside the SFR Regional domain (Figure 3-1). As described above, this is accomplished by merging the two hydrogeological models at the domain boundary of the SFR Regional model area. To avoid artificial overlaps in the merging process, the sub-volume of the SFR Regional domain is first truncated from the SR-Site Forsmark model files. The principle of merging truncated data from SDM-/SR-Site Forsmark with SDM-PSU data is identical to that used in Öhman et al. (2014). The removal of fractures/deformation-zone geometry inside the SFR Regional domain is indicated by filename tags ("WITH_HOLE" and "med_hål_i_mitten" in Table A-6, as explained in Öhman et al. 2013). The SDM-Site sheet joints are also truncated inside the SFR Regional domain, as described in Öhman et al. 2013 (Table A-6).

HRD parameterisation outside the SFR Regional domain

Three cases of HRD parameterisation outside the SFR Regional domain are included in the sensitivity analysis:

- EXT_0: Constant hydraulic conductivity, KHRD = 6.5×10^{-9} m/s, implemented for rock mass outside deformation zones. Hard-coded implementation in [SR-PSU_TD18_Model_parameterisation.f] (not based on fracture input files).
- EXT_1: Stochastic DFN realisation R01, identical to that used in the preceding sensitivity analysis (Öhman et al. 2014). Based on SR-Site's heterogeneity case, but expanded to cover the entire domain for flow modelling. File used: [UPDATED_SERCO_DFN_WITH_HOLE] (Table A-6; Figure 4-10).
- EXT_2: Stochastic DFN realisation R02, partly based on SR-Site's heterogeneity case, but merged with anomalous realisation identified in Öhman and Odén (2017b). Files used: [UPDATED_SERCO_DFN_HOLE_TEMPLATE] and [Connected_DFN_OUTSIDE_SFR_R02_knwn] (Table A-6; Figure 4-15).

It should be noted that the DFN realisation outside SFR Regional domain lack DFN coverage above $z = 0$ m elevation (referring to fracture-centre points). This is compensated by applying a minimum bedrock conductivity of 3×10^{-8} m/s above $z = -10$ m elevation (see Table 4-4).

The fracture files representing the bedrock outside the SFR Regional domain are specified in Table A-6. It should be noted that all fracture files used in the model are rotated into the DarcyTools coordinate system, which tags the prefix "R_" to all filenames with rotated data.

Table A-6. Fracture files used outside SFR Regional domain.

Description*	Data files
Parameterized HCD, outside SFR Regional domain Exclusion of HCD geometry inside SFR Regional domain (and ZFM871; Section 3.3.2 in Öhman 2010). Converted to “known-fracture format”.	Source: [861006_DZ_PFM_REG_v22_SJ.dt] Output: [PFM_zoner_med_hål_i_mitten]
Stochastic DFN realisation R01, outside SFR Regional domain (Figure 4-10). Taken from SR-Site Forsmark, but expanded to cover flow domain (Öhman et al. 2014;). Converted to “known-fracture format”.	Source: [SRS-FFM01-06_v4_alterFinal_nocpm_r1_sets1-65_all_96.asc] [Update_Sercos_DFN.f90] Output: [UPDATED_SERCO_DFN_WITH_HOLE]
Stochastic DFN realisation R02, outside SFR Regional domain. The parameterisation is based on SR-Site, but the sub-volume north of SFR (Figure 4-15) is replaced by an anomalous DFN realisation that affects particle-tracking exit locations (Öhman and Odén 2017b). “known-fracture format”.	Source: [UPDATED_SERCO_DFN_WITH_HOLE] Output: [UPDATED_SERCO_DFN_HOLE_TEMPLATE] Output: [Connected_DFN_OUTSIDE_SFR_R02_knwn]
Hydraulic deterministic structures (HCD), converted from ifz into “known-fracture format”, and locally reduced transmissivity near SFR ramp, as described in Section 3.4.1 in Öhman et al. (2012).	Source: [081006_sheet_joints_v5.ifz] Output: [PLU_sheet_joints_truncated]
Used to fill in geometric discontinuities when merging SFR HCDs with those in SDM-Site Forsmark. Parameterised and converted from xml into “known-fracture format” via RVSinfo.	Source: [SFR DZ MASTER v1.0-bridges.xml] Output: [Parameterized_SFR_BRIDGES]

* All fracture files are rotated into the local model coordinate system. The prefix “R_” is added to all rotated files, denoting the rotated coordinate system.

A3 Management of model files in simulation

Computational grids are generated by means of the DarcyTools module GridGen (Section 5.1). The grids are unstructured, which allows the flexibility of local refinement (e.g. near ground surface and tunnel geometry). The discretization is carried out via a sequence of commands specified in the standardised Compact Input File on xml-format, [cif.xml] (Svensson et al. 2010). Each discretisation command in this control file consists of:

- geometric reference to a model subdomain (e.g. tunnels, lakes, and soil layer). These are defined by geometrical DarcyTools objects (Chapter 3). The geometric reference is accompanied by either:
  - specification on local maximum cell side length (Table A-7), and/or
  - identification of grid subdomains by means of a cell marker ID (Table A-7). Cell-marker IDs have a key role in subsequent modelling; for example they are used in property assignment, boundary conditions, and particle release points.

Table A-7. Grid generation.

Input files	**Description**
[SR-PSU_TD18_cif_GGN_<time slice>.xml]	Compact Input File in xml-format, specifying the sequence of discretisation commands (i.e. commands specify local grid refinement via geometry of DarcyTools objects).
Geometry data	Prepared in so-called DarcyTools-object format (Chapter 3, main report). Complete list of input geometry used is traceable via the Compact Input File.

Output files	**Description**
[xyz_<time slice>_L26]	Computational grid used in flow simulations. Nine grids generated with identical discretisation, but different cell classification to reflect the landscape dynamics modelled in RLDM. The identical discretisation implies time-independent compatibility with upscaled ECPM properties.
[ggnSFR_<time slice>.plt]	Tecplot output, visualising discretisation and cell marking in tunnels (e.g. Figure 3-2) and flow-domain cross sections.
[SR-PSU_TD18_GGN-<time slice>_L26.log]	Log file per default generated by GridGen.

Grid discretisation, in summary[1]	Max. cell side length[2] (m)		
Domain, defined by [geometric object]	Delimitation	ΔL_H	ΔL_z
Flow domain [R_Updated_WD_model_domain.dat]	Outside SFR Regional domain	128	
−1 100 m ≤ z ≤ [R_MAX_Filled_DEM_2000AD_to_9000AD(onlyRLDM).dat]			
SFR Regional domain Inside [R_SFR_modellområde_v01.dat]	z ≥ −180 m	8	
	−400 ≤ z < −180 m	16	
	−1 100 ≤ z < −400 m	64	
Singö deformation zone	Inside Singö deformation zone[6]	8	
HSD Above [R_bedrock_up_v2_2000 AD.dat]	Outside SFR Regional domain	32	1
	Inside SFR Regional domain	8	0.5
Tunnels (including disposal rooms and tunnel plugs) [R_anlaggning_SFR3_sammanslagen_L26.dat] and [R_Entire_SFR1_(silo_mod).dat] [3]		2	
Silo walls: border [R_SFR-1_Silo_Outer_bnd.dat][3]		1	
Volume enclosing particle-exit locations[4]	z ≥ −60 m	16	
	−200 ≤ z < −60 m	32	
Volume enclosing Sheet-joints[4]		16	

Domain		**Delimitation**	**Cell marker ID**
Bedrock	Outside Singö deformation zone	Outside SFR Regional domain	1
		Inside SFR Regional domain	10
	Inside core of Singö deformation zone[7]		9
RLDM objects	Cell inactivation	Above [R_Filled_pdem<time slice>_Fixed_bedrock.dat]	999
	HSD	Above [R_bedrock_up_v2_2000AD.dat]	100
	Ground surface	[R_Filled_pdem<time slice>_Fixed_bedrock.dat]	101
	Rivers	[R_Filled_Streams_<time slice>_z25.dat]	102
	Lakes	[R_Lake_<Lake ID>_<time slice>.dat]	Table A-3
Tunnels	SFR 1	Backfilled tunnel sections (Table B-1)	16
	SFR 3	Backfilled tunnel sections (Table B-1)	28

Disposal rooms	1BTF	[R_1BTF_del1_yellow.dat]	11
	2BTF	[R_2BTF_del1_yellow.dat]	12
	1BLA	[R_1BLA_del1_yellow.dat]	13
	1BMA	[R_1BMA_del1_yellow.dat]	14
	Silo, interior	[R_Silo_del4_mitt_yellow.dat]	15[5)]
	2BLA	[R_2BLA_del1_yellow.dat]	22
	3BLA	[R_3BLA_del1_yellow.dat]	23
	4BLA	[R_4BLA_del1_yellow.dat]	24
	5BLA	[R_5BLA_del1_yellow.dat]	25
	2BMA	[R_2BMA_del1_yellow.dat]	26
	1BRT	[R_1BRT_del1_yellow.dat]	27
Plugs	Blue plugs	Mechanical concrete plugs (Table B 1)	30
	Brown	Bentonite plugs (Table B 1)	31
	Green	Filter-material plugs (Table B 1)	32
	Pink	Bentonite plugs in ramp (Table B 1)	33
	Silo, exterior	[R_SFR-1_Silo_Outer_bnd.dat]3)	21[5)]

1. This summary only presents an overview of grid discretisation. Full details are traceable via [SR-PSU_TD18_cif_GGN_<time slice>.xml] and [SR-PSU_TD18_GGN-<time slice>_L26.log].
2. Refinement expressed in terms of maximum side lengths of cells, in the horizontal and/or vertical direction, ΔL_H and ΔL_z, respectively.
3. Discretisation of tunnel geometry based on CAD definitions for TD10.
4. Approximate refinement volumes for particle-exit locations and sheet joints specified directly in Compact Input File (i.e. not based on formal CAD geometry). Details provided in [SR-PSU_TD18_cif_GGN_<time slice>.xml].
5. The differentiation between Silo interior and Silo exterior is demonstrated in Figure 4-2.
6. Defined by [R_WNW0001_In_SFR_REG_108m.dat] and [R_WNW0001_OUT_SFR_REG_165_m.dat].
7. Defined by [R_WNW0001_In_SFR_REG_36m.dat] and [R_WNW0001_OUT_SFR_REG_55_m.dat].

Two types of inconsistencies are noted in the generated grids:

1. HSD cells on top of: a) an inactivated cell, b) a lake cell, or c) a river cell, are inactivated,
2. particle-release locations inside the silo (Mk = 15) are constrained to a maximum elevation of z = −80 m elevation (any Mk = 15 above z = −80 are set to Mk = 21; Figure 4-2).

In a secondary step, these inconsistencies are edited by means of the DarcyTools module PropGen, as compiled from: [SR-PSU_TD18_GRID_RE-write.f].

File management in ECPM translation

As explained in Section 5.2, DarcyTools employs a geometric upscaling concept to transfer fracture-network characteristics onto its computational grid, in terms of Equivalent Continuous Porous Medium (ECPM) properties. These ECPM properties are the result of: 1) a given set of input fracture files and 2) a given grid discretisation. Owing to the unstructured gridding in DarcyTools, the validity of the upscaled properties are limited to the specific grid discretisation. The addressed stages of landscape dynamics, as modelled in RLDM, are represented by nine grids with “time-dependent” cell marking (Section 5.1). However, the *discretisation* is identical in all grids and therefore ECPM properties are generic for all grids.

ECPM upscaling is featured by the DarcyTools module FracGen (GEHYCO algorithm) (Svensson et al. 2010), for which all input data are specified in a standardised Compact Input File, on xml-format [cif.xml]. The file management is automatized (Figure A-1). The ECPM upscaling is managed by means of [SR-PSU_TD18_Manage_ECPM.f90] in 6 steps:

1. Identify a <Bedrock case> from the manual input file [List_of_model_setups_for_ECPM.txt]
2. Ensure existence of all required input files (Table A-8),
3. write the Compact Input File for FracGen, i.e. a temporary cif.xml specifying input files for the given <Bedrock case>,

4. execute FracGen with the temporary cif.xml,
5. write control file [ECPM_setup.txt],
6. write and execute [Store_data.bat], which creates the folder [<Bedrock case>] in which ECPM-property files are stored (Table A-8).

Table A-8. ECPM conversion [DarcyTools module FracGen].

Input files	Description
List_of_model_setups_for_ECPM.txt	List of bedrock cases (Table 2-2).
Cif.xml	Compact Input File in xml-format, which is the default input file for the DarcyTools module FracGen, specifying involved indata for ECPM upscaling (fracture files and computational grid). The input file is automatically generated by [SR-PSU_TD18_Manage_ECPM.f90] and is not stored.
[xyz_L26]	Computational grid (i.e. time-independent, as discretisation is static in all grids).
Inside SFR Regional domain	
[SFR_DFN_connected_RXX_L26_knwn] [Unresolved_PDZ_RXX_knwn]	Stochastic DFN realisations, RXX (Table 4-2), for heterogeneous HRD parameterisation variants.
	No HRD fracture input file is upscaled in the homogeneous variants.
[Param_SFR_HCD_<HCD variant>]	Parameterisation variant of the 40 deterministic deformation zones inside the SFR Regional domain (Table 4-3). Assumes minimum extension of the six HCDs extending north from SFR (Figure 4-11a).
[HCD_North_<HCD variant>]	Only included in cases assuming maximum extension of the six HCDs extending north from SFR (Figure 4-11b).
[Parameterized_SFR_SBA1_to_SBA8]	Deterministic representation of SBA structures, inside the SFR Regional domain.
Outside SFR Regional domain	
[Parameterized_SFR_BRIDGES] [PLU_sheet_joints_truncated] [PFM_zoner_med_hål_i_mitten]	Static files for bedrock parameterisation outside the SFR Regional domain (Table A-6).
[UPDATED_SERCO_DFN_WITH_HOLE] [UPDATED_SERCO_DFN_HOLE_TEMPLATE] [Connected_DFN_OUTSIDE_SFR_R02_knwn]	Heterogeneous HRD realisation R01. Heterogeneous HRD realisation R02.
Output files[1)]	
[ECPM_setup.txt]	Control file specifying <Bedrock case>.
[<Bedrock case>_condx.dat]	Cell-wall ECPM conductivity in x-direction (rotated coordinate system).
[<Bedrock case>_condy.dat]	Cell-wall ECPM conductivity in y-direction (rotated coordinate system).
[<Bedrock case>_condz.dat]	Cell-wall ECPM conductivity in z-direction.
[<Bedrock case>_frevol.dat]	Cell ECPM free volume (i.e. intersectional volume sum of fracture aperture, Eq. (5-1), used to calculate bedrock porosity).
[<Bedrock case>_fws.dat]	Cell ECPM flow-wetted surface area (i.e. intersectional sum of fracture area).

[1)] <Bedrock case> = <HCD variant>"_DFN_RXX" (see Table 2-2).

Managing flow simulations

The execution of flow simulations (Section 5.3) is managed by the Fortran code [Td18_Manage_DT_runs.f90] in 6 steps:

1. Identify a <Bedrock case> from the manual input file [List_of_model_setups_for_DTS.txt].
2. Retrieve and ensure the existence of required input files (Table A-9).
3. Loop steps 4 to 6 for all six <time slice>.
4. Write the control file [DTS_setup.txt], which is used in subsequent model parameterisation, flow simulations, and particle tracking.
5. Write Compact Input Files for the subsequent flow simulations (cif.xml for the recharge and steady state simulations, respectively).

6. Write and execute [Run_DarcyTools.bat], which:
   a. Creates a local folder [RUN_<time slice>] in the working folder [<Bedrock case>].
   b. Finalises the model setup, by launching [SR-PSU_TD18_Model_parameterisation.f] (Table A-9).
   c. Solves head for the model top boundary in a recharge phase, under premises specified in [SR-PSU_TD18_DTS_RECHARGE.f] (Table A-10).
   d. Applies the top-boundary condition to solve the full flow field, under premises specified in [SR-PSU_TD18_DTS_Steady_state.f] (Table A-11).
   e. Renames output/input to tag <Bedrock case> and <time slice> in file names.
   f. Moves simulation input/output files into the local run folder [RUN_<time slice>].

Following the standard procedure in DarcyTools modelling, the upscaled bedrock properties (Table A-8) and the HSD parameterisations are combined (Table A-9) to form the final model setup, i.e. Step 6b above. However, DarcyTools does not facilitate inbuilt functions for the implementation of HSD layering, and therefore the approach taken is presented below.

Numerical implementation of HSD conductivity

Soil cells are identified by two DarcyTools cell markers: 1) Mk = 100, representing general soil, defined as cells above bedrock surface, and 2) Mk = 101, representing the uppermost, contiguous cell-layer intersected by the DEM of the current time slice. The HSD parameterisation is facilitated by a separate subroutine "HSD" of [SR-PSU_TD18_Model_parameterisation.f], which can be summarized in 6 steps:

1. Use DarcyTools cell markers to identify grid cells classified as HSD.
2. Match the DarcyTools grid cell, by coordinate, to relevant raster point(s) in RLDM (Table A-1).
   a) DarcyTools cells below the RLDM resolution are matched to the *nearest* RLDM point.
   b) DarcyTools cells exceeding RLDM resolution are matched to *an array* of RLDM points.
   c) Matching cells by coordinate requires back-rotation and translation into the RT90 coordinate system.
3. Calculate an effective HSD conductivity for the cell, based on the fractional intersection thicknesses, b_i, between the cell-wall control volume and the layer i, which has hydraulic conductivities K_{hi} and K_{vi} (Table 4-4).
   a. Effective horizontal conductivity is calculated as *arithmetic* mean of all $b_i \times K_{hi}$
   b. Effective vertical conductivity is calculated as *harmonic* mean of all $b_i \times K_{vi}$
4. Defaults are applied at inconsistencies between the DarcyTools grid and the RLDM data (i.e. for cells where $\Sigma b_i = 0$ m.
   a. *Outcrops* are set to K = 10^{-7} m/s, for cell markers = 101 where RLDM thickness = 0 m.
   b. *Till* is assumed, for cells located outside the horizontal coverage of RLDM.
   c. The *uppermost* or *lowest* RLDM layer with non-zero thickness is assumed, respectively, if the grid and RLDM layer elevations should mismatch vertically.
5. To avoid model artefacts (Figure 4-17), the conductivity of filling in the SFR pier, and its surroundings, are propagated 2 grid cells horizontally (i.e. 2 × 8 = 16 m horizontally; performed outside subroutine).
6. the SFR pier, and its surroundings, is parameterized as *till* below an elevation of −3 m.

Table A-9. Final model setup [SR-PSU_TD18_Model_parameterisation.f].

Input files	Description
[DTS_setup.txt]	Defines <Bedrock case> and <time slice>[1)]
[xyz_<time slice>_L26]	Computational grid (Table A-7).
[<Bedrock case>_condx.dat] [<Bedrock case>_condy.dat] [<Bedrock case>_condz.dat]	Cell-wall ECPM bedrock conductivity in x, y, and z-directions (Table A-8). In bedrock cases of constant K_{HRD}, K_{ECPM} refers only to HCD. In Singö variants, K_{ECPM} is overwritten for the Singö core.
[<Bedrock case>_frevol.dat]	Cell ECPM free volume (Table A-8; i.e. intersectional volume sum of fracture aperture, Eq. (5-1))
[Filled_pdem<time slice>_Fixed_bedrock.asc]	Upper surface of basin-filled DEM, z (m, elevation; fixed-bedrock format)
[lpgd<time slice>_Fixed_bedrock.asc]	Upper surface of lacustrine accumulation of postglacial deposits, z (m, elevation; fixed-bedrock reference).
[mpgd<time slice>_Fixed_bedrock.asc]	Upper surface of marine accumulation of post glacial deposits, z (m, elevation; fixed-bedrock reference).
[gkl<time slice>_Fixed_bedrock.asc]	Upper surface of glacial clay, z (m, elevation; fixed-bedrock reference).
[fill<time slice>_Fixed_bedrock.asc]	Upper surface of filling, z (m, elevation; fixed-bedrock reference).
[glfl<time slice>_Fixed_bedrock.asc]	Upper surface of glaciofluvial-material, z (m, elevation; fixed-bedrock reference).
[till<time slice>_Fixed_bedrock.asc]	Upper surface of till, z (m, elevation; fixed-bedrock reference).
[bedr<time slice>_Fixed_bedrock.asc]	Static bedrock surface, z (m, elevation; fixed-bedrock reference).
Table 4-4	Hydraulic conductivity for HSD layers (K_{HSD} hard-coded in separate subroutine)
Table 4-1	Tunnel backfill parameterisation (K_{Tunnel} hard-coded in separate subroutine). Identification via cell markers.
Output files	
[<Bedrock case>_<time slice>_PERMX] [<Bedrock case>_<time slice>_PERMY] [<Bedrock case>_<time slice>_PERMZ]	Cell-wall permeability in x, y, and z-directions, merged from bedrock K_{ECPM}, regolith K_{HSD} and tunnel backfill, K_{Tunnel}.
[<Bedrock case>_<time slice>_PORO]	Cell ECPM porosity for bedrock.
[<Bedrock case>_<time slice>_ECPM_K.plt]	Tecplot output for visualisation. Contains conductivity of tunnel-walls (e.g. Figure 4-3) and flow-domain cross sections.

[1)] <Bedrock case> = <HCD variant>"_DFN_RXX" (see Table 2-2). <time slice> defined in Table 2-1. Separate variables for: 1) Singö variant, 2) constant K_{HRD} inside the SFR Regional domain, 3) HCD extension north of the SFR domain, and 4) HRD parameterisation outside the SFR Regional domain.

Input/output of the ”Recharge-phase” simulation

Table A-10. “Recharge-phase” simulation [SR-PSU_TD18_DTS_RECHARGE.f].

Input files	Description
[DTS_setup.txt]	Defines <Bedrock case> and <time slice>[1)]
[cif.xml]	Automatically generated standard Compact Input File. Replaced by final CIF (Table A-11).
[xyz_<time slice>_L26]	Computational grid (Table A-7).
[<Bedrock case>_<time slice>_PERMX] [<Bedrock case>_<time slice>_PERMY] [<Bedrock case>_<time slice>_PERMZ]	Cell-wall permeability in x, y, and z-directions, merged from bedrock K_{ECPM}, regolith K_{HSD} and tunnel backfill, K_{Tunnel}. (Table A-9).
[Filled_pdem<time slice>_Fixed_bedrock.asc]	Upper surface of basin-filled DEM, z (m, elevation; fixed-bedrock format). Defines maximum-head criterion for ground-surface cells.
Output files	
[<Bedrock case>_<time slice>_hist<1-8>]	History files logging convergence statistics (e.g. Figure 6-5 and Figure 6-6).
[<Bedrock case>_<time slice>_rstslv]	Flow solution (standardised DarcyTools restart file). The head solution in ground-surface cells is propagated as a top-boundary condition for the “Steady-state phase”.
[<Bedrock case>_<time slice>_GWT_recharge.plt	Tecplot ground-surface output for visualisation (e.g. Figure 6-1 to Figure 6-4).

[1)] <Bedrock case> = <HCD variant>”_DFN_RXX” (see Table 2-2). <time slice> defined in Table 2-1. Separate variables for: 1) Singö variant, 2) constant K_{HRD} inside the SFR Regional domain, 3) HCD extension north of the SFR domain, and 4) HRD parameterisation outside the SFR Regional domain.

Input/output of the ”Steady-state” phase

Table A-11. “Steady-state” phase simulation [SR-PSU_TD18_DTS_Steady_state.f].

Input files	Description
[DTS_setup.txt]	Defines <Bedrock case> and <time slice>[1)]
[xyz_<time slice>_L26]	Computational grid (Table A-7).
[<Bedrock case>_<time slice>_cif.xml]	Automatically generated standard Compact Input File.
[<Bedrock case>_<time slice>_PERMX] [<Bedrock case>_<time slice>_PERMY] [<Bedrock case>_<time slice>_PERMZ]	Cell-wall permeability in x, y, and z-directions, merged from bedrock K_{ECPM}, regolith K_{HSD} and tunnel backfill, K_{Tunnel} (Table A-9).
[<Bedrock case>_<time slice>_rstslv]	Flow solution from the “Recharge phase” (Table A-10), defining a fixed-head condition for the top boundary (standardised DarcyTools restart file).
Output files	
[<Bedrock case>_<time slice>_hist<1-8>]	History files, logging convergence statistics, appended from the Recharge phase (Table A-10). See Section A5 for analysis of history files.
[<Bedrock case>_<time slice>_rstslv]	Final steady-state solution (DarcyTools restart file). Not used.
[<Bedrock case>_<time slice>_Flow_solution.dat]	Final steady-state solution, accessible for Post processing (Section 5.4; Table A-12; Table A-13). Contains cell-wall Darcy velocity and cell-centre pressure.
[<Bedrock case>_<time slice>_Tunnel_flows.dat]	Disposal-room cross-flows, ASCII text.
[<Bedrock case>_<time slice>_Tunnel_walls.plt]	Tecplot output for visualisation (containing conductivity, head, and cross-flow for all tunnel walls).
[<Bedrock case>_<time slice>_DTS_output.plt]	Tecplot output for visualisation (containing conductivity, head, cell markers, and Darcy flux for vertical and horizontal flow-domain cross sections).

[1)] <Bedrock case> = <HCD variant>”_DFN_RXX” (see Table 2-2). <time slice> defined in Table 2-1. Separate variables for: 1) Singö variant, 2) constant KHRD inside the SFR Regional domain, 3) HCD extension north of the SFR domain, and 4) HRD parameterisation outside the SFR Regional domain.

A4 Post-processing model output

The performance measures are extracted from the flow solutions by means of post processing the obtained flow solutions (details in Section 5.4.1 and 5.4.2). Disposal-facility cross flow is extracted by means of the FORTRAN code [SR-PSU_TD18_GET_flows.f90], and particle tracking is executed by means of the code [SR-PSU_Td18_p-track_random_deplete_loops.f]. The input/output of the flow analysis is documented in Table A-12, while the input/output for particle tracking is documented in Table A-13.

Table A-12. Flow-field analysis [SR-PSU_TD18_GET_flows.f90].[1)]

Input files	Description
[Directory_Get_flow.txt]	Defines <Bedrock case>
[xyz_<time slice>_L26]	Computational grid (from Table A-7).
[<Bedrock case>_<time slice>_Flow_solution.dat]	Final steady-state solution, containing cell-wall Darcy velocities and cell-centre pressures (result from Table A-11).
[objects_sfr_20121130.asc][2)]	Raster data identifying biosphere objects.
Output files	
[Cell-net_flows.dat]	Calculated cell-net flow over tunnel walls, maximum local disposal-room gradient and overall disposal-room gradient.
[Biosphere_Cell-net_flows.dat]	Net recharge/discharge across bedrock surface inside biosphere objects (mm/yr).
[<Bedrock case>_<time slice>Bio_Q.plt]	Tecplot output for verification and visualisation purposes.

[1)] See Table 2-2 for <Bedrock case> and Table 2-1 for <time slice>.

[2)] Delivered by Emma Bosson, 2013-03-18. Raster data linked to biosphere object ID via [objects_sfr_20121130.dbf].

The input and output data files are summarized in Table A-13. In addition to the standardised output [<Bedrock case>_<time slice>_<Release location>_<File type>.dat], so-called disposal-room *interactions* are exported in a separate output file [Assembled_Cross-List.dat] (ASCII format). Disposal-room interactions are statistics on the fraction of released particles from one disposal room that crosses one or more adjacent disposal rooms.

Table A-13. Particle tracking [SR-PSU_Td18_p-track_random_deplete_loops.f].*

Input files	Description
[Directory_for_P-tracking.txt]	Defines <Bedrock case> and <time slice>
[xyz_<time slice>_L26]	Computational grid (from Table A-7).
[<Bedrock case>_fws.dat]	ECPM flow-wetted surface area (cell property from Table A-8).
[<Bedrock case>_<time slice>_PORO]	ECPM porosity (cell property from Table A-9).
[<Bedrock case>_<time slice>_Flow_solution.dat]	Final steady-state solution, containing cell-wall Darcy velocities and cell-centre pressures (result from Table A-11).

Output files: <Bedrock case>_<time slice>_<Release location>_<File type>.dat

<Release location>	Markers		Tunnels	No. particles
All_SFR1_D_	11–15	SFR-1	All 5 disposal rooms	1 000 000
SFR-1_1BTF_(11)	11	SFR-1	1BTF	10 000
SFR-1_2BTF_(12)	12	SFR-1	2BTF	10 000
SFR-1_1BLA_(13)	13	SFR-1	1BLA	10 000
SFR-1_1BMA_(14)	14	SFR-1	1BMA	10 000
SFR-1_Silo_(15)	15	SFR-1	Silo1	10 000
All_SFR2_D_	22–27	SFR-3	All 6 disposal rooms	1 000 000
SFR-2_2BLA_(22)	22	SFR-3	2BLA	10 000
SFR-2_3BLA_(23)	23	SFR-3	3BLA	10 000
SFR-2_4BLA_(24)	24	SFR-3	4BLA	10 000
SFR-2_5BLA_(25)	25	SFR-3	5BLA	10 000
SFR-2_2BMA_(26)	26	SFR-3	2BMA	10 000
SFR-2_1BRT_(27)	27	SFR-3	1BRT_del1	10 000

<File type>.dat

Exit_loc	Exit locations, or recharge locations, at the bedrock surface depending on direction of particle tracking. 15 data columns defined in TD11_Exit_locations_2013-01-30__READ_ME_____.txt
Discharge	2-D histogram of exit locations used for visualisation in TecPlot format, resolving number of particles per m^2 and mean travel time.
Recharge	2-D histogram of recharge locations used for visualisation in TecPlot format, resolving number of particles per m^2 and mean travel time.
FORWARD_Paths	3-D trajectories from forward particle tracking (max 3000 exported). Used to visualise user-specified performance measures in TecPlot.
BACKWD_Paths	3-D trajectories from backward particle tracking (max 3000 exported). Used to visualise user-specified performance measures in TecPlot.

* See Table 2-2 for <Bedrock case> and Table 2-1 for <time slice>. “deplete_loops” refer to a version of the algorithm where artificial bedrock retention properties, accumulated in “looping trajectory segments” (see separate PM on <nbgrad>), are removed.

A5 Convergence

DarcyTools allows several options of monitoring the convergence during simulations, for example the pressure at given points or flux over control volumes. The monitored values are stored in so-called history files (Table A-11). The root-mean-square (RMS) of errors in the pressure (head) solution and the mass balance of a large volume of SFR host rock is exemplified for an arbitrary model case (here: case 26, 2000 AD; Figure A-2).

The RMS error is expected to improve by c. 6 to 7 orders of magnitude in a well-converged flow solution, from the first iteration to the last. In the given example, the RMS-error improves by almost 8 orders of magnitude (Figure A-2a). Analysis of all simulated bedrock cases (270 model setups) demonstrates that the RMS improvement typically ranges from 6 to 9 orders of magnitude (Table A-14). Early time slices, where the pressure-gradients are lower, exhibit a larger improvement, compared to the later time slices, where gradients are stronger. Note that case 6 is particularly well-converged for two early time slices (i.e. 10 orders of magnitude improvement); the reason for this is that its two model setups 2000 AD and 2100 AD had to be run 25 additional iterations (in addition to the standard 25 iterations) in its fixed-phase to fulfil the 1 % mass-balance criterion for disposal-room crossflow (Figure 6-8).

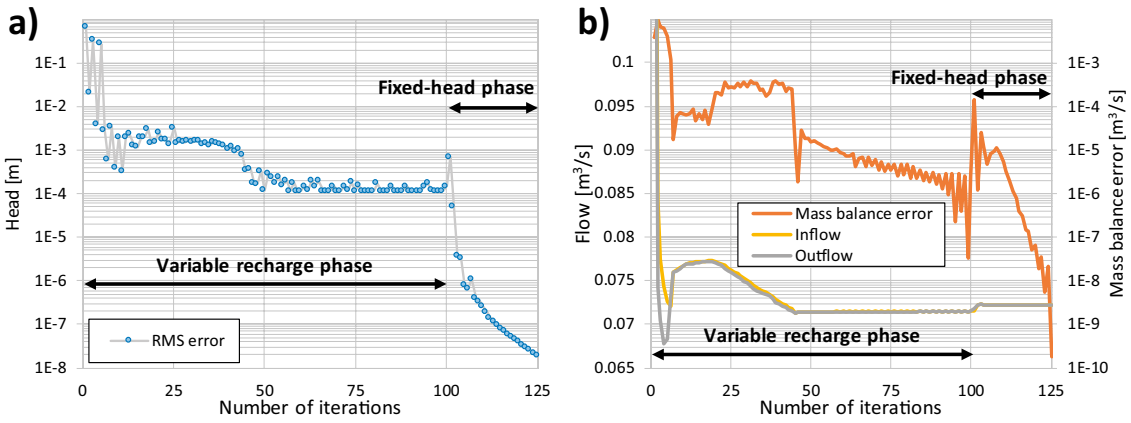

Figure A-2. *Convergence measures in flow simulation; a) root-mean-square of errors and b) mass balance over a relevant volume of host rock (horizontal extent of c. 1 km × 2 km; vertical extending from z = −20 m to z = −145 m; partly containing SFR1 and SFR3). Note linear scaling of flow (left y-axis) and logarithmic scaling of the mass balance error (right y-axis).*

Table A-14. Compilation of RMS-error improvement (orders of magnitude).

No.	Bedrock case[1)]	2000	2100	2250	2500	2750	3000	3500	5000	9000
1*	BASE_CASE1_DFN_R85_EXT1	7.88	7.99	7.67	8.21	6.50	7.14	7.47	6.34	6.38
2	BASE_CASE1_DFN_R85_EXT02	9.02	9.11	8.46	8.59	8.19	8.03	7.75	6.80	6.76
3	BASE_CASE1_DFN_R85_EXT11	8.82	8.81	8.39	8.91	8.89	8.14	7.84	7.00	6.36
4	BASE_CASE1_DFN_R85_EXT12	9.11	9.01	8.46	8.59	8.21	8.03	7.81	6.98	6.83
5	nc_Si1_HOM_HRD_C02_EXT01	8.82	8.94	8.49	8.45	8.83	8.25	7.86	6.85	6.95
6	nc_Si1_R01_HRD_C01_EXT01	10.42	10.59	8.30	8.67	7.02	7.82	7.48	6.83	6.72
7	nc_Si1_R01_HRD_C02_EXT01	9.15	8.63	8.50	8.35	8.82	8.34	8.04	6.33	6.72
8	nc_Si1_R01_HRD_C03_EXT01	8.87	8.87	8.40	8.30	8.81	7.90	7.86	6.53	6.68
9	nc_Si1_R01_DFN_R03_EXT02	8.97	8.78	8.30	8.56	8.43	7.90	8.12	7.03	6.69
10	nc_Si1_R01_DFN_R03_EXT01	8.80	8.72	8.47	8.65	8.44	7.96	8.02	7.03	6.76
11*	nc_DEP_R07_DFN_R85_EXT1	7.98	8.00	7.70	8.23	6.49	7.17	7.42	6.74	6.20
12	nc_Si1_R07_HRD_C02_EXT01	9.21	8.71	8.41	8.92	8.53	8.14	7.73	6.78	6.67
13	CD_Si1_R07_DFN_R85_EXT01	7.95	8.04	7.83	7.02	6.87	6.97	6.78	6.69	6.61
14	nc_Si1_R01_DFN_R85_EXT01	8.71	8.47	8.20	7.47	7.33	7.20	7.03	6.54	6.59
15*	nc_NoD_R01_DFN_R18_EXT1	7.84	7.96	7.67	8.14	6.51	7.14	7.46	6.72	6.10
16	nc_Si1_R07_DFN_R85_EXT02	8.64	8.77	8.43	8.71	7.38	7.91	7.81	7.07	6.95
17	nc_Si1_R07_DFN_R18_EXT02	8.90	8.64	8.38	8.50	8.57	7.91	7.71	7.07	6.50
18	nc_Si1_R07_DFN_R03_EXT02	8.82	8.62	8.42	8.67	8.12	8.02	7.78	6.50	6.70
19	CD_Si2_HOM_DFN_R85_EXT01	8.78	8.78	8.12	6.82	6.79	6.92	6.79	6.71	6.23
20	CD_Si3_HOM_DFN_R85_EXT01	8.47	8.40	8.13	6.81	6.83	6.93	6.79	6.89	6.82
21	CD_Si4_HOM_DFN_R85_EXT01	8.52	8.44	7.90	7.11	6.80	8.18	7.97	7.00	6.80
22	nc_Si1_R07_DFN_R85_EXT11	8.67	8.88	8.45	8.71	8.73	7.87	7.83	7.02	6.89
23	nc_Si1_R07_DFN_R85_EXT12	8.31	8.31	8.01	7.44	7.19	7.05	6.82	6.72	6.59
24	nc_Si1_R01_DFN_R85_EXT11	8.73	8.47	8.19	7.47	7.33	7.19	7.03	6.62	6.52
25	nc_Si1_R01_DFN_R85_EXT12	8.70	8.44	8.17	7.44	7.33	7.21	7.06	7.01	6.80
26	BASE_CASE1_DFN_R85_EXT00	7.91	7.87	8.07	7.10	6.77	6.93	6.76	6.43	6.68
27	BASE_CASE1_DFN_R85_EXT10	8.09	8.00	8.47	8.57	7.35	8.53	7.88	6.75	7.18
28	nc_Si1_HOM_HRD_C02_EXT00	8.28	8.01	7.94	7.42	7.30	7.33	7.19	7.05	7.25
29	nc_Si1_HOM_HRD_C02_EXT10	8.29	8.00	7.95	7.44	7.31	7.33	7.17	6.54	6.72
30	BASE_CASE1_DFN_R85_EXT01	8.34	8.37	7.83	7.12	6.85	6.93	6.80	6.76	6.86

* Three bedrock cases selected as representative for covering the range of disposal-room flow related to uncertainty in bedrock parameterisation.

[1)] See Table 2-2 for annotation of bedrock cases.

A large rock-mass volume is selected as representative for monitoring the SFR flow conditions during flow simulations. The relative mass balance over this rock volume is taken as another measure of convergence in the flow solution (e.g. case 26, 2000 AD, in Figure A-2b). This rock volume[2] contains all the rock vaults of SFR1 and SFR3 (except the silo) and covers a horizontal extent of c. 1 km × 2 km and a vertical extent from z=−20 m to z=−145 m. For the given example (Figure A-2b), the relative mass-balance error at the end of simulations is $\Delta Q_{Error}/Q = 2 \times 10^{-8}/0.072 \approx 4 \times 10^{-7}$. Analysis of all simulated bedrock cases (270 model setups) demonstrates that the relative mass-balance error typically ranges from 10^{-10} to 10^{-5} orders of magnitude (Table A-15).

[2] In the rotated DarcyTools coordinate system, xDT ranges from 6 350 to 8 000, yDT ranges from 9 350 to 10 150, and y ranges from −145 m to −20 m (fixed-bedrock reference).

Table A-15. Compilation of relative mass-balance error of SFR host rock.

No.	Bedrock case[1)]	2000	2100	2250	2500	2750	3000	3500	5000	9000
1*	BASE_CASE1_DFN_R85_EXT1	5.1E-8	1.5E-8	3.8E-9	2.5E-7	2.1E-7	4.9E-8	2.2E-8	7.5E-8	3.6E-9
2	BASE_CASE1_DFN_R85_EXT02	8.6E-9	3.5E-9	4.1E-10	6.0E-8	4.0E-9	1.8E-9	1.7E-8	5.3E-8	1.3E-7
3	BASE_CASE1_DFN_R85_EXT11	4.5E-9	2.5E-9	7.1E-11	1.1E-8	1.6E-8	8.2E-10	4.3E-9	6.0E-8	1.6E-8
4	BASE_CASE1_DFN_R85_EXT12	6.6E-9	4.1E-9	3.8E-10	3.0E-8	7.9E-10	1.8E-9	1.4E-8	7.1E-8	1.6E-7
5	nc_Si1_HOM_HRD_C02_EXT01	4.2E-9	1.5E-9	1.2E-10	2.0E-8	7.1E-9	5.7E-10	6.8E-9	8.8E-8	2.2E-8
6	nc_Si1_R01_HRD_C01_EXT01	1.4E-9	6.7E-10	4.0E-9	5.4E-9	3.5E-7	3.3E-8	6.4E-8	5.0E-7	9.1E-8
7	nc_Si1_R01_HRD_C02_EXT01	2.6E-8	2.6E-8	1.1E-11	3.1E-8	3.9E-8	3.5E-9	5.2E-9	1.7E-7	6.5E-9
8	nc_Si1_R01_HRD_C03_EXT01	4.7E-9	1.5E-11	2.7E-10	9.2E-9	6.2E-9	6.6E-9	4.1E-9	1.2E-7	6.2E-7
9	nc_Si1_R01_DFN_R03_EXT02	4.7E-9	6.8E-9	9.3E-9	7.2E-9	7.6E-10	8.0E-9	5.0E-9	1.4E-7	9.8E-7
10	nc_Si1_R01_DFN_R03_EXT01	1.7E-8	5.9E-10	1.1E-8	9.8E-9	8.4E-9	5.4E-9	1.2E-8	1.1E-7	1.0E-7
11*	nc_DEP_R07_DFN_R85_EXT1	6E-10	3.3E-9	2.0E-9	1.1E-7	3.3E-7	2.1E-8	1.5E-8	9.9E-8	1.4E-6
12	nc_Si1_R07_HRD_C02_EXT01	1.8E-9	2.1E-8	1.2E-9	6.0E-8	1.1E-8	5.7E-9	5.2E-9	1.1E-7	1.0E-7
13	CD_Si1_R07_DFN_R85_EXT01	3.9E-7	9.8E-7	2.8E-7	9.9E-6	7.6E-6	1.3E-6	1.5E-6	9.0E-7	6.6E-7
14	nc_Si1_R01_DFN_R85_EXT01	2.7E-8	3.1E-8	7.6E-8	3.3E-7	1.7E-7	3.8E-7	3.7E-7	2.2E-9	1.3E-7
15*	nc_NoD_R01_DFN_R18_EXT1	1.2E-7	4.8E-9	4.3E-9	1.7E-10	6.4E-7	9.9E-9	1.0E-7	2.6E-7	8.3E-8
16	nc_Si1_R07_DFN_R85_EXT02	2.7E-9	2.5E-9	3.5E-9	2.7E-8	3.4E-8	2.1E-9	4.7E-8	5.2E-8	2.3E-8
17	nc_Si1_R07_DFN_R18_EXT02	1E-9	2.1E-9	3.3E-9	5.5E-10	1.3E-9	4.5E-9	7.8E-9	9.4E-8	4.1E-7
18	nc_Si1_R07_DFN_R03_EXT02	8.5E-9	5.3E-9	1.1E-9	4.3E-9	2.7E-8	5.8E-9	8.9E-9	8.8E-8	3.2E-8
19	CD_Si2_HOM_DFN_R85_EXT01	7.6E-7	1.4E-7	5.1E-7	2.5E-5	3.0E-6	2.4E-6	2.3E-6	1.8E-6	2.9E-7
20	CD_Si3_HOM_DFN_R85_EXT01	7.8E-8	2.7E-7	3.7E-7	2.5E-5	6.9E-6	2.6E-6	2.1E-6	6.5E-8	4.4E-8
21	CD_Si4_HOM_DFN_R85_EXT01	6.1E-7	7.6E-7	1.3E-7	4.1E-6	6.4E-6	1.8E-10	9.6E-9	9.0E-8	1.1E-7
22	nc_Si1_R07_DFN_R85_EXT11	4.1E-9	5.1E-10	3.0E-9	1.4E-7	1.5E-9	4.2E-9	8.1E-9	6.3E-8	2.8E-8
23	nc_Si1_R07_DFN_R85_EXT12	3.5E-8	2.3E-8	1.9E-7	4.2E-7	3.1E-7	1.7E-7	2.3E-7	4.3E-7	2.2E-7
24	nc_Si1_R01_DFN_R85_EXT11	2.8E-8	3.1E-8	7.6E-8	3.5E-7	1.8E-7	3.8E-7	3.7E-7	4.6E-8	8.5E-8
25	nc_Si1_R01_DFN_R85_EXT12	2.9E-8	3.3E-8	6.6E-8	1.8E-6	4.5E-9	3.1E-7	3.3E-7	1.1E-7	1.0E-6
26	BASE_CASE1_DFN_R85_EXT00	3.9E-7	5.1E-7	1.2E-7	3.9E-6	5.9E-6	2.2E-6	1.4E-6	1.3E-6	1.9E-6
27	BASE_CASE1_DFN_R85_EXT10	2.6E-8	2.7E-8	6.6E-10	9.6E-8	6.2E-8	9.2E-9	4.5E-8	4.2E-8	1.7E-7
28	nc_Si1_HOM_HRD_C02_EXT00	4.8E-6	3.6E-6	2.0E-6	9.2E-6	6.8E-6	3.6E-6	3.7E-6	8.1E-8	1.2E-7
29	nc_Si1_HOM_HRD_C02_EXT10	4.8E-6	3.3E-6	2.2E-6	1.0E-5	7.4E-6	3.7E-6	4.0E-6	5.8E-6	2.7E-6
30	BASE_CASE1_DFN_R85_EXT01	5.8E-7	7.7E-7	1.3E-7	5.7E-6	9.0E-6	2.0E-6	1.7E-6	5.5E-8	1.1E-7

* Three bedrock cases selected as representative for covering the range of disposal-room flow related to uncertainty in bedrock parameterisation.

[1)] See Table 2-2 for annotation of bedrock cases.

Appendix B

Data processing for DarcyTools implementation

The implementation of tunnel geometry (Figure 3-2) into the DarcyTools computational grid requires processing of delivered data (Table B-1):

1. all geometric tunnel data (original CAD format *.stl) are converted into the so-called DarcyTools-object format (changing file extension to *.dat). The file conversion is a standard procedure, and managed by the DarcyTools module OGN.
2. all geometric objects (*.dat) are translated and rotated into the local model coordinate system (adding the prefix “R_”*.dat). Filename traceability from original CAD files to the applied DarcyTools-object files is provided by means of Table B-1.

Tunnel geometry data

All tunnel geometry data, i.e. SFR 1, SFR 3 and tunnel plugs (Section 3.2), are available in the CAD format (Odén and Öhman 2017). The implementation of tunnel geometry in the DarcyTools computational grid (Figure 3-2) requires processing of delivered data (Table B-1). The original CAD files are converted into the so-called DarcyTools-object format (changing file extension to *.dat; Table B-1). These geometric objects (*.dat) are translated and rotated into the local model coordinate system (adding the prefix “R_”*.dat). Filename of DarcyTools objects are shortened, as DarcyTools has an upper limit of 32 characters in object names. Typically, the substrings “plugg” can be omitted. Filename traceability from original CAD files to the applied DarcyTools object files is provided by means of Table B-1.

Table B-1. Used tunnel/tunnel plug geometry.

Source data (CAD STereoLithography format)	Rotated DarcyTools object
Disposal rooms of SFR 1	
SFR1_1BLA_del1_yellow.stl	R_1BLA_del1_yellow.dat
SFR1_1BMA_del1_yellow.stl	R_1BMA_del1_yellow.dat
SFR1_1BTF_del1_yellow.stl	R_1BTF_del1_yellow.dat
SFR1_1TT_del7_yellow.stl	R_1TT_del7_yellow.dat
SFR1_2BTF_del1_yellow.stl	R_2BTF_del1_yellow.dat
SFR1_Silo_del1_topp_yellow.stl	R_Silo_del1_topp_yellow.dat
SFR1_Silo_del2_under_topp_yellow.stl	R_Silo_del2_under_topp_yellow.dat
SFR1_Silo_del3_yttre_yellow.stl	R_Silo_del3_yttre_yellow.dat
SFR1_Silo_del4_mitt_yellow.stl	R_Silo_del4_mitt_yellow.dat
SFR1_Silo_del5_undre_yellow.stl	R_Silo_del5_undre_yellow.dat
Backfilled tunnels of SFR 1	
SFR1_1BT_del1_white.stl	R_1BT_del1_white.dat
SFR1_1BT_del2_white.stl	R_1BT_del2_white.dat
SFR1_1BT_del3_white.stl	R_1BT_del3_white.dat
SFR1_1BT_del4_genomstick_white.stl	R_1BT_del4_genomstick_white.dat
SFR1_1BT_del5_white.stl	R_1BT_del5_white.dat
SFR1_1BT_del7_white.stl	R_1BT_del7_white.dat
SFR1_1BT_del9_white.stl	R_1BT_del9_white.dat
SFR1_1BT_del10_genomstick_white.stl	R_1BT_del10_genomstick_white.dat
SFR1_1BT_del11_white.stl	R_1BT_del11_white.dat
SFR1_1BT_del12_white.stl	R_1BT_del12_white.dat
SFR1_1BT_del13_nedre_stick_white.stl	R_1BT_del13_nedre_stick_white.dat
SFR1_1BT_del14_nedre_stick_white.stl	R_1BT_del14_nedre_stick_white.dat
SFR1_1BT_del15_white.stl	R_1BT_del15_white.dat
SFR1_1BT_del16_white.stl	R_1BT_del16_white.dat
SFR1_1BT_del17_white.stl	R_1BT_del17_white.dat
SFR1_1BT_del18_white.stl	R_1BT_del18_white.dat

Source data (CAD STereoLithography format)	Rotated DarcyTools object
SFR1_1BT_del19_white.stl	R_1BT_del19_white.dat
SFR1_1BT_del20_white.stl	R_1BT_del20_white.dat
SFR1_1BT_del21_silotunnel_white.stl	R_1BT_del21_silotunnel_white.dat
SFR1_1BT_del22_silotunnel_white.stl	R_1BT_del22_silotunnel_white.dat
SFR1_1BT_del23_silotunnel_white.stl	R_1BT_del23_silotunnel_white.dat
SFR1_1BT_del26_white.stl	R_1BT_del26_white.dat
SFR1_1BT_del27_white.stl	R_1BT_del27_white.dat
SFR1_1BT_del28_white.stl	R_1BT_del28_white.dat
SFR1_1BT_del29_white.stl	R_1BT_del29_white.dat
SFR1_1BT_del34_white.stl	R_1BT_del34_white.dat
SFR1_1BT_del35_anslutning_schakt_white.stl	R_1BT_del35_ansl_schakt_white.dat
SFR1_1BT_del36_undre_del_white.stl	R_1BT_del36_undre_del_white.dat
SFR1_1BT_del37_undre_del_white.stl	R_1BT_del37_undre_del_white.dat
SFR1_1BT_del38_undre_del_white.stl	R_1BT_del38_undre_del_white.dat
SFR1_1BT_del39_undre_del_white.stl	R_1BT_del39_undre_del_white.dat
SFR1_1BT_del40_undre_del_white.stl	R_1BT_del40_undre_del_white.dat
SFR1_1BT_del41_undre_del_white.stl	R_1BT_del41_undre_del_white.dat
SFR1_1BT_del42A_undre_del_white.stl	R_1BT_del42A_undre_del_white.dat
SFR1_1BT_del42B_undre_del_white.stl	R_1BT_del42B_undre_del_white.dat
SFR1_1BT_del42C_undre_del_white.stl	R_1BT_del42C_undre_del_white.dat
SFR1_1BT_del53_undre_del_white.stl	R_1BT_del53_undre_del_white.dat
SFR1_1BT_del54_undre_del_schakt_white.stl	R_1BT_del54_undre_del_sch_white.dat
SFR1_1BTF_ut_del5_white.stl	R_1BTF_ut_del5_white.dat
SFR1_1DT_del1_white.stl	R_1DT_del1_white.dat
SFR1_1DT_del2_white.stl	R_1DT_del2_white.dat
SFR1_1DT_del3_white.stl	R_1DT_del3_white.dat
SFR1_1DT_del4_white.stl	R_1DT_del4_white.dat
SFR1_1DT_del5_white.stl	R_1DT_del5_white.dat
SFR1_1DT_del6_white.stl	R_1DT_del6_white.dat
SFR1_1DT_del7_white.stl	R_1DT_del7_white.dat
SFR1_1DT_del8_white.stl	R_1DT_del8_white.dat
SFR1_1DT_del11_white.stl	R_1DT_del11_white.dat
SFR1_1DT_del12_white.stl	R_1DT_del12_white.dat
SFR1_1DT_del15_white.stl	R_1DT_del15_white.dat
SFR1_1DT_del16_white.stl	R_1DT_del16_white.dat
SFR1_1DT_del17_white.stl	R_1DT_del17_white.dat
SFR1_1DT_del18_white.stl	R_1DT_del18_white.dat
SFR1_1DT_del19_white.stl	R_1DT_del19_white.dat
SFR1_1DT_del20_white.stl	R_1DT_del20_white.dat
SFR1_1DT_del21_white.stl	R_1DT_del21_white.dat
SFR1_1DT_del22_white.stl	R_1DT_del22_white.dat
SFR1_1DT_del23_white.stl	R_1DT_del23_white.dat
SFR1_1DT_del24_white.stl	R_1DT_del24_white.dat
SFR1_1DT_del25_white.stl	R_1DT_del25_white.dat
SFR1_1DT_del26_white.stl	R_1DT_del26_white.dat
SFR1_1DT_del27_white.stl	R_1DT_del27_white.dat
SFR1_1DT_del28_white.stl	R_1DT_del28_white.dat
SFR1_1DT_del29_white.stl	R_1DT_del29_white.dat
Mechanical concrete plugs in SFR 1 (Blue)	
SFR1_1BT_del24_silotunnel_blue_plugg.stl	R_1BT_del24_silotunnel_blue.dat
SFR1_1BT_del25A_silotunnel_blue_plugg.stl	R_1BT_del25A_silotunnel_blue.dat
SFR1_1BT_del30A_blue_plugg.stl	R_1BT_del30A_blue_plugg.dat
SFR1_1BT_del30B_blue_plugg.stl	R_1BT_del30B_blue_plugg.dat
SFR1_1BT_del33_blue_plugg.stl	R_1BT_del33_blue_plugg.dat
SFR1_1BT_del42D_undre_del_blue_plugg.stl	R_1BT_del42D_undre_del_blue.dat
SFR1_1BT_del45_undre_del_blue_plugg.stl	R_1BT_del45_undre_del_blue.dat

Source data (CAD STereoLithography format)	Rotated DarcyTools object
SFR1_1BT_del50_undre_del_blue_plugg.stl	R_1BT_del50_undre_del_blue.dat
SFR1_1BT_del51_undre_del_blue_plugg.stl	R_1BT_del51_undre_del_blue.dat
SFR1_1BT_del52_undre_del_blue_plugg.stl	R_1BT_del52_undre_del_blue.dat
SFR1_1BTF_ut_del2_blue_plugg.stl	R_1BTF_ut_del2_blue.dat
SFR1_1BTF_ut_del4_blue_plugg.stl	R_1BTF_ut_del4_blue_plugg.dat
SFR1_1TT_del1_blue_plugg.stl	R_1TT_del1_blue.dat
SFR1_1TT_del4_blue_plugg.stl	R_1TT_del4_blue.dat
SFR1_1TT_del6_blue_plugg.stl	R_1TT_del6_blue_plugg.dat
SFR1_1TT_del10_blue_plugg.stl	R_1TT_del10_blue.dat
Bentonite plugs in SFR 1 (Brown)	
SFR1_1BST_del4_brown_plugg.stl	R_1BST_del4_SFR1_brown.dat
SFR1_1BST_del6_brown_plugg.stl	R_1BST_del6_brown.dat
SFR1_1BST_del7_brown_plugg.stl	R_1BST_del7_brown.dat
SFR1_1BST_del8_brown_plugg.stl	R_1BST_del8_brown.dat
SFR1_1BST_del10_brown_plugg.stl	R_1BST_del10_brown.dat
SFR1_1BST_del11_brown_plugg.stl	R_1BST_del11_brown.dat
SFR1_1BST_del12_brown_plugg.stl	R_1BST_del12_brown.dat
SFR1_1BST_del14_brown_plugg.stl	R_1BST_del14_brown.dat
SFR1_1BST_del15_brown_plugg.stl	R_1BST_del15_brown.dat
SFR1_1BST_del16_brown_plugg.stl	R_1BST_del16_brown.dat
SFR1_1BST_del18_brown_plugg.stl	R_1BST_del18_brown.dat
SFR1_1BST_del19_brown_plugg.stl	R_1BST_del19_brown.dat
SFR1_1BT_del25B_silotunnel_brown_plugg.stl	R_1BT_del25B_silotunnel_brown.dat
SFR1_1BT_del30C_brown_plugg.stl	R_1BT_del30C_brown_plugg.dat
SFR1_1BT_del31_brown_plugg.stl	R_1BT_del31_brown_plugg.dat
SFR1_1BT_del32_brown_plugg.stl	R_1BT_del32_brown_plugg.dat
SFR1_1BT_del42E_undre_del_brown_plugg.stl	R_1BT_del42E_undre_del_brown.dat
SFR1_1BT_del43_undre_del_brown_plugg.stl	R_1BT_del43_undre_del_brown.dat
SFR1_1BT_del44_undre_del_brown_plugg.stl	R_1BT_del44_undre_del_brown.dat
SFR1_1BT_del46_undre_del_brown_plugg.stl	R_1BT_del46_undre_del_brown.dat
SFR1_1BT_del47_undre_del_brown_plugg.stl	R_1BT_del47_undre_del_brown.dat
SFR1_1BT_del48_undre_del_brown_plugg.stl	R_1BT_del48_undre_del_brown.dat
SFR1_1BT_del49_undre_del_brown_plugg.stl	R_1BT_del49_undre_del_brown.dat
SFR1_1BTF_ut_del3_brown_plugg.stl	R_1BTF_ut_del3_brown_plugg.dat
SFR1_1TT_del2_brown_plugg.stl	R_1TT_del2_brown.dat
SFR1_1TT_del3_brown_plugg.stl	R_1TT_del3_brown.dat
SFR1_1TT_del5_brown_plugg.stl	R_1TT_del5_brown.dat
SFR1_1TT_del6_brown_plugg.stl	R_1TT_del6_brown_plugg.dat
SFR1_1TT_del8_brown_plugg.stl	R_1TT_del8_brown.dat
SFR1_1TT_del9_brown_plugg.stl	R_1TT_del9_brown.dat
SFR1_1TT_del11_brown_plugg.stl	R_1TT_del11_brown.dat
SFR1_1TT_del12_brown_plugg.stl	R_1TT_del12_brown.dat
Earth-dam plugs in SFR 1 (Green)	
SFR1_1BST_del1_green_plugg.stl	R_1BST_del1_green.dat
SFR1_1BST_del2_green_plugg.stl	R_1BST_del2_green.dat
SFR1_1BST_del3_green_plugg.stl	R_1BST_del3_green.dat
SFR1_1BST_del5_green_plugg.stl	R_1BST_del5_green.dat
SFR1_1BST_del9_green_plugg.stl	R_1BST_del9_green.dat
SFR1_1BST_del13_green_plugg.stl	R_1BST_del13_green.dat
SFR1_1BST_del17_green_plugg.stl	R_1BST_del17_green.dat
Bentonite plugs in ramp of SFR 1 (Pink)	
SFR1_1BT_del6_pink_plugg.stl	R_1BT_del6_pink_plugg.dat
SFR1_1BT_del8_pink_plugg.stl	R_1BT_del8_pink_plugg.dat
SFR1_1DT_del9_pink_plugg.stl	R_1DT_del9_pink.dat
SFR1_1DT_del10_pink_plugg.stl	R_1DT_del10_pink.dat

Source data (CAD STereoLithography format)	Rotated DarcyTools object
SFR1_1DT_del13_pink_plugg.stl	R_1DT_del13_pink.dat
SFR1_1DT_del14_pink_plugg.stl	R_1DT_del14_pink.dat
SFR1_1BT_del6_pink_plugg.stl	R_1BT_del6_pink_plugg.dat
Disposal rooms of SFR 3	
anlaggning_1BRT_L2-6_RT90.stl	R_anlaggning_1BRT_L26.dat
anlaggning_2BLA_L2-6_RT90.stl	R_anlaggning_2BLA_L26.dat
anlaggning_3BLA_L2-6_RT90.stl	R_anlaggning_3BLA_L26.dat
anlaggning_4BLA_L2-6_RT90.stl	R_anlaggning_4BLA_L26.dat
anlaggning_5BLA_L2-6_RT90.stl	R_anlaggning_5BLA_L26.dat
anlaggning_2BMA_L2-6_RT90.stl	R_anlaggning_2BMA_L26.dat
Backfilled tunnels of SFR 3	
anlaggning_SFR3_sammanslagen_L2-6_RT90.stl	R_anlaggning_SFR3_sammanslagen_L26.dat
anlaggning_SFR3_nedfartstunnlar_L2-6_RT90.stl	R_SFR3_nedfartstunnlar_L26.dat
anlaggning_4VB-5VB_L2-6_RT90.stl	R_anlaggning_4VB-5VB_L26.dat
Mechanical concrete plugs in SFR 3 (Blue)	
betongplugg_SFR3_L2-6_RT90.stl	R_betongplugg_SFR3_L26.dat
Bentonite plugs in SFR 3 (Brown)	
bentonitplugg_2NDB_SFR3_L2-6_RT90.stl	R_bentonitplugg_2NDB_SFR3_L26.dat
bentonitplugg_3NDB_SFR3_L2-6_RT90.stl	R_bentonitplugg_3NDB_SFR3_L26.dat
bentonitplugg_tunnlar_SFR3_L2-6_RT90.stl	R_bentonitplugg_tunnlar_SFR3_L26.dat

Appendix C

Inflow under open tunnel conditions

Tunnel inflow for the operative phase of to the planned extension (SFR3) is simulated to provide the basis for dimensioning its pumping system. An estimate of the uncertainty in simulation results is provided by comparing the output from three bedrock-parameterisation variants, combined with two parameterisation variants for the tunnel-wall rock mass. A reality-check is also provided by comparing simulated inflow to the existing facility (SFR1) against measured inflow. The measured inflow to SFR1 has declined continuously since its earliest control-programme measurements in June 1988 (Figure C-1); the simulated inflow to SFR3 represent the early inflow.

The simulated inflow is differentiated per:

- Disposal room (11).
- Drainage basin (4).

These simulations reflect the operative period of SFR (i.e. c. 100 years, prior to repository closure). An atmospheric pressure is therefore assumed for the open tunnel system (i.e. H(z) = z m), combined with the present shoreline (i.e. 2000 AD, $z_{sea} = -0.17$ m). During this operative phase, the tunnel inflow is assumed be decreased by grouting efficiency II, i.e. corresponding to a flow resistance in the tunnel wall modelled as a threshold for hydraulic conductivity: $K_{tunnel\ wall} = (K_{ECPM}, 10^{-8}\ m/s)_{min}$. The grouting material is not assumed to be persistent over the time scales addressed in long-term safety assessment (on the order of hundreds or thousands of years after repository closure), and therefore grouting is not normally accounted for in SR-PSU modelling.

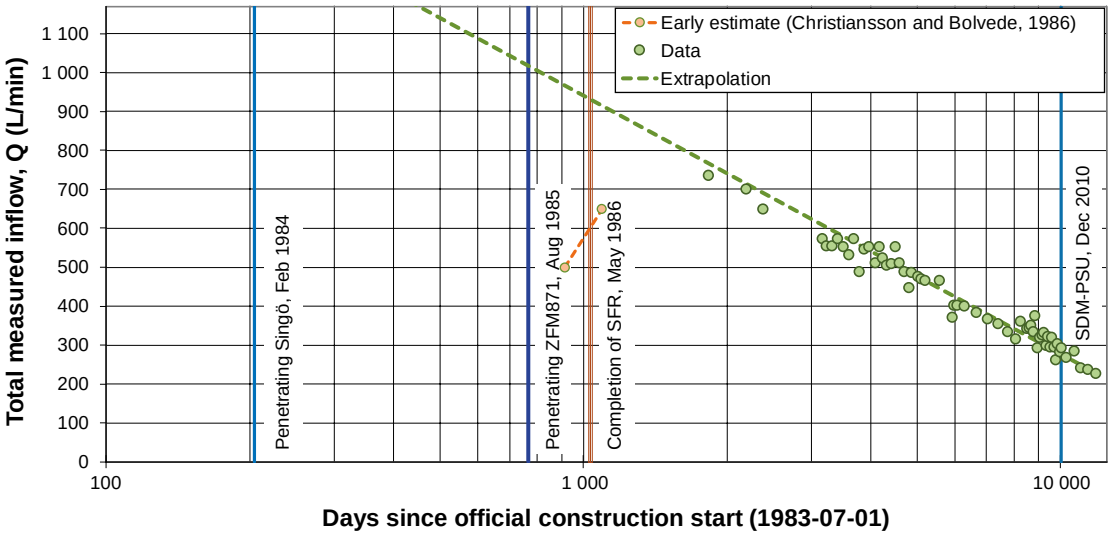

Figure C-1. *Declining inflow to drainage basins 1ÖDB and 1NDB since the start of the control programme for SFR1 in June 1988.*

C1 Background and model setup

To cover uncertainties in model parameterisation, the three bedrock parameterisation variants 1, 11, and 18 (Table 2-2) are employed in the simulations, as they are considered to span a realistic range of tunnel flow (Table C-1). Two variants are considered for the parameterisation of tunnel walls, referred to as K_{ECPM} and K_{Skin} (Table C-1). Here, K_{ECPM} refers to the undisturbed rock-mass properties, while K_{Skin} refers to a flow resistance in the bedrock closest to the tunnel wall (i.e. a rock-mass thickness of 2 m). This flow resistance primarily refers to the reduction in hydraulic conductivity achieved by grouting efforts, but it may also include natural sealing phenomena (i.e. discussed in Öhman et al. 2013). The skin is implemented as a maximum value for hydraulic conductivity of the tunnel wall (i.e. the tunnel-wall conductivity is not modified where K_{ECPM} is lower than K_{skin}).

A constant tunnel-wall skin, $K_{skin} = 10^{-8}$ m/s, is assumed for the entire SFR3, which corresponds to grouting-efficiency level II (e.g. Svensson and Follin 2010). The tunnel-wall skin for SFR1 is differentiated per deformation-zone intercept, based on the SDM-PSU calibration to match the measured inflow in 2010 (Öhman et al. 2013). The SDM-PSU calibration was made for an assumed constant rock-mass conductivity, $K_{HRD} = 6.5 \times 10^{-9}$ m/s, and to match the inflow per 2010. In this study the bedrock (HRD) parameterisation is based on stochastic DFN simulations, and therefore the inflow data may not necessarily be reproduced. Moreover, it should be noted that the SFR1 inflow has continued to decrease since 2010, which can be interpreted as either

1. the hydrogeological system is slow and is still in a transient state,
2. the flow resistance in the tunnel wall is non-static.

ZFM871 was extensively grouted in the area around its 1NDB intercept. This is modelled as a modest flow resistance, $K_{skin} = 1.3 \times 10^{-7}$ m/s, but applied over a larger rock volume (i.e. within a cylinder of 55 m radius; Figure C-2).

Table C-1. Model setups in open-tunnel inflow simulations.

Bedrock parameterisation variant			**Representing (see Öhman et al. 2014)**
nc_NoD_R01_DFN_R18			Low tunnel flow
BASE_CASE1_DFN_R85			Base case
nc_DEP_R07_DFN_R85			High tunnel flow
Tunnel-wall parameterisation variants			
ECPM	Non-disturbed hydraulic bedrock properties (Equivalent Continuum Porous Media), as upscaled from its underlying bedrock case (fracture-network and deformation-zone data).		
Skin	**SFR1**	$K_{skin} = 1.04 \times 10^{-8}$	Southern boundary belt[1)]
		$K_{skin} = 4.55 \times 10^{-9}$	ZFMWNW1035, ZFMNNE0869, ZFMNE0870, ZFMNE3118, ZFNNW1209
		$K_{skin} = 1.3 \times 10^{-7}$	ZFM871[2)]
		$K_{skin} = 10^{-10}$	Silo
		$K_{skin} = 6.5 \times 10^{-10}$	HRD (rock mass outside deformation-zone intercepts).
	SFR3	$K_{skin} = 10^{-8}$ m/s[3)]	Entire SFR3 (i.e. irrespectively if deformation-zone intercept, or not).

[1)] The southern geologic deformation-zone belt in defined in SDM-PSU (ZFMWNW0001, ZFMWNW3259, ZFMWNW0813, ZFMNW0002, and ZFMWNW1035).

[2)] Not applied over a 2 m thickness of the tunnel wall, but over a 55 m radius (as illustrated by pink cylinder in Figure C-2).

[3)] Grouting-efficiency level II in Svensson and Follin (2010).

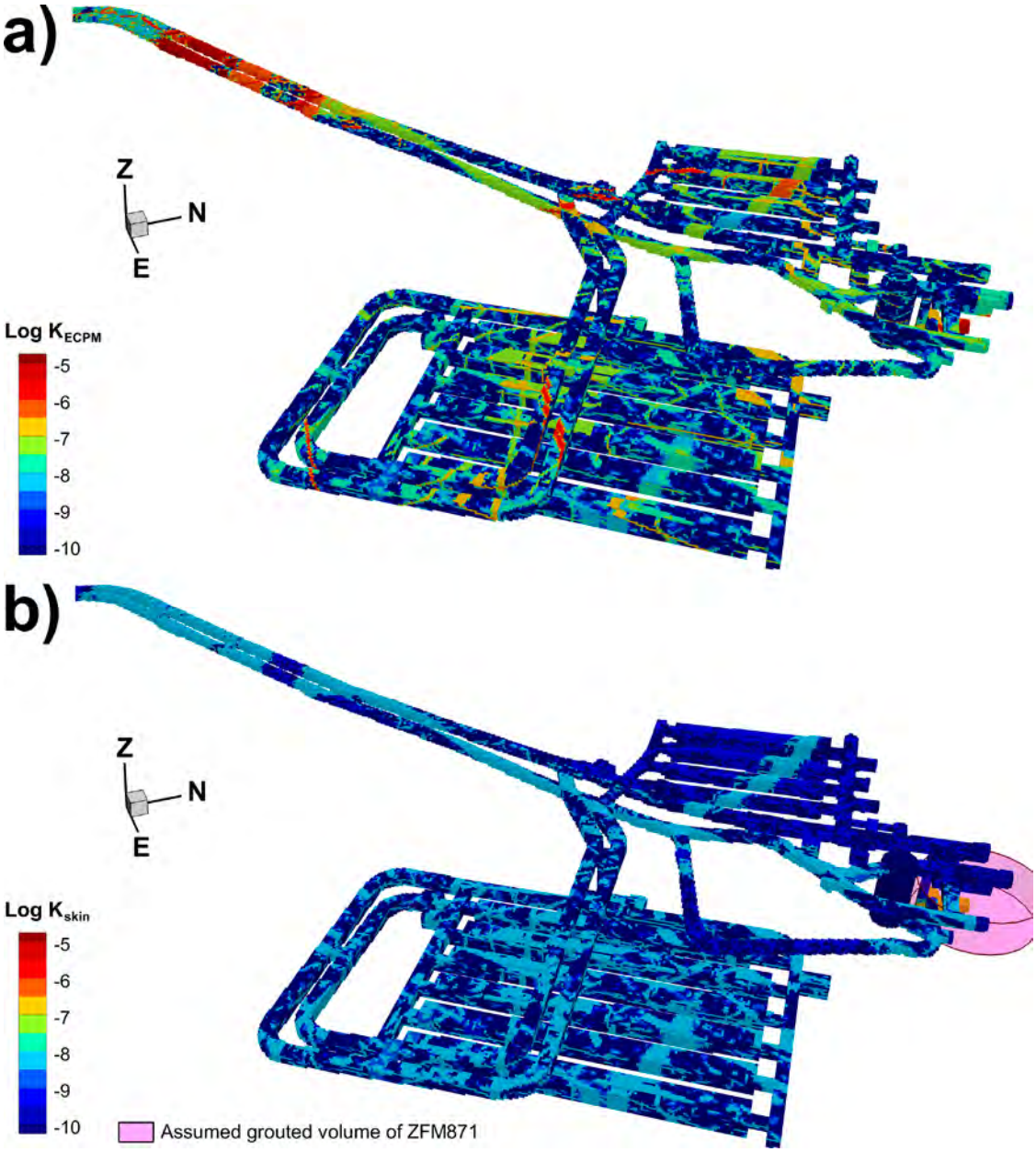

Figure C-2. *Tunnel-wall conductivity in the base-case setup; a) no skin (K_{ECPM}), and b) modelled flow resistance (K_{skin}, which is deformation-zone specific for SFR1, and generalized for SFR3, $K_{skin} = 10^{-8}$ m/s). The grouting of ZFM871 is modelled as a maximum conductivity of 1.3×10^{-7} m/s within a 55 m radius of its 1NDB-intercept (pink cylinder).*

Differentiation of the tunnel system per drainage areas

The inflow to the existing facility is pumped from an upper and a lower basin: 1ÖDB (*Swe*: Övre DränageBassäng) and 1NDB (*Swe*: Nedre DränageBassäng); another pair of pumping pits is planned for SFR3: 2NDB and 3NDB. Based on a conceptual sketch of the planned drainage design (Figure C-3), the implemented tunnel geometry in the DarcyTools grid is differentiated in terms of corresponding drainage areas (Figure C-4 and Table C-2).

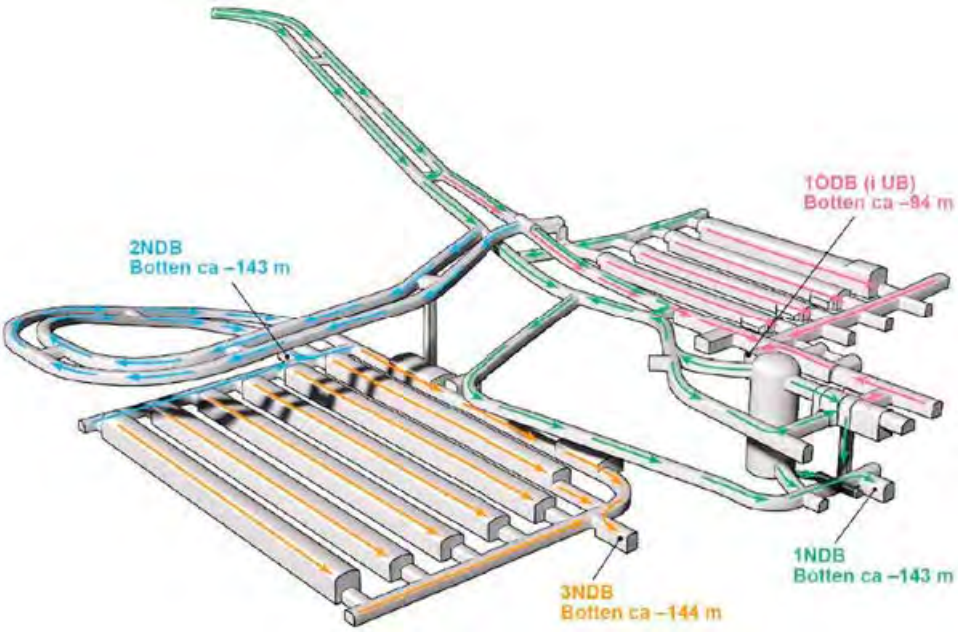

Figure C-3. *Designed drainage of the tunnel system (coloured by drainage basin).*

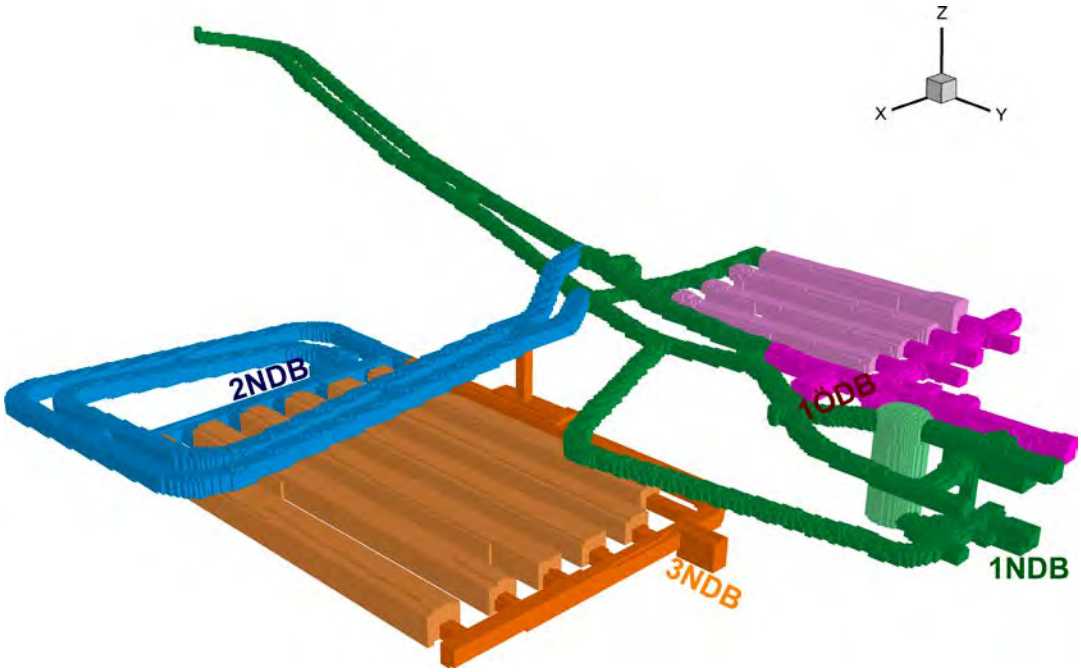

Figure C-4. *Discretised tunnel system in simulations, differentiated by drainage to the four basins 1ÖDB, 1NDB, 2NDB, and 3NDB (coloured by drainage basin; c.f. Figure C-3).*

Table C-2. Differentiation of the tunnel system in simulations (c.f. Figure C-4).

Drainage basin	Colour	Tunnel unit	DarcyTools ID
1ÖDB	Pale pink	1BTF	11
		2BTF	12
		1BLA	13
		1BMA	14
	Pink	Tributary 1ÖDB (1BST, 1DT)	30
1NDB	Pale green	Silo	15
	Green	Tributary, 1NDB (1BT, 1DT, NDB, IB, 1TT)	31
2NDB	Blue	Tributary, 2NDB (2BT, 2DT, 2TT)	32
3NDB	Pale orange	2BLA	22
		3BLA	23
		4BLA	24
		5BLA	25
		2BMA	26
		1BRT	27
	Orange	Tributary, 3NDB (TIT, 4VB, 5VB, 3FS)	33

C2 Results

The simulated inflow to 1ÖDB ranges from 38 to 55 L/min, if skin is assumed, which compares well to the measured inflow 48.8 L/min in 2010 (Table C-3). The simulated inflow to 1NDB, on the other hand ranges from 424 to 492 L/min, which is about twice the measured inflow in 2010 (237.6 L/min). It should, however, be noted that the skins were not calibrated for stochastic DFN realisations or variants of the HCD parameterisation.

Grouting is modelled as an upper threshold in hydraulic conductivity of the tunnel wall, and as such, the largest effect of grouting is found at the points of largest inflow, whereas it leaves the background inflow more or less unaffected. The highest inflows are associated to the deformation-zone intercepts of the ramp with the Southern boundary belt (ZFMWNW0001, ZFMWNW3259, ZFMWNW0813, ZFMNW0002, and ZFMWNW1035) and the ZFM871 intercept in 1NDB (Figure C-5). The grouting effects are manifested as a reduction in inflow at the highest inflow anomalies (c.f. Figure C-5a and b).

As a rough average, grouting reduces the simulated inflow by c. 25–75 % (Table C-3). In the current design of SFR3, the transport tunnels are connected to the existing ramp for SFR1 (se description of layout L2.6 in Section 3.2). As SFR3 does not require a separate ramp for direct ground access (through the Singö deformation zone), its simulated inflow is considerably lower (c. 70 %) than that to the existing facility.

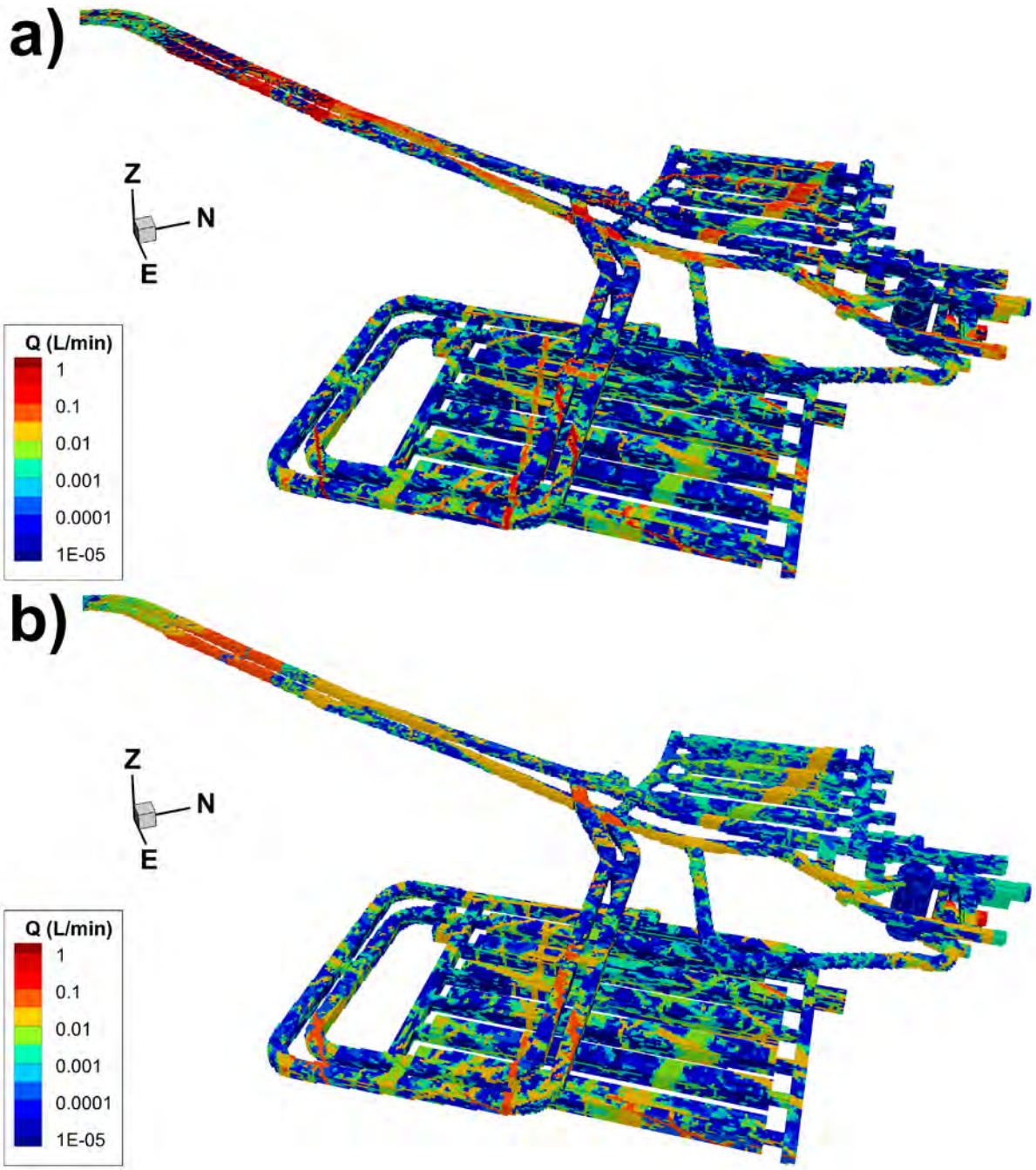

Figure C-5. *Simulated inflow for the base-case setup; a) no skin (K_{ECPM}), and b) modelled flow resistance (K_{skin}, which is deformation-zone specific for SFR1, and generalized for SFR3, $K_{skin} = 10^{-8}$ m/s).*

Table C-3. Simulated inflow to the tunnel system, differentiated per drainage area (L/min).

Drainage area	nc_NoD_R01_DFN_R18		BASE_CASE1_DFN_R85		nc_DEP_R07_DFN_R85	
	Q_{ECPM}	Q_{Skin}	Q_{ECPM}	Q_{Skin}	Q_{ECPM}	Q_{Skin}
1BTF	9.5	6.0	4.4	3.4	9.5	6.8
2BTF	11.2	6.7	14.6	8.8	23.2	10.1
1BLA	14.8	8.4	47.1	14.2	45.5	15.7
1BMA	24.6	10.9	18.6	10.7	65.7	14.9
Tributary, 1ÖDB	35.3	5.9	15.7	7.5	17.8	7.1
Total 1ÖDB[1)]	**95**	**38**	**100**	**45**	**162**	**55**
Silo	3.4	0.6	3.9	0.6	4.7	0.6
Tributary, 1NDB	1 327	423	1 996	491	1 870	468
Total 1NDB[2)]	**1 331**	**424**	**2 000**	**492**	**1 875**	**469**
Tributary, 2NDB	110	86	217	140	256	151
Total 2NDB	**110**	**86**	**217**	**140**	**256**	**151**
2BLA	11.3	10.3	13.3	12.8	14.4	16.1
3BLA	11.0	11.4	14.9	14.8	22.8	25.6
4BLA	14.1	14.4	13.2	13.8	32.4	31.7
5BLA	16.7	17.3	10.5	11.8	37.8	32.2
2BMA	39.3	32.4	37.8	29.9	220.3	75.4
1BRT	7.8	8.1	12.1	11.6	19.4	17.8
Tributary, 3NDB	21.8	21.8	34.4	33.7	31.4	33.2
Total 3NDB	**122**	**116**	**136**	**128**	**378**	**232**
Total: SFR1	**1 426**	**462**	**2 100**	**537**	**2 037**	**524**
Total: SFR3	**232**	**202**	**353**	**268**	**634**	**383**

[1)] Q_{skin} can be compared to the measured inflow in 2010: $Q_{1ÖDB}$ = 48.8 ±1 L/min.

[2)] Q_{skin} can be compared to the measured inflow in 2010: Q_{1NDB} = 237.6 ±10 L/min.

The simulated total inflow to 1ÖDB, Q_{skin} = 38 to 55 L/min, agrees well with the corresponding to the measured inflow in 2010 ($Q_{1ÖDB}$ = 48.8 L/min). For individual disposal rooms in SFR1, the simulated inflow, Q_{skin}, is a factor 2–4 higher than that measured in 2010 (Figure C-6). The simulated inflow to the silo agrees well with recorded data in 2010 (Q_{silo} = 0.5 ± 0.1 L/min).

The calculated inflows to SFR3 exhibit a comparatively smaller difference between non-disturbed bedrock, Q_{ECPM}, and the grouted case, Q_{skin} (Table C-3 and Figure C-6). One reason for this is the difference in parameterisation of skin, where SFR1 is based on an inflow calibration, while a grouting standard for SFR3. Notably, the simulated inflow to 2BMA ranges almost an order of magnitude, from 30 L/min (base case, with skin) to 220 L/min (for the non-conditioned heterogeneous HCD realisation R07), which signifies the uncertainty related to the parameterisation of deformation zone ZFMWNW0835. The inflow to disposal rooms and their relative contribution to the total inflow to the drainage basins is illustrated by stacked histogram bars (Figure C-7).

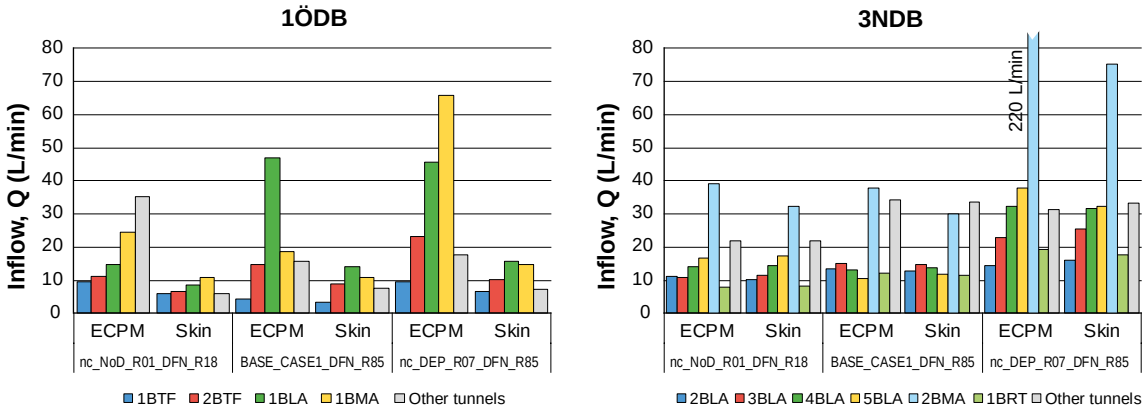

Figure C-6. *Simulated inflow to disposal rooms and the tributaries of 1ÖDB/3NDB; a) in SFR1, and b) in SFR3. Inflow for non-disturbed tunnel-wall bedrock, Q_{ECPM}, compared to that for grouted tunnel properties, Q_{skin}.*

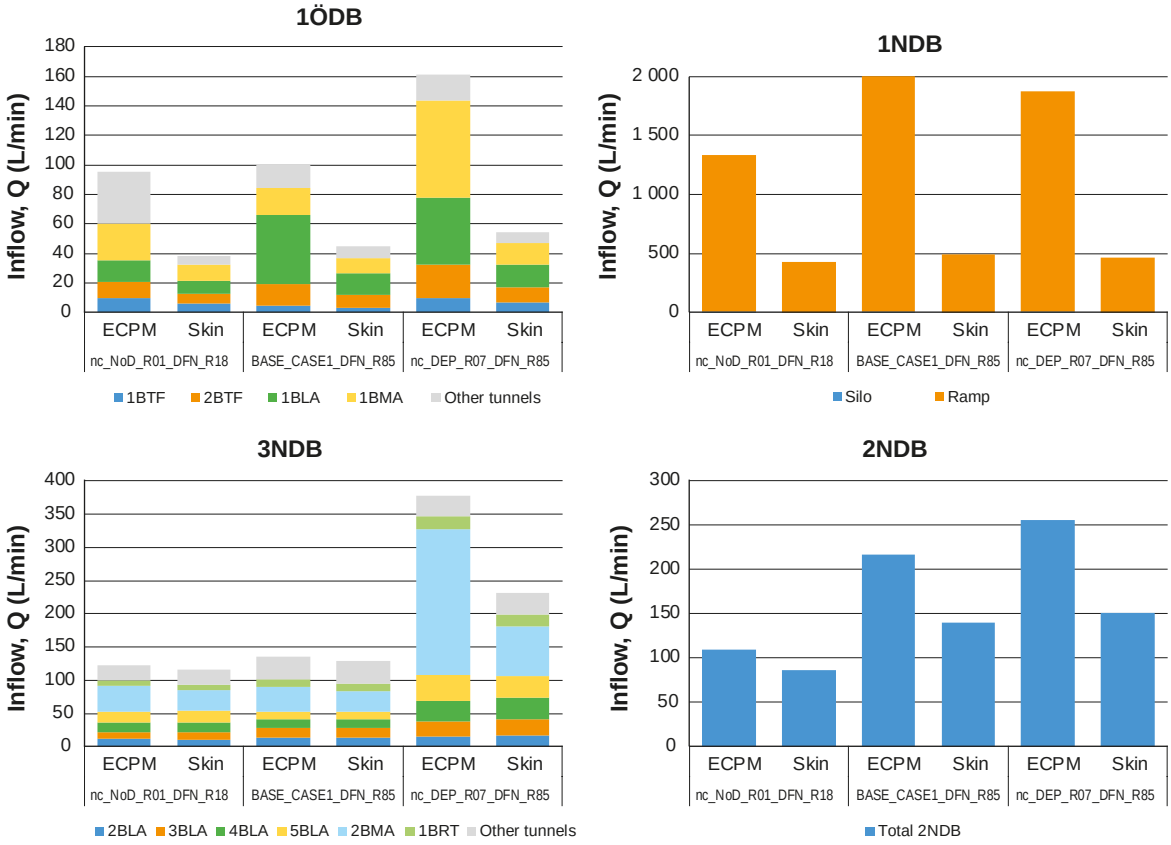

Figure C-7. *Simulated inflow to the four drainage basins; the relative contribution from disposal rooms shown by stacked histogram bars.*

Appendix D

Data controlling ground-surface conditions

The data controlling ground-surface conditions in flow simulations (Öhman et al. 2014) were provided from RLDM modelling per 500 year intervals (Brydsten and Strömgren 2013). This appendix describes the data preparations and data-consistency checks that were executed at the onset of this study.

D1 Early time slices

Preceding flow simulations in SR-PSU (e.g. Öhman et al. 2014) demonstrate that the transient hydrogeological setting of SFR undergoes its most abrupt changes during the early stages of land uplift (i.e. the first 500 years, or so). To better resolve this early development of shore-line retreat, three additional time slices: 2100 AD, 2250 AD, and 2750 AD, have been introduced to the current sensitivity analysis (Figure D-1). Inclusion of these time slices in flow simulations requires the following preparation/modification of input data:

- Relative sea-level displacement: the driving potential in the hydrogeological setting of SFR is determined by the groundwater level relative to the sea level. This potential increases over time due to the ongoing land uplift, which is modelled as relative lowering of the sea level (see main report, Section 3.3.2). The relative sea levels for 2100 AD, 2250 AD, and 2750 AD are interpolated from the time slices that are provided per 500-year in RLDM (Figure D-1; Table 3-2). In simulations, the relative sea-level displacement is hard coded in [SR PSU_TD18_DTS_RECHARGE.f] and [SR-PSU_TD18_DTS_Steady_state.f].
- River system: Head is prescribed along the river trajectories provided from RLDM. With the retreating shoreline, the river system grows over time and its level may be somewhat affected by erosion and sedimentation (i.e. which affects the prescribed head values). In essence, SFR is submerged the first 1 000–2 000 years, and thus, the changes to the river system are negligible during the early time slices. The river trajectories for 2100 AD, 2250 AD, and 2750 AD are terminated against the retreating shoreline, and their head values are interpolated from the time slices used in TD11 (stored in the file [SR-PSU_TD18_River_head.in]).
- Lake evolution: Lake objects are provided per 500 year from RLDM. No new lake objects are introduced for the intermediate time slices; instead, they are taken from the modelled sequence of lake succession (new lakes forming above sea level and removal of choked-up lakes), based on the modelled lake levels relative to the sea level (see Figure D-2 and Table D-1).
- HSD thickness: HSD layers are provided every 500 years from RLDM, which means that the HSD thickness must be interpolated for the three intermediate time slices, 2100 AD, 2250 AD, and 2750 AD. However, these time slices span a relatively short time period during which the changes in HSD thickness are relatively small (i.e. typically less than 0.1 m; Figure D-3).
- Basin-filled DEM: The DEM is used in the mixed-boundary condition to control the maximum simulated head at ground surface. However, during this early period, the topographical changes (i.e. above sea level) are very small (Figure D-3), compared to the significance of the relative shoreline displacement (Figure D-1). All basin-filled DEMs are checked for consistency with the lake/river systems (Figure D-4 to Figure D-12).

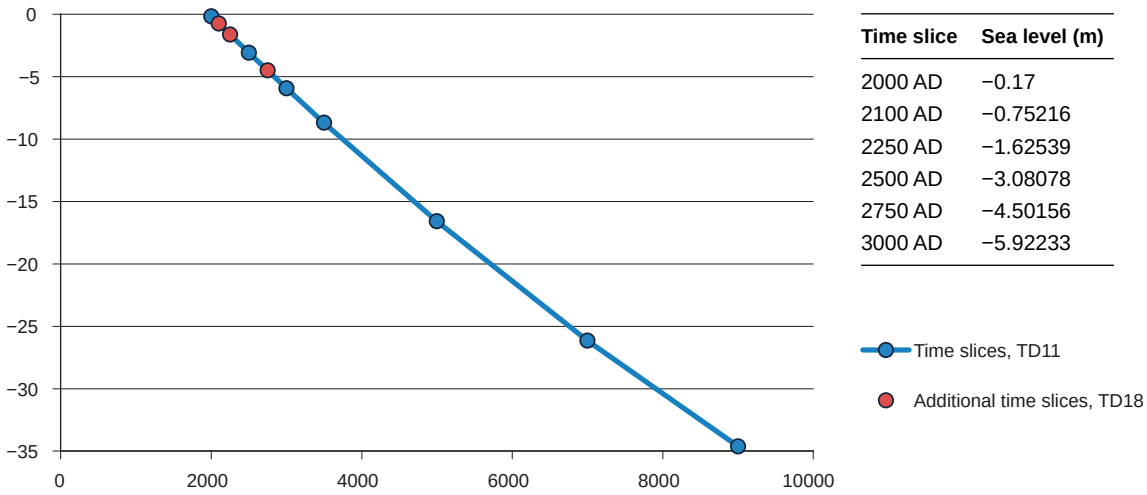

Figure D-1. *Relative sea-level displacement in the fixed-bedrock reference.*

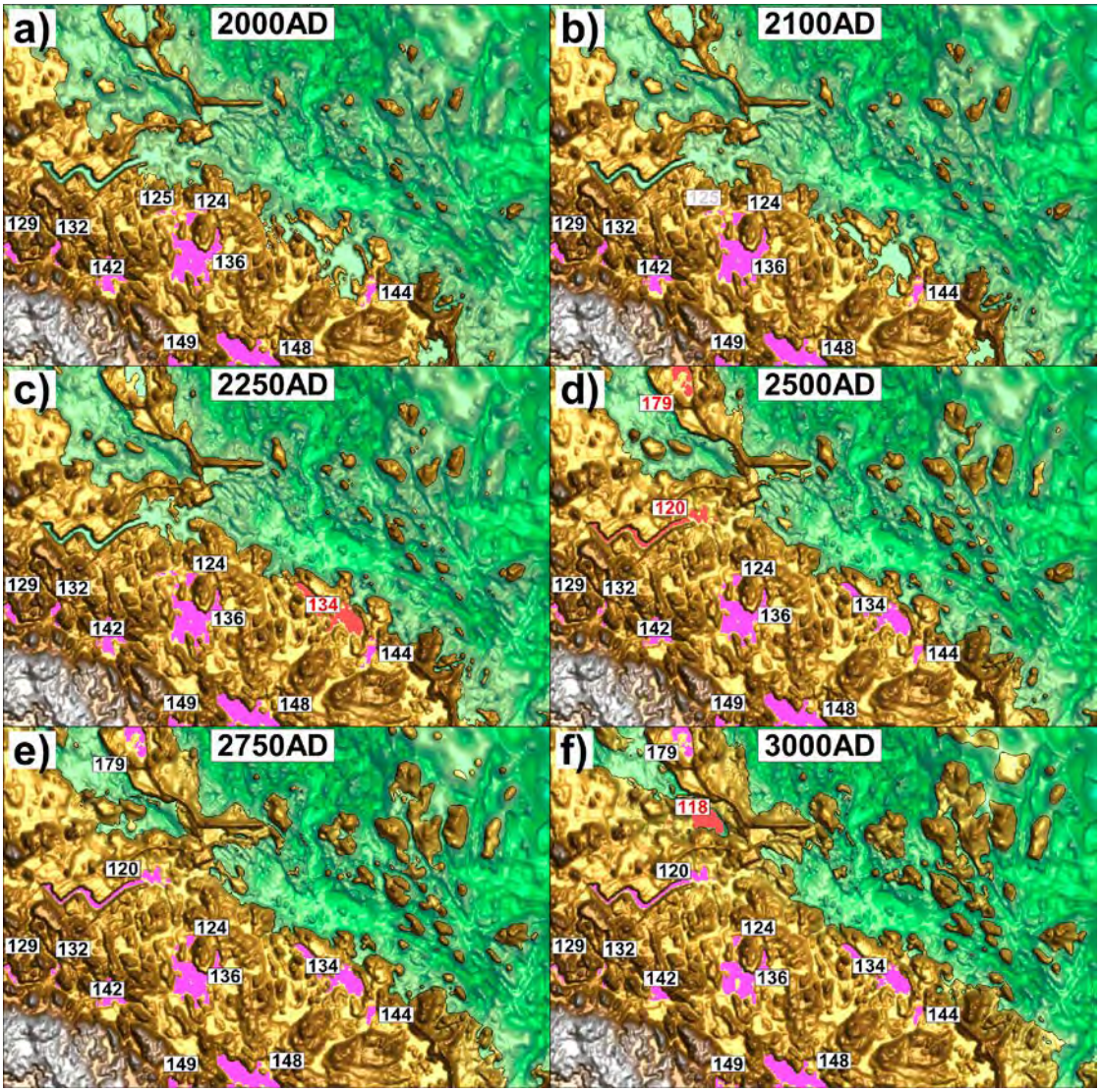

Figure D-2. *Interpreted existence of lakes over the early stages of shoreline retreat (c.f. Table D-1). Newly formed lakes in red and choked-up lakes in grey.*

Table D-1. Interpreted existence of lakes over time, based on shoreline retreat (Y/N).

Lake ID	Level	2000 AD −0.17	2100 AD −0.752	2250 AD −1.625	2500 AD −3.081	2750 AD −4.502	3000 AD −5.922
118	−5.13	N	N	N	N	N	Y
120	−2.6	N	N	N	Y	Y	Y
124	0.48	Y	Y	Y	Y	Y	Y
125	0.4	Y	N	N	N	N	N
129	5.82	Y	Y	Y	Y	Y	Y
132	3.66	Y	Y	Y	Y	Y	Y
134	−1.35	N	N	Y	Y	Y	Y
136	0.42	Y	Y	Y	Y	Y	Y
142	1.82	Y	Y	Y	Y	Y	Y
144	0.41	Y	Y	Y	Y	Y	Y
148	0.56	Y	Y	Y	Y	Y	Y
149	5.32	Y	Y	Y	Y	Y	Y
176	−4.95	N	N	N	N	N	Y
179[1)]	−1.67	N	N	N	Y	Y	Y

[1)] Bio-test lake defined from 2000 AD in RLDM. Modelled as sea-level until 2500 AD in flow simulations.

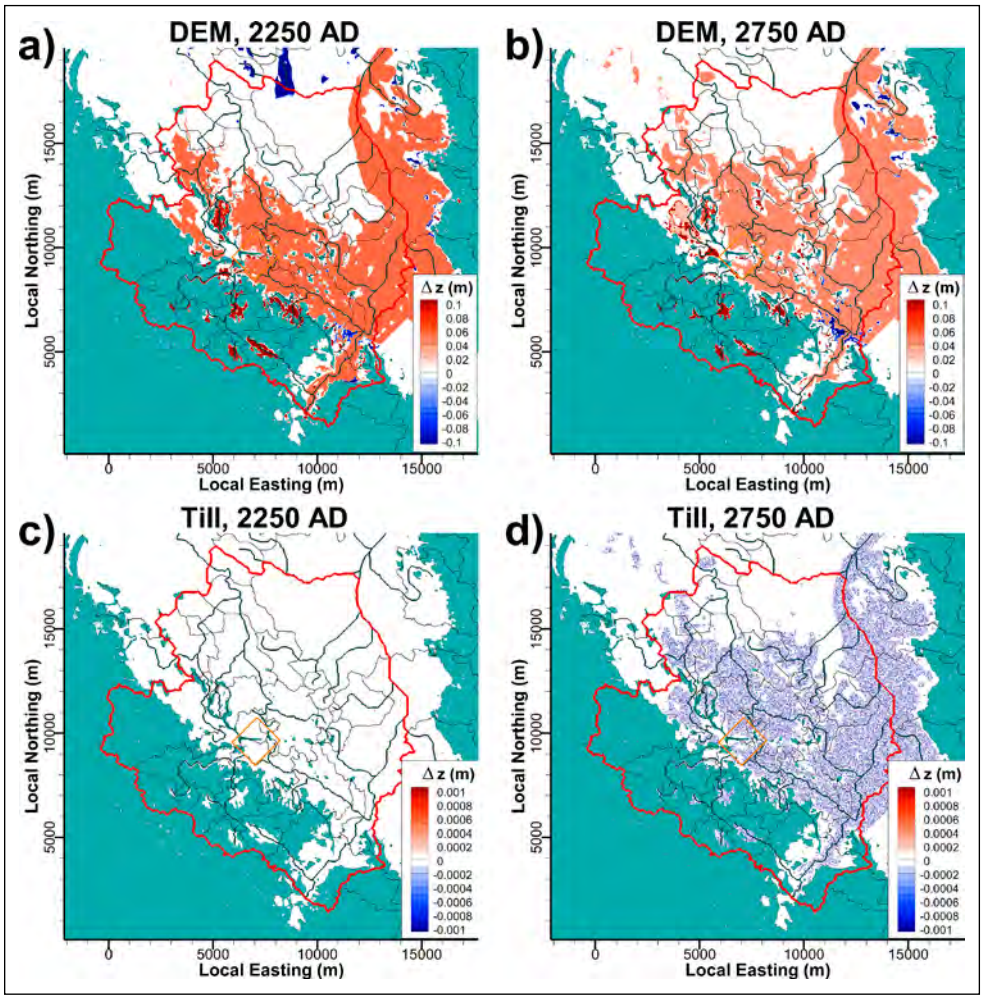

Figure D-3. *Visual inspection of regolith-layer interpolation for early time slices, expressed as change Δz (m) relative to preceding time slice. Lacustrine/marine accumulation increases total HSD thickness (red contoured), whereas local erosion of glacial clay decreases the HSD thickness (blue contoured). The underlying layers, fill, glaciofluvial, till, and bedrock are static (only millimetre-scale round-off errors, contoured in blue).*

D2 Consistency check of data controlling ground-surface

All basin-filled DEMs are checked for consistency with the lake/river systems (Figure D-4 to Figure D-12). This is done by tracing surface runoff by means of balls dropped uniformly over the basin-filled DEMs (all nine time slices). The balls will roll along the topographical gradient, downhills towards the coast line. The balls are expected to reach a water object: rivers, lakes or the sea. Data inconsistencies are identified by trapped balls that do not reach a water object (i.e. river/lake/coast). The following inconsistencies were made identified and corrected (judged to have a minor impact)

- To resolve small topographical gradients, the precision of DEM data is increased from centimetres to millimetres.
- The river system 2000 AD is extended slightly to reach the cooling-water canal (Figure D-4).
- The river system at 2500 AD is extended slightly to adjoin the cooling-water canal to the sea (Figure D-7).
- The river system is extended to adjoin lakes 107 and 156, at 3500 AD (Figure D-10).
- A “topographical hole” is identified between peripheral lake 149 and sea. The hole is filled to remove an artificial sink at 9000 AD.
- the Bio-test lake is modelled as z = 0 m at 2000 AD in RLDM (Figure D-4). To simplify DarcyTools simulations, the Bio-test lake is not included before its lake level exceeds the sea level, which occurs after 2250 AD (Table D-1). For all time slices prior to 2500 AD, the Bio-test lake is modelled as part of the sea.
- By 9000 AD, the Bio-test lake has choked up in RLDM (Figure D-12), and hence its surface boundary condition per automatic should become defined by its basin threshold (i.e. its basin-filled level, z = 0.43 m). However, this is not very realistic as the Bio-test area is enclosed by rock-blast material. Instead, its surface boundary condition is re-set to the non-filled DEM inside the Bio-test area (i.e. original pdem delivered by RLDM, c. −1.4 m, which is just above the modelled lake level of object 179, z = −1.67 m in Table D-1).

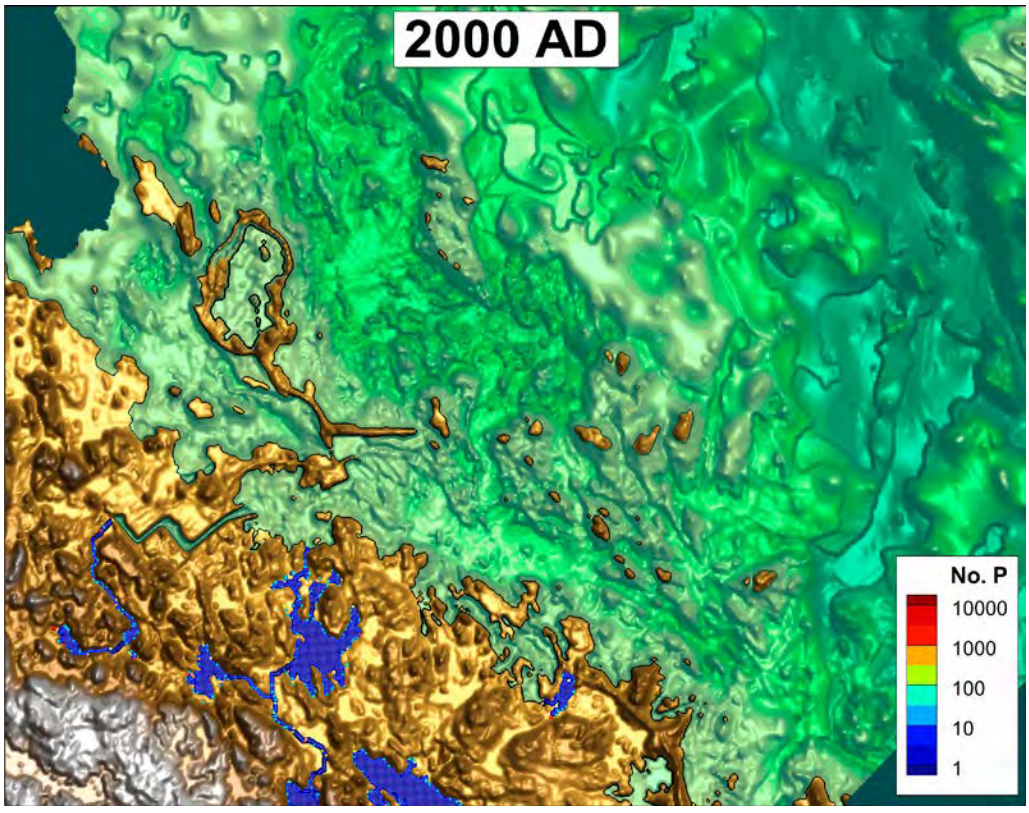

Figure D-4. *Consistency-check of basin-filled DEM, 2000 AD; balls uniformly released over land rolls along the topographical gradient to reach rivers or lakes (density of termination points contoured).*

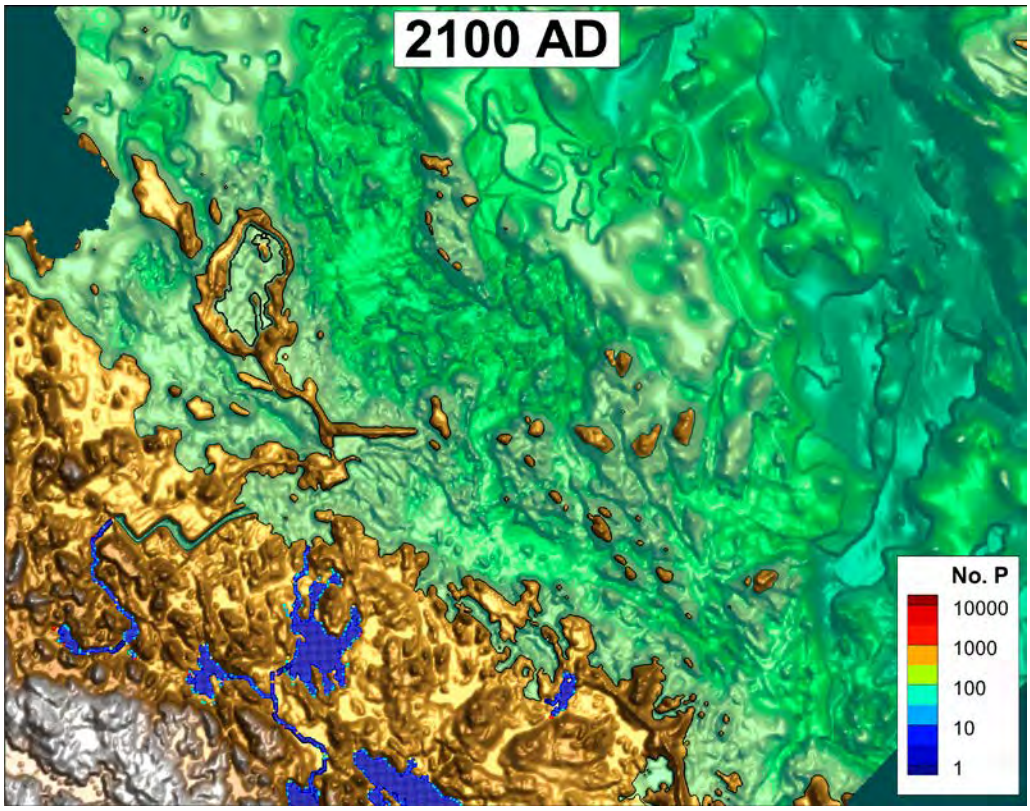

Figure D-5. *Consistency-check of basin-filled DEM, 2100 AD; balls uniformly released over land rolls along the topographical gradient to reach rivers or lakes (density of termination points contoured).*

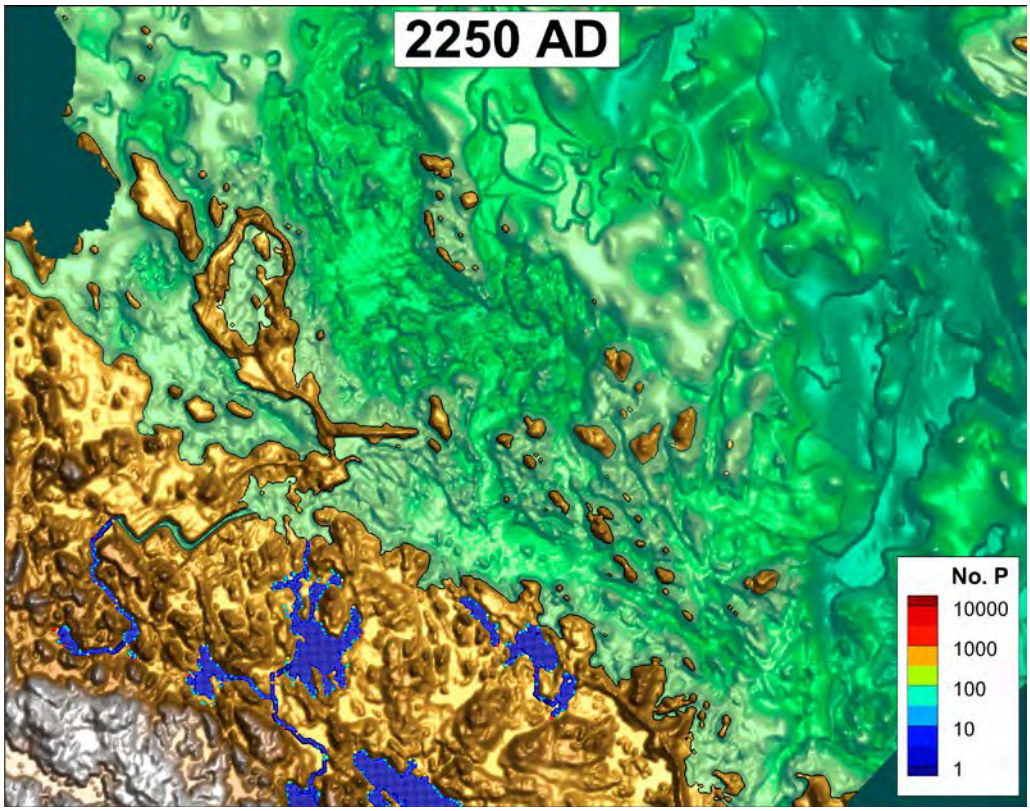

Figure D-6. *Consistency-check of basin-filled DEM, 2250 AD; balls uniformly released over land rolls along the topographical gradient to reach rivers or lakes (density of termination points contoured).*

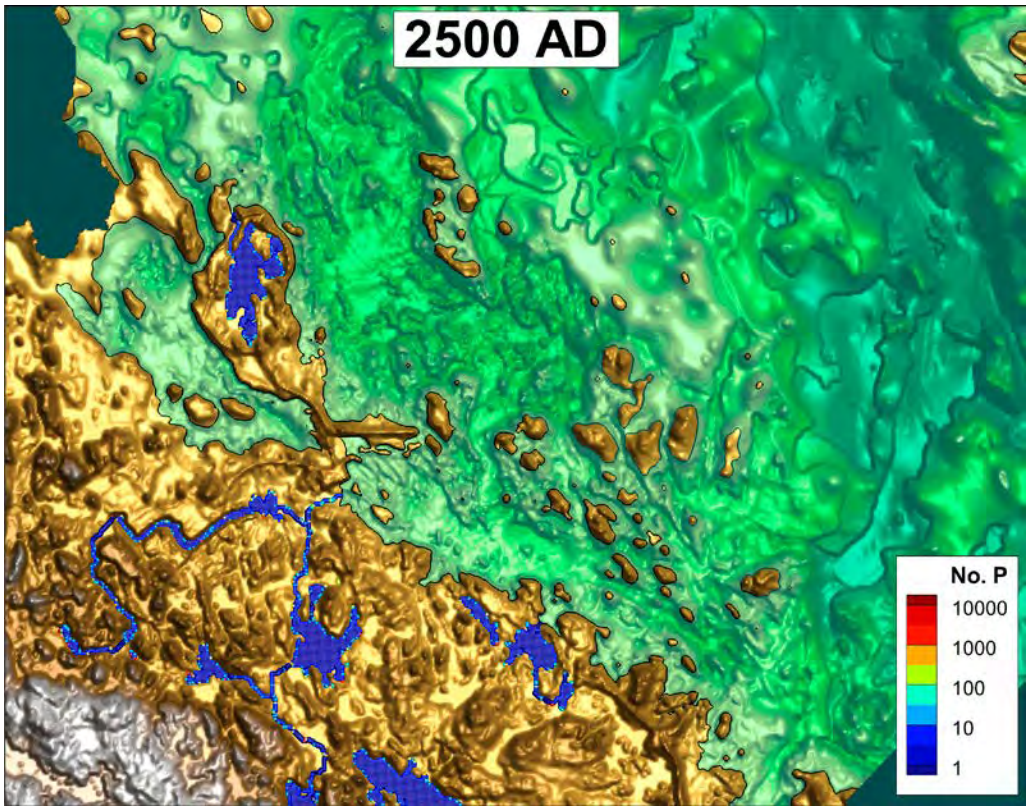

Figure D-7. *Consistency-check of basin-filled DEM, 2500 AD; balls uniformly released over land rolls along the topographical gradient to reach rivers or lakes (density of termination points contoured).*

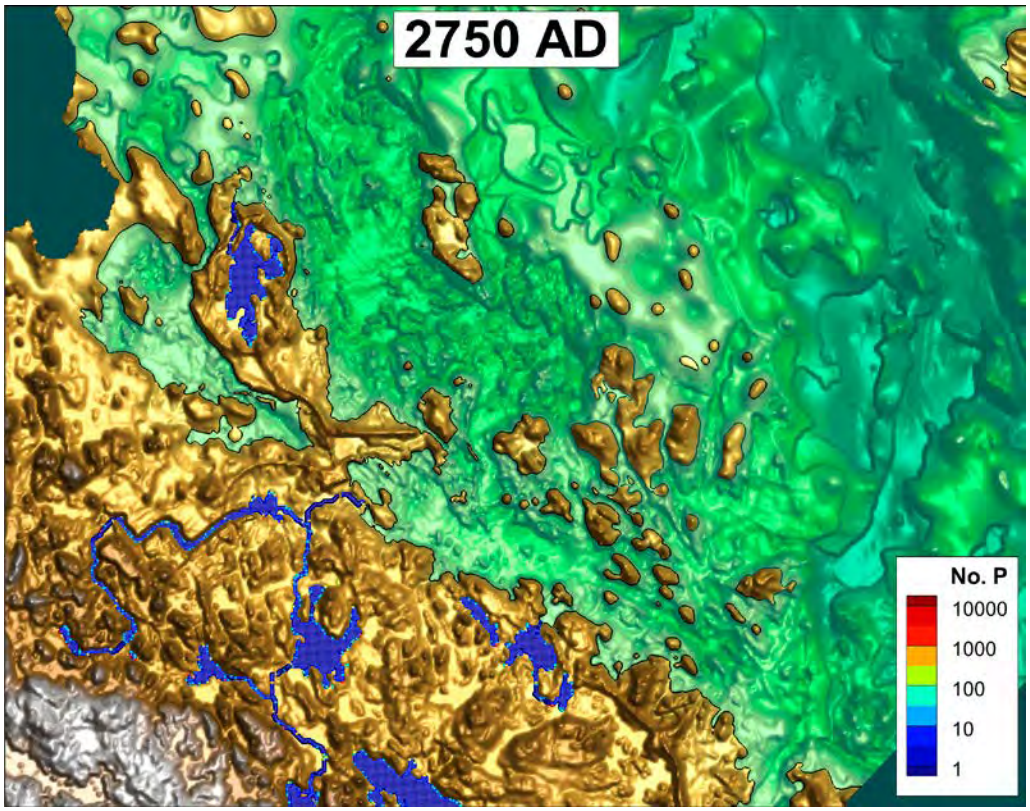

Figure D-8. *Consistency-check of basin-filled DEM, 2750 AD; balls uniformly released over land rolls along the topographical gradient to reach rivers or lakes (density of termination points contoured).*

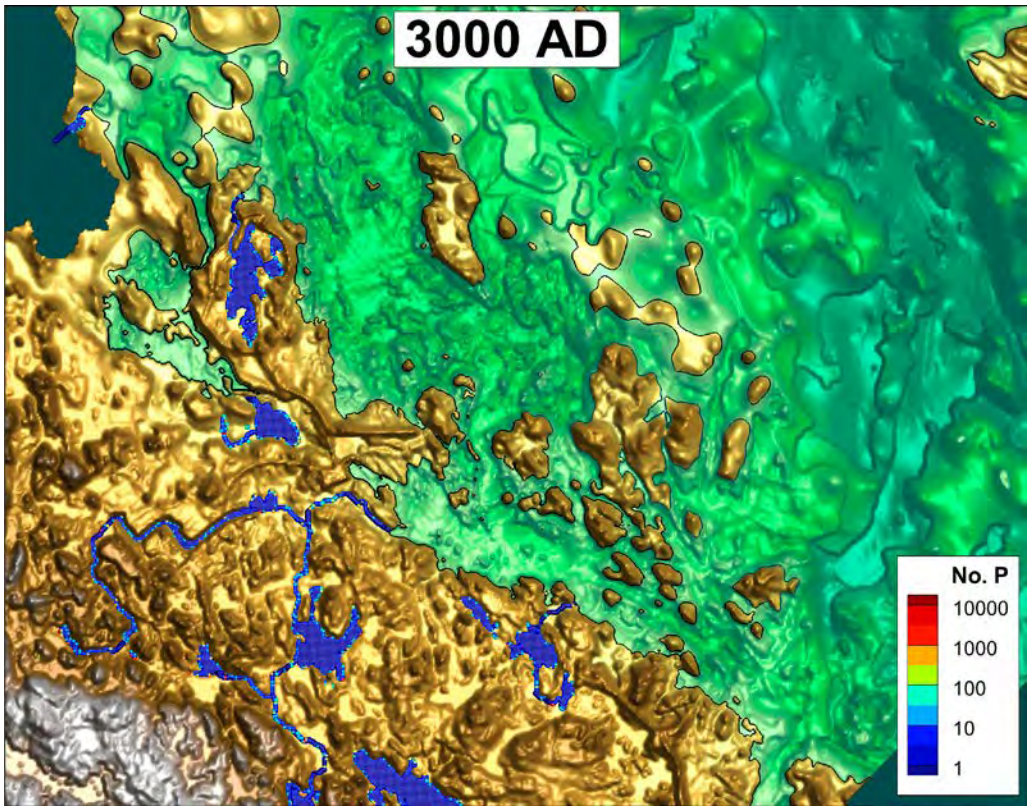

Figure D-9. *Consistency-check of basin-filled DEM, 3000 AD; balls uniformly released over land rolls along the topographical gradient to reach rivers or lakes (density of termination points contoured).*

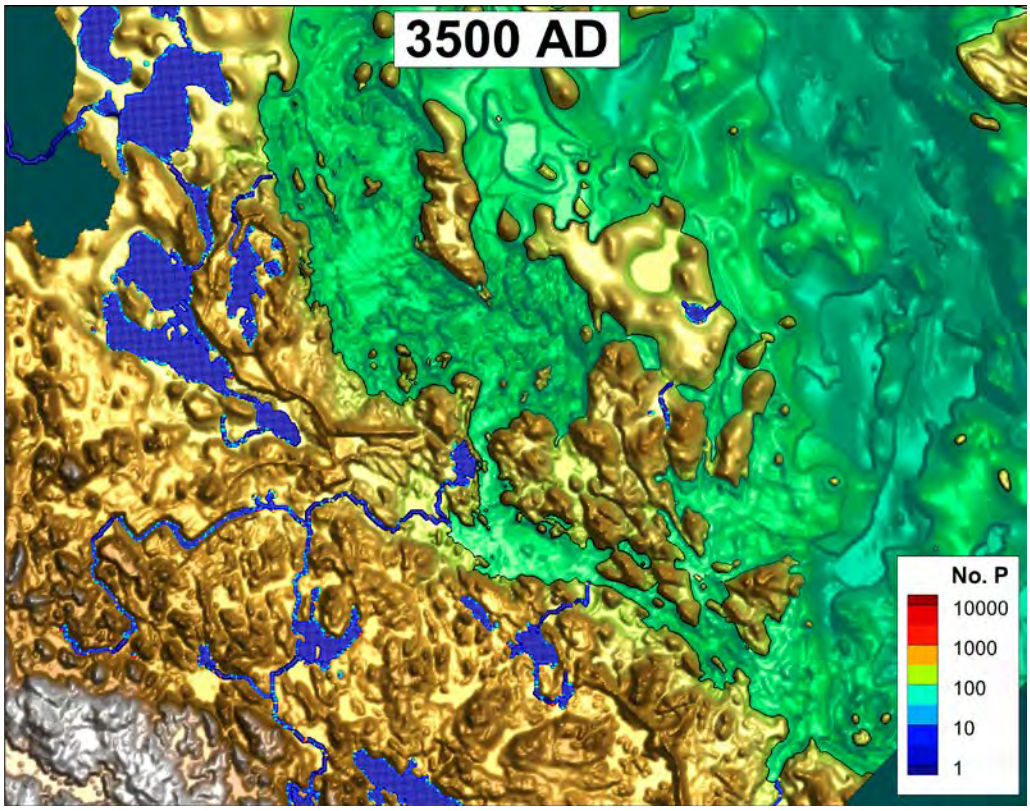

Figure D-10. *Consistency-check of basin-filled DEM, 3500 AD; balls uniformly released over land rolls along the topographical gradient to reach rivers or lakes (density of termination points contoured).*

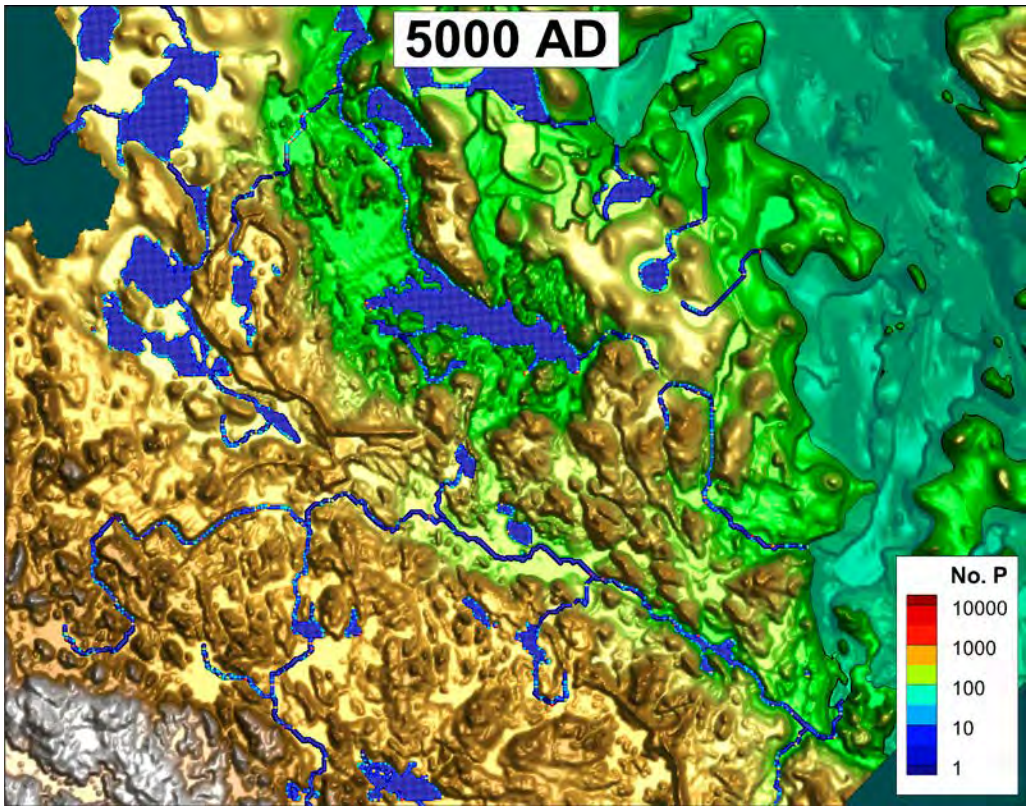

Figure D-11. *Consistency-check of basin-filled DEM, 5000 AD; balls uniformly released over land rolls along the topographical gradient to reach rivers or lakes (density of termination points contoured).*

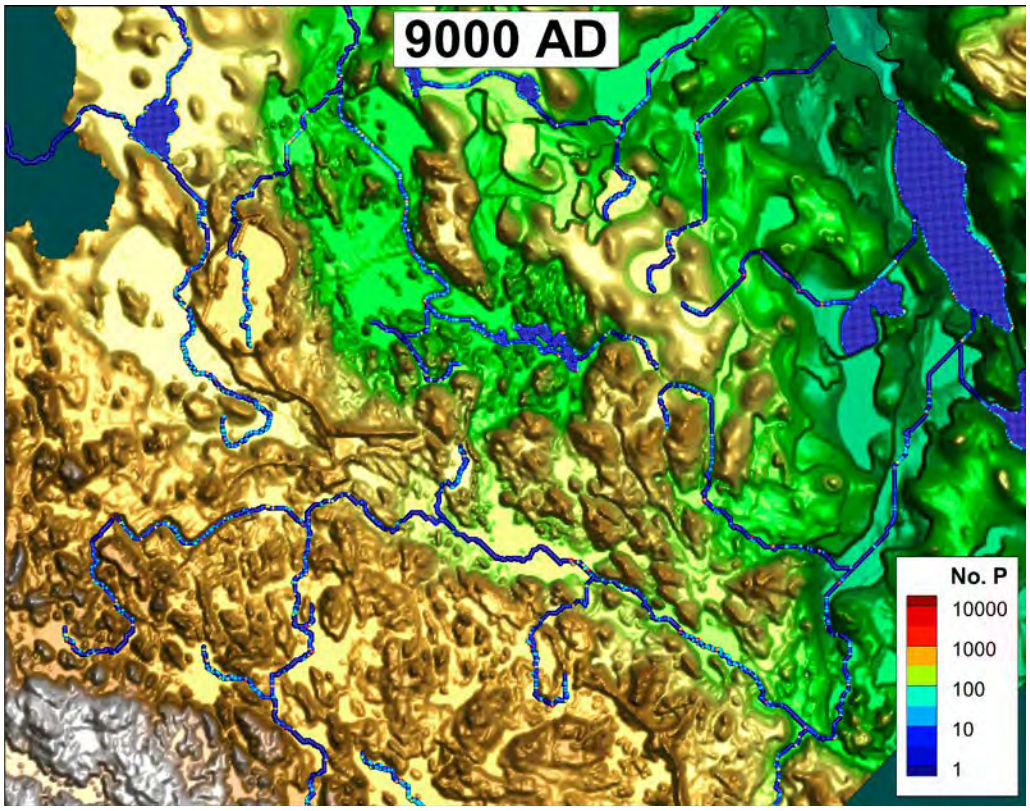

Figure D-12. *Consistency-check of basin-filled DEM, 9000 AD; balls uniformly released over land rolls along the topographical gradient to reach rivers or lakes (density of termination points contoured).*

Arkitektkopia AB, Bromma, 2018

SKB is responsible for managing spent nuclear fuel and radioactive waste produced by the Swedish nuclear power plants such that man and the environment are protected in the near and distant future.

skb.se